

**Defining a mechanism for *Heligmosomoides polygyrus bakeri*
exacerbation of colorectal cancer development**



Ella Katie Reed

Thesis submitted for the award of PhD

January 2025

Supervisor: Dr Katherine Smith

Co-supervisors: Dr Mark Young and Professor Valerie O'Donnell

Table of Contents

Acknowledgements	6
Abbreviations	7
Summary	10
Chapter 1: General Introduction.....	11
1.1 The healthy colon.....	11
1.1.1 Structure & function	11
1.1.2 Stem cells.....	13
1.1.2.1 <i>Intestinal stem cells</i>	13
1.1.2.2 <i>Signalling pathways involved in intestinal stem cell differentiation</i>	15
1.2 Colorectal Cancer.....	17
1.2.1 Genetics of colorectal cancer.....	17
1.2.2 Mechanisms of colorectal cancer development.....	19
1.2.2.1 <i>Colorectal cancer stem cell theory</i>	21
1.2.2.2 <i>Dysregulation of intestinal barrier function</i>	23
1.3 Changing epidemiology.....	24
1.4 Risk factors for colon cancer development.....	24
1.4.1 High omega-6 diet.....	25
1.4.1.1 <i>Prostaglandin E₂</i>	26
1.5 Soil-transmitted helminths.....	29
1.5.1 <i>Heligmosomoides polygyrus bakeri</i>	31
1.5.2 <i>Heligmosomoides polygyrus bakeri</i> excretory/secretory products.....	33
1.6 Link Between Soil-transmitted Helminth Infection and Colorectal Cancer.....	34
1.6.1 Helminth regulation of tight-junction markers and intestinal permeability.....	35
1.6.2 Helminth regulation of cancer stem-cell function.....	36
1.6.3 Helminth regulation of omega-6 polyunsaturated fatty acid metabolism.....	38
1.7 Project Aims and Hypothesis.....	41
Chapter 2: Materials and Methods.....	43
2.1 Cell culture.....	43
2.1.1 Established cell line.....	43
2.1.2 Cell line maintenance.....	43
2.1.3 Defrosting cells from liquid nitrogen and seeding.....	44
2.1.4 Passaging cells.....	44
2.1.5 Freezing cells.....	44
2.1.6 Seeding cells for functional assays.....	45
2.1.7 Preparation of drug solutions for cell treatment.....	45
2.1.8 Treatment of cell lines.....	45
2.2 <i>In vitro</i> experiments.....	46
2.2.1 FD4 cell permeability assay.....	46
2.2.2 Western blotting.....	48
2.2.2.1 <i>Whole cell lysate harvesting and protein extraction</i>	49
2.2.2.2 <i>Tissue harvesting and protein extraction</i>	50
2.2.2.3 <i>Sample preparation and loading</i>	50
2.2.2.4 <i>Gel production and protein separation</i>	51
2.2.2.5 <i>Semi-dry membrane transfer</i>	52

2.2.2.6 Membrane blocking and primary antibody staining.....	53
2.2.2.7 Secondary antibody staining.....	54
2.2.2.8 Protein detection.....	55
2.2.2.9 Protein quantification.....	55
2.2.3 BCA protein quantification assay.....	56
2.2.4 PCR.....	56
2.2.4.1 PCR primer design.....	57
2.2.4.2 RNA extraction.....	57
2.2.4.3 DNase treatment.....	58
2.2.4.4 cDNA synthesis.....	58
2.2.4.5 DNA amplification.....	58
2.2.4.6 Gel electrophoresis.....	59
2.2.5 Molecular cloning into <i>E. coli</i>	59
2.2.5.1 DNA preparation and Gibson assembly.....	60
2.2.5.2 Bacterial transformation.....	61
2.2.5.3 Colony PCR.....	62
2.2.5.4 Plasmid extraction and sequencing.....	62
2.2.5.5 Protein expression in <i>E. coli</i>	63
2.3 HES analysis.....	64
2.3.1 <i>Heligmosomoides polygyrus bakeri</i> larvae and HES preparation.....	64
2.3.2 HES heat-inactivation, protease inhibition and size fractionation.....	65
2.3.3 Oxylipin analysis.....	66
2.3.4 Phospholipase A ₂ activity assay.....	70
2.3.5 Nano-LC mass spectrometry.....	71
2.3.5.1 Proteomic data analysis.....	71
2.4 <i>In vivo</i> experiments.....	72
2.4.1 Animal husbandry.....	72
2.4.2 AOM/DSS model.....	72
2.4.3 Tissue harvest and processing.....	74
2.4.4 Immunohistochemistry.....	74
2.4.5 Faecal calprotectin ELISA.....	75
2.5 RNA expression: RNA sequencing data (RNASeq).....	76
2.5.1 Sample collection and quality control.....	76
2.5.2 Library construction, quality control and sequencing.....	77
2.5.3 Bioinformatic analysis pipeline.....	77
2.5.3.1 Data quality control.....	78
2.5.3.2 Reads mapping to reference genome.....	78
2.5.3.3 Reads indexing, sorting and final QC.....	79
2.5.3.4 Differential expression analysis.....	79
2.5.3.5 Enrichment analysis of differentially expressed genes.....	79
2.6 Computational studies.....	80
2.6.1 Molecular modelling and docking studies.....	80
2.6.2 Bioinformatic sequence analysis.....	81
2.7 Statistical analysis.....	81
Chapter 3: Role of prostaglandin signalling in helminth exacerbation of CAC.....	83
3.1 Introduction.....	83
3.1.1 Relationship of prostaglandin E ₂ signalling with colitis-associated colorectal cancer...84	84
3.1.2 How might helminths modify intestinal permeability and drive CAC?.....85	85

3.2 Chapter aims.....	86
3.3 Hypothesis.....	86
3.4 Results.....	86
3.4.1 <i>H. polygyrus</i> infection increases PGE ₂ receptor activation in the colon at day 14 post-infection.....	86
3.4.2 <i>H. polygyrus</i> infection has no significant effect on E-cadherin expression in the colon at day 14 post-infection.....	88
3.4.3 <i>H. polygyrus</i> infection increases PGE ₂ receptor activation in the colon in the AOM/DSS model.....	89
3.4.4 <i>H. polygyrus</i> infection decreased E-Cadherin expression in the colon in the AOM/DSS model.....	92
3.4.5 Addition of EP2 & EP4 inhibitors during AOM/DSS model.....	93
3.4.6 <i>H. polygyrus</i> infection results in a significant increase in intestinal inflammation which is reduced with EP2/EP4 inhibitors.....	96
3.4.7 HES causes an increase in <i>in vitro</i> intestinal cell permeability in a similar manner to a PGE ₂ receptor agonist.....	98
3.4.8 The ability of HES to increase <i>in vitro</i> intestinal cell permeability is mediated primarily through EP2 receptor signalling.....	100
3.4.9 HES causes an increase in phosphorylation of β -catenin Ser ⁵⁵² <i>in vitro</i> which is significantly reduced with EP2 & EP4 inhibitors.....	103
3.4.10 HES causes a decrease in expression of E-cadherin <i>in vitro</i> which is rescued with EP2 & EP4 inhibitors.....	104
3.5 Discussion.....	105
Chapter 4: Analysis of the HES to determine what is driving the increase in cellular permeability.....	110
4.1 Introduction.....	112
4.2 Chapter aims.....	112
4.3 Hypothesis.....	112
4.4 Results.....	112
4.4.1 Protease inhibition had no significant impact on the ability of HES to increase cellular permeability.....	112
4.4.2 Size fractionation of HES reveals a predicted molecular weight of molecule(s) responsible for increasing cellular permeability.....	114
4.4.3 Oxylipins were below the level of detection in HES using LC/MS.....	115
4.4.4 HES contains three homologues of secreted phospholipase A ₂	117
4.4.5 HES-dependent increases in cell permeability are cyclooxygenase-dependent.....	119
4.4.6 HES encodes several homologues of metabolic enzymes.....	120
4.4.7 PGES2 gene is expressed in the adult life-stage of <i>H. polygyrus</i>	122
4.4.8 <i>H. polygyrus</i> PGES2 enzyme homologue shows highly conserved primary and tertiary amino acid structures to human and murine enzyme.....	125
4.4.9 Addition of a recombinant human PGES2 increases cellular permeability.....	127
4.4.10 <i>H. polygyrus</i> PGES2 is not predicted to be secreted.....	128
4.4.11 <i>H. polygyrus</i> has PLA ₂ activity in the HES and adult antigen.....	129
4.4.12 Addition of recombinant PLA ₂ increases cellular permeability.....	130
4.4.13 <i>H. polygyrus</i> PLA ₂ enzyme homologues show highly conserved primary and tertiary structures to human enzymes.....	132
4.4.14 <i>sPLA₂</i> gene is expressed in the adult life-stage of <i>H. polygyrus</i>	136
4.4.15 <i>H. polygyrus sPLA₂</i> is predicted to be secreted.....	138

4.5 Discussion.....	139
Chapter 5: <i>H. polygyrus</i> secretory phospholipase A2 drug development and linking its activity to increased cell permeability.....	144
5.1 Introduction.....	144
5.2 Chapter aims.....	148
5.3 Hypothesis.....	148
5.4 Results.....	148
5.4.1 Structure-based identification of potential <i>H. polygyrus</i> secretory phospholipase A ₂ inhibitors and molecular docking studies.....	148
5.4.2 Selected inhibitors of <i>H. polygyrus</i> secretory phospholipase A ₂ show activity against <i>H. polygyrus</i> adult supernatant.....	155
5.4.3 Inhibiting the <i>H. polygyrus</i> secretory phospholipase A ₂ significantly reduces the ability of <i>H. polygyrus</i> excretory/secretory products from increasing intestinal cell permeability.....	156
5.4.4 Off-target effects of <i>H. polygyrus</i> PLA ₂ G1B inhibitor AF-399/14183760.....	158
5.5 Discussion.....	161
Chapter 6: Profiling the colonic transcriptome of <i>H. polygyrus</i> infected mice....	163
6.1 Introduction.....	163
6.2 Chapter aims.....	164
6.3 Hypothesis.....	164
6.4 Results.....	164
6.4.1 RNA extraction quality control results.....	164
6.4.2 Differential gene expression in the colon of <i>H. polygyrus</i> infected mice vs uninfected.....	169
6.4.3 Upregulated genes and their corresponding biological process and molecular function.....	171
6.4.4 Downregulated genes and their corresponding biological process and molecular function.....	173
6.4.5 Gene set enrichment analysis reveals significantly enriched pathways in the colon of <i>H. polygyrus</i> infected mice.....	175
6.4.6 Expression profiling of the PGE ₂ synthetic and signalling pathway in the colon of <i>H. polygyrus</i> infected mice.....	179
6.4.7 Differential immune cell content in the colon of <i>H. polygyrus</i> infected mice.....	182
6.4.8 Effect of <i>H. polygyrus</i> infection on the colonic stem cell compartment.....	185
6.5 Discussion.....	187
Chapter 7: General Discussion.....	192
7.1 Summary of results.....	192
7.2 Limitations.....	195
7.3 Future work.....	196
7.4 Overall implications.....	198
References.....	200
Appendix.....	223

Acknowledgements

Firstly, I would like to thank my supervisor Dr Katherine Smith for the opportunity to undertake my PhD project in her lab and for providing me with support and guidance as I navigated this long journey. Thank you for introducing me to the weird and wonderful world of helminths, your enthusiasm for this topic of research is endearing and inspiring, and has ignited my interest in host-pathogen interactions in cancer. I would also like to thank my second supervisors Dr Mark Young and Professor Valerie O'Donnell, for always being available to offer their expertise in the world of proteins and lipidomics respectively. Additionally, I would like to acknowledge the support of Dr Marcella Bassetto, without whom the structure-based drug identification would not have been possible, by providing much-appreciated expertise and knowledge. I would like to thank Dr Alex Gibbs for extensive support with the RNA sequencing analysis. Finally, I would like to thank Dr Victoria Tyrrell for providing support with the lipidomics experiment and data analysis.

I am hugely grateful to my colleagues and friends in the MMI lab who supported me through the project and made these three years the most enjoyable. I would like to thank Lucile Hubert, Gordon Webster, Rebecca Weiser, Laura Rushton, Brooklyn Rowlands, Naomi Hughes, Owen Griffiths, Alex Mullins, Teresa Paradell-Gill, Nico Bruyniks, Doyle Millard, and Holly-Anne Smith for all the technical and emotional support and for making the MMI office a fun and enjoyable place to be. I would like to extend a special thank you to Dr Helen Brown, who offered significant mentorship and guidance on career development throughout my PhD, I am indebted to you for providing such support.

Finally, I would like to extend a massive thank you to my friends and family for their support and providing a welcome escape when things got tough. Particularly, my parents, Carmel and Simeon Reed, my lab bestie Lucile Hubert, my rock Caitlin Jones, and my partner Joel Thomas, who always reminded me that despite everything I am good enough and to never give up.

Abbreviations

AOM – azoxymethane

APC – adenomatous polyposis coli

BCA – bicinchoninic acid

CAC – colitis-associated colorectal cancer

COX – cyclooxygenase

CRC – colorectal cancer

DEG – differential gene expression

DMEM/F12 – Dulbecco's modified eagle medium F12

DMSO – dimethylsulfoxide

dmPGE2 – dimethyl prostaglandin E2

DSS – dextran sodium sulfate

EDTA – ethylenediaminetetraacetic acid

ELISA – enzyme-linked immunosorbent assay

ESPs – excretory/secretory products

FBS – foetal bovine serum

FDR – false discovery rate

FD4 – fluorescein isothiocyanate-dextran 4kDa

GAPDH - glyceraldehyde 3-phosphate dehydrogenase

GC – goblet cell

GIT – gastrointestinal tract

GO – gene ontology

HES – helminth excretory/secretory products

HI – heat-inactivation

Hpb – *Heligmosomoides polygyrus bakeri*

HTVS – high-throughput virtual screening

IBD – inflammatory bowel disease

IECs – intestinal epithelial cells

I-TASSER - Iterative Threading ASSEmbly Refinement

KEGG – Kyoto encyclopedia of genes and genomes

LA – linoleic acid

LB – lysogeny broth

LC/MS – light chromatography/mass spectrometry

LGR5 - Leucine-rich repeat-containing G-protein coupled receptor 5

MMPs – matrix metalloproteases

MOE – molecular operating environment

MW – molecular weight

MWCO – molecular weight cut-off

PCA – principle component analysis

PBS – phosphate buffered saline

PBS-T - phosphate buffered saline with Tween

PCA – principle component analysis

PCR – polymerase chain reaction

PC – Paneth cell

PGE2 – Prostaglandin E2

PGES2 – prostaglandin E synthase 2

PGH2 – prostaglandin H2

PI – protease inhibition

PLA2 – phospholipase A2

PLANTS - Protein-Ligand ANT System

P/S - penicillin and streptomycin

PUFA – polyunsaturated fatty acid

RIN – RNA integrity

RNA – ribonucleic acid

SDS – sodium dodecyl sulphate

SEM – standard error of the mean

STH – soil-transmitted helminth

SP – standard precision

TBS-T – Tris-buffered saline with Tween

TC – tuft cell

VAL – venom allergen-like

XP – extra precision

ZO-1 – zonula occludens 1

Summary

Around 10-15% of patients with inflammatory bowel disease (IBD) develop colitis-associated colorectal cancer (CAC). Recent findings indicate that a diet high in linoleic acid (ω -6) and infection with the small intestinal nematode *Heligmosomoides polygyrus bakeri* increase the risk of CAC separately, with the combination resulting in further exacerbation of disease. In a murine CAC model, inhibition of cyclooxygenase (COX) metabolites, products of linoleic acid, and subsequent prostaglandin signalling, significantly reduced tumour formation in *H. polygyrus* infected mice. Notably, activating COX-derived prostaglandin E₂ (PGE₂) receptors EP2 and EP4 prior to disease onset enhanced tumour formation, similar to the effect of *H. polygyrus* infection.

This thesis demonstrates that *H. polygyrus* infection activates EP2 and EP4 receptors in the colon *in vivo*, and that excretory/secretory products (HES) increase cell permeability *in vitro* via EP2 and EP4 signalling. Biochemical analysis identified a heat-stable, non-protease molecule between 10,000-50,000 MW in HES responsible for this effect. The *H. polygyrus* genome revealed 17 proteins similar to human secretory phospholipase A₂ (PLA₂), with proteomic analysis confirming the presence of three in the 10-50,000 MW fraction. Among these, HPOL_0000384601 showed the highest similarity to human PLA₂G1B active sites. Using an *in vitro* fluorescence assay, PLA₂ activity was confirmed in HES. With commercial inhibitors of human and murine PLA₂G1B showing no effect against *H. polygyrus* PLA₂G1B, a structure-based design approach was taken to identify novel compounds to inhibit its activity. Using a crystal model of *H. polygyrus* PLA₂G1B generated through protein threading, a known inhibitor was docked into the active site, and important ligand interactions used to identify compounds that interact with these residues. Testing of the IC₅₀ of the best ten compounds based on *in silico* visual inspection revealed AF-3999/14183760 as having the highest potency, and addition of this compound along with HES *in vitro* resulted in a reduction in the ability of HES to increase cell permeability, suggesting *H. polygyrus* PLA₂G1B plays a central role in HES-mediated increase in cell permeability.

To explore the mechanisms by which *H. polygyrus* may exacerbate CAC, transcriptomic analysis of infected mice colons revealed upregulation of inflammatory and oncogenic pathways, alongside downregulation of cell cycle regulatory and tumour suppressor pathways. These findings offer new insights into *H. polygyrus*-driven CAC progression and open avenues for further functional studies.

Chapter 1: General Introduction

1.1 The Healthy Colon

1.1.1 Structure & function

The colon forms an integral part of the large intestine, which accounts for one-fifth of the length of the gastrointestinal (GI) tract (1). In healthy individuals, the colon has three main functions; absorbing water and electrolytes, producing and absorbing vitamins, and propelling faeces towards the rectum for elimination (1). These functions are carried out in specific regions of the colon, which is divided into four parts: the ascending colon, transverse colon, descending colon, and the sigmoid colon (2). The ascending colon has the role of absorbing the remaining water and other key nutrients from indigestible material which hasn't been absorbed in the small intestine (2). This material is then solidified and stored in the descending colon as faeces which will eventually be secreted via the rectum (2). The sigmoid colon is able to contract to increase the pressure inside the colon, causing the faeces to move into the rectum where it is subsequently excreted (2).

The anatomy of the intestinal architecture is shown in **Figure 1**, made up of four layers. The colon contains an additional mucus layer on top of the epithelium. This mucus layer is imperative in forming the intestinal barrier, which is a direct barrier between the external environment and the internal host (3). There are several examples of these mucosal barriers throughout the human body, with one of the largest being found within the GI tract (4). The intestinal barrier plays a critical role in the regulation of the immune system in health and disease; and critical to this function is its complex structure as seen in **Figure 2** (3).

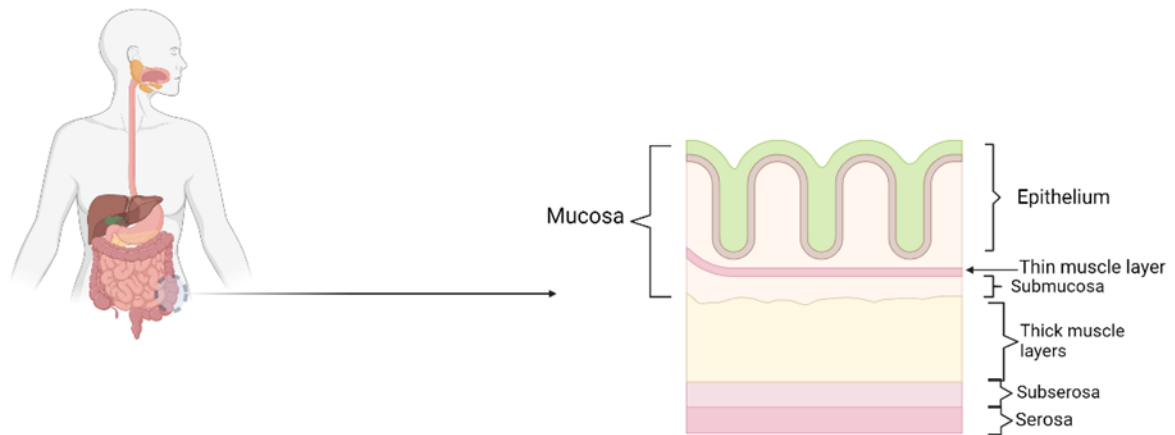


Figure 1. Figure showing the structure of the human colon. The architecture consists of continuous villi and crypts known collectively as the epithelium. There is a thick mucus layer over the top of the epithelium to prevent the entry of pathogens. The colon also contains several layers of muscle which contract to enable the movement of faeces to the rectum and also the elimination of intestinal pathogens. Image made using Biorender.

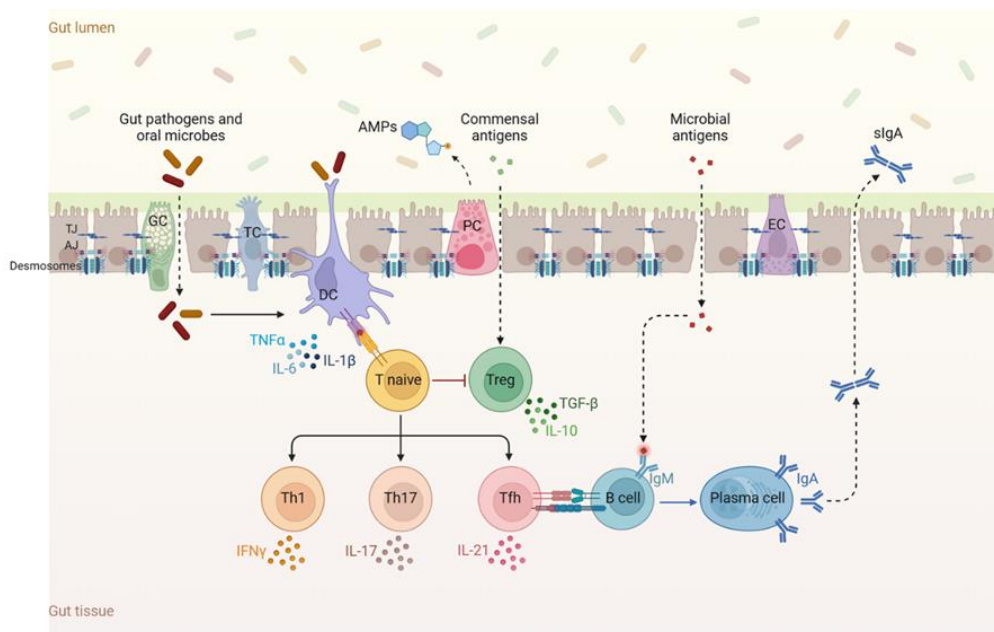


Figure 2. Interactions between gut microbiota, epithelial cells, and immune responses in the intestinal mucosa. The gut lumen contains pathogens, oral microbes, and commensal antigens interacting with the epithelial barrier. Goblet cells (GC) secrete mucus, forming a protective layer, while tight junctions (TJ) and adherens junctions (AJ) maintain epithelial integrity. Dendritic cells (DC) sample antigens and present them to naïve T cells, promoting differentiation into Th1, Th17, Tfh, or regulatory T cells (Treg). Th1 cells produce IFN- γ , Th17 cells produce IL-17, and Tregs secrete anti-inflammatory cytokines TGF- β and IL-10. Microbial antigens also stimulate B cells, which differentiate into plasma cells producing secretory Immunoglobulin A (sIgA) for mucosal immunity. Paneth cells (PC) secrete antimicrobial peptides (AMPs), while enteroendocrine cells (EC) contribute to gut homeostasis. Image made using Biorender.

The first line of physical defence against invading and commensal bacteria from being able to directly contact the epithelial cells is the mucus layer (5). The mucus layer is composed of several highly glycosylated mucin proteins, most notably mucin 2 (MUC2) which is the most abundant mucus protein secreted by goblet cells (6). The importance of MUC2 in colonic protection was demonstrated in a MUC2 knockout mouse model, where these knock out mice spontaneously developed colitis; inflammation of the large intestine (7). The mucus layer also releases mediators such as secretory immunoglobulin A (sIgA), which prevents pathogens and toxins from attaching to mucosal surfaces by binding antigens and trapping them in mucus (8). Below the mucus layer are the intestinal epithelial cells (IECs), which form the strongest physical component of the intestinal barrier (3). Within the IECs are a pool of pluripotent stem cells which reside in the intestinal crypts giving rise to five distinct cell types (3). These cell types include goblet cells, tuft cells, Paneth cells and enteroendocrine cells (3). Altogether, these cells form a monolayer separating the intestinal lumen from the lamina propria (3). The transport of molecules from the intestinal lumen to the blood stream is highly regulated by three junctional complexes: tight junctions, adherens junctions, and desmosomes (9).

1.1.2 Stem cells

Stem cells are undifferentiated cells with three key traits: extensive proliferation, derivation from a single cell, and the ability to differentiate into various cell types and tissues (10). Pluripotent stem cells, from the inner embryonic cell mass or reprogrammed somatic cells, can form tissues from all three germ layers. In contrast, multipotent stem cells, such as mesenchymal stem cells, differentiate into tissues from a single germ layer, like adipose, bone, and cartilage (10).

1.1.2.1 Intestinal stem cells

The architecture of the large intestine consists of continuous villi and crypts as shown in **Figure 3A**. The villi contains differentiated mature epithelial cells which are no longer capable of proliferating, but have the ability to de-differentiate in response to injury (11). These mature epithelial cells can be categorised based on their differing functions (11). The main function of enterocytes is digestion and the absorption of ions, water, nutrients, vitamins, and unconjugated bile salts (12). Enterocytes have also been shown to play a key role in maintaining the intestinal immune environment, by regulating the inflammatory responses (12). They achieve this by producing anti-inflammatory cytokines, such as interleukin-10 (IL-10), which help dampen excessive immune activation, thereby protecting the intestinal tissue from damage (13). Simultaneously, enterocytes can secrete pro-inflammatory mediators like interleukin-8 (IL-8) in response to pathogenic threats, activating and recruiting immune cells to contain infections (13). The next category of cells are goblet cells, which as previously discussed

play a critical role in maintaining the integrity of the mucus barrier by secreting MUC2 (6). Enteroendocrine cells are responsible for the secretion of several peptide hormones which regulate intestinal metabolism (14). Like the other cells of the intestinal epithelium, enteroendocrine cells are in a continuous state of cell turnover, being replaced every 3-5 days by a cycle of local stem cell division in the small and large intestine (14). Tuft cells have been related to taste cells, where they share similar chemosensory molecules (15). Using this ability to sense their environment, tuft cells can trigger the type 2 immune response in the presence of infection (15). In response to infection, they secrete interleukin-25 (IL-25), which activates group 2 innate lymphoid cells (ILC2s). ILC2s release type 2 cytokines, including interleukin-13 (IL-13) and interleukin-5 (IL-5), which promote mucus production, smooth muscle contraction, and eosinophil activation to expel parasites and mediate inflammation (16). These cytokines also recruit additional immune cells, such as mast cells and basophils, and create feedback loops to amplify the response, ensuring effective defence and tissue repair. Finally, Paneth cells are highly specialised secretory epithelial cells which unlike the other categories of epithelial cells discussed, are located at the base of the small intestinal crypts of Lieberkühn (17). Paneth cells can secrete granules which contain antimicrobial peptides and immunomodulating proteins which function to regulate the composition of the intestinal flora (17). The crypts of Lieberkühn contain undifferentiated and rapidly dividing cells which are responsible for providing the incredible rate of cell turnover in the intestinal epithelium (**Figure 3B**) (18). As these cells begin to differentiate, they then migrate up the toward the tip of the villus where they are eventually shed (18).

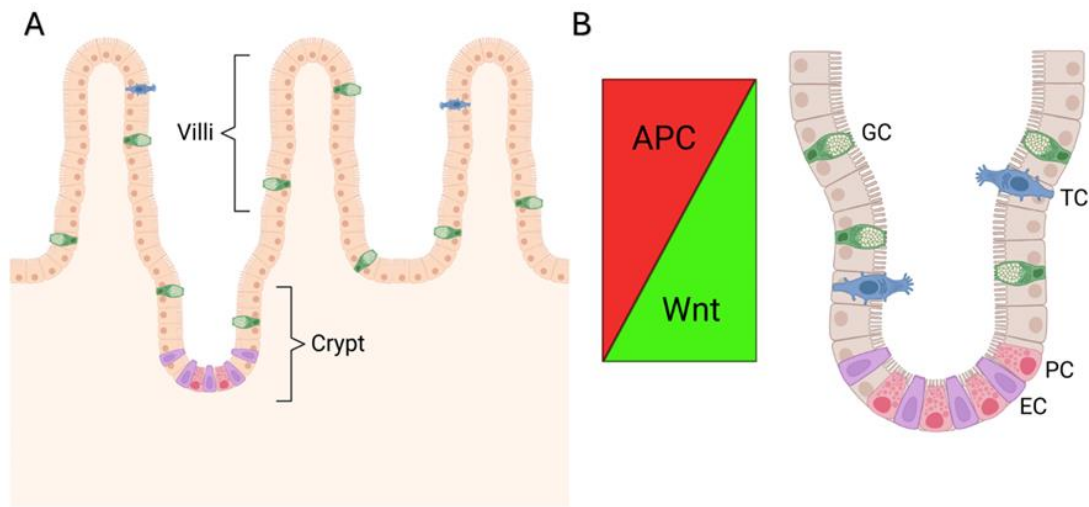


Figure 3. Architecture of the intestinal crypt. (A) Figure showing the structure of the intestine, with the villi and crypt clearly distinguished. (B) Figure showing the composition of the small intestinal crypt, showing the different types of cells which are present. The levels of APC and Wnt signalling show an inverse relationship, with adenomatous polyposis coli (APC) being prominent at the top of the villus whereas Wnt signalling is at its highest at the bottom of the crypt. This is to control the levels of cell proliferation throughout the small intestinal crypt. Image made using Biorender.

1.1.2.2 Signalling pathways involved in intestinal stem cell differentiation

The predominant signalling pathway involved in regulating intestinal stem cell (ISC) differentiation is the canonical Wingless-related integrated site (Wnt) cascade (**Figure 4**) (19). The Wnt signalling cascade is activated once Wnt binds to its frizzled/Low-density lipoprotein receptor-related proteins (LRP) receptor complex (19). When this receptor is engaged, it releases β -catenin from the destruction complex made up of adenomatous polyposis coli (APC), axin, and glycogen synthase kinase-3 beta (GSK3- β). Once β -catenin is released from the destruction complex, it can be phosphorylated at several sites determining its fate (20). For example, it is phosphorylated at Ser⁵⁵² ($p\beta$ -catenin Ser⁵⁵²) allowing it to translocate to the nucleus where it can cause the transcription of Wnt target genes (**Figure 4**) (19). When the Wnt receptor is not engaged, the destruction complex binds to β -catenin where it becomes ubiquitinated for degradation (19).

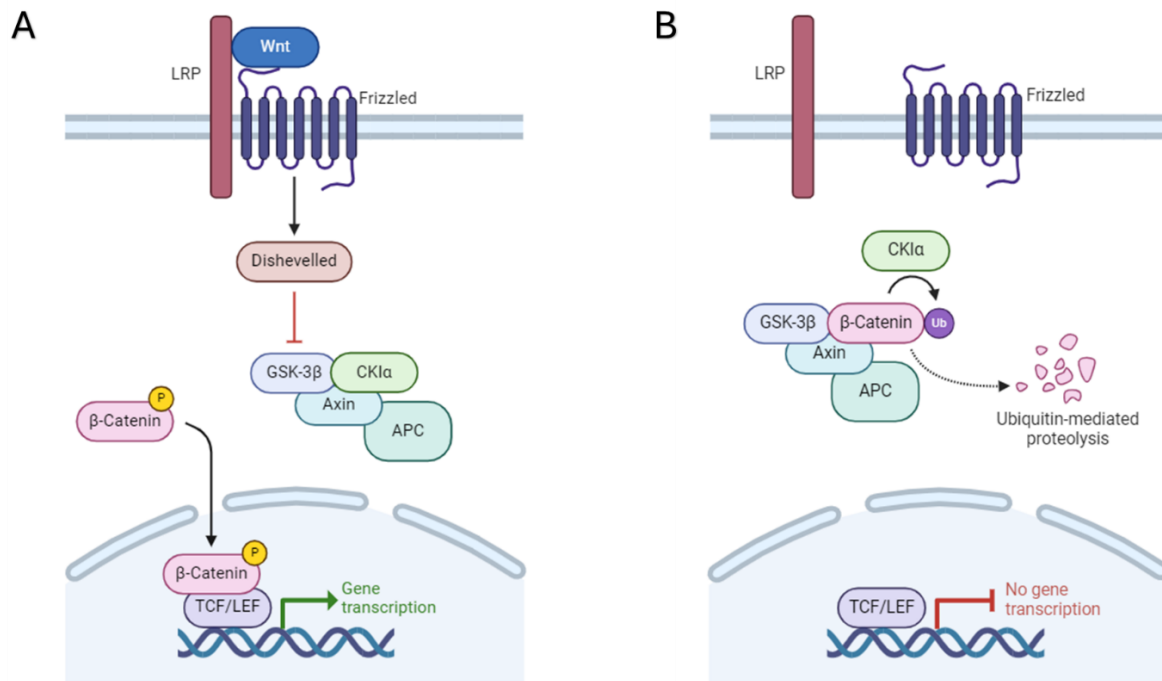


Figure 4. Figure showing a schematic of the Wnt canonical signalling pathway. **(A)** When Wnt is bound to its receptor complex, axin prevents GSK3-β from phosphorylating β-catenin. This leaves β-catenin free in the cytoplasm, where it can translocate to the nucleus and promote the transcription of Wnt target genes. **(B)** When Wnt is not bound to its receptor complex, β-catenin is bound to a “destruction complex” formed of axin, APC, and GSK3-β. Whilst bound to this complex GSK3-β tags β-catenin therefore targeting it for ubiquitination, leading to the transcription of Wnt target genes being switched off. Image made using Biorender.

As shown in **Figure 3B**, the levels of Wnt signalling increase from the crypt up to the tip of the villi which is the opposite of APC expression (19). There is an incredible demand within the intestinal crypt to keep up with the need for cell turnover due to high levels of mechanical stress and to maintain homeostasis (21), therefore Wnt signalling is key for this in the base of the crypt (19). Moving up from the crypt to the villi, levels of APC then start to increase, resulting in a reduced rate of cellular proliferation (19). APC is a well-known tumour suppressor gene and mutations within this gene have been well characterised in pathology, in particular colorectal cancer (CRC) (22). Aberrant activation of the Wnt pathway, often through mutations in key components such as APC, β-catenin, or Axin, leads to uncontrolled cell growth and resistance to apoptosis (23). This dysregulation is commonly associated with colorectal cancer but also contributes to other malignancies like breast, liver, and prostate cancer (23).

1.2 Colorectal Cancer

1.2.1 Genetics of colorectal cancer

CRC is the second leading cause of cancer-related mortality worldwide, with an estimated 881,000 deaths being accredited to CRC in 2018 (24). There are several factors linked to an increased risk of developing CRC, including inherited genetic mutations, diet and lifestyle factors, including smoking and alcohol (25). Chronic inflammatory conditions of the large intestine, such as inflammatory bowel disease (IBD), are also known to increase the risk of developing colitis-associated colorectal cancer (CAC) by 10-15% (26, 27).

Non-inherited adenocarcinomas account for 80% of CRC diagnoses, with the risk of these increasing with age (>90% are over 50) as well as other factors such as obesity and a diet high in red meat (28). It is estimated that patients with IBD have a 10-15% increased risk of developing CAC (26, 27). The other 20% of CRC diagnoses are known as hereditary adenocarcinomas where the risk is significantly increased with a strong family history (29). Approximately 1% of these hereditary adenocarcinomas are due to familial adenomatous polyposis (FAP) which is driven by a mutation in the APC gene, which is part of the β -catenin destruction complex (19). A loss of heterozygosity mutation in APC prevents the proteolytic degradation of β -catenin so it can translocate to the nucleus and cause the transcription of Wnt target genes such as cellular-myelocytomatosis oncogene (c-myc) and cyclin D1 (**Figure 4**) (30). C-myc is a proto-oncogene whose transcription is dysregulated in the majority of human CRC cases and is thought to contribute to at least 40% of CRC tumours (31). C-myc is also able to promote the transcription of pro-proliferative genes such as cyclin D1 (32). Cyclin D1 is an important regulator of the G1 to S phase in the cell cycle (**Figure 5**) and has been found to be important for the development and progression of several cancers, including breast and lung (33). It is estimated that all FAP positive patients will develop CRC by the age of 45 and all are offered prophylactic colectomy (29).

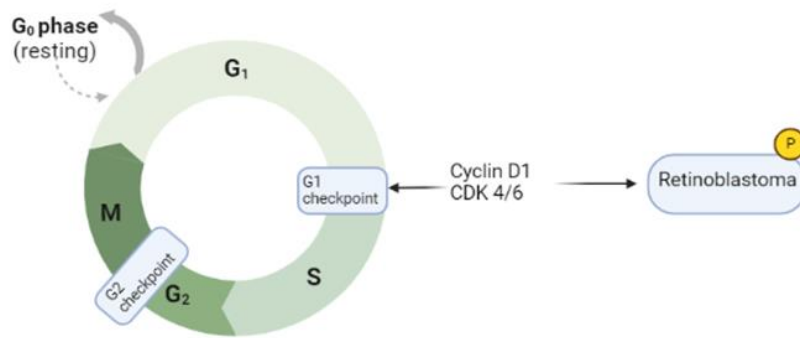


Figure 5. Schematic figure of the cell cycle, including details of the G₁/S checkpoint. Cyclin D1 acts with cyclin dependent kinase 4/6 (CDK 4/6) to phosphorylate and inactivate the retinoblastoma protein. Image made using Biorender.

Another form of hereditary adenocarcinoma is hereditary non-polyposis colorectal cancer (HNPCC) which is also known as Lynch syndrome (29). Lynch syndrome accounts for 3% of CRC diagnoses and is driven by error in DNA repair genes (29). These tumours are characterised by a high level of microsatellite instability, which is a characteristic of CRC arising from defective mismatch repair (MMR) genes, causing errors in DNA to go uncorrected (29). The MMR system includes several genes, such as human mutS homologue 2 (hMSH2) and human mutL homologue 1 (hMLH1), and is imperative for maintaining genomic stability (34). The MMR system does this by correcting single-base mismatches and insertion-deletion loops that form during DNA replication (34). The most commonly mutated MMR genes are hMSH2 and hMLH1 which account for up to 90% of Lynch Syndrome cases (35).

Patients who are identified as having genetic susceptibility to developing CRC are routinely screened in the UK with the NHS screening programme. However, most patients will present with advanced CRC in accident & emergency (A&E) departments or general practice (GP) surgeries due to the early stages of CRC being asymptomatic (36). It is in more advanced stages of CRC where clinical symptoms start to appear, examples of these include weight loss, abdominal pain, and changes in bowel habits (37).

Among colon cancers, the most common sites are the sigmoid colon (55%), followed by the ascending colon (23.3%), transverse colon (8.5%), descending colon (8.1%), cecum (8.0%), and crossing site (2.1%) (38). CRC may also metastasise to distant organs by invading the lymph vessels and the bloodstream (39). This is where patient prognosis severely decreases, and current treatment strategies are redundant. Current treatment modalities for CRC are limited to either surgery or chemotherapy (40), both of which have detrimental impacts on the patient such as neutropenia, anaemia, diarrhoea, nausea, vomiting, fatigue, hematologic disorders, and liver toxicity (41). These side effects and the development of drug resistance mean that treatment outcomes to date have not been highly efficacious (42).

1.2.2 Mechanisms of colorectal cancer development

The timeline of events which characterise CRC development were first described by Bert Vogelstein in what he later called the “Vogelgram” model of cancer development (**Figure 6**) (43).

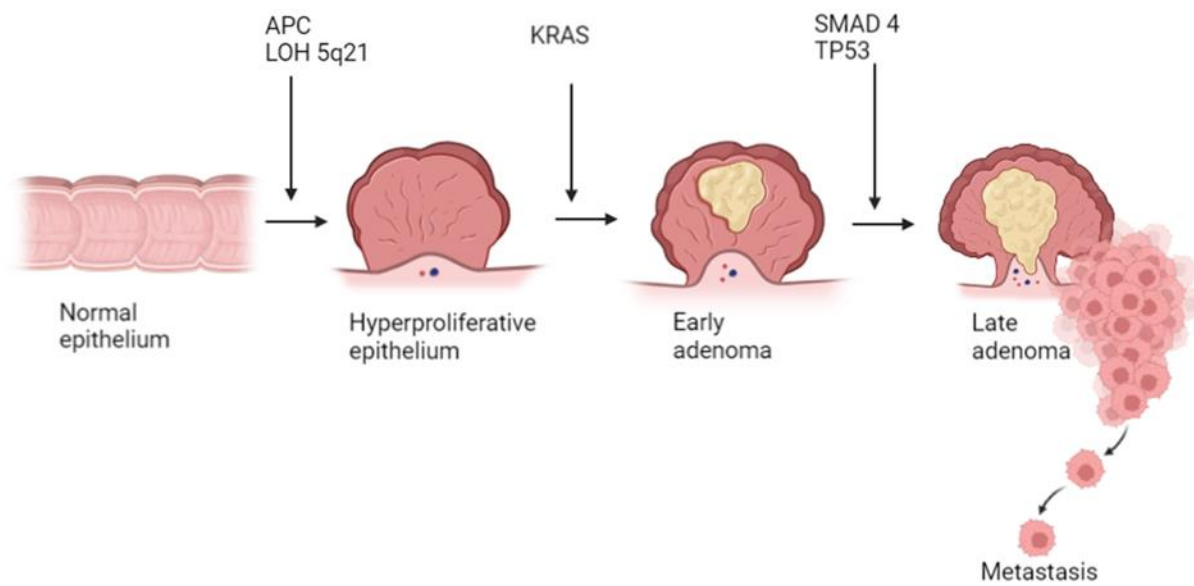


Figure 6. A schematic diagram detailing the Vogelstein model of colorectal cancer progression.

The figure shows the different stages of carcinogenesis and the genetic mutations which occur to allow progression from healthy epithelium to cell metastasis. The first mutational event is a loss of heterozygosity (LOH) mutation on chromosome 5 at position q21 in the APC gene, leading to the accumulation of β -catenin resulting in a hyperproliferative epithelium. Next is a mutation in Kirsten rat sarcoma viral oncogene homologue (KRAS) which acts as a molecular switch to control intracellular signalling pathways such as phosphatidylinositol 3-kinase (PI3K)/ protein kinase B (AKT) and mitogen activated protein kinase (MAPK). The mutation in KRAS allows these pathways to be constantly switched on resulting in uncontrolled cellular proliferation. Finally, mutations in tumour protein 53 (TP53) and Suppressor of Mothers Against Decapentaplegic 4 (SMAD4) occur in the later stages on CRC development. TP53 is activated when DNA damage occurs and promotes the transcription of cell cycle arrest genes to prevent the mutation progressing through the cell cycle. A loss of TP53 allows mutations in DNA to be replicated allowing for mutant clones to form. SMAD4 is a member of the SMAD family of proteins who respond to transforming growth factor-beta (TGF- β) signalling. The SMAD family of proteins are tumour suppressors and promote the transcription of genes which inhibit epithelial cell proliferation. Image made using Biorender.

The “Vogelgram” model of cancer development is a well-established model which assumes that CRC originate from a monoclonal tumour origin, that originates from a single mutated cell (43). While the Vogelstein model provides a foundational framework for understanding colorectal cancer progression, its linear, mutation-centric approach is increasingly challenged by emerging evidence of tumour complexity, heterogeneity, and the interplay of genetic, epigenetic, and environmental factors that can influence disease (44).

The colorectal cancer stem cell (CSC) theory offers an alternative framework to the Vogelstein model for understanding colorectal cancer development. While the Vogelstein model focuses on the linear accumulation of genetic mutations driving tumour progression through a clonal evolution process, the CSC theory emphasizes the role of a subpopulation of cancer cells in differing lineages with stem-like properties that drive tumour initiation, growth, and recurrence (45).

1.2.2.1 Colorectal cancer stem cell theory

As previously discussed, stem cells are defined by their ability to self-renew and differentiate into cells of the tissue of origin (10). Adult colonic stem cells are characterised as being Leucine-rich repeat-containing G-protein coupled receptor 5 (Lgr5) positive and are located at the base of the intestinal crypt (46). Lgr5-positive cells in the colon serve as ISCs that are crucial for maintaining and regenerating the epithelial lining of the colon (47). Lgr5 is a ligand of the Wnt signalling pathway, and is therefore constitutively activated at the base of the intestinal crypt to promote cellular proliferation towards the peak of the intestinal villi (48). Therefore, it is these Lgr5⁺ ISC which play a pivotal role in maintaining the plethora of functional intestinal cells, including goblet cells (GC), Paneth cells (PC), tuft cells (TC), and enteroendocrine cells (EC) (Figure 7) (49).

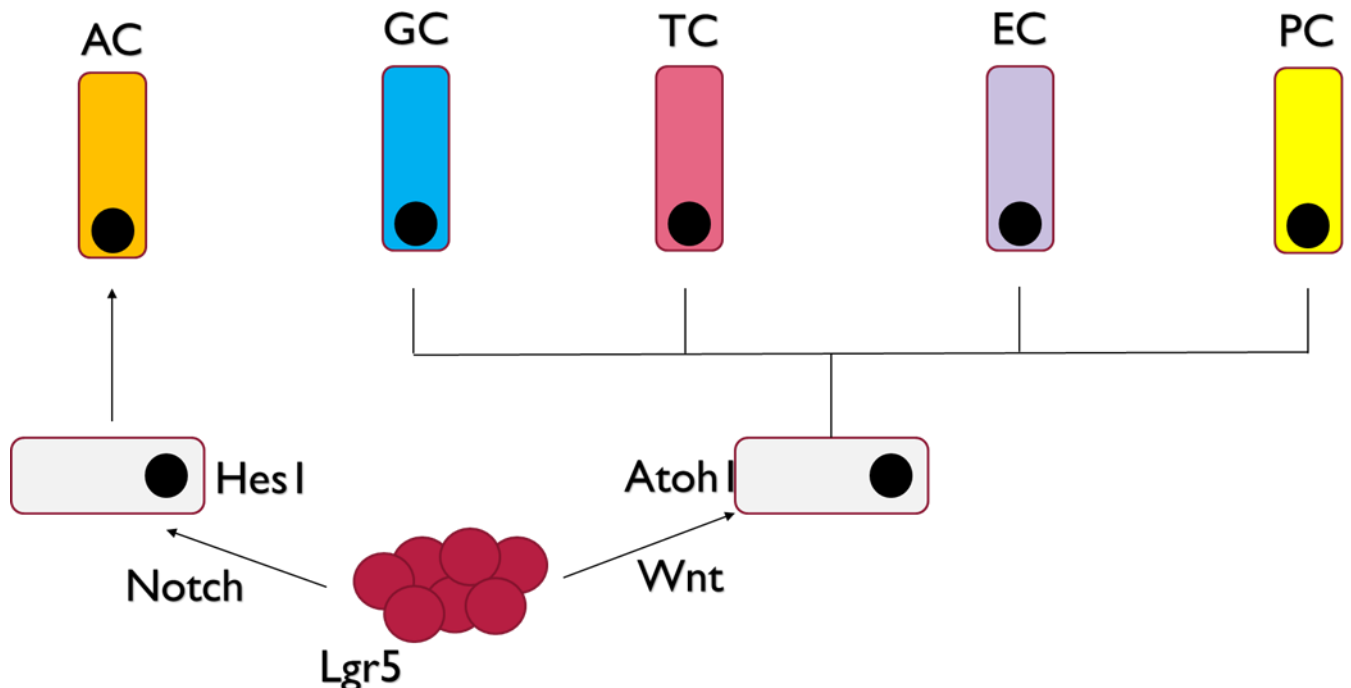


Figure 7. Figure showing the process by which Lgr5 ISCs can differentiate into functional intestinal cells. There are two groups of cells which the ISCs can differentiate into, absorptive cells (AC) and secretory cells. The secretory cells include goblet cells (GC), tuft cells (TC), enteroendocrine cells (EC), and Paneth cells (PC). In terms of which lineage the ISCs differentiate into, this is dependent on the signaling pathway activated. Image made using Biorender.

According to CSC theory, also known as the “hierarchical model”, tumours contain cells with different tumorigenic potential; cells that have lost the ability to propagate the tumour and cells which retain their clonogenic ability (50). In fact, biologically distinct populations of CSC have been identified in most solid tumours, including colon cancer (51). CSCs are thought to have three key characteristics; the capacity of self-renewal indefinitely, the potential for multilineage differentiation, and the expression of a distinctive set of surface biomarkers (52) such as cluster of differentiation (CD) 24, CD44 and CD133 (53). CSCs have also been shown to display alterations of DNA repair mechanisms, due to the presence of cytoprotective properties such as telomerase activation and a high expression of anti-apoptotic factors (54). CSCs also display a relatively low proliferative potential, which underpins the failure of most anti-tumour therapies as they target rapidly dividing cells, leaving CSCs to proliferate slowly (55). CSCs are also known to express high levels of proteins belonging to the adenosine triphosphate (ATP) binding cassette (ABC) membrane transporters family, which are involved in resistance to chemotherapeutic drugs such as paclitaxel and cisplatin (55).

Although the characteristics of CSCs has been well studied, there is still debate surrounding the origin of cancer formation (50). There are two possible hypothesis which have been suggested: the so-called “bottom-up” and the “top-down” theories (56). The “bottom-up” hypothesis proposes that an ISC, either a progenitor or a differentiated cell, is the first transformed cell that differentiates to give rise directly to cancer cells (56). This is typically an APC mutation in the intestinal crypt, leading to increased levels of β -catenin and cellular proliferation (57). Evidence for the “bottom-up” model is shown with the significant increase in expression of Lgr5 in human CRC (58). Conversely, a study showed that the dysplastic cells at the tops of the crypts often exhibited genetic alterations of APC and neoplasia-associated patterns of gene expression (59). In contrast, cells located at the base of these same crypts did not contain such alterations and were not clonally related to the contiguous transformed cells above them (59). These results imply that development of adenomatous polyps proceeds through a “top-down” mechanism.

1.2.2.2 Dysregulation of intestinal barrier function

Disruption of the intestinal barrier has been linked to several pathologies, most notably IBD and CRC (60). Research performed by Michielan and D'Inca found that 40-50% of patients with colitis had increased gut permeability, as measured by functional tests such as the sugar absorption tests (61). This was further assessed using the novel imaging technique of confocal laser endomicroscopy, with the highest values observed in patients with chronic disease. (61). Permeability tests in explants of tissue from IBD patients have shown increased intestinal fluxes and changes in tight junction protein expression, with alteration in the mucus layer being described (62). Evidence points towards a role for inflammatory cytokines in promoting this increase in intestinal permeability (3). Tumour necrosis factor-alpha (TNF- α), a traditional therapeutic target for IBD, has been attributed to causing the dysfunction of the intestinal barrier by altering the expression of tight junction proteins (63). Further evidence of its role in driving disease comes from a study of Crohn's patients, whereby treatment with an anti-TNF- α antibody appears to normalise intestinal permeability (64). However, the safety and effectiveness of such therapies has been shown to differ between younger and older IBD patients (65, 66). One study found that anti-TNF α therapy in IBD patients over 60 years old was associated with an increased risk of developing serious infections compared to those not on anti-TNF α therapy (67), therefore this treatment is not a safe option.

A further mechanism for this increase in intestinal permeability is a dysregulation of the protease/anti-protease balance in the gut, contributing to epithelial damage and increased permeability (68). Proteases can be produced by both the IECs (69) and certain species of bacteria within the microbiome (70). Proteases are enzymes that catalyse proteolysis, by breaking the peptide bonds of proteins, and are categorised into seven groups based on the catalytic residue (71). The largest group of proteolytic enzymes present in the human and mouse genome are the matrix metalloproteases (MMPs), which have been implicated in several cancers due to their ability to break down physical barriers by cleavage of tight junction proteins (72). In physiological conditions, MMPs are produced at very low levels by IECs generally in the non-pathogenic form and are involved in the normal tissue turnover (73). However, the expression of MMPs significantly increases in inflammatory disorders such as IBD, where MMPs are suggested to play a role in degrading the intestinal barrier (69, 73). Serine proteases, a group of proteases characterised by the presence of serine in its catalytic site, are also shown to be upregulated in IBD patients (74, 75) and thought to contribute to disease pathology by loss of the tight junction protein occludin and myosin light chain phosphorylation (76).

Disruption of the inner mucus layer is thought to result in colitis as the resulting penetration of the intestinal barrier by commensal bacteria resident in the gut leads to inflammation (77). This was demonstrated in a dextran sodium sulfate (DSS) murine model of colitis, shown by analysing bacterial localisation using immunofluorescence, with bacteria shown to translocate from the gut lumen into the usually sterile gut tissue (77). DSS is widely used as it induces the intestinal barrier dysfunction and inflammation seen in the human colitis (78). These observations in a colitis mouse model have also been seen in ulcerative colitis patients where bacteria are shown to be present in the epithelium instead of being localised to the gut lumen (79). This crossing over results in bacteria being present in a usually sterile environment, therefore triggering an immune response, including the production of inflammatory cytokines such as tumour necrosis factor-alpha (TNF- α) resulting in an overall increase in intestinal inflammation (77). The mechanism behind this is mediated by myosin light chain kinase-mediated phosphorylation of myosin light chains which promotes tight junction disruption (80). Inhibition of this ability to phosphorylate myosin light chain restored intestinal barrier function, highlighting the important role of tight junctions for maintaining barrier function (80).

The increase in penetration of the intestinal barrier by bacteria forms the basis of the 'leaky-gut' hypothesis, which provides an explanation for the increase in systemic inflammation seen in IBD and CRC (81). A clinical study reveal elevated gut permeability, circulating bacterial DNA in the blood, and pro-inflammatory markers in affected patients (82). Animal models with genetic mutations affecting gut barrier proteins exhibit similar permeability and inflammation, while dysbiosis—characterized by reduced beneficial bacteria and increased pathobionts (a microorganism normally part of a host's microbiome but can become harmful under certain conditions)—further weakens the intestinal barrier (83). These findings highlight the central role of gut barrier dysfunction in systemic inflammatory conditions.

1.3 Changing epidemiology

Currently, the highest incidence of CRC is within high-income regions such as Europe and Northern America. However, the incidence is rapidly starting to increase in low- and middle-income regions, primarily found in Africa and Asia (84). The incidence of CRC in low- and middle-income regions overall is estimated to increase rapidly by 71.3% by 2040, in comparison to an increase of 33.8% in the United Kingdom (84). There are several reasons for this predicted trend, which will now be discussed in more detail.

1.4 Risk factors for colorectal cancer development

1.4.1 High omega-6 diet

The dietary ratio of omega-6 (ω -6) to omega 3 (ω -3) polyunsaturated fatty acids (PUFAs) has emerged as one of the key risk factors for developing CRC, with several studies proving its significance (85-89). The average ω -6: ω -3 ratio in the western diet is estimated to be 20:1-50:1, whereas in Asia it is estimated to be 4:1 (90). This coincides with the low incidence of CRC diagnoses in Asia, where a high consumption of sources of ω -3 such as fish oil and flax seeds are common (90). The ω -6 PUFA found in the diet is linoleic acid (LA), which is commonly found in sunflower and corn oils and are prominent features of the western diet (90). The metabolism of ω -6 and ω -3 PUFAs is shown in **Figure 8**, where production of oxylipins is linked to activation of pro/anti-inflammatory responses, e.g. production of cytokines (91). Whether these oxylipins result in a pro- or anti-inflammatory response is context dependent, for example prostaglandin E₂ (PGE₂) produced at sites of tissue injury can promote an anti-inflammatory neutrophil response (92), but also a pro-inflammatory response by inducing TNF- α production (93).

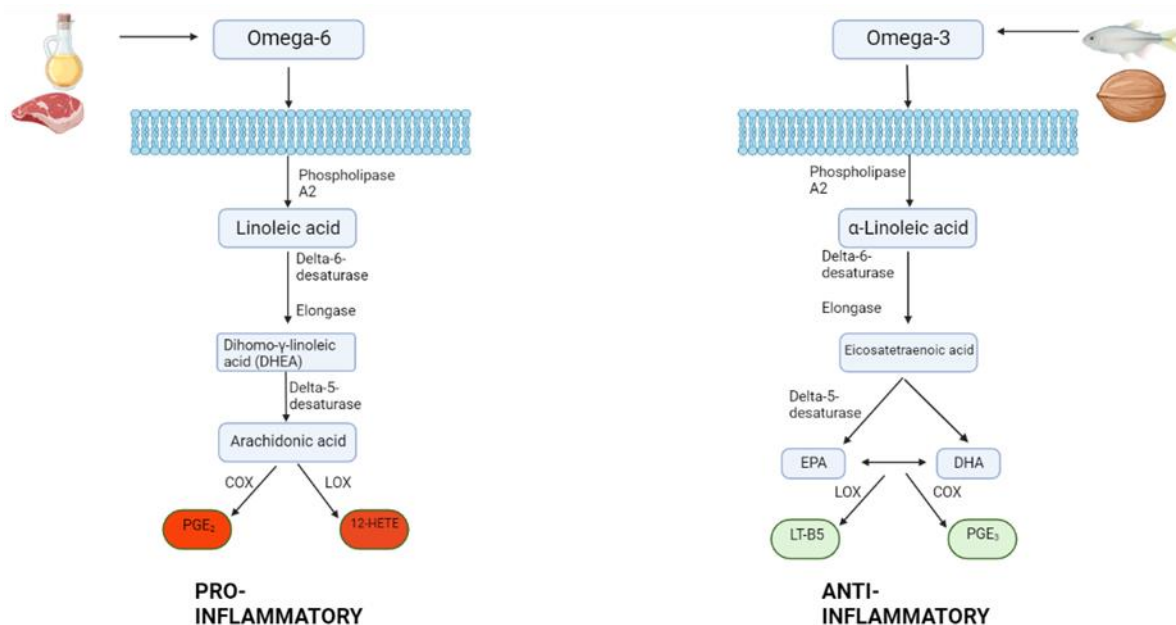


Figure 8. A schematic diagram showing the stages of both ω -6 and ω -3 PUFA metabolism. Sources of ω -6 include sunflower oil and red meat, whereas ω -3 is found in fish oils and walnuts. Once ingested, both ω -6 and ω -3 are stored in the phospholipid bilayer where they are released by phospholipase A₂ enzymes. Once released, ω -6 forms arachidonic acid. Arachidonic acid is metabolized via lipoxygenase (LOX) and cyclooxygenase (COX) enzymes to form pro-inflammatory oxylipins such as prostaglandin E₂ (PGE₂) and 12-hydroxyeicosatetraenoic acid (12-HETE). Once ω -3 is released from the phospholipid bilayer it forms α -linoleic acid. This is converted to eicosatetraenoic acid and then to eicosapentaenoic acid (EPA) and docosahexaenoic acid (DHA). EPA and DHA are metabolized by COX and LOX to form anti-inflammatory oxylipins such as leukotriene B5 (LTB5) and prostaglandin E₃ (PGE₃). Image made using Biorender.

Diets rich in the ω -6 PUFA LA, which is converted into arachidonic acid (AA) *in vivo*, are associated with increased IBD and CRC in humans and mouse models of disease (94-98). Murine studies have demonstrated a role for AA-derived oxylipins generated by cyclooxygenase (COX), such as PGE₂ in CAC using pharmacological tools such as aspirin, which also significantly reduces the risk of CRC incidence and improves disease-associated survival in humans (99, 100).

1.4.1.1 Prostaglandin E₂

PGE₂ is derived from AA downstream of the ω -6 PUFA LA, whereby the substrate prostaglandin H₂ (PGH₂) is converted to PGE₂ by prostaglandin E synthase (PGES) (Figure 9) (91). PGE₂ is able to exert its effects throughout the body through binding prostaglandin E2 (EP) receptors EP1, EP2, EP3, and EP4 (101). These receptors are differentially expressed throughout the body, EP2 and EP4 are predominantly found in the colon, whilst EP1 and EP3 are found largely in the kidney (101).

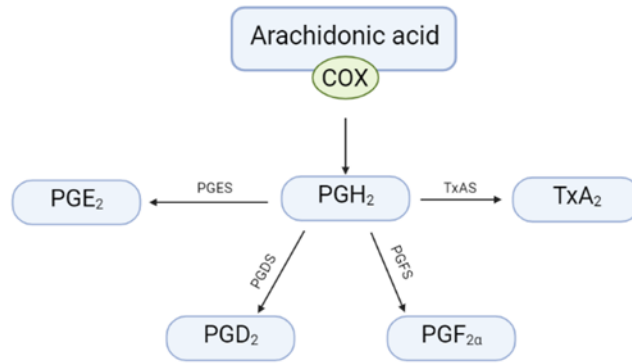


Figure 9. A schematic diagram showing the prostaglandin synthesis pathway. Arachidonic acid is metabolized by cyclooxygenase (COX) to produce PGH₂ which acts as the substrate for the prostaglandin synthase and thromboxane A synthase (TxAS) enzymes. PGH₂ is metabolized by prostaglandin E synthase (PGES), prostaglandin D synthase (PGDS), prostaglandin F synthase (PGFS) and TxAS to form PGE₂, PGD₂, PGF_{2α}, and TxA₂ respectively. Image made using Biorender.

In the context of CRC, the role of PGE₂ has been well characterised and is shown to play a significant role in promoting tumorigenesis by increasing tumour growth and invasion, whilst reducing apoptosis (102, 103). Levels of PGE₂ have been shown to be elevated in the colon tissue of patients with CRC (104). Recently, the role of the EP4 receptor has been highlighted in the context of CRC, with the use of an EP4 antagonist significantly reducing liver metastasis from the colon following intrasplenic injection of MC26 colon cancer cells (105, 106). Furthermore, global deletion of the EP4 receptor inhibited colorectal tumorigenesis *in vivo* (107).

Binding of PGE₂ to EP1, EP2, and EP4 receptors has been linked with increasing intestinal cell permeability (**Figure 10**), which as previously discussed is one of the key initiating events in CRC (108, 109). PGE₂-EP1/EP2/EP4 signalling results in the activation of G_αs proteins, leading to elevated cyclic adenosine monophosphate (cAMP) levels and activation of protein kinase A (PKA) (110). PKA phosphorylates tight junction proteins such as occludin and claudins, weakening their integrity and reducing cell-cell adhesion (111). Additionally, PGE₂ signaling can activate small guanine triphosphatase (GTPases) like Ras homolog family member A (RhoA) and Ras-related C3 botulinum toxin substrate 1 (Rac1), disrupting actin cytoskeleton dynamics and further destabilizing tight junctions (112).

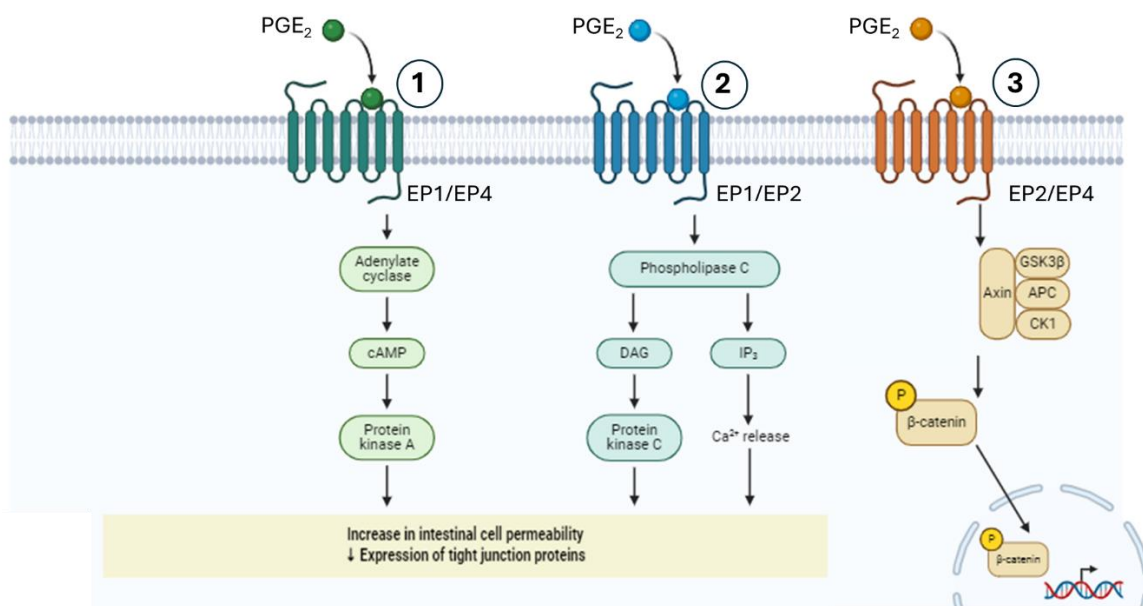


Figure 10. Summary of the mechanisms by which PGE₂ signalling has been implicated in increasing intestinal cell permeability. 1. Binding to EP1/EP4 activates protein kinase A leading to decrease in expression of tight junction proteins. 2. Binding to EP1/EP2 activates phospholipase C, which causes increase in calcium release. 3. Binding to EP2/EP4 phosphorylates β-catenin at Ser⁵⁵² enabling it to translocate to the nucleus which can lead to a decrease in tight junction expression. Image made using Biorender.

As the downstream effects of PGE₂ signalling have been suggested to promote CRC progression by increasing tumour growth and invasion, this pathway has become a very attractive therapeutic target for the treatment of malignancies (113). One such therapeutic to target prostaglandin biosynthesis is acetylsalicylic acid, also known as aspirin, which targets both COX-1 and COX-2 (114). By inhibiting these key enzymes in prostaglandin synthesis, the production of pro-inflammatory prostaglandins such as PGE₂ is significantly reduced in the urine of CRC patients (114, 115). Data from observational studies and clinical trials both strongly support the use of low-dose aspirin in CRC, with one study showing a 69% reduction in the development of metastases by patients who developed cancer whilst taking aspirin (116-118). Meta-analyses and other systematic reviews of large observational cohort studies have estimated that aspirin reduces risk for colorectal neoplasia by approximately 20–30% (119). Estimates from adenoma prevention trials typically enrolling higher-risk individuals with a personal history of colorectal adenoma have demonstrated that risk for recurrent neoplasia is reduced by 13–18% (120-123). Despite aspirin showing efficacy in the treatment of CRC, it is not recommended for long-term use due to a high risk of developing severe side effects, such as gastrointestinal and intracranial bleeding (124, 125).

1.5 Soil-transmitted Helminths

Soil-transmitted helminths (STHs) refer to the intestinal worms that are transmitted through soil contaminated with infective larvae or embryonated eggs (126). STHs are classed as a neglected tropical disease (NTD), a group of about 20 communicable conditions that disproportionately affect the poorest and most vulnerable communities (127). There are three main STH infections, which are hookworm (*Ancylostoma duodenale* and *Necator americanus*), *Ascaris lumbricoides*, and whipworm (*Trichuris trichiura*), and together they account for a major burden of parasitic disease worldwide (128). STHs have also been shown to have a detrimental impact on livestock, increasing mortality, reducing growth rate, inducing weight loss, and causing economic losses (129). It is estimated that 1.45 billion people worldwide are affected by STH infection, with particularly high prevalence in regions such as Africa (**Figure 11**) (129, 130). The morbidity of STH infection can be estimated using the disability-adjusted life (DALY) indicator, which is expressed as the number of years lost due to ill-health, disability or early death (131). STH infections have been attributed to approximately 20 million DALYs worldwide (130). This is significantly lower than other infectious diseases, with HIV/AIDS accounting for approximately 42 million DALYs (132), and malaria 49 million DALYs (133). Patients with a low STH infection burden tend to be asymptomatic and so potentially may not know they have an infection (126). Those with a higher worm burden will however experience a variety of health problems, which could include abdominal pain, diarrhoea, and rectal prolapse (126).

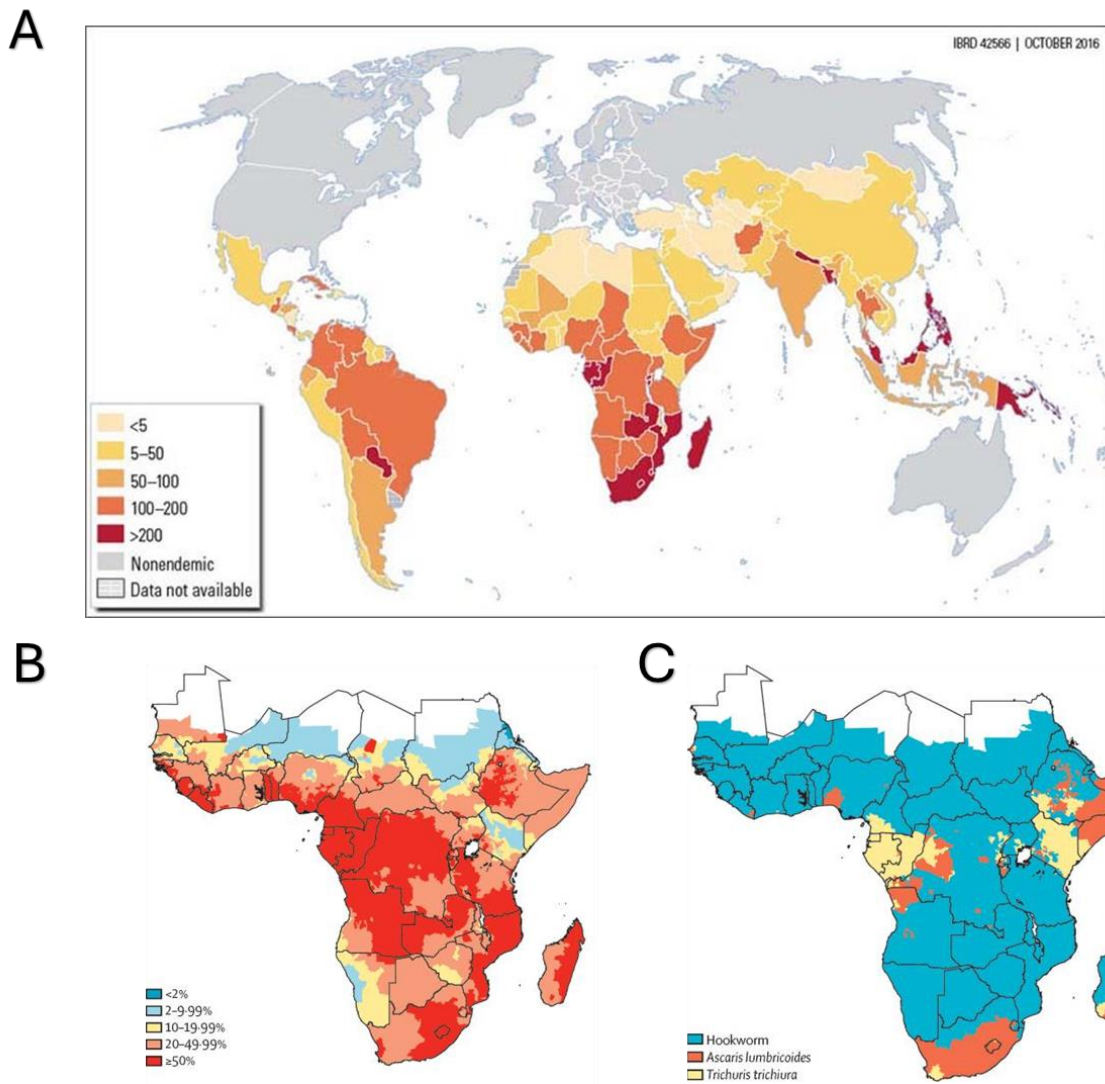


Figure 11. Global prevalence of soil-transmitted helminth infections. (A) Figure showing the global distribution of soil-transmitted helminth (STH) infection in 2016 per 100,000 population. (B) Map of Africa highlighting the prevalence of any STH infection with predominant STH species being highlighted in (C). Figures from Daley *et al* 2016 and Sartorius *et al* 2021.

Infection with *Ascaris* or whipworm occurs when the eggs are ingested, invade the intestinal mucosa, and are carried via the portal, then systemic circulation to the lungs (128). The larvae mature further in the lungs (10 to 14 days), penetrate the alveolar walls, ascend the bronchial tree to the throat, and are swallowed (134). Upon reaching the small intestine, they develop into adult worms (134). Hookworm eggs hatch in the soil, releasing larvae which mature into a form which can penetrate human skin (128). On contact with the human host, typically bare feet, the larvae penetrate the skin and are carried through the blood vessels to the heart and then to the lungs (135). They penetrate into the pulmonary alveoli, ascend the bronchial tree to the pharynx, and are swallowed (135). The larvae reach the jejunum of the small intestine, where they reside and mature into adults (135). Adult worms live in the lumen of the small intestine, typically the distal jejunum, where they attach to the intestinal wall with resultant blood loss by the host (135).

Current diagnosis of STH infection involves a labour-intensive method of identifying eggs in a stool specimen using a microscope (136). The use of this conventional technique is potentially going to be replaced with molecular techniques such as qPCR and ELISA, as this is estimated to have a higher sensitivity to a lower worm burden, can easily distinguish between species, and can detect if an individual has had previous exposure to infection (137). In terms of treatment, there are a variety of broad-spectrum anthelmintics such as albendazole and mebendazole which are used to treat parasitic infections (138). Albendazole typically has higher efficacy, curing 95–100% of *Ascaris lumbricoides* infections, 70–95% of hookworm, and 28–54% of *Trichuris trichiura* (139). Mebendazole also achieves high cure rates for *A. lumbricoides* (90–95%) but is less effective against hookworm and *T. trichiura* (139). This class of drug has been known to block the microtubule systems of developing larva and adult helminths, thus leading to a cease in the cell cycle ultimately causing cell death (138). Recently, cases of drug resistance to both albendazole and mebendazole have been reported in hookworm infections which is predicted to become a significant global issue (140). There is currently no vaccine available against human STH infection (140), but a vaccine for *Necator americanus* is currently in development with early studies showing the vaccine is safe and well-tolerated (141).

1.5.1 *Heligmosomoides polygyrus bakeri*

The rodent intestinal nematode *Heligmosomoides polygyrus bakeri* has been extensively used to model human STH infection **Figure 12** (142). *H. polygyrus* is a roundworm, causing chronic long-lasting infections, whilst replicating the human immune response to infection (142). The chronicity of *H. polygyrus* infections in rodents has been shown to be strain dependent (143). This was demonstrated by Filbey *et al* who compared adult worm burden and egg production in SJL, BALB/c, C57BL/6, and CBA mice (143). Filbey *et al* showed that C57BL/6 and CBA mice had a significantly higher adult worm burden and egg count at day 28 post-infection in comparison to SJL and BALB/c mice (143). Using *H. polygyrus* as a model for intestinal infection offers researchers an incredible insight into the parasite-host relationship.

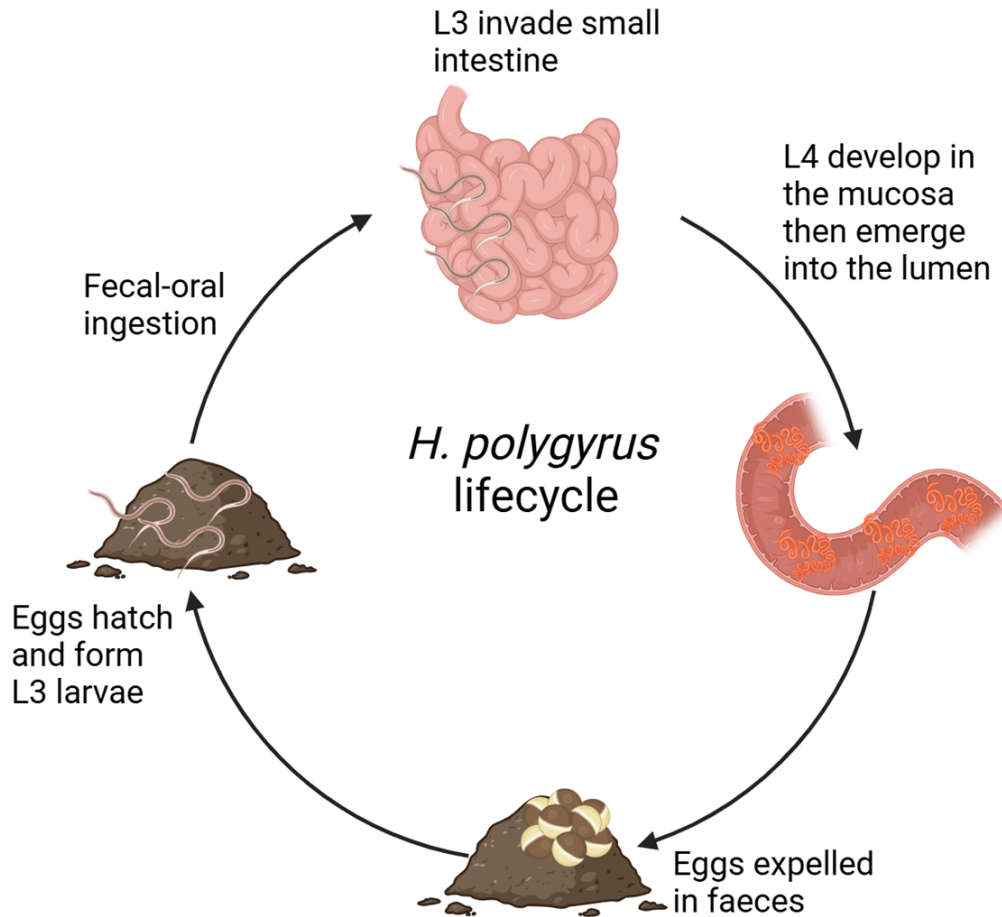


Figure 12. The lifecycle of *Heligmosomoides polygyrus bakeri*. The L3 larvae of *H. polygyrus* reside in the soil of warm and humid climate countries, where they are ingested via the fecal-oral route. The L3 larvae then invade the intestinal barrier of the small intestine which is where they reside. At day 8, the L4 adults have developed from the L3 larvae in the mucosa and emerge in the lumen of the small intestine. At day 10, the L4 adults begin to mate and produce eggs which are excreted via the faeces back into the soil. The eggs in the faeces then hatch and form L3 larvae. Image made using Biorender.

Despite residing in the small intestine, *H. polygyrus* can have both local and systemic consequences on the inflammatory response to infection (144). This is thought to be due to a number of mechanisms, including the release of excretory/secretory products (HES) during chronic parasitic infection, modulation of host immune responses to evade detection, suppression of inflammatory pathways to reduce immune-mediated damage, alteration of cytokine production to favour a regulatory immune environment, and interference with antigen presentation by host immune cells, thereby diminishing the host's ability to mount an effective defence (144).

1.5.2 *Heligmosomoides polygyrus bakeri* excretory/secretory products

HES is a complex mixture of proteins, lipids, carbohydrates, exosomes, extracellular vesicles, and mRNAs (145) which has been characterised by proteomic analysis as containing 446 different proteins (145). Several secreted enzyme families have been identified in the HES, with predominant examples including proteases, lysozymes, apyrases, and acetylcholinesterase (145). Along with different enzyme families, many HES proteins have also been identified, with the most abundant being members of the venom allergen-like (VAL) family (145). The VAL family of proteins are the major immunogens, which lead to an immune response in the host and an increase in antibody production (145). Immune-regulatory proteins have also been discovered in HES, such as a transforming growth factor-beta (TGF- β) mimic promoting the expansion of T regulatory (Treg) cells (146), and the *H. polygyrus* Binds Alarmin Receptor and Inhibits (HpBARI) protein which inhibits the alarmin cytokine interleukin-33 (IL-33) binding to its receptor and activating mast cell degranulation (147).

1.6 Link Between Soil-transmitted Helminth Infection and Colorectal Cancer

It is currently estimated that infectious diseases are estimated to contribute to 33% of cancer diagnoses and up to 20% of cancer-related mortality (148). There is growing evidence in both murine and human epidemiological studies that STH are an emerging risk factor for increased CRC (149-152). However, the role for STH in CRC and colitis is controversial, as a range of helminths—in particular those involving the gastrointestinal tract—have been found to alleviate inflammation in rodent models (153-156), and there is epidemiological evidence that helminth-infected children are less prone to develop IBD (157). The therapeutic application of helminths during colitis has been suggested, however due to the tumour promoting effects discussed in detail in this section, these risks should be taken into account.

Recent evidence from Pastille *et al* utilised *H. polygyrus* infection and the AOM/DSS model of CAC to investigate a link between helminth infection and tumour development (151). The AOM/DSS model consists of azoxymethane (AOM) and dextran sodium sulfate (DSS) (158). The first component, AOM, is a procarcinogen which is metabolised by cytochrome P450 2E1 (CYP2E1) into methylazoxymethanol (MAM). MAM is a highly reactive alkylating species which induces O⁶ methylguanine adducts in DNA, causing a guanine to alanine transition (159). After AOM is excreted into the bile, it is taken up by colonic epithelium where it induces DNA damage (159). The second component of the model, DSS, is dissolved in the drinking water and acts as a direct chemical toxin to the colonic epithelium resulting in epithelial cell injury and a loss of intestinal barrier integrity (160). Interestingly, *H. polygyrus* infection

had no impact on carcinogenesis when given at week 8 of the AOM/DSS model when disease is established, whereas when mice were infected one day after AOM injection there was a significant increase in tumour burden (151). Infection exacerbated DSS colitis with an increase in interleukin-6 (IL-6), a prognostic biomarker for IBD (161), being observed. Pastille *et al* then neutralised IL-6 *in vivo* resulting in a reduction in *H. polygyrus* exacerbation of CAC (151).

Hayes *et al* showed that infection with the murine gut-dwelling nematode *Trichuris muris* led to changes in the caecum of the mouse that were comparable to those seen with mice administered AOM (150). In addition to this, *T. muris* infection was also able to increase the development of adenomas in the small intestine of APC^{min/+} mice that spontaneously develop tumours (150). This change was abrogated if a Treg cell type was blocked during infection (150), suggesting that although the Treg cell type that arises during infection has been shown to play an important role in protecting the host from damage caused by the parasite (146), they may have a negative impact in the context of cancer development.

1.6.1 Helminth regulation of tight-junction markers and intestinal permeability

Most research has focussed on the impact of helminth infection on local epithelial permeability in the small intestine, as this is where helminths live. The results of these studies show a clear trend toward helminth infection causing an increase in local epithelial permeability, in the regions where the helminth parasite inhabits. For example, infection with *Trichinella spiralis* was shown to result in a decrease in the expression of occludin in the tight junction, leading to an increase in epithelial permeability of the jejunum (162). Infection with *Nippostrongylus brasiliensis* resulted in a decreased expression of E-cadherin and a subsequent loss of adhesion in the epithelial cells of the small intestine (163). An infection with *H. polygyrus* was also shown to increase the mucosal permeability of the small intestine (164).

The effect of helminth infection on systemic intestinal permeability in the colon has also been shown. Research by Su *et al* were able to demonstrate that infection with *H. polygyrus* caused a significant increase in colonic epithelial permeability, increasing susceptibility to *Citrobacter rodentium* infection and the severity of *C. rodentium*-induced colitis (165). Histological analysis of the colon tissue after *H. polygyrus* infection revealed severe structural abnormalities, including alterations in the apical junction and distortion of the paracellular space (165). These results indicate that *H. polygyrus* infection can compromise the integrity of the colonic epithelium at a location distinct from where the parasite typically resides in the small intestine (165). Western blot and immunofluorescence analysis also revealed that *H. polygyrus* causes a reduction in E-cadherin expression and distribution in the colonic epithelium, whilst causing no effect in expression or distribution of ZO-1 (165). The distribution of E-cadherin in uninfected mice was located on the cell membrane, whereas in infected mice the

distribution had changed to the cytoplasm (165). These findings suggest the molecular mechanism by which helminth infection can increase intestinal permeability, as altering the amount and distribution of E-cadherin inevitably will contribute to the opening of tight junctions and subsequent increase in epithelial permeability. Su *et al* then repeated the same experiments in immune-deficient mice to determine if there is a required role for the immune system (165). In contrast to the immunocompetent BALB/c mice, *H. polygyrus* infection appeared to have no impact on E-cadherin expression or distribution, suggesting a role for adaptive immune activation in the increase of intestinal epithelial barrier permeability (165). Reconstitution of the *H. polygyrus*-infected SCID mice with T and B lymphocytes derived from the spleen of BALB/c mice resulted in the same effects on E-cadherin and intestinal permeability as previously seen in *H. polygyrus*-infected BALB/c mice (165). These findings highlight the importance of the type-2 adaptive immune response to helminth infection in causing the increase in intestinal barrier permeability. This finding is supported by *in vitro* research on CRC cell lines and keratinocytes, which show that type-2 cytokines IL-4 and IL-13 downregulate the expression of E-cadherin (166, 167).

A role for helminth excretory/secretory products (ESPs) has also been suggested in their ability to increase cell permeability. Both the ability of the ESPs of *T. muris* and *T. spiralis* to increase cell permeability was demonstrated to be dependent on the activity of a serine protease, as shown by experiments involving heat inactivation and the addition of protease inhibitors (168, 169). Furthermore, Hiemstra *et al* demonstrated how the ESPs of *Trichuris suis* reduce the barrier function and expression of the tight junction protein claudin-4 in a colon cancer cell monolayer *in vitro* in a glycan-dependent manner (170).

The importance of the adaptive immune response to helminths in contributing to a decrease in epithelial integrity has also been shown in an acute infection with the intestinal parasite *T. muris* (171). Like other intestinal parasites, infection with *T. muris* was shown to cause an increase in the activation of epithelial mast cells (172). These mast cells have been shown to have a role in regulating epithelial barrier function, with mast cell-derived proteases shown to regulate epithelial permeability (173). The most notable mast cell-derived protease is MCPT-1, which is a characteristic of mucosal mast cells (172). In this study by Sorobetea *et al* levels of MCPT-1 were measured in both infected and non-infected mice in the small and large intestine (171). Levels of MCPT-1 were shown to increase significantly during infection when compared to naïve mice (171). Increased intestinal permeability also correlated with increased serum levels of MCPT-1, with depletion of mast cells reversing this effect (171).

1.6.2 Helminth regulation of cancer stem-cell function

The intestinal epithelium undergoes drastic remodelling during the “weep and sweep” response against parasitic infection, driven by the type-2 immune response and its signature cytokines IL-4 and IL-13 (174). There is an expansion of goblet, Paneth, and tuft cells which are detrimental to the survival of the helminth parasite (16, 175, 176).

Nusse *et al* revealed how *H. polygyrus* is able to alter the stem cell population in the crypts overlying larvae-associated granulomas, with a loss in Lgr5⁺ cells and an increase in Sca1⁺ cells (177). These granulomas also exhibited loss of the Paneth cell marker MMP7 and the goblet cell marker MUC2, with expansion of both these cell types being previously recognised in helminth infections (175). Interestingly, non-granuloma-associated crypts retained expression of Lgr5 (177). Thus, the epithelium overlying granulomas exhibits loss of ISC markers and disruption of the ISC niche (178), creating a favourable environment for helminth survival.

Drurey *et al* investigated the impact on stem cell differentiation of the helminth secretions (HES) using small intestinal organoids (179). The addition of HES was found to skew stem cell differentiation induced by the type-2 cytokines IL-4 and IL-14 away from goblet cells, tuft cells, Paneth cells, and enteroendocrine cells (**Figure 13**) (179). HES resulted in the downregulation of several tuft cell necessary genes upregulated during the type-2 immune response, such as *Dclk1* and *Trpm5* (179). HES also suppressed the induction of MUC2, which is a key goblet cell product and may be crucial for maintaining the integrity of the mucosal layer (7, 179). Drurey *et al* then investigated whether these findings of inhibition of tuft cell expansion occur *in vivo* (179). To do this, they performed a co-infection with *H. polygyrus* and another GI nematode *N. brasilienses* (179). Expression of the tuft cell markers *Dclk1* and *Trpm5* were significantly increased in *N. brasilienses*-alone infected mice but were then significantly decreased in *H. polygyrus* and *H. polygyrus* /*N. brasilienses* co-infected mice (179). These same effects were also observed for levels of the MUC2 gene and numbers of goblet cells (179). From this data, it was suggested that *H. polygyrus* and not *N. brasilienses* can alter the differentiation of secretory-lineage cell types to favour its survival (179). To investigate this, Drurey *et al* analysed the expression of key developmental genes in the intestinal epithelium (179). Most notably, HES caused a significant decrease in the expression of *Atoh1*, which is also induced with the addition of IL-4 and IL-13 (179). *Atoh1* is known to play a key role in the differentiation of intestinal epithelium towards the secretory lineage, which include goblet, Paneth, and tuft cells (180). Genes downstream of *Atoh1*, for example *Neurog3*, were also suppressed with the addition of HES (179). *Neurog3* is also a key player in the secretory cell lineage, as it specifies differentiation to enteroendocrine cells (181). Another transcription factor *Hes1* is known to repress *Atoh1* and shift the cell lineage towards an absorptive

cell and away from secretory cells (182). Although levels of *Hes1* were not affected by IL-4/IL-13, the addition of HES caused a significant increase in expression levels of this transcription factor (179).

Furthermore, Drurey *et al* acknowledge that the small intestinal organoids with the addition of HES showed an altered morphology which resembled organoids produced from stem cells collect from *H. polygyrus* infected mice (177). Here, it is proposed that these stem cells have switched from being *Lgr5*⁺ stem cells to *Sca1*⁺ stem cells, which corroborates findings *in vivo* from Nusse *et al* and Karo-Atar *et al* (177, 183). While this may initially protect the epithelium under stress, it can impair long-term homeostasis and create conditions that favour chronic inflammation, epithelial dysfunction, and increased risk of colon cancer development (184-186). The induction of *Sca1*⁺ stem cells has been linked to the injury response in the intestinal crypt and have been shown to have a more spheroidal morphology (177, 187). This spheroid morphology has been linked to a pro-proliferative tissue repair processes which could be essential to recover from epithelial destruction caused by the helminth infection itself (177).

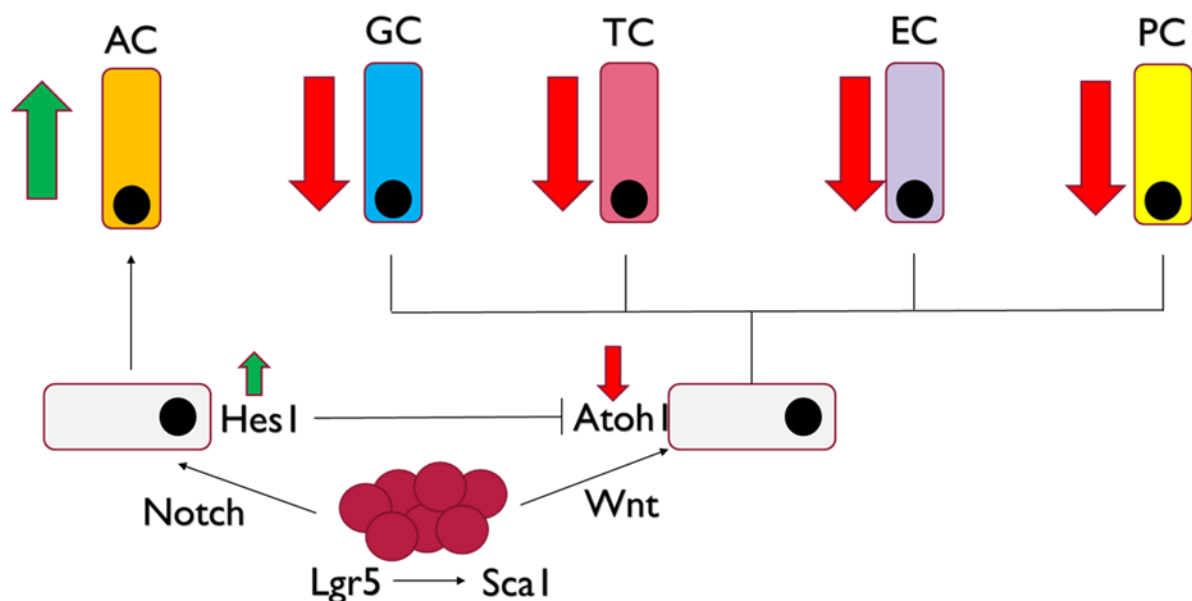


Figure 13. Figure showing the effect of HES on small intestinal organoids. The addition of HES causes a skew towards Notch signaling and an increase in expression of *Hes1*. This increase in *Hes1* expression inhibits *Atoh1* expression, a ligand of Wnt signaling. *Hes1* causes the differentiation of intestinal stem cells to absorptive cells (AC). The decrease in expression of *Atoh1* leads to a decrease in differentiation of secretory cells, which include goblet cells (GC), tuft cells (TC), enteroendocrine cells (EC). And Paneth cells (PC). The addition of HES also causes a switch in the intestinal stem cell marker *Lgr5* to *Sca1*, which is indicative of a more proliferative phenotype. Figure based on results from Drurey *et al*.

1.6.3 Helminth regulation of omega-6 polyunsaturated fatty acid metabolism

As previously discussed, a diet high in ω -6 has been associated as a risk factor for developing CRC, with its metabolism leading to the production of pro-inflammatory metabolites such as PGE₂ and 12-hydroxyeicosatetraenoic acid (12-HETE) (91). Recent evidence has shown that infection with *N. brasiliensis* or addition of HES was shown to cause alterations in oxylipin production (188, 189). Henkel *et al* compared the eicosanoid profiles in the airways of mice that had either been exposed to house dust mite or *N. brasiliensis* infection (188). Comparison of the infected and non-infected eicosanoid profiles revealed a significant increase in the levels of oxylipins derived from ω -6, such as PGE₂, thromboxane B₂ (TxB₂), and prostaglandin F_{2 α} (PGF_{2 α}) in the airways (188). de los Reyes *et al* showed that addition of *H. polygyrus* larvae extract to murine or human monocytes resulted in increased production of PGE₂ and TxB₂ and decreased production of 5-HETE and LTB₄ (189). These changes in oxylipin production correlated with altered transcriptional changes in the metabolic enzymes responsible for their production, including increased expression of *PTGS2* and microsomal prostaglandin E synthase 1 (mPGES-1) and decreased expression of 5 lipoxygenase (5-LOX) and leukotriene c₄s (Ltc₄s) (189).

The changes described by the studies discussed point towards an anti-inflammatory eicosanoid switch in the context of airway allergy (189). However, in the context of carcinogenesis, these alterations in PUFA metabolism could be causing more harm than good. Findings from Smith *et al* show that helminth infection can exacerbate tumour burden and weight loss in mice fed a “western diet” with a high omega-6:omega 3 ratio (**Figure 14A&B**). Evidence from the colon showed that both the “western diet” or helminth infection increased the production of AA-derived oxylipins (**Figure 14C**) (190). This study indicated a potential link between helminth alterations in PUFA metabolism and exacerbation of CAC.

There are various studies showing that parasitic helminths can produce their own prostaglandins to have an effect on the host (191). Examples of this include *Schistosoma mansoni*, *Onchocerca volvulus*, and *Trichuris suis* (192-194). *S. mansoni* has been shown to produce PGD₂ that mediates pro-inflammatory effects in the host, including activation of eosinophils, as well as immunomodulatory PGE₂ that can induce production of IL-10 that promotes migration and survival of the parasite (192, 195, 196). In addition, other helminth parasites such as *B. malayi*, have also been shown to produce PGE₂, PGD₂, and TxB₂ (197, 198). These lipids have been shown to play an immunomodulatory role in the host, preventing platelet aggregation around the parasites as they grow in blood vessels (197, 198). Furthermore, *T. suis* produces PGE₂ that can directly suppress the production of cytokines from activated dendritic cells (194).

Parasite products have also been shown to regulate PUFA metabolic enzyme expression, or contain secreted metabolic enzymes that can promote prostaglandin production. Secretory phospholipase A₂ (sPLA₂), a subfamily of PLA₂ enzymes, has been identified within the secretions of helminths like *Steinernema carpocapsae* and *Clonorchis sinensis* (199-201). The release of sPLA₂ is considered an immunomodulatory strategy utilized by helminths, where the resulting prostaglandins produced play a role in regulating the host immune response to pathogens (199, 202). Prodjinotho *et al* show that glutamate dehydrogenase from viable cysts of *Taenia solium* instructs tolerogenic monocytes to release IL-10 and the lipid mediator PGE₂ (203). These act in concert, converting naive CD4⁺ T cells into Tregs, through the EP2 and EP4 and the IL-10 receptors, unearthing an immune evasion mechanism of these cysts (203).

Although these are all possible mechanisms for how helminths exacerbate CAC, there are still many unanswered questions remaining. Throughout this thesis, I will aim to define a mechanism for how helminths exacerbate CAC by using similar techniques as described in this section, as well as taking a more in-depth transcriptomics approach.

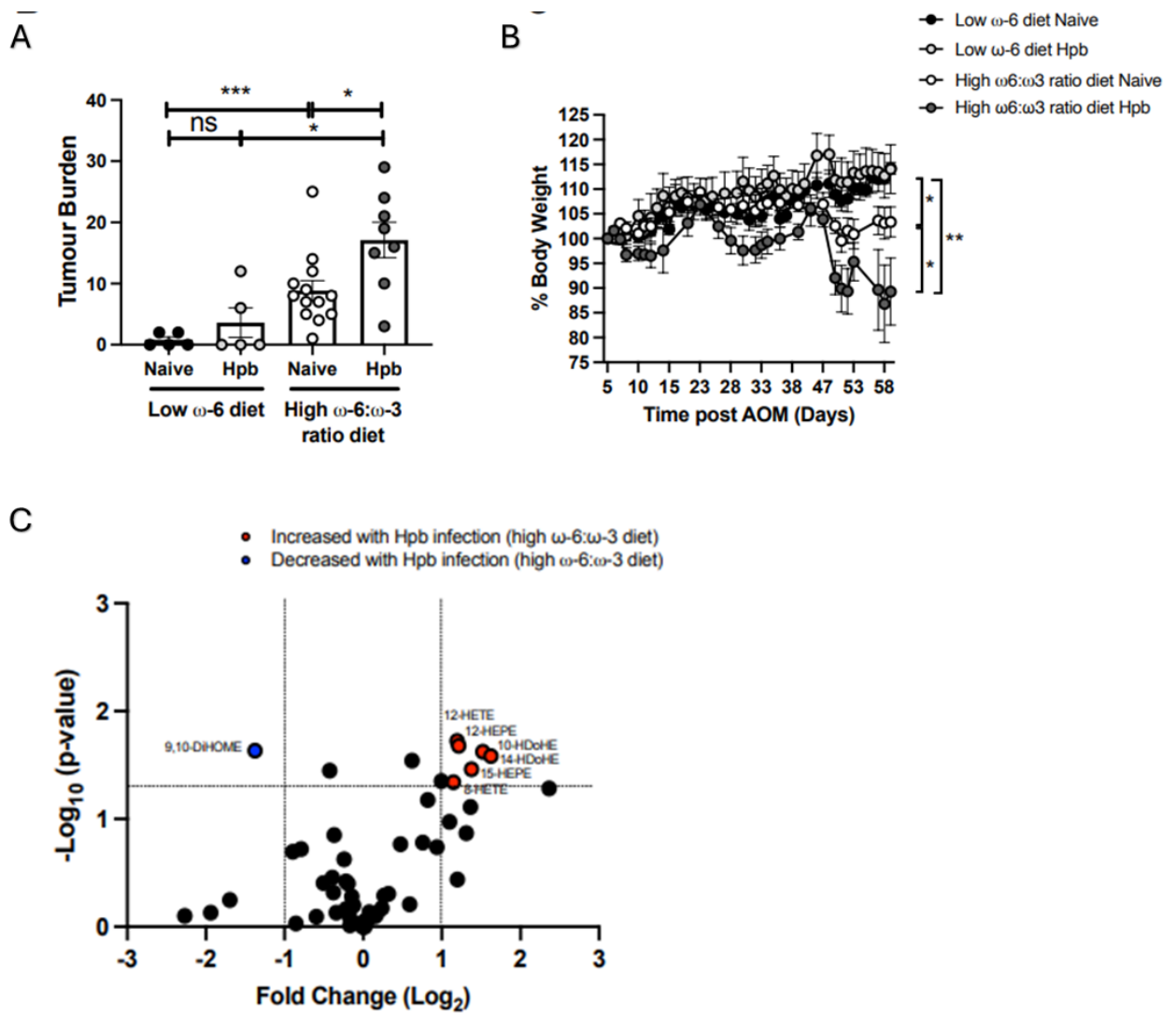


Figure 14. Effect of *H. polygyrus* on PUFA metabolite production in the colon and tumour development. The effect of *H. polygyrus* infection can also be seen on **(A)** tumour burden and **(B)** weight loss. **(C)** Volcano plot showing the metabolites which are increased and decreased with *H. polygyrus* infection. Figures taken from Smith *et al.* 2025

1.7 Project Aims and Hypothesis

The overall aim of this thesis was to determine a mechanism by which *H. polygyrus* exacerbates CAC, with the following objectives:

1. Establish a role for prostaglandin signalling in *H. polygyrus* exacerbation of CAC
2. Establish a role for secreted helminth products in increasing clinical signs associated with CAC
3. Utilise an *In silico* approach to target secreted factor believed to exacerbate CAC
4. Take an unbiased transcriptomic approach to see what other pathways are altered in the colon

Hypothesis:

1. Based on section 1.6.3 we hypothesis that helminths exacerbate CAC through prostaglandin signalling
2. Based on section 1.6.1 we hypothesis that helminth secretions mediate this effect on prostaglandin signalling *in vitro*
3. That an *in silico* drug design can be effectively used to design a specific inhibitor of this secreted factor
4. That an unbiased transcriptomic approach will reveal potential other pathways that may be contributing to helminth exacerbation of CAC

Chapter 2: Materials and Methods

2.1 Cell Culture

2.1.1 Established cell line

The CMT-93 cell line used throughout this thesis were kindly provided by Dr. Cedric Berger (School of Biosciences, Cardiff University) and tested negative for Mycoplasma contamination (**Figure 1**). This cell line is derived from *Mus musculus*, and is from a large intestinal polyploid carcinoma (204). These cells have an epithelial morphology, and are regularly used *in vitro* for preclinical colon cancer research and to assess the impact of intestinal parasite infections (205, 206). The cells were maintained for a maximum of 20 passages.

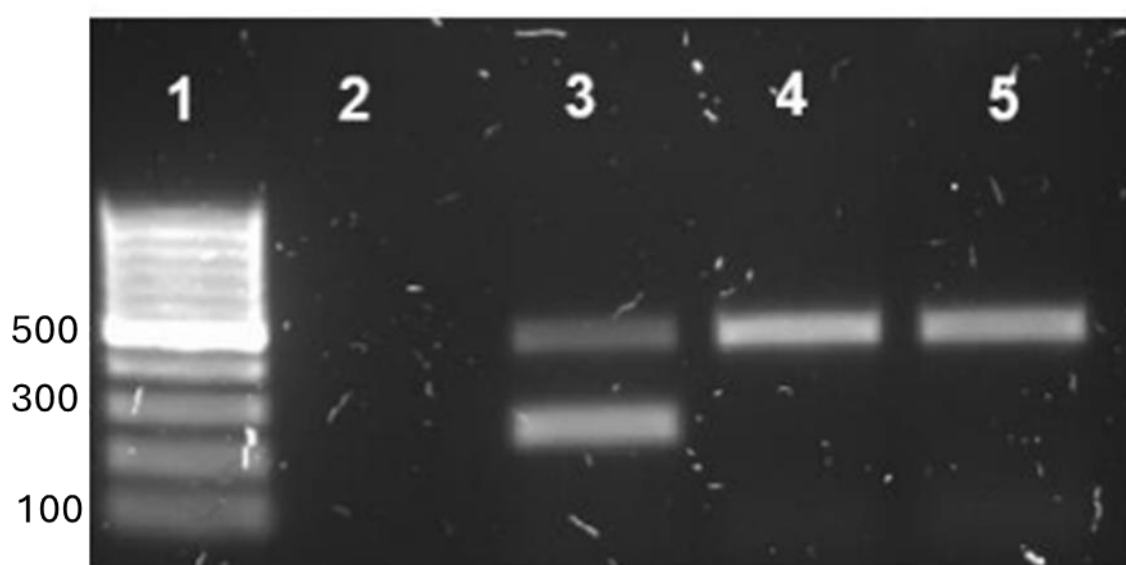


Figure 1. CMT-93 Mycoplasma test. 1. 100 base pair (bp) ladder, 2. Empty lane, 3. Positive control, 4. Negative control, 5. CMT-93 cell supernatant.

2.1.2 Cell line maintenance

The CMT-93 cell line was maintained in the appropriate media as recommended by the American Type Culture Collection (ATCC) (Manassas, VA, USA) with some modifications (**Table 1**).

Table 1. Media requirements for CMT-93 cell line

Component	Add	Final concentration	UK Catalogue number
Dulbecco's Modified Eagle Medium F12 (DMEM/F-12)	500 mL	-	21331020 (ThermoFisher Scientific)
Foetal Bovine Serum (FBS), heat-inactivated	50 mL	10%	10500064 (ThermoFisher Scientific)
Penicillin/streptomycin (100X stock)	5 mL	0.5 mg/mL	P7539-100ML (ThermoFisher Scientific)
L-glutamine (200 mM)	5 mL	2 mM	A2916801 (ThermoFisher Scientific)
NEAA (100X stock)	5 mL	1X	11140050 (ThermoFisher Scientific)

2.1.3 Defrosting cells from liquid nitrogen and seeding

Cells taken from liquid nitrogen were transferred on ice before being rapidly defrosted using a water bath set to 37°C and added to 5 mL of pre-warmed culture medium just before ice pellet had completely melted. Cells were then centrifuged at 2,000 *x g* for 5 mins to remove the freezing medium. The supernatant was then removed and cells resuspended in 1 mL culture medium before seeding into a T25 flask. Cells were supplemented with 5% FBS and medium was changed every day until the cells reached 70-80% confluency, before being passaged as described in section 1.1.4.

2.1.4 Passaging cells

The CMT-93 cells were grown in media described in **Table 1** in a 37°C incubator containing 5% CO₂. When 70-80% confluency was achieved, ~ 2.5 x 10⁶ cells were passaged in a 1:5 ratio as recommended by ATCC (VA, USA). DMEM/F-12 media was aspirated from the T25 flask (ThermoFisher Scientific, MA, USA, Cat #156340) and replaced with 2 mL 0.25% (w/v) trypsin-disodium ethylenediaminetetraacetic acid (EDTA) 0.53 mM (Invitrogen, CA, USA, Cat #15400054) to cause cell detachment from the flask surface. Cells were detached following five to seven minutes of incubation in trypsin, at 37°C with 5% CO₂. Once all cells became detached from the flask surface, 5 mL of cell culture medium supplemented with FBS was added. The media, trypsin and cells were added to a 15 mL falcon and centrifuged at 2,000 *x g* for 5 mins. Following centrifugation, the supernatant was aspirated and the pellet was resuspended in 5 mL culture medium, with 1 mL containing ~ 7 x 10⁵ cells seeded into a new T25 flask containing 4 mL fresh DMEM/F-12 and returned to the incubator.

2.1.5 Freezing cells

Cultures of CMT-93 that had undergone low passage numbers were selected for freezing, to avoid genetic drift which may occur with increasing passage numbers (207). Cells at 70-80% confluence were detached from the T25 flask and centrifuged as described in 1.1.4. The supernatant was aspirated and the pellet resuspended in 5 mL Recovery™ Cell Culture Freezing Medium (ThermoFisher Scientific, MA, USA, Cat #12648010) before 1 mL aliquots were added to cryopreserve vials (ThermoFisher Scientific, MA, USA, Cat #4000200). Tubes were stored in the Mr Frosty™ Freezing Container (ThermoFisher Scientific, MA, USA, Cat #5100-0001) for one week at -80°C before being transferred on ice to liquid nitrogen.

2.1.6 Seeding cells for functional assays

To seed specific quantities of cells for functional assays, cells were detached from the flask surface and resuspended in 1 mL media as previously described in section 2.1.4. Cells were then counted manually using a hemacytometer (Fisher Scientific Ltd, Cat #10200872) and trypan blue exclusion (ThermoFisher Scientific, MA, USA, Cat #15250061). Appropriate dilutions were performed to account for different types of plates. For experiments using Transwell inserts in 24-well plates, 100 μL of cells at $3.3 \times 10^5/\text{mL}$ in media were added to the apical chamber of each insert before growing to confluency (3-5 days) (section 2.2.1). For Western blot analysis, cells were seeded in 6-well plates by adding 2.5 mL of the 1:5 dilution from a T75 to each well before growing to confluency (48 hrs) (section 2.2.2.1).

2.1.7 Preparation of drug solutions for cell treatment

The PGE₂ antagonists PF-04418948 and ONO-AE3-208, (Cambridge Bioscience, Cat #15016-10mg-CAY & Cat #14522-10mg-CAY) were purchased and made up to a final concentration of 10 mg/mL in 0.1% dimethylsulfoxide (DMSO) (Sigma, Missouri, USA, Cat #D8418) and stored at -20°C ready for use. Aspirin (ThermoFisher Scientific, MA, USA, Cat #158180500) was made up to a final concentration of 100 μM in deionised H₂O and stored at -20°C ready for use.

2.1.8 Treatment of cell lines

The CMT-93 cell line was used to determine effects of *Heligmosomoides polygyrus bakeri* excretory/secretory products (HES) (see section 2.3.1), the prostaglandin receptor agonist 16,16-dimethyl prostaglandin E₂ (dmPGE₂) (Cambridge Bioscience, Cat #14750-1mg-CAY), the prostaglandin E₂ receptor antagonists PF-04418948 and ONO-AE3-208, and Aspirin on cellular PGE₂ receptor signalling and cellular permeability (see section 2.2.1 and 2.2.2). For assessments of PGE₂ receptor signalling, cells were seeded in triplicate into a 6-well plate as described in section 1.1.6. After 3-5 days,

cells received either 10 µg/mL HES, 200 ng/mL diMe-PGE₂, 1 µM PF-04418948 and ONO-AE3-208 in 0.1% DMSO or DMSO alone. For cell permeability experiments, cells were seeded in triplicate in Transwell inserts as described in section 2.1.6. After 3-5 days when the cells have formed a monolayer in the insert, cells were treated with either 10 µg/mL HES, 200 ng/mL dmPGE₂, 10mM Aspirin, 1 µM PF-04418948 and/or ONO-AE3-208 in 0.1% DMSO or 0.1% DMSO alone as a vehicle control. Trypsin-EDTA 0.25% was added in triplicate at a concentration of 1 µM as a positive control for permeability (208).

2.2 *In vitro* Experiments

2.2.1 FD4 cell permeability assay

The set up of the experiment is summarised in **Figure 2**. CMT-93 cells were seeded into 6.5 mm Transwell inserts with 0.4 µm pore size (Sarstedt Ltd, Cat #83.3932.041) as described in section 2.1.6. After forming a monolayer 3-5 days from being seeded, cells were treated as described in section 2.1.8 as well as Fluorescein isothiocyanate–dextran 4kDa (FD4) (Merck Life Science Ltd, Cat #FD4-100MG) being added to the apical chamber at a concentration of 1 mg/mL. In the basolateral chamber, 600 µL of the same cell culture medium that is in the apical chamber is added. The plate is incubated in the 37°C incubator with 5% CO₂ for 20 hrs, then the contents of the basolateral chamber are collected into a 1.5 mL Eppendorf tube wrapped in tinfoil. Then, 100 µL of each sample is loaded in triplicate into a black opaque-bottomed 96-well plate (ThermoFisher Scientific, MA, USA, Cat #M33089). A 2-fold serial dilution of FD4 ranging from 200 µg/mL to 0.1 µg/mL was prepared in cell media and added to the black opaque-bottomed 96-well plate in duplicate to generate a standard curve to quantify FD4 concentrations in the basolateral chamber using the equation from the graph (**Figure 3**). Trypsin was included as a positive control at a concentration of 1 µM, whilst a Transwell containing only CMT93 cells and no FD4 was used as a negative control. To account for background fluorescence, values obtained from the negative control were subtracted from all values. Fluorescence was determined at 530/485 nm excitation/emission using a plate reader (Tecan Infinite M200 Pro).

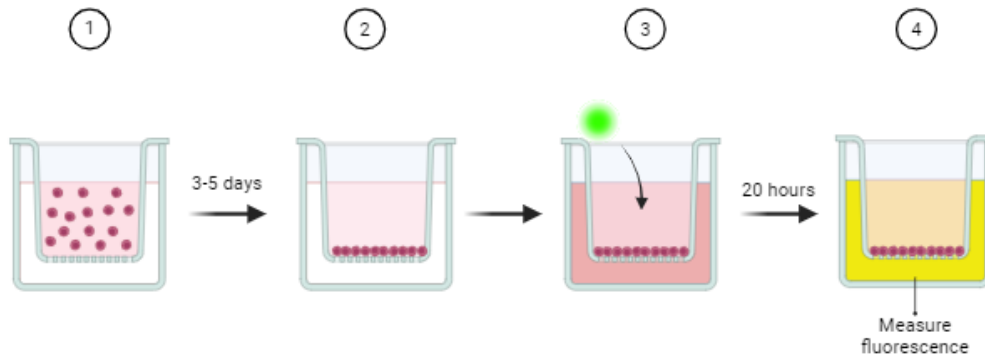


Figure 2. General FD4 cell permeability assay workflow. **1.** Cells were seeded in a Transwell insert in a 24-well plate at a density of 3.3×10^4 . **2.** The cells are left for 3-5 days to form a monolayer with the cell media being changed every day. **3.** Once the monolayer is formed, FD4 is added to the apical chamber at a final concentration of 1 mg/mL and cell media is added to the basolateral chamber. **4.** After 20 hours, the contents of the basolateral chamber are collected and fluorescence measured. Image created in Biorender.com

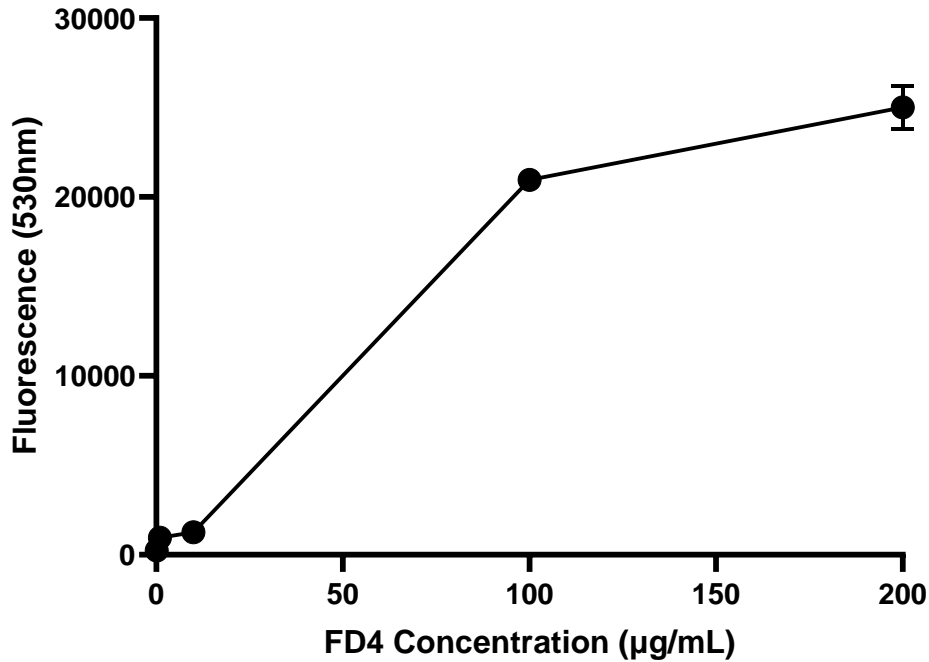


Figure 3. Example standard curve used to determine FD4 concentrations in samples. All values are corrected for background fluorescence. Data shown is the mean of one experiment performed in duplicate. Error bars Mean \pm SD.

2.2.2 Western Blotting

Differences in PGE₂ receptor signalling and E-cadherin expression in CMT-93 cells and murine colon tissue was evaluated, to assess the effect of HES treatment and *H. polygyrus* infection respectively. Western blot enables the identification of proteins through molecular weight-based separation (209). Separation is achieved using gel electrophoresis, producing a band for each protein. The gel is then transferred to a membrane which can be incubated with antibodies specific to the protein of interest and detected by developing the membrane. A single band corresponding to the molecular weight of the peptide recognised by the antibody is expected. The intensity of the protein bands is measured using ImageJ, which assigns numerical values to the band intensities based on pixel density. The band intensity is normalised to the loading control glyceraldehyde 3-phosphate dehydrogenase (GAPDH) to account for variations in sample loading. The process is summarised in **Figure 4**.

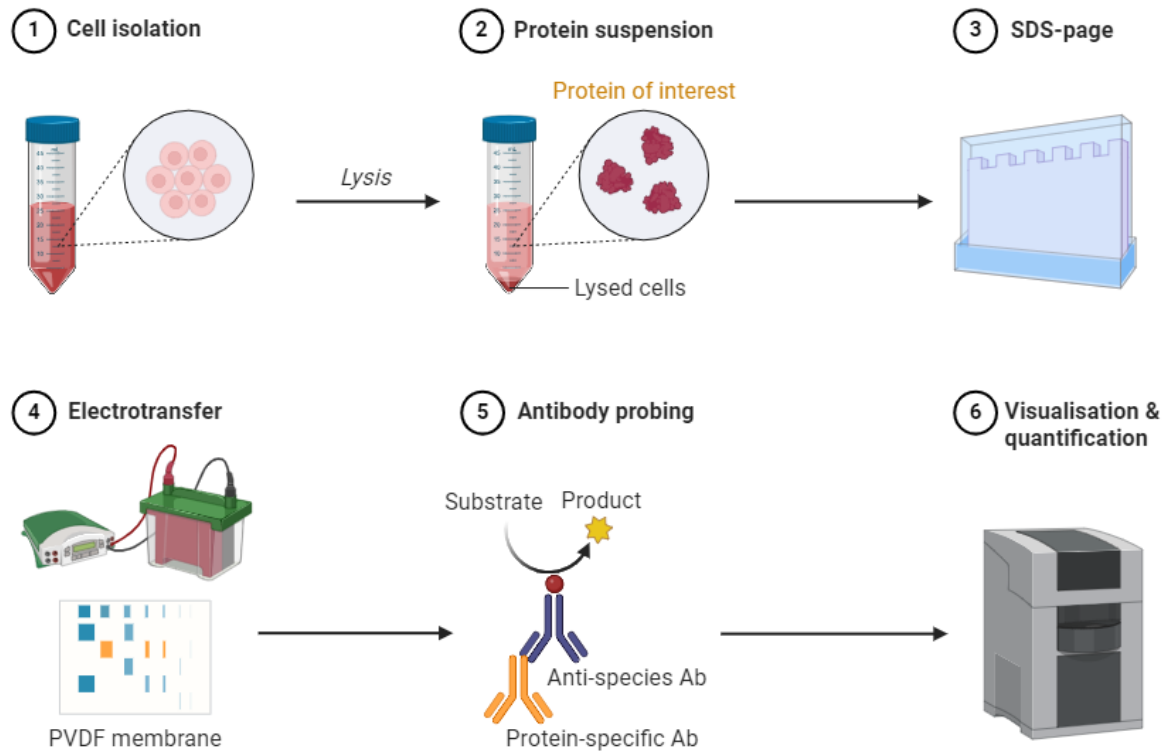


Figure 4. General western blot workflow. 1. Cells are isolated from a sample and prepared for protein extraction. 2. Cells undergo lysis to release proteins, including the target protein of interest. 3. The proteins are separated by size using SDS-PAGE (sodium dodecyl sulfate-polyacrylamide gel electrophoresis). 4. Separated proteins are transferred from the gel to a PVDF (polyvinylidene difluoride) membrane for detection. 5. The membrane is probed with a primary antibody specific to the target protein, followed by a secondary antibody conjugated to a detection enzyme. The enzyme reacts with a substrate to produce a detectable signal. 6. The signal is captured using an imaging system for visualization, and band intensity is quantified to measure protein levels. Image created in Biorender.com

2.2.2.1 Whole cell lysate harvesting and protein extraction

Cells were seeded in a 6-well plate as described in section 2.1.6 and left for 24 hrs before being treated as described in section 2.1.8, then left for a further 24 hrs to form 70-80% confluency. After 48 hrs had elapsed, the cell media was aspirated and wells washed with ice cold phosphate buffered saline (PBS) before being aspirated. The plate was placed on ice and 250 μ L lysis buffer (**Table 2**) added to each well. Each well was scraped thoroughly using a cell scraper and the contents collected into 1.5 mL Eppendorf tubes which were kept on ice. To chelate DNA, a 21-gauge needle is placed on a 1 mL syringe and the sample is pipetted up and down 20-25 times. The protein is isolated from the cells by centrifuging the sample at $9,600 \times g$ for 15 mins at 4°C . The supernatants are moved to a fresh 1.5 mL Eppendorf and stored at -20°C ready for use. Protein concentrations were determined using a Pierce™

BCA Protein Assay Kit (ThermoFisher Scientific, MA, USA, Cat #23227) as described in section 2.2.3 with standards mixed with lysis buffer.

Table 2. Lysis buffer 7X components

Component	Quantity	Concentration	UK Catalogue number
Tris 1 M pH 7.4	7 mL	350 mM	RC-107 (VWR International)
NaCl	1.22 g	1.05 M	71380-1KG-M (Merck Life Science Ltd)
EDTA	104 mg	14 mM	46-034-CI (Scientific Laboratory Supplies)
NP-40	1.4 mL	7%	85124 (ThermoFisher Scientific, MA, USA)
H ₂ O	11.6 mL		

2.2.2.2 Tissue harvesting and protein extraction

Colon tissue harvested from *in vivo* experiments for protein extraction was immediately stored in 1 mL 1X RIPA buffer (VWR International, Cat #PIER89901) containing 1X protease/phosphatase inhibitor cocktail (ThermoFisher Scientific, MA, USA, Cat #78430) and stored in -80°C until ready for protein extraction. For extraction, 2-3 ceramic beads were added to the sample and homogenised using a bead beater (BeadBug™) by pulsing at maximum speed for 30 sec x 2 and immediately placed on ice. To chelate DNA, a 21-gauge needle is placed on a 1 mL syringe and the sample is pipetted up and down 20-25 times. The protein is isolated from the tissue by centrifuging the sample at 9,600 x *g* for 15 mins at 4°C. The supernatants are moved to a fresh 1.5 mL Eppendorf and stored at -20°C ready for use. Protein concentrations were determined using a Pierce™ BCA Protein Assay Kit (ThermoFisher Scientific, MA, USA, Cat #23227) as described in section 2.2.3 with standards mixed with RIPA buffer.

2.2.2.3 Sample preparation for loading

The correct volume of sample was added to 10 µL 4X loading buffer (**Table 3**) to a final volume of 30 µL and final protein concentration of 20 µg. The protein solution was boiled at 100°C for 5 mins before brief centrifugation at maximum speed to remove condensation.

Table 3. Components of sample loading buffer for western blot

Component	Quantity	Concentration	UK Catalogue number
Tris 0.5 M pH 6.8	5 mL	250 mM	RC-107 (VWR International)
Glycerol	4 mL	25%	17904 (ThermoFisher Scientific, MA, USA)
SDS	600 mg	6%	1610301 (Bio-Rad Laboratories Ltd)
1% Bromophenol blue	200 µL		14331-25g-CAY (Cambridge Bioscience)
β-mercaptoethanol	800 µL		BC98 (VWR International)

2.2.2.4 Gel production and protein separation

Proteins within cell and tissue lysates were separated according to size by gel electrophoresis using a mini 7.5 or 12% gel depending on the size of the protein of interest. Gel components are listed in **Table 4 & 5**. The resolving gel (pH 8.8) was cast between two glass plates separated by a 1 mm spacer (Bio-Rad Laboratories Ltd, Cat #1653308 & #1653311). A small layer of butanol was then added on top of the liquid resolving gel to ensure gel integrity and then the gel was incubated at room temperature until the residual gel left over had set (approximately one hour). Once the resolving gel had set, a stacking gel (pH 6.8) was then loaded between the plates, on top of the solid resolving gel. A 1 mm comb (Bio-Rad Laboratories Ltd, Cat #1653359) was immediately inserted into the stacking gel, which was then left to set at room temperature for approximately 30 mins.

Table 4. Western blot resolving gel composition

	7%	12%	
Component	Quantity	Quantity	UK Catalogue number
H₂O	5.1 mL	3.4 mL	
Acrylamide/Bis-acrylamide (30%/0.8% w/v)	2.3 mL	4 mL	A3574-100ML (Merck Life Science Ltd)
1.5 M Tris-HCl pH 8.8	2.5 mL	2.5 mL	RC-107 (VWR International)
20% Sodium dodecyl sulfate (SDS)	50 µL	50 µL	1610301 (Bio-Rad Laboratories Ltd)
10% Ammonium persulfate (APS)	50 µL	50 µL	HC2005 (ThermoFisher Scientific, MA, USA)
Tetramethylethylenediamine (TEMED)	6.6 µL	6.6 µL	HC2006 (ThermoFisher Scientific, MA, USA)

Table 5. Western blot stacking gel composition

Component	Quantity	UK Catalogue number
H₂O	3.075 mL	
Acrylamide/Bis-acrylamide (30%/0.8% w/v)	670 µL	A3574-100ML (Merck Life Science Ltd)
0.5 M Tris-HCl pH 6.8	1.25 mL	RC-107 (VWR International)
20% Sodium dodecyl sulfate (SDS)	25 µL	1610301 (Bio-Rad Laboratories Ltd)
10% Ammonium persulfate (APS)	25 µL	HC2005 (ThermoFisher Scientific, MA, USA)
Tetramethylethylenediamine (TEMED)	5 µL	HC2006 (ThermoFisher Scientific, MA, USA)

Once the stacking gel had set, 30 µL of the sample containing 20 µg protein was loaded into wells using gel loading tips (ThermoFisher Scientific, MA, USA, Cat #LC1001) for accuracy. A 10-250 kDa ladder (Bio-Rad Laboratories Ltd, Cat #1610374) was used to ensure detected bands were of the expected

size for the protein of interest. The space between the gels was flooded with 1X running buffer (**Table 6**) and a 300V power pack (Bio-Rad Laboratories Ltd, Cat #1645070) was set to 120V and used to run the gel at room temperature for approximately 90 mins.

Table 6. Western blot running buffer composition

Component	Quantity	UK Catalogue number
SDS-PAGE tank buffer Tris-Glycine-SDS (10X)	900 mL	B9-0032 (Geneflow Ltd)
H ₂ O	100 mL	

2.2.2.5 Semi-dry membrane transfer

To transfer the separated proteins from the gel to a low fluorescence poly(vinylidene fluoride) (LF-PVDF) membrane (Bio-Rad Laboratories Ltd, Cat #1620262) for antibody staining, a rapid semi-dry transfer was performed once the gel had completed its run and the protein ladder had visibly separated enough so that different molecular weight bands were easily distinguishable.

All transfer equipment including gels and membranes were soaked in 1X transfer buffer (**Table 7**) for at least 5 mins to ensure they remained wet throughout the procedure. The LF-PVDF membrane was cut to size and initially soaked in 100% methanol for 10 sec before being added to 1X transfer buffer separate from the incubating gel and filter paper. Care was taken throughout to avoid contact of the membrane with potential sources of protein contamination including gloves, with tweezers being used to handle the membrane at all times.

Table 7. Western blot transfer buffer composition

Component	Quantity	UK Catalogue number
10X Tris/glycine buffer	200 mL	1610734 (Bio-Rad Laboratories Ltd)
100% Ethanol	200 mL	10680993 (Fisher Scientific)
H ₂ O	600 mL	

Transfer equipment was assembled as shown in **Figure 5**, with the membrane being carefully placed over the gel and sandwiched between filter paper. Assembled transfer equipment was then placed in the Trans-Blot Turbo Transfer System (Bio-Rad Laboratories Ltd, Cat #1704150) which is set at 1.3A and 25V which runs for 7 mins.

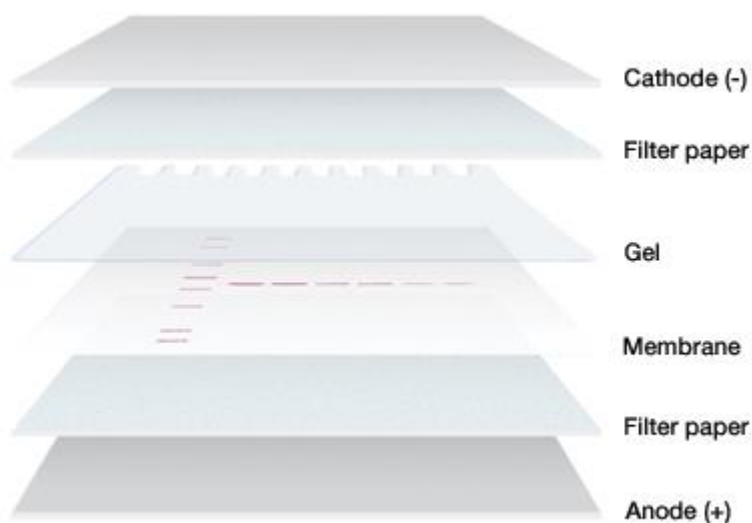


Figure 5. Gel and membrane setup for electrophoretic transfer. Image adapted from Bio-rad.com

2.2.2.6 Membrane blocking and primary antibody staining

Once proteins had transferred from the gel to the membrane, the membrane was blocked to prevent non-specific binding of the primary antibodies. Blocking was achieved by incubating the membrane in blocking buffer (**Table 8**) in a sealed bag for at least 30 mins at room temperature on a shaker set to 40 rpm. Membranes were then incubated with primary antibody at the dilution detailed in **Table 9** at 4°C overnight on a rocker.

Table 8. Western blot blocking buffer composition

Component	Quantity	Concentration	UK Catalogue number
Tris 1 M pH 7.4	10 mL	10 mM	RC-107 (VWR International)
NaCl	8.76 g	0.15 M	71380-1KG-M (Merck Life Science Ltd)
EDTA	372 mg	1 mM	46-034-CI (Scientific Laboratory Supplies)
Bovine Serum Albumin (BSA)	30 g	3%	A7030-50G (Merck Life Science Ltd)
Gelatine	5 g	0.5%	48722-100G-F (Merck Life Science Ltd)
H₂O	1L		

2.2.2.7 Secondary antibody staining

Following primary antibody incubation, membranes were washed for 3 x 15 mins with Tris buffer saline-Tween 20 (TBS-T) on a shaker set to 40 rpm. Membranes were then placed in a new sealable plastic bag and secondary antibodies dissolved in blocking buffer at the recommended dilution factor (**Table 9**) were added. Membranes were incubated with secondary antibody for one hour at room temperature on a shaker set to 40 rpm. Washing, as described above, was repeated before detection.

Table 9. Antibodies used for western blot

Target	Host species	Species reactivity	Classification	Dilution	UK Catalogue number
GAPDH	Rabbit	Human, mouse	Primary antibody	1:1000	ab9485-100ug (Abcam)
Total β-catenin	Rabbit	Human, mouse, rabbit, monkey	Primary antibody	1:1000	8480T (Cell Signalling Technology)
Phosphorylated β-catenin Ser552	Rabbit	Human, mouse	Primary antibody	1:1000	9566S (Cell Signalling Technology)
E-cadherin	Rat	Dog, human, mouse	Primary antibody	1:250	14-3249-80 (ThermoFisher Scientific, MA, USA)
Alexa Fluor 790-conjugated AffiniPure donkey anti-rabbit IgG	Donkey	Rabbit	Secondary antibody	1:10,000	711-655-152 (Jackson ImmunoResearch Laboratories Inc.)
IRDye800CW Goat anti-Rat	Goat	Rat	Secondary antibody	1:10,000	926-32219 (Li-Cor Bio)

2.2.2.8 Protein detection

To visualise the protein bands, membrane sections were placed face-up inside the Li-Cor Odyssey cXL system (Li-Cor Biosciences) which uses a 2-channel near-infrared fluorescent imager to detect the signal produced. The infrared lasers excite the fluorophore conjugated to the secondary antibody to give the signal.

2.2.2.9 Protein quantification

Density of target bands normalised to density of internal control protein (GAPDH) was used to indicate expression of the target protein. Analysis was conducted in ImageJ (210) with data being presented using GraphPad Prism 10.2.0 (GraphPad, CA, USA).

2.2.3 BCA protein quantification assay

To quantify protein quantification in samples, the Pierce™ Bicinchoninic Acid (BCA) Protein Assay Kit (ThermoFisher Scientific, MA, USA, Cat #23227) was used following manufacturers instructions. In brief, BCA reagent A was mixed with BCA reagent B at a 50:1 ratio to make the working reagent (WR). To a 96-well microplate (ThermoFisher Scientific, MA, USA, Cat #15041), 200 μ L of WR was added followed by 25 μ L of sample. To quantify protein concentration, a standard curve using BSA (20-2000 μ g/mL) was generated (**Figure 7**) by performing a dilution series in the same diluent as the sample. A negative control of diluent alone with no BSA was included. To account for background absorbance, values obtained from the negative control were subtracted from all values. The plate was covered in foil and incubated at 37°C for 30 mins, before measuring absorbance at 562 nm (Tecan Infinite M200 PRO).

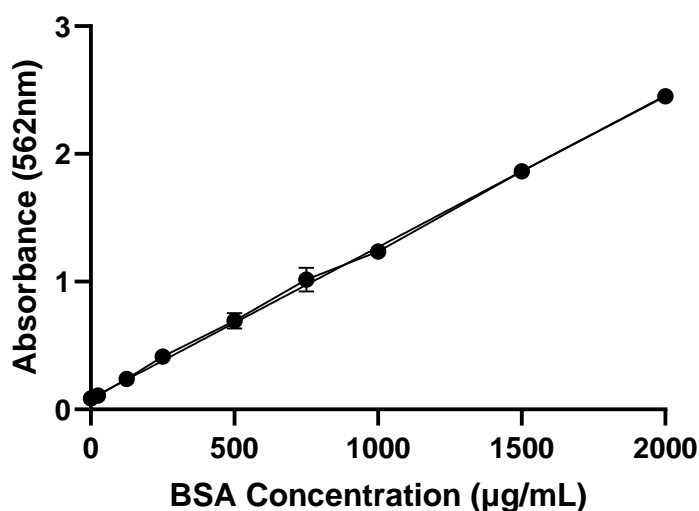


Figure 7. Example standard curve used to determine BSA concentrations in samples. All values are corrected for background fluorescence. Data shown is the mean of one experiment performed in duplicate. Error bars Mean \pm SD.

2.2.4 PCR

Following methods published by Harcus *et al* (211), expression levels of prospective metabolic enzyme homologues of prostaglandin E synthase 2 (PGES2) and phospholipase A₂ (PLA₂) were investigated in different lifecycle stages of *H. polygyrus* using polymerase chain reaction (PCR).

2.2.4.1 PCR primer design

PCR primers were designed using National Centre for Biotechnology Information (NCBI) Primer-BLAST (212). For primer pair specificity checking parameters, the organism against which primers were designed was 'Nematoda' (taxid: 6231). Consideration was made to optimal primer parameters when designing primers, these included; forward and reverse primer length of between 18-24 bases, product size maximum of 200 base pairs, melting temperatures (T_m) less than 3°C apart, a guanine and cytosine (GC) content of between 40-60% and as close to the 3' end of the target sequence as possible. Once potential candidates were identified, they were aligned to the target sequence using the sequence alignment software, Multalin (213). The reverse primer was reverse complemented using a reverse complement tool to ensure correct binding (214). If the chosen primer pair sequences aligned well to the target sequence and the predicted product size matched with the size proposed by NCBI Primer-Blast, then primers were ordered (Eurofins genomics). The sequences of the designed primers are shown in **Table 10**. The primer sequences for *H. polygyrus* actin were obtained from published work by Harcus *et al* (211).

Table 10. Primers used for PCR reactions

Gene name	Primer sequence (5'-3')	Species
Actin	TGAGCACGGTATCGTCACCAAC	Nematoda
	TTGAAGGTCTCGAACATGATCTG	
PGES2	CGCCATTGGACCGAATAGGA	Nematoda
	CGACACCTAGTTCGCCTGAA	
PLA2	GATAGGTGGGTGAGCTGTCCG	Nematoda
	TGTCTTTGGTGTCCGGTCTCG	

2.2.4.2 RNA extraction

RNA was extracted from *H. polygyrus* eggs, L3 larvae, and adults using TRIzol reagent (ThermoFisher Scientific, MA, USA, Cat #15596026). Samples were homogenised by adding 1-2 ceramic beads and homogenising using the BeadBug™ homogeniser on 4,000 rpm for 2 x 30 sec pulses. The samples are incubated in the TRIzol reagent for 5 mins to allow complete dissociation of the nucleoproteins complex. To each sample, 0.2 mL chloroform (Merck Life Science Ltd, Cat #366927) was added and shaken thoroughly, followed by centrifugation (12,000 x g, 15 mins, 4°C) to allow separation of the phases. The upper aqueous phase was then transferred to a new tube for further processing. Here, 0.5 mL isopropanol (Merck Life Science Ltd, Cat #I9516-25ML) was added to each sample, incubated and centrifuged (12,000 x g, 10 minutes, 4°C) to allow precipitation of the RNA. Supernatant was discarded and pellet resuspended in 1 mL 75% ethanol (Fisher Scientific, Cat #16606002), vortexed and

centrifuged again to precipitate the pellet (7500 x g, 5 mins, 4°C). Supernatant was discarded, and pellet was left to air dry for 10 mins. Once dry, the pellet was resuspended in 20 µL nuclease-free water (ThermoFisher, MA, USA, Cat #R0581) and stored at -80°C. Quantity (ng/ µL) and purity (260/280 ratio) of extracted RNA were measured using a Nanodrop-1000 spectrophotometer (ThermoFisher, MA, USA).

2.2.4.3 DNase treatment

To 1 µg of each RNA sample, 1 µL RQ1 RNase 10x reaction buffer (Promega, Cat #M6101), 1 U/ µg RNA RNase free DNase (Promega, Cat #M6101) and DNase and RNase free water (up to 10 µL were added and the reaction mixture incubated at 37°C for 30 minutes. Following this, 1 µL RQ1 DNase stop solution (Promega, Cat #M6101) was added to terminate the reaction and incubated at 65°C for 5 mins.

2.2.4.4 cDNA synthesis

Using the DNase digested RNA, cDNA mixes were prepared. For each sample, 1 µL random hexamer primers (50 µM) (Invitrogen, Cat #N8080127), 1 µL deoxyribonucleotide triphosphate (dNTPs) (10 mM) (New England Biolabs, Cat #N0447S), up to 5 µg RNA and DNase and RNase free water to make the total reaction mixture up to 14 µL were all added. The reaction mixture was then heated at 65°C for 5 mins and allowed to cool at 4°C. To the cDNA mix, 4 µL 5X First Strand Buffer, 1 µL 0.1M dithiothreitol (DTT) and 1 µL SuperScript III (Invitrogen, Cat #18080093) were added. The 20 µL total mix was then incubated in a thermocycler, programmed as follows: 25°C for 5min, 50°C for 1hr, and 70°C for 15min. Samples were allowed to cool and then stored at -20°C.

2.2.4.5 DNA amplification

The PCR BIO Ultramix (PCR BIO, Cat # PB10.32-01) master mix was prepared according to manufacturer instructions for the required number of samples +1 to account for error. 22 µL of the master mix was aliquoted into 0.2 mL non-stick PCR tubes (Starlabs, Cat #I1402-8100), and to each aliquot 1 µL template DNA, 1 µL forward primer (10 µM) and 1 µL reverse primer (10 µM) were added. Samples were then placed in the thermocycler with the programme in **Table 11** used to amplify the DNA.

Table 11. Thermocycler conditions used during DNA amplification

Cycles	Temperature (°C)	Time
1	95	5 mins
35-40	95	30 sec
	60	30 sec
	72	50 sec/kb
1	72	10 mins

2.2.4.6 Gel electrophoresis

A 2% agarose gel was made combining agarose and Tris-acetate EDTA (TAE) buffer and microwaving until molten, before being poured into the gel caster and comb immediately inserted. To allow visualisation, 5 µL SYBR safe (Invitrogen, Cat # S33102) per 100 mL of agarose gel was added prior to pouring into the gel caster. Once set, the agarose gel was placed into the gel electrophoresis tank and submerged in TAE buffer. 8 µL of sample was mixed with 2 µL 6X sample loading dye (PCRBIO, Cat # PB40.12-01) on parafilm before being loaded into the designated wells. For product size reference, 5 µL of 10 – 10,000 bp ladder was loaded (PCRBIO, Cat #PB40.12-01). The gel electrophoresis tank was connected to a PowerPac™ Basic Power Supply (Bio-Rad Laboratories Ltd, Cat #1645070) set to 90V and run for 30 – 40 mins. Once the sample loading dye had run to the bottom, the gel was visualised on the GelDoc Go Imaging System (Bio-Rad Laboratories Ltd).

2.2.5 Molecular cloning into *E. coli*

Gibson cloning was performed in an attempt to express the proposed *H. polygyrus* PGES2 enzyme to investigate its function. The Gibson cloning technique was chosen as it is a relatively quick and inexpensive method of joining multiple overlapping DNA fragments in a single-tube isothermal reaction (215). The overview of the Gibson cloning process is shown in **Figure 8**.

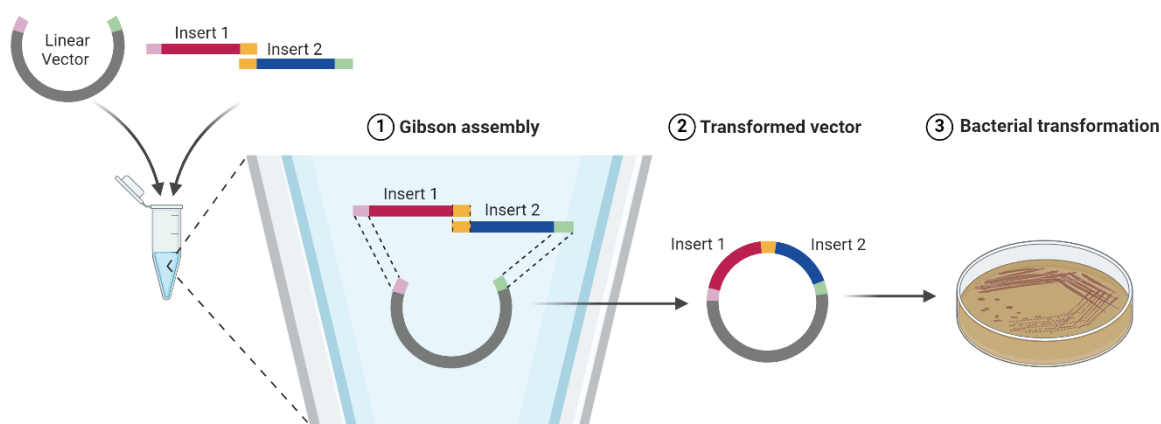


Figure 8. Overview of Gibson assembly process. 1. Insert sequence is ligated into the chosen vector using the Gibson assembly mix. 2. The successfully transformed vector is then 3. transformed into bacteria. Image created using Biorender.com

2.2.5.1 DNA preparation and Gibson assembly

The pET15b vector used for cloning of the PGES2 sequence was kindly provided by Dr Mark Young (School of Biosciences, Cardiff University). Primers used to amplify the PGES2 insert sequence and the pET15b vector were obtained using Benchling software (**Table 12**).

Table 12. Primer sequences of pET15b vector and PGES2 insert

Primer name	Sequence (5'-3')
pET15b	ATC ATC ATC ATC AT CAT TAG GAT CCG GCT GCT AAC AAA GC
	TCA ATA TGA AAC GTC AGC ATG GTA TAT CTCC TTC TTA AAG TTA AAC AA
PGES2	CTT TAA GAA GGA GAT ATA CCA TGC TGA CGT TTC ATA TTG AG
	GCT TTG TTA GCA GCC GGA TCC TAA TGA TGA TGA TGA TGA TGA TTT G

For the PCR amplification, the pET15b vector was diluted 1:50 with nuclease free water to a final concentration of 2ng/mL. The insert sequence is supplied at a concentration of 2µg/mL which was made up to 100ng/µL by adding 20 µL of nuclease free water. The PCR amplification involved using high fidelity Q5 DNA polymerase (New England Biolabs, Cat #M0491S) as opposed to a low fidelity

DNA polymerase due to its exonuclease activity resulting in a low mutation rate. The reaction mix was put in the thermocycler using the conditions found in **Table 13**.

Table 13. Thermocycling conditions used during DNA amplification

pET15b vector		
Cycles	Temperature (°C)	Time
1	98	30 sec
35	98	10 sec
	60	30 sec
	72	4 mins
1	72	2 mins
PGES2 insert		
1	98	30 sec
35	98	10 sec
	65	30 sec
	72	30 sec
1	72	2 min

The PCR was performed as previously described in section 2.2.8.6 only with a 1% gel so that it is easier to cut through in the fragment extraction step. To estimate fragment size, 5µL of a 1kbp DNA ladder (Meridian science, Cat #BIO33053) was run alongside. Both amplified fragments were PCR extracted by using the Monarch DNA Gel Extraction Kit (New England Biolabs, Cat #T1120). The extracted fragments were then quantified using a Qubit dsDNA broad range (BR) assay kit (ThermoFisher, MA, USA, Cat #Q33265) with the Qubit fluorometer (Invitrogen, Cat #Q33238). The PGES2 insert fragment was then cloned into the pET15b vector using a Gibson Assembly Cloning Kit (New England Biolabs, Cat #E5510S) with the following mix shown in **Table 14**. The fragment assembly mix was then heated at 50°C for 30 mins and stored at -20°C ready for bacterial transformation

Table 14. Details of Gibson assembly mix

Component	Fragment assembly (μL)	Positive control (μL)
Fragments	2	10
Gibson assembly master mix (10X)	10	10
H ₂ O	7	0

2.2.5.2 Bacterial transformation

The bacteria used for transformation were 5-alpha competent *E. coli* cells supplied by (New England Biolabs, Cat #C29871) and stored at -80°C until ready to perform the transformation. Cells were thawed on ice for 30 mins before 2 μL of the Gibson assembled plasmid DNA was added directly to the cells and incubated on ice for a further 30 mins. The plasmid DNA was introduced into the cells by using the heat shock transformation method, where the vial was submerged in a water bath set to 42°C for exactly 30 sec and placed back on ice for 5 min. To the vial, 950 μL SOC media (New England Biolab, Cat #B9020S) was added and the mix was placed on a shaker set at 37°C and 250 rpm for 1 hr. A 1 in 10 serial dilution of the cells was performed down to 10⁻⁷ with 100 μL being spread onto lysogeny broth (LB) agar (Merck Life Sciences, Cat #BP9724-500) supplemented with 100 μg/mL ampicillin (ThermoFisher, MA, USA, Cat #11593027) to select for positive colonies.

2.2.5.3 Colony PCR

To confirm positive transformation of the plasmid into the bacteria, a colony PCR was performed on randomly selected single colonies. The DNA was extracted from the colonies by picking a single colony and mixing it with 50 μL 5%- Chelex-100 (Bio-Rad Laboratories, Cat #1421253) by pipetting up and down. The sample was heated to conditions shown in **Table 15**.

Table 15. Thermocycling conditions used for DNA extraction with Chelex-100 resin

Cycles	Temperature (°C)	Time
1	95	5 min
	4	5 min
	95	5 min
	4	5 min

The Chelex resin can be seen at the bottom of the tube after this heating step, so we next took 1 μ L of colony DNA from the top of the tube and added to a PCR BIO ultramix and primers for the PGES2 insert sequence were used. The sample was then heated in the thermocycler using conditions shown in **Table 16**.

Table 16. Thermocycling conditions for colony PCR

Cycles	Temperature (°C)	Time
1	95	5 min
35	95	30 sec
	62	30 sec
	72	1 min
1	72	10 min

The samples were loaded onto a 1.2% agarose gel as previously described in section 2.2.4.6. Colonies showing successful transformation were grown in an overnight culture of 10 mL LB broth supplemented with 100 μ g/mL ampicillin to maintain selection pressure on a shaker in a 37°C incubator set at 250 rpm for plasmid extraction the next day.

2.2.5.4 Plasmid extraction and sequencing

The plasmid extraction was performed using the Monarch plasmid miniprep kit (New England Biolab, Cat #T1010S) following manufacturer instructions, with the workflow being summarised in **Figure 9**. In brief, transformed colonies were inoculated into LB broth with 100 μ g/mL ampicillin and grown overnight. The culture is centrifuged, and the bacterial cells lysed with lysis buffer before cell debris being removed. The plasmid DNA is then added to a spin column, with multiple wash steps allowing the plasmid DNA to bind to the matrix and be eluted in nuclease-free water. Once extracted, plasmid was stored in -20°C ready for subsequent use. To ensure the plasmid had the correct insert sequence transfected, 20 μ L of plasmid was sent to Eurofins for sequencing against a standard T7 primer. Once

the sequencing was complete, the resulting plasmid sequence was blasted against the PGES2 insert sequence using NCBI-Blast to ensure both sequences matched.

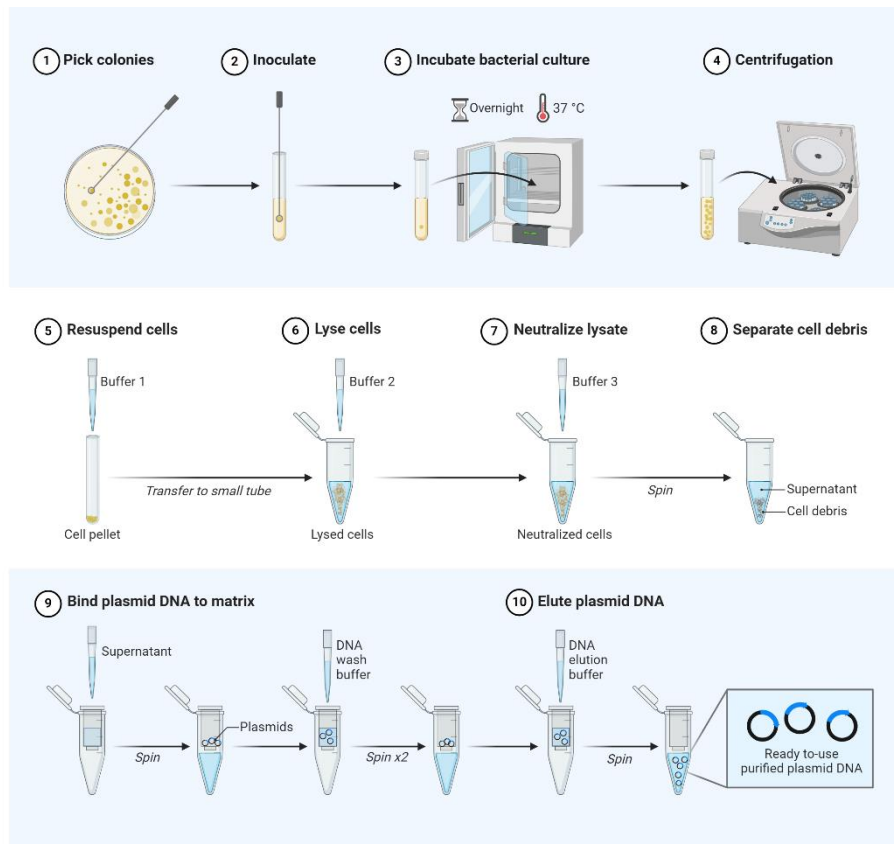


Figure 9. Schematic summarizing the process of plasmid extraction using the Monarch plasmid miniprep kit. Image created using Biorender.com

2.2.5.5 Protein expression in *E. coli*

To express the PGES2 protein, the transformed pET15b plasmid is next transformed into a T7 express *E. coli* strain (New England Biolab, Cat #C2566H). In the T7 system, the target gene is cloned into an expression vector downstream of the T7 promoter and this construct is introduced into a T7 expression host. T7 expression hosts carry a chromosomal copy of the phage T7 RNA polymerase gene. When an inducer is added, such as Isopropyl β - d-1-thiogalactopyranoside (IPTG), T7 RNA polymerase is expressed and becomes dedicated to target gene transcription (216).

The pET15b plasmid was transformed into the T7 express *E. coli* strain using the heat shock method as previously described in section 2.2.9.2. A 5ml culture of LB broth (Merck Life Sciences, Cat #12801660) containing 100 μ g/mL of ampicillin was inoculated with a colony from this culture and grown overnight at 37°C in a shaking incubator set to 250 rpm. A 10 mL culture of LB broth was inoculated with 0.5 mL of the overnight culture and grown at 37°C until an optical density (OD)₆₀₀ of 0.6 was reached. Optical density was measured by taking 100 μ L of culture and mixing with 900 μ L LB broth (1 in 10) in a microcuvette (ThermoFisher, MA, USA, Cat #221S). The OD was quantified at 600 nm using a

spectrophotometer (Jenway 6300) then multiplied by 10 to account for the dilution factor. Once the OD₆₀₀ was equal to 0.6, a 1ml sample was taken (time 0) and added into a 1.5mL Eppendorf. The remaining culture was split into two 50mL Falcon tubes and 9µL of IPTG (Cambridge Bioscience, Cat #15300-5g-CAY) from 1M frozen stock was added to each tube. One tube was placed in a shaking incubator at 37°C for 3hr whilst the other tube was placed in a shaking incubator at 18°C for 20hr. The samples were then centrifuged at maximum speed in a microcentrifuge for 30sec, with the supernatant being discarded. The pellet was stored at -20°C until ready to process.

The cell pellets were suspended in 100µL of lysis buffer consisting of 1mL Bugbuster and 2µL Lysonase (Merck Life Science Ltd, Cat #71370-3) and rotated at room temperature for 5 mins. The samples were then centrifuged in a microcentrifuge at maximum power for 2 mins to remove inclusion bodies and cell debris. The soluble supernatant was then pipetted into a fresh tube and 10µL being taken for SDS-PAGE. The insoluble cell debris was resuspended in 100 µL H₂O and 10 µL was taken for SDS-PAGE. The 10 µL sample was combined with 10 µL 4X loading buffer (section 2.2.2.3) and heated at 100°C for 2 mins and centrifuged at maximum speed in a microcentrifuge. The samples were loaded alongside a 10-180 kDa molecular weight ladder (Bio-Rad Laboratories) on a 12% SDS-PAGE gel (section 2.2.2.4). The gel was run at 120V for 90 mins and then stained with Instant blue stain (Abcam, Cat #ab119211-1000ml) before being washed with deionised water 3 x 5 mins. The gel was imaged using the GelDoc Go imaging system (Bio-Rad Laboratories).

2.3 HES Analysis

2.3.1 *Heligmosomoides polygyrus bakeri* larvae and HES preparation

The *H. polygyrus* lifecycle was performed using an established protocol by Johnston *et al* (217) summarised in **Figure 10**. Male, 8-week-old C57BL/6 mice (Charles River) were maintained on standard chow diet and infected with 400 L3 *H. polygyrus* larvae (donated to us from Dr Benjamin Dewals, University of Liege), by oral gavage, with the adult worms being collected from the small intestine 14 days post-infection. The adult worms were then washed repeatedly with Hank's Balanced Salt Solution (HBSS) (Merck Life Science Ltd, Cat #H9394-1L) with 100 U/mL penicillin/streptomycin before incubation with Roswell Park Memorial Institute-1640 (RPMI-1640) medium (ThermoFisher, MA, USA, Cat #21875091), supplemented with 2mM L-glutamine (ThermoFisher, MA, USA, Cat #A2916801), 100 U/mL penicillin/streptomycin, and 100 µg/mL gentamicin (ThermoFisher, MA, USA, Cat #15710049). The pooled culture supernatants collected twice weekly for three weeks were then concentrated in 1xPBS over a 3000MW Amicon membrane (Merck Life Science Ltd, Cat #UFSC05001). The protein concentration of the HES was quantified using a BCA assay as described previously (section 2.2.3) and

then stored at -80°C ready for use. For the *H. polygyrus* larvae preparation, faecal material containing the eggs are removed from the lower gut. The faecal material is then mixed with washed activated charcoal (Merck Life Science Ltd, Cat #1096310100) and smeared onto filter paper in a large petri dish. This is kept in a humid box for 12-14 days, with the larvae being removed from day 5 onwards. The filter paper is removed, and the larvae left on the plate is washed with water into a 50 mL falcon tube. The wash step is repeated and then spun at $13,800 \times g$ for 10 mins to obtain the L3 larvae.

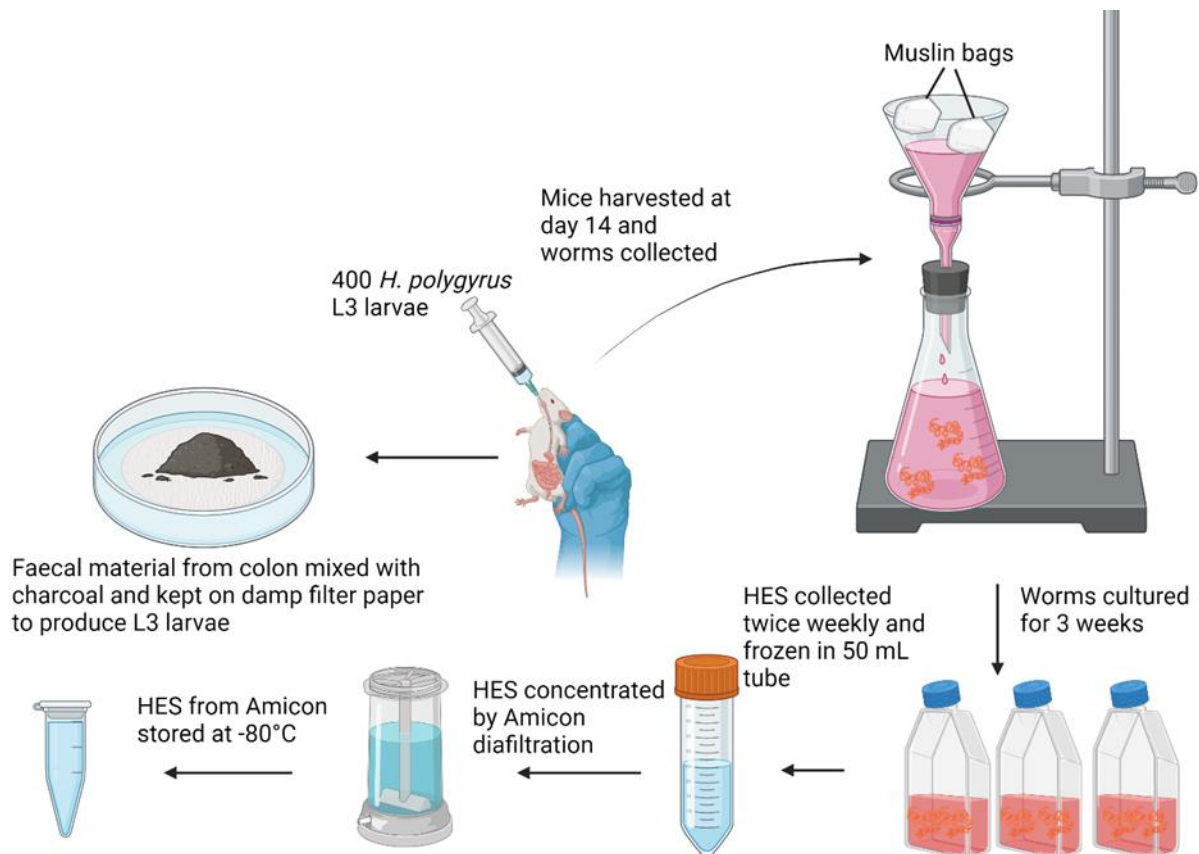


Figure 10. Animated schematic of *H. polygyrus* cultivation. Summary of key events during cultivation of *H. polygyrus* and isolation of HES. Image made using information from Johnston *et al.* Image created in Biorender.com

2.3.2 HES heat-inactivation, protease inhibition and size fractionation

Where indicated, HES was heat-inactivated by incubating at 95°C for 20 mins in accordance with a published protocol (146). For protease inhibition, the Halt™ protease inhibitor cocktail, EDTA-free 100X stock (ThermoFisher Scientific, MA, USA, Cat #78430) was added to cells at a final concentration of 1X. To perform size fractionation, Vivaspin 500 molecular weight cut off (MWCO) spin columns with 10,000 and 50,000 MWCO filters were used (VWR International, Cat #28-9322-25&28-9322-36). To the 50,000 MWCO spin column, 100 μL of HES was added and centrifuged at $9,600 \times g$ for 5 mins with the concentrate and filtrate collected and stored at -20°C . To the 10,000

MWCO spin column, 50 μ L of the filtrate from the 50,000 MWCO spin column was added and centrifuged at 9,600 $\times g$ for 5 mins with the concentrate and filtrate collected and stored at -20°C . To evaluate % efficiency, a sample of bovine serum albumin (BSA) was run on the spin column and protein concentration quantified using the BCA assay as described previously (section 2.2.3).

2.3.3 Oxylin analysis

HES was made up to 500 μ L with water, with 100 μ L being used for analysis. To this 100 μ L of sample, 2.1-2.9ng of 13(S)-HODE-d4, 5(S)-HETE-d8, 12(S)-HETE-d8, 15(S)-HETE-d8, 20-HETE-d6, LTB4-d4, Resolvin D1-d5, PGE2-d4, PGD2-d4, PGF2 α -d4, TXB2-d4, 11-dehydro-thromboxane B2-d4 standard (Cayman chemicals) was added. Lipids were then extracted following sequential additions of isopropanol/hexane/acetic acid extraction buffer and hexane before removal of the upper layer of lipids following centrifugation at 2,000 $\times g$ for 5 mins. Lipid extraction from the lower layer was then completed according to the Bligh and Dyer technique using sequential additions of methanol and chloroform before vacuum drying of the sample and reconstitution of the lipid extract with 200 μ L high-performance liquid chromatography (HPLC) grade methanol. Samples were separated by liquid chromatography (LC) using gradients of two mobile phases and an Eclipse Plus C18 Column (Agilent) and analysed on a QTRAP[®] 6500 LC-MS/MS system (Sciex) according to established multiple reaction monitoring (MRM) transitions (**Table 17**). Following quantification of each oxylin to the internal standard using MultiQuant[™] software (Sciex).

Table 17. Multiple reaction monitoring (MRM) transitions.

Analyte	Retention Time (RT; min)	Declustering potential (DP)	Collision energy (CE)	Transition	
				Q1 (m/z)	Q3 (m/z)
5-HETE	14.4	-55	-19	319.20	115.2
8-HETE	14.1	-65	-18	319.20	155.201
9-HETE	14.27	-50	-20	319.20	167.2
11-HETE	13.91	-60	-19	319.20	167.202
12-HETE	14.11	-65	-18	319.20	179.2
15-HETE	13.65	-55	-18	319.20	219.2
20-HETE	12.64	-85	-21	319.20	275.1
5-HEPE	13.17	-60	-20	317.20	115.1
8-HEPE	12.8	-65	-19	317.20	155.2
9-HEPE	12.99	-50	-18	317.50	167.2
11-HEPE	12.69	-50	-20	317.20	167.201

12-HEPE	12.91	-65	-18	317.20	179.2
15-HEPE	12.63	-65	-16	317.20	219.2
18-HEPE	12.25	-50	-15	317.20	259.2
4-HDOHE	14.66	-50	-17	343.20	101.1
7-HDOHE	14.2	-50	-21	343.20	141.2
8-HDOHE	14.31	-50	-19	343.20	189.2
10-HDOHE	13.99	-55	-21	343.20	153.201
11-HDOHE	14.14	-60	-18	343.20	121.1
13-HDOHE	13.87	-55	-19	343.20	193.1
14-HDOHE	13.99	-45	-17	343.20	205.2
16-HDOHE	13.73	-55	-17	343.20	233.201
17-HDOHE	13.79	-70	-15	343.20	201.2
20-HDOHE	13.47	-55	-17	343.20	241.201
9-HODE	13.34	-85	-23	295.20	171.1
13-HODE	13.28	-85	-23	295.20	195.2
9-HOTrE	12	-60	-20	293.20	171.2
13-HOTrE	12.2	-70	-22	293.20	195.101
5-HETrE	15.49	-70	-19	321.20	115.1
15-HETrE	14.29	-70	-21	321.20	221.2
9-OxoODE	14	-85	-23	293.20	185.1
13-OxoODE	13.72	-85	-25	293.20	195.1
5-OxoETE	15.06	-65	-20	317.20	273.2
12-OxoETE	14.36	-75	-20	317.20	153.1
15-OxoETE	14	-60	-22	317.20	113.1
9,10-DiHOME	10.9	-80	-29	313.20	201.2
12,13-DiHOME	10.62	-80	-28	313.20	183.2
5,6-DiHETrE	12.64	-75	-24	337.20	145.1
8,9-DiHETrE	12.14	-70	-25	337.20	127.1
11,12-DiHETrE	11.79	-65	-26	337.20	167.1
14,15-DiHETrE	11.45	-65	-25	337.20	207.1
5,6-DiHETE	11.2	-60	-23	335.20	115.2
5,15-DiHETE	9.92	-60	-21	335.30	115.2
8,15-DiHETE	9.63	-65	-22	335.20	235.2

14,15-DiHETE	10.35	-65	-23	335.30	207.2
17,18-DiHETE	9.97	-65	-24	335.30	247.2
RvE1	3.21	-65	-22	349.30	195.1
RvD1	7.47	-55	-23	375.50	215.1
RvD2	6.8	-65	-21	375.20	141.2
RvD3	6.49	-65	-24	375.20	147.1
RvD5	10.09	-65	-22	359.20	199.1
LTB3	11.5	-65	-22	337.20	195.2
LTB4	10.22	-70	-23	335.20	195.1
20-carboxy LTB4	3.24	-80	-25	365.20	347.2
20-hydroxy LTB4	3.55	-80	-25	351.20	195.2
6-trans LTB4	9.89	-65	-23	335.20	195.101
LXA4	7.32	-55	-19	351.20	115.2
Mar-01	10.1	-60	-23	359.50	250.2
7,17-DiHDPA	10.38	-65	-20	361.50	263.3
9(10)-EpOME	14.86	-80	-21	295.30	171.1
12(13)-EpOME	14.74	-80	-19	295.30	195.2
5(6)-EET	15.37	-60	-16	319.20	191.1
8(9)-EET	15.15	-60	-15	319.30	167.201
11(12)-EET	15.15	-60	-18	319.30	167.2
14(15)-EET	14.84	-65	-18	319.20	219.3
8(9)-EpETE	14.2	-70	-18	317.20	127.2
11(12)-EpETE	14.12	-70	-15	317.20	167.2
14(15)-EpETE	14.04	-70	-18	317.20	207.2
17(18)-EpETE	13.7	-75	-16	317.20	215.2
7(8)-EpDPA	15.2	-60	-16	343.20	113.1
10(11)-EpDPA	15.08	-65	-15	343.20	153.2
13(14)-EpDPA	15.02	-70	-15	343.20	193.2
16(17)-EpDPA	14.97	-55	-16	343.20	233.2
19(20)-EpDPA	14.71	-70	-18	343.20	241.2
PGD1	6.65	-55	-16	353.30	317.202
PGD2	6.61	-50	-22	351.20	271.302
PGD3	5.26	-50	-17	349.30	269.201

PGE1	6.53	-60	-18	353.30	317.2
PGE2	6.2	-60	-19	351.20	271.3
PGE3	4.86	-60	-17	349.30	269.2
PGB2	8.82	-60	-24	333.30	175.1
13,14-dihydro-15-keto PGE2	7.33	-55	-19	351.20	235.2
13,14-dihydro-15-keto PGD2	8.16	-50	-25	351.50	207.2
13,14-dihydro-15-keto PF2α	7.43	-55	-23	353.50	113.001
11β-PGE2	6.38	-55	-23	351.20	271.2
6-keto PGE1	3.22	-55	-23	367.20	143.1
8-iso PGE2	5.94	-55	-21	351.20	271.001
15-deoxy-Δ12,14-PGJ2	12.44	-65	-18	315.20	271.2
8-iso-15-keto PGF2α	5.37	-50	-23	351.20	289.2
PGF2α	5.89	-85	-24	353.20	309.2
6-keto PGF1α	3.3	-75	-26	369.30	163.2
TXB2	4.83	-60	-22	369.20	169.1
11-dehydro TXB2	6.24	-60	-20	367.20	305.2
13(S)-HODE-d4	13.22	-60	-25	299.2	198.1
5(S)-HETE-d8	14.32	-55	-19	327.2	116.1
12(S)-HETE-d8	14.02	-60	-20	327.2	184.1
15(S)-HETE-d8	13.55	-65	-22	327.2	226.1
20-HETE-d6	12.6	-70	-21	325.2	281.1
Leukotriene B4-d4	10.17	-65	-21	339.2	197.1
Resolvin D1-d5	7.41	-75	-18	380.2	141.1
Prostaglandin E2-d4	6.16	-60	-23	355.2	275.101
Prostaglandin D2-d4	6.58	-55	-23	355.2	275.1
Prostaglandin F2α-d4	5.86	-80	-24	357.2	313.2
Thromboxane B2-d4	4.79	-55	-22	373.2	173.1
11-dehydro Thromboxane B2-d4	6.21	-55	-21	371.2	309.2
11(12)-EET (EpETrE) -d11	15.09	-65	-18	331.2	167.1

2.3.4 Phospholipase A₂ activity assay

Phospholipase A₂ (PLA₂) enzymatic activity was measured using the EnzChek™ Phospholipase A₂ Assay kit, (ThermoFisher Scientific, MA, USA, Cat #E10217) following manufacturers protocol. Honey-bee

venom PLA₂ was used to produce a standard curve by diluting the 500 U/mL stock in 1X reaction buffer to a concentration range of 0-10 U/mL in a 96-well black plate (ThermoFisher Scientific, MA, USA, Cat #M33089) (Figure 11). The *H. polygyrus* adult supernatant was prepared by homogenising *H. polygyrus* adults in 1X reaction buffer at 4,000 rpm for 2 x 30 secs (BeadBug™), centrifuged at maximum speed in a microcentrifuge, and supernatant removed and stored at -80°C. Assays were performed at 100 µL total reaction volume, each well containing 50 µL of the sample supernatant and 50 µL Substrate-Liposome (SL) mix and left for 10 minutes in the dark. As a negative control, 50 µL 1X reaction buffer was added with the SL mix. To account for background fluorescence, values obtained from the negative control were subtracted from all values. Fluorescence was measured at 460/515 nm excitation/emission (Tecan Infinite M200 PRO).

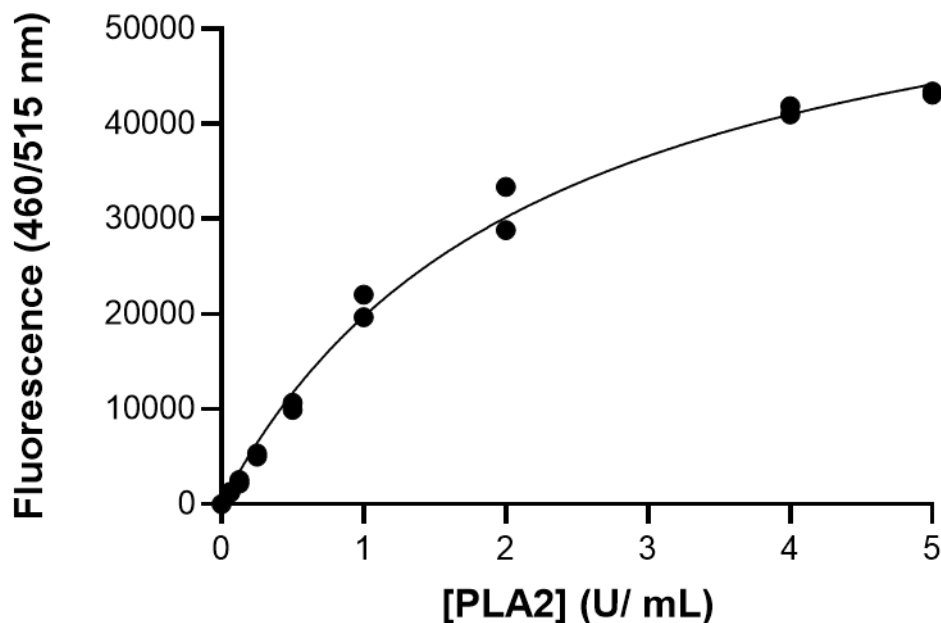


Figure 11. Example standard curve used to determine PLA₂ activity in samples. All values are corrected for background fluorescence. Data shown is the mean of one experiment performed in duplicate.

2.3.5 Nano-LC mass spectrometry

This methodology was performed by Dr Kate Heesom (Proteomics Facility, Biomedical Sciences Building, University of Bristol, Bristol, UK). The 10,000-50,000 MW HES sample was run on a 10% SDS-PAGE gel until the dye front had migrated approximately 1cm into the separating gel. The gel lane was then excised as a single slice and subjected to in-gel tryptic digestion using a DigestPro automated digestion unit (Intavis Ltd.).

The resulting peptides were fractionated using an Ultimate 3000 nano-LC system in line with an Orbitrap Fusion Lumos mass spectrometer (ThermoFisher Scientific, MA, USA). In brief, peptides in 1% (vol/vol) formic acid were injected onto an Acclaim PepMap C18 nano-trap column (ThermoFisher Scientific, MA, USA). After washing with 0.5% (vol/vol) acetonitrile 0.1% (vol/vol) formic acid peptides were resolved on a 250 mm × 75 μm Acclaim PepMap C18 reverse phase analytical column (ThermoFisher Scientific, MA, USA) over a 150 min organic gradient, using 7 gradient segments (1-6% solvent B over 1min., 6-15% B over 58min., 15-32%B over 58min., 32-40%B over 5min., 40-90%B over 1min., held at 90%B for 6min and then reduced to 1%B over 1min.) with a flow rate of 300 nl min⁻¹. Solvent A was 0.1% formic acid and Solvent B was aqueous 80% acetonitrile in 0.1% formic acid. Peptides were ionized by nano-electrospray ionization at 2.2 kV using a stainless-steel emitter with an internal diameter of 30 μm (ThermoFisher Scientific, MA, USA) and a capillary temperature of 300°C.

All spectra were acquired using an Orbitrap Fusion Lumos mass spectrometer controlled by Xcalibur 3.0 software (ThermoFisher Scientific, MA, USA) and operated in data-dependent acquisition mode. FTMS1 spectra were collected at a resolution of 120 000 over a scan range (m/z) of 350-1550, with an automatic gain control (AGC) target of 4E5 and a max injection time of 50ms. Precursors were filtered according to charge state (to include charge states 2-7), with monoisotopic peak determination set to peptide and using an intensity threshold of 1E3. Previously interrogated precursors were excluded using a dynamic window (40s +/-10ppm). The MS2 precursors were isolated with a quadrupole isolation window of 0.7m/z. ITMS2 spectra were collected with an AGC target of 2E4, max injection time of 35ms and HCD collision energy of 30%.

2.3.5.1 Proteomic data analysis

The raw proteomic data analysis was performed by Dr Kate Heesom (Proteomics Facility, Biomedical Sciences Building, University of Bristol, Bristol, UK). The raw data files were processed and quantified using Proteome Discoverer software v2.1 (Thermo Scientific) and searched against the UniProt *Heligmosomoides polygyrus* database (downloaded February 2024; 31791 sequences) using the SEQUEST HT algorithm. Peptide precursor mass tolerance was set at 10ppm, and MS/MS tolerance was set at 0.6Da. Search criteria included oxidation of methionine (+15.995Da), acetylation of the protein N-terminus (+42.011Da) and Methionine loss plus acetylation of the protein N-terminus (-89.03Da) as variable modifications and carbamidomethylation of cysteine (+57.021Da) as a fixed modification. Searches were performed with full tryptic digestion and a maximum of 2 missed cleavages were allowed. The reverse database search option was enabled and all data was filtered to satisfy false discovery rate (FDR) of 5%.

To determine GO terms, the accession gene IDs were inputted into g:Profiler using the g:GO functional profiling tool and searched against the *H. polygyrus* genome (PRJEB15396) (218). Uniqueness of protein expression to *H. polygyrus* was also determined in g:Profiler. Signal peptide sites were predicted using SignalP 6.0 (219).

2.4 *In vivo* Experiments

2.4.1 Animal husbandry

All animal experiments were conducted with Cardiff University Animal Welfare and Ethical Review Board (AWERB) approval, in accordance with UK Home Office regulations and under valid Personal and Project licences (PIL: I94048829 and PPL: PP8622667). Mice received free access to standard animal diet unless otherwise stated and water, with a maximum of six mice of the same sex housed per cage. Appropriate environmental enrichment was provided for experimental animals, with regular health and well-being inspections occurring in accordance with regulatory requirements. Tick@Lab software (A-Tune Software Inc, USA) was used for population management.

2.4.2 AOM/DSS model

The azoxymethane (AOM)/dextran sodium sulfate (DSS) was chosen as a model of CAC as it is a reproducible and relatively inexpensive model which utilises chemical induction of DNA damage followed by repeated cycles of colitis (220). We followed an established AOM/DSS protocol published by Parang *et al*, (158) with a basic schematic outlining the protocol shown in **Figure 12**.

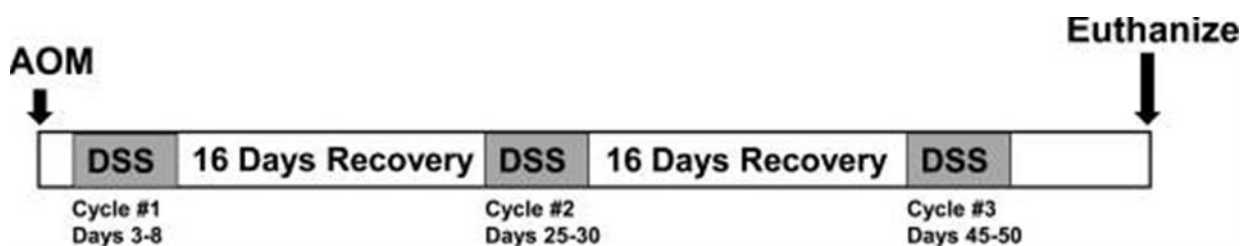


Figure 12. Schematic timeline for AOM/DSS induced inflammatory carcinogenesis. Adapted using information from Parang, *et al* 2016

Female 6-8 week old BALB/c mice (Charles River) were housed for one week prior to initiation of experiment to climatise. The mice were randomly allocated to a cage upon arrival which corresponded to the experimental condition. The infected group were given 200 *H. polygyrus* L3 using a 21-gauge oral gavage needle in 200 μ L sterile water, with the non-infected group receiving just sterile water. All mice were maintained on a modified pro-inflammatory high sucrose American Institute of Nutrition (AIN)-76A rodent diet (221) with a high ω -6: ω -3 ratio of 120:1 (Product #D16083101, ResearchDiets,

USA) for one week before helminth infection. The diet composition is shown in **Table 18** showing how the mAIN-76A diet differs from the standard chow diet. AOM (Merck Life Science Ltd, Cat #A5486-25MG) was administered intraperitoneally (i.p.) at a dose of 10 mg/kg followed by three fortnightly 7 day cycles of 2% 40,000-50,000 MW DSS (Fisher Scientific Ltd, Cat #J14489.22) in the water. EP2 and EP4 inhibitors PF-04418948 and ONO-AE3-208 were given i.p. at a dose 10mg/kg at day -10, -7, -4 and -1 before AOM administration, with control mice receiving 200 μ L 1:1 DMOS:PBS i.p. as a vehicle control. Mice were monitored daily for weight loss, physical, and behavioural changes and were immediately euthanised if the humane endpoint was reached.

Table 18. Composition of rodent diets.

Diet	Standard Laboratory Chow		Modified AIN-76A	
	g/kg	g%	g/kg	g%
Protein	225	22.5	200	20 (casein)
Carbohydrate	509	50.9	660	66 (corn starch, sucrose, cellulose)
Fiber	44	4.4	50	5 (all cellulose)
Fat	42	4.2	50	5 (sunflower oil, high linoleic)
Ingredient	g/kg	g%	g/kg	g%
Linoleic acid (ω-6)	12.6	1.26	30.1	3.01
α-linoleic acid (ω-3)	1.7	0.17	0.25	0.025
ω-6:ω-3 ratio	25:3		120:4	

2.4.3 Tissue harvest and processing

Once mice reached the end-point of the experiment or an ethical related humane endpoint (**Table 19**), mice were culled using a Schedule 1 approved method and colon tissue immediately dissected and harvested. Approximately 0.2 cm sections of tissue were stored in either RIPA buffer or Trizol reagent (ThermoFisher Scientific, MA, USA) at -80°C for subsequent protein and RNA extractions respectively.

Table 19. Clinical scoring chart to prevent suffering of pre-clinical models. The chart was used to monitor all animal models included in this thesis, according to guidelines stipulated in the AWERB- and Home Office-approved project licence. Experimental animals were regularly monitored and scored against the morbidity chart. Clinical illness severity score: 1-2 observe daily, 3-6 examine daily, >6 cull by Schedule 1 method.

Parameter	Animal ID	Score
Appearance	General lack of grooming	1
	Staring coat, ocular and nasal discharges	2
	Piloerection, hunched up	3
Food and water intake	5% weight loss	1
	Up to 10% weight loss	2
	Up to 15% weight loss	3
Natural behaviour	Minor changes e.g. lack of nest	1
	Less mobile and alert, isolated	2
Provoked behaviour	Minor depression or exaggerated response	1
	Moderate change in expected behaviour	2
Tumour growth	Discharge	3
	Ulceration	3
	Redness	3
Foot lesion	Impaired motility	3

2.4.4 Immunohistochemistry

For tumour burden quantification and immunohistochemical staining, the entire colon was removed from below the caecum to the anus, measured, weighed, and flushed with PBS and opened longitudinally before rolling around a toothpick and fixing in 100% ethanol overnight at 4°C. Following overnight incubation, ethanol-fixed tissues were transferred to the Cardiff University School of Biosciences Bioimaging Research Hub for paraffin embedding, sectioning, and haematoxylin and eosin (H&E) staining. Mounted Hematoxylin and eosin (H&E) stained tissues were scanned and digitised using an Olympus Slide Scanner (Olympus Corp, Japan). Infiltrating immune cells were quantified using ImageJ using the Cell Concentration Calculator plugin (222). Histological severity score was performed to evaluate the grade of malignant tissue transformation (223) (lymphocyte infiltration: 0 – normal, 3

– dense inflammatory infiltration; goblet cell hyperplasia: 0 – absent, 3 – severe; muscle thickening: base of crypts sits on the muscularis mucosae – 0, marked muscle thickening – 3). This was conducted blind, with the order of images being randomised before analysis.

2.4.5 Faecal calprotectin ELISA

The mouse S100A8 DuoSet enzyme-linked immunosorbent assay (ELISA) (R&D systems, Cat #DY3059) was purchased as it has previously been used to quantify calprotectin in the faecal material (224, 225). This is a sandwich ELISA, with the mechanism detailed in **Figure 13**.

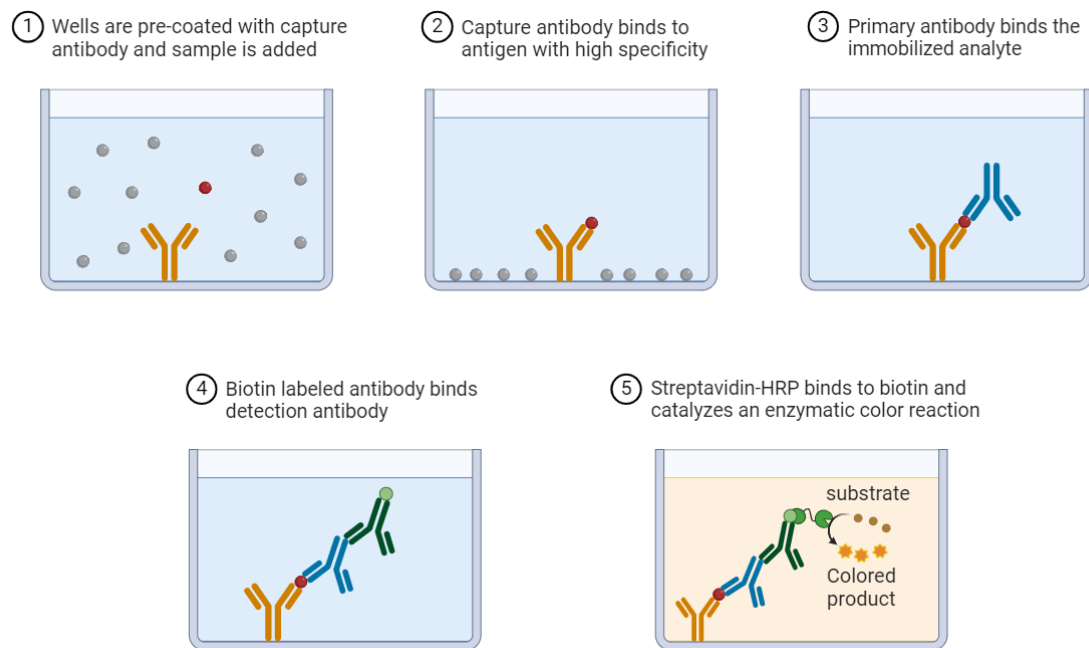


Figure 13. General concept of sandwich ELISA. Image created in Biorender.com

Faecal samples were first weighed, then homogenised in PBS + 0.1% Tween-20 (PBS-T) for 15 mins before being centrifuged at $22,500 \times g$ for 10 mins at 4°C . The supernatant was removed and stored at -80°C before performing the ELISA. To prepare the ELISA plate, each well was coated with $100 \mu\text{L}$ rat anti-mouse S100A8/S100A9 heterodimer capture antibody (give clone number) then covered with a plate sealer and incubated overnight at room temperature. The capture antibody was then aspirated and wells thoroughly washed with wash buffer (0.05% PBS-T). After 3x washes, wells were blocked with $300 \mu\text{L}$ 0.1% PBS-T and incubated at room temperature for 1 hr. Wells were again washed with wash buffer and then $100 \mu\text{L}$ of samples and standards were added in duplicate. To prepare the standard curve, a 2-fold dilution series of recombinant mouse S100A8/S100A9 heterodimer standard was prepared in 0.1% PBS-T ranging from 31.2 to 2,000 pg/mL . A negative control of 0.1% PBS-T alone was included, with values from these wells subtracted from all values to account for background fluorescence. After samples and standards were added, the plate was covered and incubated at room

temperature for 2 hrs before being washed. 100 μL of biotinylated goat anti-mouse S100A8/S100A9 heterodimer detection antibody (give clone number) was added to each well, incubated for room temperature for 2 hrs then washed. Next, 100 μL of streptavidin-horseradish peroxidase (HRP) was added to each well and incubated for 20 mins in the dark, then washed before 100 μL of substrate solution (1:1 mixture of Colour Reagent A (H_2O_2) and Colour Reagent B (Tetramethylbenzidine) was added and incubated in the dark for a further 20 mins. Finally, 50 μL of stop solution ($2\text{NH}_2\text{SO}_4$) was added to each well before absorbance was immediately read using a plate reader (Tecan Infinite M200 Pro) set to 450 nm. Concentrations of faecal calprotectin in each sample was determined using the standard curve (**Figure 14**), with the sample weights used to standardised concentrations to pg/mg.

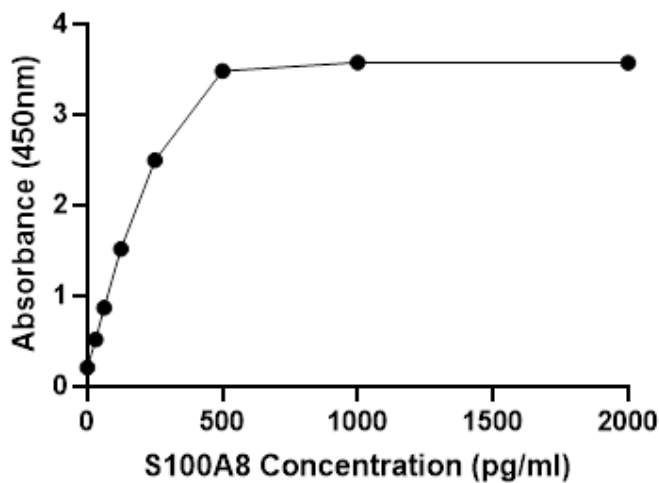


Figure 14. Example standard curve used to determine S100A8 concentrations in samples. All values are corrected for background fluorescence. Data shown is the mean of one experiment performed in duplicate. Data presented as Mean \pm SD. Graph generated using GraphPad Prism

2.5 RNA expression: RNA sequencing data (RNASeq)

2.5.1 Sample collection and quality control

Ten Female 6-8 week old BALB/c mice (Charles River) were randomly divided into two cages of five mice upon arrival and immediately fed the mAIN-76A diet. After one week of acclimatisation, one group of five were infected with 200 L3 *H. polygyrus* larvae in sterile water by oral gavage, with the other group given 200 μL sterile water alone as a control. After two weeks, mice were culled by Schedule 1 and 0.5 cm of the distal colon taken and immediately stored in RNAprotect tissue reagent (Qiagen, Cat #76104) at -80°C overnight ready for RNA extraction. RNA was extracted from samples using the RNeasy Mini Kit (Qiagen, Cat #Q10210) following the manufacturer guidance. Briefly, samples were first homogenised using the BeadBugTM as previously described (section 2.2.2.1). The

lysate is then loaded onto the RNeasy silica membrane and RNA binds to the silica membrane, and all contaminants are efficiently washed away. Residual DNA is removed using on-column RNase-Free DNase treatment (Qiagen, Cat #79254). The pure RNA is eluted in nuclease free water. After extraction, RNA yield was quantified using the Qubit™ RNA BR assay kit (ThermoFisher, MA, USA, Cat #Q10210), and DNA yield by using the Qubit™ DNA BR assay kit (ThermoFisher, MA, USA, Cat #Q33265) to estimate the percentage of DNA contamination. Samples were loaded onto the Nanodrop-1000 spectrophotometer (ThermoFisher, MA, USA) with 260/280 and 260/230 used to estimate sample purity, with ratios > 1.8 being acceptable. TapeStation software (Agilent) was used to show the ribosomal integrity number (RIN), with values > 4 acceptable for sequencing. Samples were made up to a final concentration of 20 ng/μL in nuclease free water and sent to Novogene on dry ice for sequencing.

2.5.2 Library construction, quality control and sequencing

The library construction, quality control and sequencing was performed by Novogene. Messenger RNA (mRNA) was purified from total RNA using poly-T oligo-attached magnetic beads. After fragmentation, the first strand cDNA was synthesized using random hexamer primers, followed by the second strand cDNA synthesis using either dUTP for directional library or dTTP for non-directional library (226). For the non-directional library, it was ready after end repair, A-tailing, adapter ligation, size selection, amplification, and purification. For the directional library, it was ready after end repair, A-tailing, adapter ligation, size selection, USER enzyme digestion, amplification, and purification. The read depth selected was 30 million reads per sample, with 150 paired-end reads (227).

2.5.3 Bioinformatic analysis pipeline

The analysis pipeline is adopted from nf-core/rnaseq (228) and summarised in **Figure 15**. The pipeline was run using the Unix operating system MobaXterm.

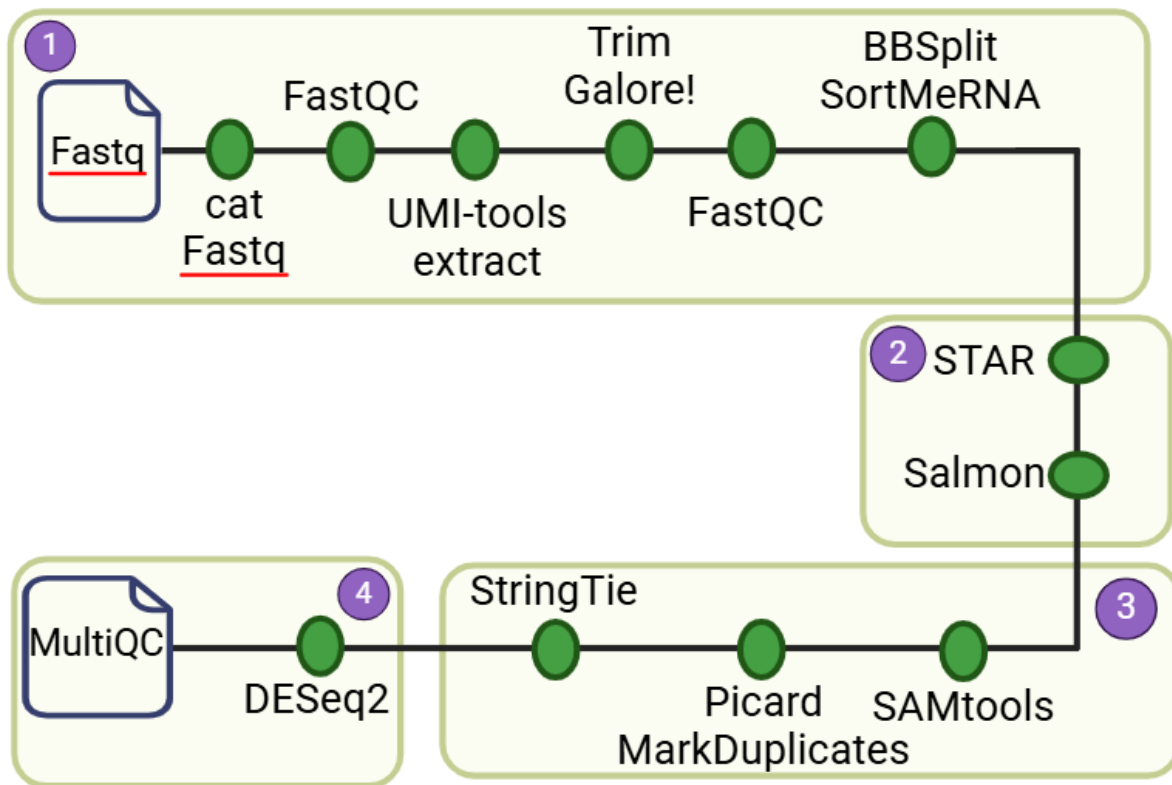


Figure 15. RNA-seq bioinformatic analysis pipeline. 1. Data pre-processing. 2. Genome alignment and quantification. 3. Data post-processing. 4. Final QC. Adapted from nf-core/rnaseq.

2.5.3.1 Data quality control

Raw data (raw reads) of fastq format were first merged using the (cat) command, then the initial QC is checked using the FastQC command line (229). The unique molecular identifiers (UMI) were extracted using the UMI-tools package and the (extract) command, to enable duplicate reads to be removed (230). The raw reads are then trimmed using the Trim Galore! script (231) to remove low-quality bases and residual adapter contamination. After trimming, the data QC is checked again using the FastQC command line to see how trimming has improved the data QC. Genome contaminants were removed using the BBSplit tool (232), then ribosomal RNA was removed using the SortMeRNA tool (233) to prepare the read counts for genome mapping.

2.5.3.2 Reads mapping to the reference genome

The *Mus musculus* BALB_cj_v1 (GCA_001632525.1) reference genome and gene model annotation files were downloaded from Ensemble (EMBL-EBI). To align the RNA-seq data to the *Mus musculus* BALB_cj_v1 genome, the free open sourced software Spliced Transcripts Alignment to a Reference (STAR) was chosen, as it is shown to outperform other aligners by a factor of > 50 in mapping speed, while at the same time improving alignment sensitivity and precision (234). To quantify the expression

of transcripts from the mapped RNA-seq data, the Salmon tool was used due to its high accuracy of abundance estimates and sensitivity compared to other methods (235).

2.5.3.3 Reads indexing, sorting and final QC

The alignments were sorted and indexed using SAMtools, allowing identification of where each read originated in the transcriptome (236). Duplicate reads were marked using the picard MarkDuplicates command line (237), with the resulting alignment assembled using StringTie (238). The DESeq2 package was used to perform the final QC step, performing principle component analysis (PCA) and comparison of gene expression levels between samples (239), with the overall QC results being compiled into a MultiQC report for inspection.

2.5.3.4 Differential expression analysis

Differential expression analysis of two conditions/groups (two biological replicates per condition) was performed using the DESeq2Rpackage (1.20.0) (239, 240). DESeq2 provide statistical routines for determining differential expression in digital gene expression data using a model based on the negative binomial distribution. The resulting p-values were adjusted using the Benjamini and Hochberg's approach, which is built in to the DESeq2Rpackage, for controlling the false discovery rate, to reduce the proportion of false positives. Genes with an adjusted p-value ≤ 0.05 found by DESeq2 were assigned as differentially expressed.

2.5.3.5 Enrichment analysis of differentially expressed genes

Gene Ontology (GO) enrichment analysis of differentially expressed genes was implemented by the clusterProfiler R package, in which gene length bias was corrected (241). Genes were annotated with their biological process (BP) and molecular function (MF) (242). GO terms with corrected P-value less than 0.05 were considered significantly enriched by differential expressed genes.

Gene Set Enrichment Analysis (GSEA) v 4.3.3 is a computational method for exploring whether a given gene set is significantly enriched in a group of gene markers ranked by their relevance with a phenotype of interest (243). The curated mouse-orthologue hallmark gene set (243) was used to compare enriched pathways in *H. polygyrus* infected mice compared to naïve. In addition, the gene sets with fewer than 1 gene or more than 1000 genes were excluded. The phenotype label was set as *H. polygyrus* infection versus naïve. The t-statistic mean of the genes was computed in each hallmark pathway using a permutation test with 1,000 replications. The upregulated pathways were defined by a normalized enrichment score (NES) 0 - 1, and the downregulated pathways were defined by an NES 0 - -1. Pathways with an FDR P value ≤ 1 were considered significantly enriched.

Leading edge analysis was performed using the leading edge analysis tool in GSEA v 4.3.3, and works by analysing the enrichment scores to identify the leading edge subset of genes in each enriched gene set.

2.5.5.6 Kaplan-Meier plotter

The relationship between enriched gene expression levels and prognosis of CRC patients was analysed using the Kaplan-Meier plotter (KM plotter) (244). The CRC KM plotter database contains data from 1,336 patients, with the analysis being run on all patient subtypes.

2.5.3.7 Immune cell population analysis

To estimate the abundance of immune cells, we used CIBERSORTx, an analytical tool to estimate abundances of immune cells in a mixed cell population without physical and expensive cell isolation (245). Using the impute cell fractions analysis mode, the transcriptome data was inputted as a mixture file and utilised a publicly available bulk RNA-seq dataset containing markers for 178 cell types obtained from C57BL/6 as part of the Immunological genome project (246-251). The analysis was run in absolute mode to compare all samples to all cell types.

2.6 Computational Studies

2.6.1 Molecular modelling and docking studies

All molecular modelling experiments were performed on Asus WS X299 PRO Intel® i9-10980XE CPU @ 3.00 GHz × 36 running Ubuntu 18.04 (graphic card: GeForce RTX 2080 Ti). Molecular Operating Environment (MOE) 2022.02 and Maestro (Schrodinger Release 2023-4) were used as molecular modelling software (252, 253). The crystal structure of the *H. polygyrus* PLA₂ protein was predicted using Iterative Threading ASSEmbly Refinement (I-TASSER) protein threading software (254). The protein was prepared using the MOE Protein Preparation tools, and saved in .mae format to be used in Maestro for docking simulations. The protein in.mae format was processed using the Schrodinger Protein Preparation wizard Wizard by adding hydrogens. A 9 Å docking grid was created for subsequent docking analysis. A high throughput virtual screening was then performed using a SPECS library consisting of 897,105 structures, keeping the default parameters and setting 1 as the number of output poses per input ligand to include. The highest scoring 750,000 compounds were scored using Glide extra precision (XP), with the highest scoring 500,000 being rescored using Protein-Ligand ANT System (PLANTS) and ScorePose functions (255, 256). The values of the three different scoring functions for each docking pose were then analysed together (consensus score) and only the docking poses falling in the top 25% of the score value range in all the three scoring functions were selected for the final

visual inspection. In total, 16,917 compounds were selected for visual screening. The visual inspection process, conducted as last step of the structure-based virtual screening, was performed using MOE 2022.02. The docking poses of the compounds obtained from the consensus score procedure were evaluated considering the following criteria:

- Ability of a compound to overall occupy the binding site;
- Number of interactions formed between the compound and specific residues in the active site (calcium, histidine, and aspartic acid)
- Coverage of different chemical scaffolds, discarding similar chemical entities

From the 16,917 compounds, 358 were selected for the final screening. The absorption, distribution, metabolism, and excretion (ADME) pharmacokinetic properties of each compound were evaluated using SwissADME screening software (257). The following criteria had to be met for the compound to be accepted:

- Complying with the Lipinski rule of 5;
- No pan assay interference compounds (PAINS);
- LogP > 2

The 10 compounds with the optimal ADME properties were purchased from the Specs library.

2.6.2 Bioinformatic sequence analysis

Sequence analysis and alignments were performed using NCBI blast and Clustal Omega (258, 259). For searches against specific sequences of the Hpb genome (PRJEB15396), WormBase Parasite (<https://parasite.wormbase.org/index.html>) was used. Sequences for human and murine enzymes were obtained in UniProt (260). Those sequences with $\geq 50\%$ identity to the human and murine enzymes, or had 100% conservation within the human and murine active sites were considered significant. To map the 3D structures together and analyse the active site configuration, PyMol software was used (261). Signal peptide sites were predicted using SignalP 6.0 (219). The subcellular locations of unknown proteins was predicted using DeepLoc 2.0 (262).

2.7 Statistical analysis

GraphPad Prism 10.2.0 (GraphPad, CA, USA) was used to analyse and present the data. Results are expressed as Mean \pm SEM. For each statistical analysis presented as part of this thesis, data was first tested for normality using GraphPad Prism 10.2.0 software to run a Shapiro-Wilk standard deviation

normality test and a quantile-quantile (QQ) plot graphical test for 37 normality. An unpaired T-test was performed comparing groups, with a Mann-Whitney post-hoc test performed when data was not normally distributed. Significance was expressed as * $p \leq 0.05$, ** $p \leq 0.01$, *** $p \leq 0.005$, **** $p \leq 0.001$. Where no statistical comparison is shown the result was not significant.

Chapter 3: Role of prostaglandin signalling in helminth exacerbation of CAC

3.1 Introduction

Research from our lab has recently shown that combining infection with the murine helminth *Heligmosomoides polygyrus bakeri* with a high ω -6: ω -3 ratio diet exacerbates tumour development in a murine model of colitis-associated colorectal cancer (CAC) (190). Prostaglandin receptor signalling was implicated playing a role in helminth exacerbation of disease, as aspirin treatment of helminth infected mice significantly reduced tumour burden in this model (**Figure 1A&B**) (190). Furthermore, the administration of a prostaglandin E₂ receptor agonist to mice fed a high ω -6: ω -3 ratio before initiation of disease increased tumour burden to the levels seen following helminth infection of mice fed this diet (**Figure 1C&D**) (190).

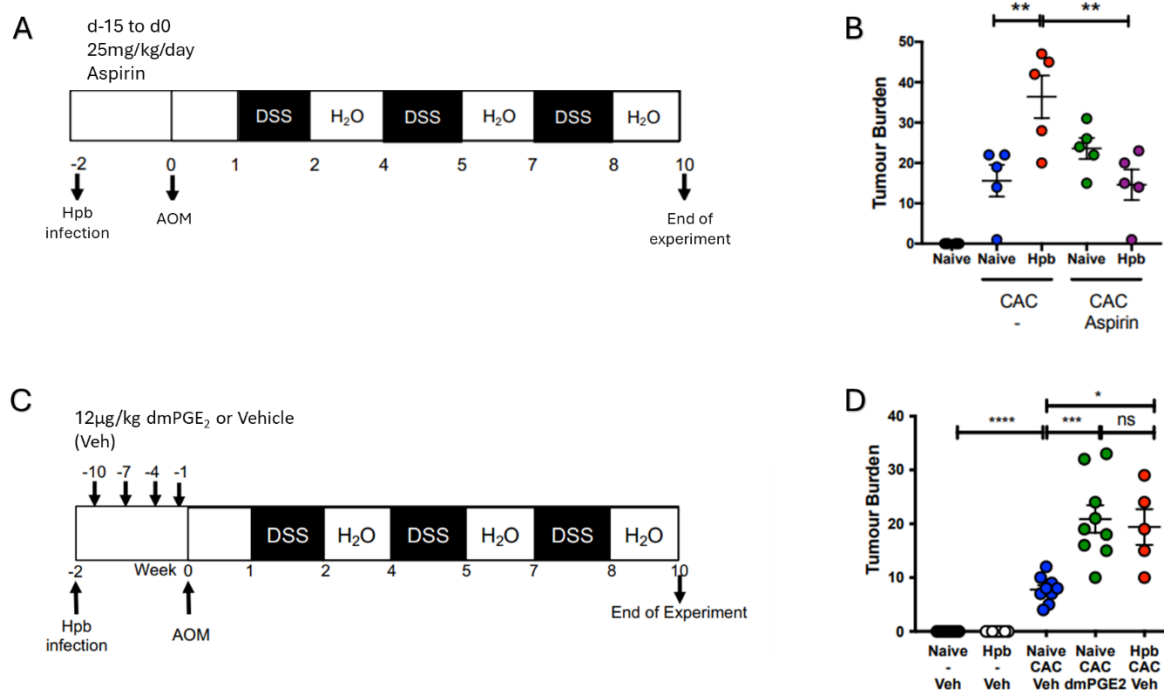


Figure 1. Experiments supporting the role for PGE₂ receptor signalling in *H. polygyrus* exacerbation of CAC. Mice fed a high ω -6: ω -3 ratio diet were given 25 mg/kg/day aspirin in the drinking water from day -15 to day 0 of *H. polygyrus* infection, or the equivalent time to uninfected (naive) mice. At day 0, aspirin-treated mice were placed onto water and CAC initiated by administering 10 mg/kg azoxymethane (AOM), followed by three fortnightly cycles of 2% dextran sulfate sodium (DSS) in the drinking water. **(A)** Tumour burden was quantified in the colon at day 59 following administration of AOM **(B)**. Mice fed a high ω -6: ω -3 ratio diet were administered 16,16-dimethyl-PGE₂ (dmPGE₂) i.p. at 12 µg/kg at day -10, -7, -4, and -1, or a vehicle control (Veh) before AOM administration at day 0, followed by three fortnightly cycles of 2% DSS in the drinking water **(C)**. Tumour burden was determined at day 61 following administration of AOM **(D)**. Experiments shown are one representative from two experiments with $n \geq 4$ mice/group **(C)** or pooled data from two separate experiments with $n \geq 4$ mice/group **(D)**. Unpaired T-test * $p < 0.05$, ** $p < 0.01$, *** $p < 0.001$, **** $p < 0.0001$, error bars SEM. Data taken from Smith *et al.*, 2025.

Although these data provided evidence that the helminth increases in tumour burden may occur due to increased prostaglandin receptor signalling, it was not clear whether this occurred following helminth infection, if this process was linked to helminth-dependent increases in tumour burden, nor how helminth infection may promote prostaglandin signalling *in vivo*.

3.1.1 Relationship of prostaglandin E₂ signalling with colitis-associated colorectal cancer

Accumulating evidence indicates that breakdown of the protective mucosal barrier of the gut, known as “leaky-gut syndrome”, plays a role in CAC development in both human disease and animal models, leading to increased intestinal inflammation and a favourable environment for mutations to occur

(263). Clinical and pre-clinical experimental data has implicated the prostaglandin E₂ (PGE₂) signalling pathway as playing a predominant role in promoting this “leaky-gut” phenotype, marked by decreased expression of tight junction proteins such as E-cadherin (108, 109, 264, 265). PGE₂ signalling through the EP2 and EP4 receptors has been implicated in promoting colon cancer development and increased intestinal permeability (109, 264, 266). Studies have shown that PGE₂ signalling through EP2 and EP4 can lead to the downregulation of E-cadherin and increased cell permeability (267, 268), or increased cancer cell detachment and invasion (106, 269, 270).

One of the mechanisms by which PGE₂ EP2/EP4 signalling has been implicated in carcinogenesis is through activation of β -catenin signalling, with phosphorylation of β -catenin at the Serine 552 site ($\rho\beta$ -catenin Ser⁵⁵²) noted as a key molecular event (269, 271, 272). Importantly, a relationship between PGE₂ signalling and $\rho\beta$ -catenin Ser⁵⁵² in intestinal carcinogenesis has been shown. PGE₂ promoted tumour development in an APC^{min/+} model through PGE₂ receptor signalling-dependent $\rho\beta$ -catenin Ser⁵⁵² (273). Furthermore, nuclear expression levels of $\rho\beta$ -catenin Ser⁵⁵² were linked with worsening progression of disease in the AOM/DSS model of CAC (274).

A further mechanism linking PGE₂ EP2/EP4 signalling to exacerbation of CAC is an increase in intestinal inflammation, with dysregulated signalling leading to chronic inflammation as indicated by an increase in faecal calprotectin concentration (266, 275, 276). Faecal calprotectin is predominantly released from neutrophils that accumulate at the site of inflammation, in this instance the colon, during disturbance of the mucosal architecture, and is also the gold-standard biomarker used in the clinic to assess the severity of colitis (277-279). As well as being used in the clinic, faecal calprotectin concentrations have also been used to quantify intestinal inflammation during the AOM/DSS model, with Rafique *et al* observing significant increases compared to an untreated group (280). It is not yet known whether Hpb exacerbation of CAC requires EP2/4-dependent regulation of E-cadherin and increased inflammation, via ρ of β -catenin Ser⁵⁵²

3.1.2 How might helminths modify intestinal permeability and drive CAC?

Loss of E-cadherin expression has been observed by Su *et al* as a consequence of *H. polygyrus* infection, which resulted in a decrease in E-cadherin expression and re-distribution in the colon at day 7 post-infection, accompanied by an increase in epithelial permeability (165). Su *et al* revealed that this impact on E-cadherin and epithelial permeability was dependent on STAT6-dependent activation of CD4⁺ T cells (165). Additionally, Shea-Donohue *et al* describe the host release of interleukin-4 (IL-4) as mediating the effect of *H. polygyrus* on the intestinal epithelial barrier (164). Both these studies highlight the importance of the host immune response to live infection in the breakdown of epithelial

barriers. However, several studies have highlighted the importance of the excretory/secretory products (ESPs) in disrupting epithelial barriers, independently of the immune system (168, 169).

Both the ESPs of larval *Trichuris suis* and *Schistosoma mansoni* ova contain PGE₂ (194, 196), although it is not known how secretion influences intestinal permeability. In addition, both the larval cysts of *Taenia solium* and the larval extract of *H. polygyrus* were shown to contain a glutamate dehydrogenase, which was found to promote PGE₂ production by human monocyte-derived macrophages (13,14). Prodjinotho *et al* then went on to show that *T. solium*-dependent production of PGE₂ promoted induction of T regulatory cells through the EP2 and EP4 receptor (203), providing evidence that helminth-promotion of PGE₂ production can activate EP2 and EP4 receptor signalling. It is not yet known whether *H. polygyrus* ESPs promote cell permeability via EP2/4-dependent regulation of E-cadherin. With the evidence that live helminth infection may promote CAC by activating PGE₂ receptor signalling in the host, the overall aims of this chapter are to 1. determine whether helminth infection modifies EP signalling *in vivo*, 2. test whether EP receptor signalling contributes to the development of CAC by modifying intestinal permeability and, 3. determine whether this effect may be mediated through its secretions. This will be address through the following objectives:

3.2 Chapter aims

1. Determine whether helminth-exacerbation of tumour development is associated with increased prostaglandin E₂ signalling and increased intestinal permeability *in vivo*
2. Investigate whether helminth secretions drive CAC by promoting PGE₂ receptor activation-dependent increases in intestinal permeability

3.3 Hypothesis

1. *H. polygyrus* exacerbation of CAC is mediated through prostaglandin signalling-dependent increases in intestinal permeability
2. *H. polygyrus*-dependent increases in intestinal permeability are driven by a secreted factor that activates prostaglandin (EP2/EP4) signalling.

3.4 Results

3.4.1 *H. polygyrus* infection increases PGE₂ receptor activation in the colon at day 14 post-infection

Considering an established link between enhanced PGE₂ (EP) receptor activation and the development of colorectal cancer (266, 272, 281), the initial investigation focused on whether *H. polygyrus* infection leads to an increase in PGE₂ receptor activation at day 14 post-infection, coinciding with when CAC was

induced in the AOM/DSS model. Western blot analysis of total β -catenin and p β -catenin Ser⁵⁵² (both 92kDa) levels in the colon were compared between helminth infected and uninfected mice. I first confirmed that expression levels of total β -catenin did not significantly change across conditions by determining the ratio of total β -catenin to the loading control protein glyceraldehyde 3-phosphate dehydrogenase (GAPDH) (37kDa) (282) (**Figure 2A, B**). I then found a significant increase in the ratio of p β -catenin Ser⁵⁵² to total β -catenin following helminth infection, when compared to naïve controls (**Figure 2C**). This data suggests that *H. polygyrus* infection can activate PGE₂ receptor signalling in the colon, as indicated by the significant increase in p β -catenin Ser⁵⁵².

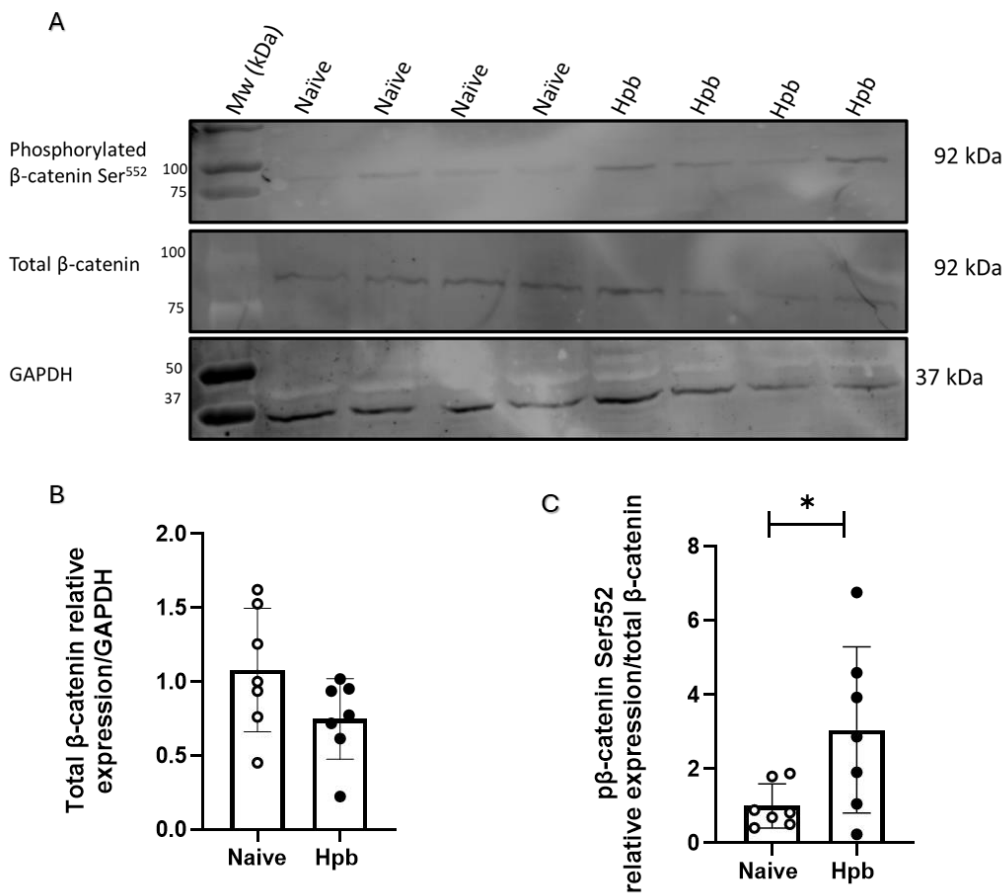


Figure 2. *H. polygyrus* infection causes a significant increase in phosphorylation of β -catenin Ser⁵⁵² *in vivo*. (A) Example western blot of total and p β -catenin Ser⁵⁵² (both 92kDa) compared to GAPDH (37kDa) from the colon of mice from day 14 following infection with *H. polygyrus*. (B) Graphical summary of the ratio of total β -catenin to GAPDH, expressed as a fold change relative to naive mice. (C) Graphical summary of the ratio of β -catenin Ser⁵⁵² normalised to total β -catenin and expressed as a fold change relative to naive mice. Data shown represents one independent experiment (Naive, n = 7; Hpb n = 7). Unpaired T-test, * p \leq 0.05, error bars Mean \pm SD.

3.4.2 *H. polygyrus* infection has no significant effect on E-cadherin expression in the colon at day 14 post-infection

Because increased EP activation has been associated with reduced E-Cadherin expression and alterations in intestinal permeability (267, 268), I then determined the impact of helminth infection on E-Cadherin expression in the colon at this time-point. Western blot analysis of E-cadherin (131 kDa) levels in the colon tissue revealed no significant difference in the ratio of E-cadherin to GAPDH between infected mice at day 14 post-infection, when compared to uninfected control mice at the same time point (Figure 3). Although sample size was limited, this result suggests that the expression of E-cadherin is not effected by *H. polygyrus* at this stage of infection.

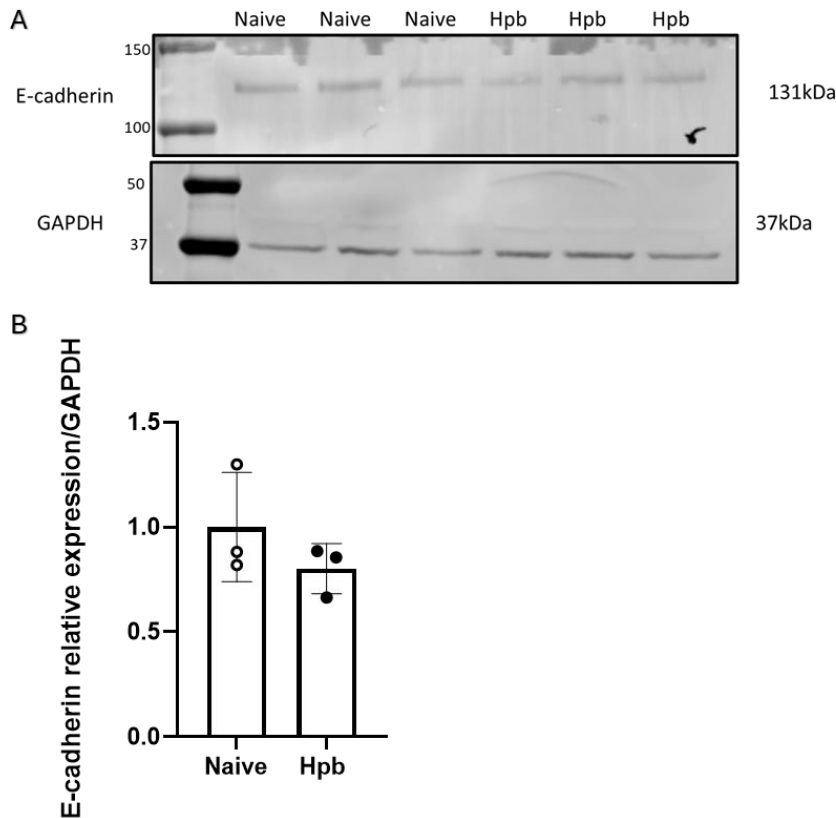


Figure 3. E-cadherin expression in the colon does not change at day 14 following *H. polygyrus* infection. Example western blot of E-cadherin (131 kDa) and GAPDH (37 kDa) from the colon of mice infected with *H. polygyrus* (Hpb) at day 14 post-infection (A) Graphical summary of the ratio of E-cadherin to GAPDH, expressed as a fold change relative to naïve mice (B). Data shown represents one independent experiment (Naïve, n = 3; Hpb n = 3). Unpaired T-test, error bars Mean ± SD.

3.4.3 *H. polygyrus* infection increases PGE₂ receptor activation in the colon in the AOM/DSS model

I then investigated whether helminth exacerbation of CAC may be due to increased PGE₂ signalling through the EP2 and EP4 receptors in the colon following helminth infection, as both have been shown to increase colorectal cancer cell development (266, 270, 281, 283). Western blot analysis of the colon of helminth infected and uninfected mice fed a high ω -6: ω -3 ratio diet was performed at day 64-post AOM administration. To demonstrate whether alterations PGE₂ signalling were mediated via EP2 and EP4 receptor signalling, the ratio of p β -catenin Ser⁵⁵² to total β -catenin was determined in helminth infected mice given 10mg/kg of the PGE₂ receptor 2 (EP2) and 4 (EP4) inhibitors (PF-04418948, ONO-AE3-208) i.p. at day -10, -7, -4 and -1 before AOM administration and compared to helminth infected mice given a vehicle control at the same time-points (Figure 4A).

Analysing the ratio of total β -catenin to GAPDH (37kDa), I found that expression levels of total β -catenin did not significantly change across conditions (**Figure 4C, E**). Following administration of AOM/DSS, there was no significant change in the levels of p β -catenin Ser⁵⁵² in naïve mice (**Figure 4D**). In line with my results from day 14-post-infection (**Figure 2C**), there was a significant increase in the ratio of p β -catenin Ser⁵⁵² to total β -catenin in helminth infected mice, when compared to naïve controls (**Figure 4D, E**). Administration of EP2 and EP4 receptor inhibitors to helminth infected mice completely prevented helminth infection-dependent increases in the ratio of p β -catenin Ser⁵⁵² to total β -catenin (**Figure 4D, E**), strongly suggesting that helminth infection can increase PGE2 signalling through EP2 and EP4.

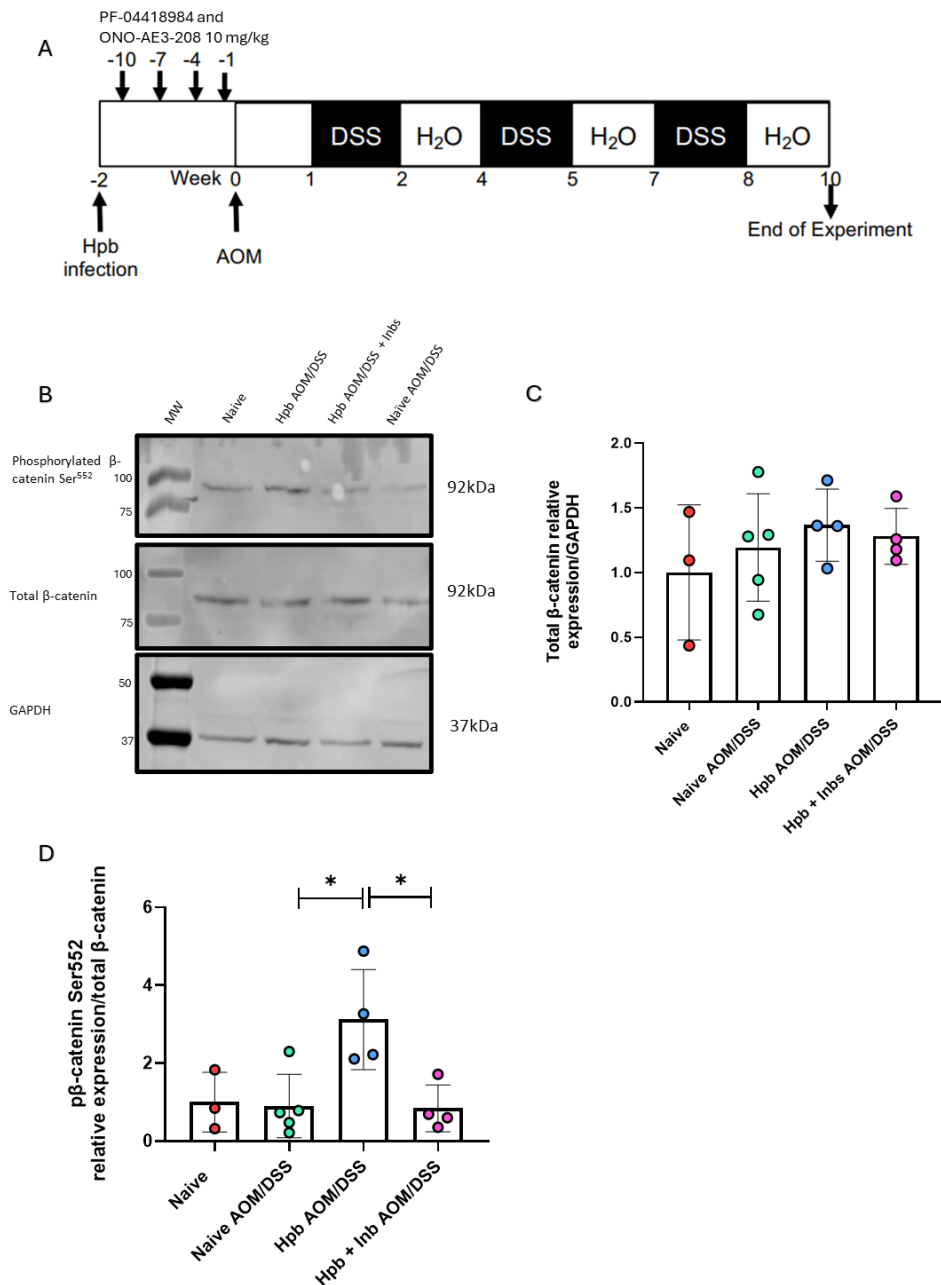


Figure 4. *H. polygyrus* infection causes a significant increase in EP2 and EP4-dependent phosphorylation of β -catenin Ser552 *in vivo*. (A) Mice infected with *H. polygyrus* (Hpb) were given 10 mg/kg of the EP2 and EP4 inhibitors (Inbs) PF-04418948 and ONO-AE3-208 i.p. at day -10, -7, -4, and -1 before AOM injection and initiation of CAC, or a vehicle control. Colon samples were taken at day 64 following administration of AOM. (B) Example western blot of total and p β -catenin Ser⁵⁵² (both 92kDa) and GAPDH (37kDa) from the colon of mice from each treatment condition at day 64 following administration of AOM. (C) Graphical summary of the ratio of total β -catenin to GAPDH, expressed as fold change relative to naïve animals. (D) Graphical summary of the ratio of p β -catenin Ser⁵⁵² to total β -catenin, expressed as a fold change relative to naïve animals. Data shown is one experiment with Naive, n = 3; Naive AOM/DSS, n = 5; Hpb AOM/DSS, n = 4; Hpb + Inb AOM/DSS, n = 4. Unpaired T-test * $p \leq 0.05$, error bars Mean \pm SD.

3.4.4 *H. polygyrus* infection decreased E-Cadherin expression in the colon in the AOM/DSS model

I found that E-cadherin levels did not change at day 14 following infection with *H. polygyrus*, despite an increase in p β -catenin Ser⁵⁵² (Figure 2). To determine whether this was the case after CAC onset, the ratio of E-cadherin expression to GAPDH expression was quantified in *H. polygyrus* infected mice 64 days post-administration of AOM and compared to control mice given vehicle. In contrast to day 14 post-infection (Figure 3), a significant reduction in the ratio of E-cadherin expression to GAPDH expression was observed in *H. polygyrus* infected mice in which CAC had been induced, when compared to naïve mice in which CAC had been induced (Figure 5). As EP2 and EP4 signalling has been linked to a decrease in E-cadherin expression (267, 268), I determined the ratio of E-cadherin expression to GAPDH following administration of EP2 and EP4 inhibitors to helminth infected mice. As shown in Figure 5, delivery of EP2 and EP4 inhibitors during helminth infection restored the ratio of E-cadherin expression to GAPDH at day 64 post-AOM to that seen in the naïve group at day 64 post-AOM, demonstrating the ability of *H. polygyrus* to decrease E-cadherin expression through PGE₂ EP2/EP4 receptor signalling.

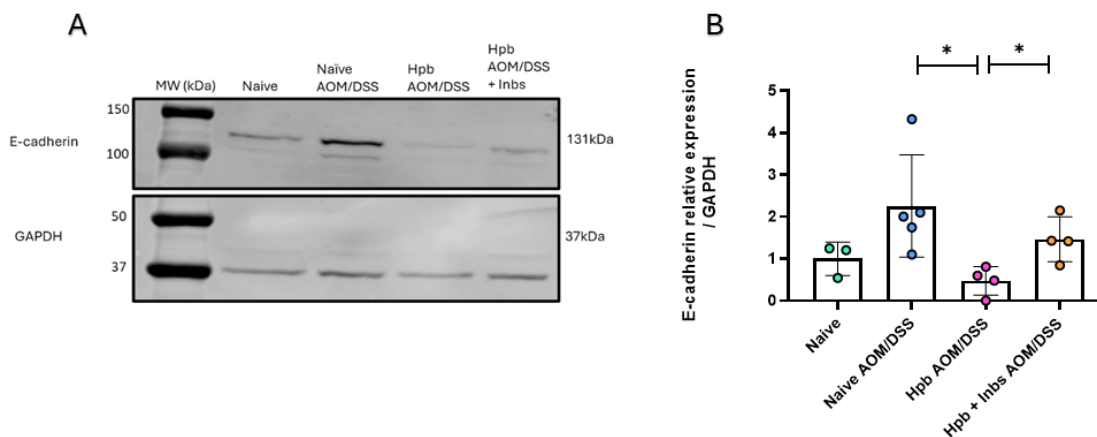


Figure 5. *H. polygyrus* infection causes a significant decrease in E-cadherin expression *in vivo* which is rescued by EP2 & EP4 inhibitors. (A) Example western blot of E-cadherin (131 kDa) and GAPDH (37kDa) from the colon of mice from each treatment condition at day 64 following administration of AOM. **(B)** Graphical summary of the ratio of E-cadherin to GAPDH, expressed as a fold change relative to naïve mice. Data shown represents one experiment (Naïve, n = 3; Naïve AOM/DSS, n = 5; Hpb AOM/DSS, n = 4; Hpb + Inb AOM/DSS, n = 4). Unpaired T-test, * p ≤ 0.05, error bars Mean ± SD.

3.4.5 Addition of EP2 & EP4 inhibitors during AOM/DSS model

So far in this chapter, an association between *H. polygyrus* infection and EP2 and EP4 receptor-dependent modulation of E-cadherin expression has been determined. To investigate whether this

pathway represents the mechanism by which *H. polygyrus* exacerbates CAC, the clinical symptoms of the AOM/DSS model were monitored following delivery of EP2 and EP4 inhibitors during helminth infection. Concerningly, no differences in weight loss or colon weight:length ratio were observed in naïve mice given AOM/DSS, when compared to naïve untreated mice (**Figure 6A, B**). Furthermore, there were no differences in weight loss and colon weight:length ratio disease between naïve and *H. polygyrus* infected mice in the AOM/DSS model (**Figure 6A, B**) and there were no visible tumours or colon shortening in any of the mice (**Figure 6C**), contradicting previous findings from our lab (190). An absence of these clinical signs and visible tumours limited the ability to determine whether inhibition of EP2 and EP4 receptor signalling had any impact on helminth-exacerbation of CAC.

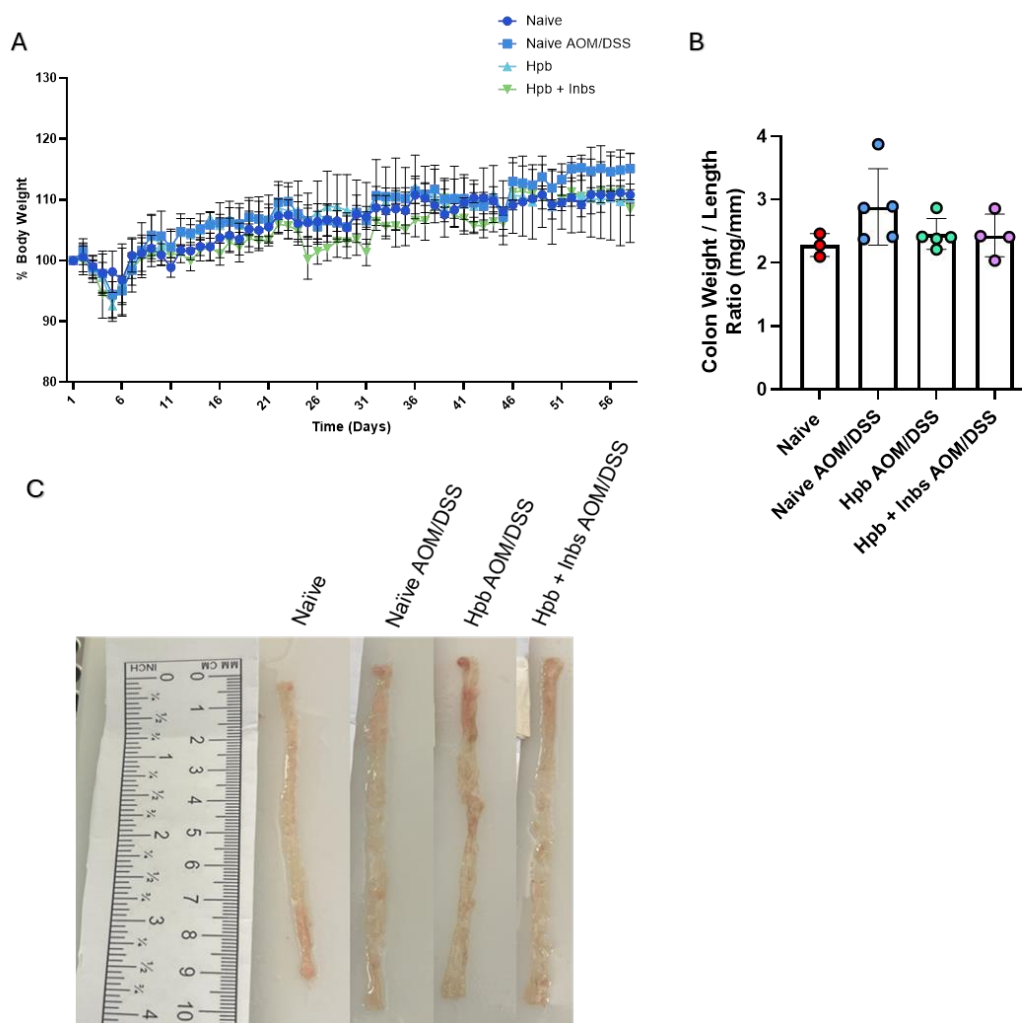


Figure 6. EP2/EP4 antagonist treatment had no effect on weight loss or colon weight/length ratio. (A) Weight loss was monitored throughout the experiment. **(B)** Colon length (mm) was determined at day 64 following administration of AOM, with **(C)** weight/length ratio calculated.

Impact of inhibitors on helminth-exacerbation of CAC were also evaluated through hematoxylin and eosin (H&E) immunohistochemical staining of the colon (**Figure 7A-E**). At sacrifice, a large area of pathology resembling a colonic polyp was observed on the luminal epithelium side in one section from one of the naïve mice in which CAC had been induced (**Figure 7B**). Closer magnification revealed structures resembling intertumoral crypt abscesses as well as hyperchromatic nuclei (**Figure 7C**). Furthermore, what appears to be a large inflammatory aggregate was observed on the luminal epithelium side in 1 out of 10 sections from 1 out of 4 *H. polygyrus* infected mice in which AOM/DSS had been induced (**Figure 7D**). Confirmation of whether these features are colonic tumours would require further analysis. Histologically, a significantly higher histology severity score, represented by high levels of goblet cell hyperplasia and large infiltration of inflammatory cells in stroma and submucosa (**Materials & Methods section 2.4.4**), was observed in the colon of both naïve and helminth treated mice in the AOM/DSS condition, when compared to naïve mice (**Figure 7B, D**). Administration of EP2 and EP4 inhibitors during helminth infection significantly reduced histology severity score, when compared to helminth infected mice given a vehicle control (**Figure 7F, G**). However, there was still some evidence of goblet cell hyperplasia and infiltrating immune cells in helminth infected mice treated with EP2/EP4 inhibitors, suggesting a level of intestinal inflammation remains (**Figure G**), possibly due to the *H. polygyrus* infection alone.

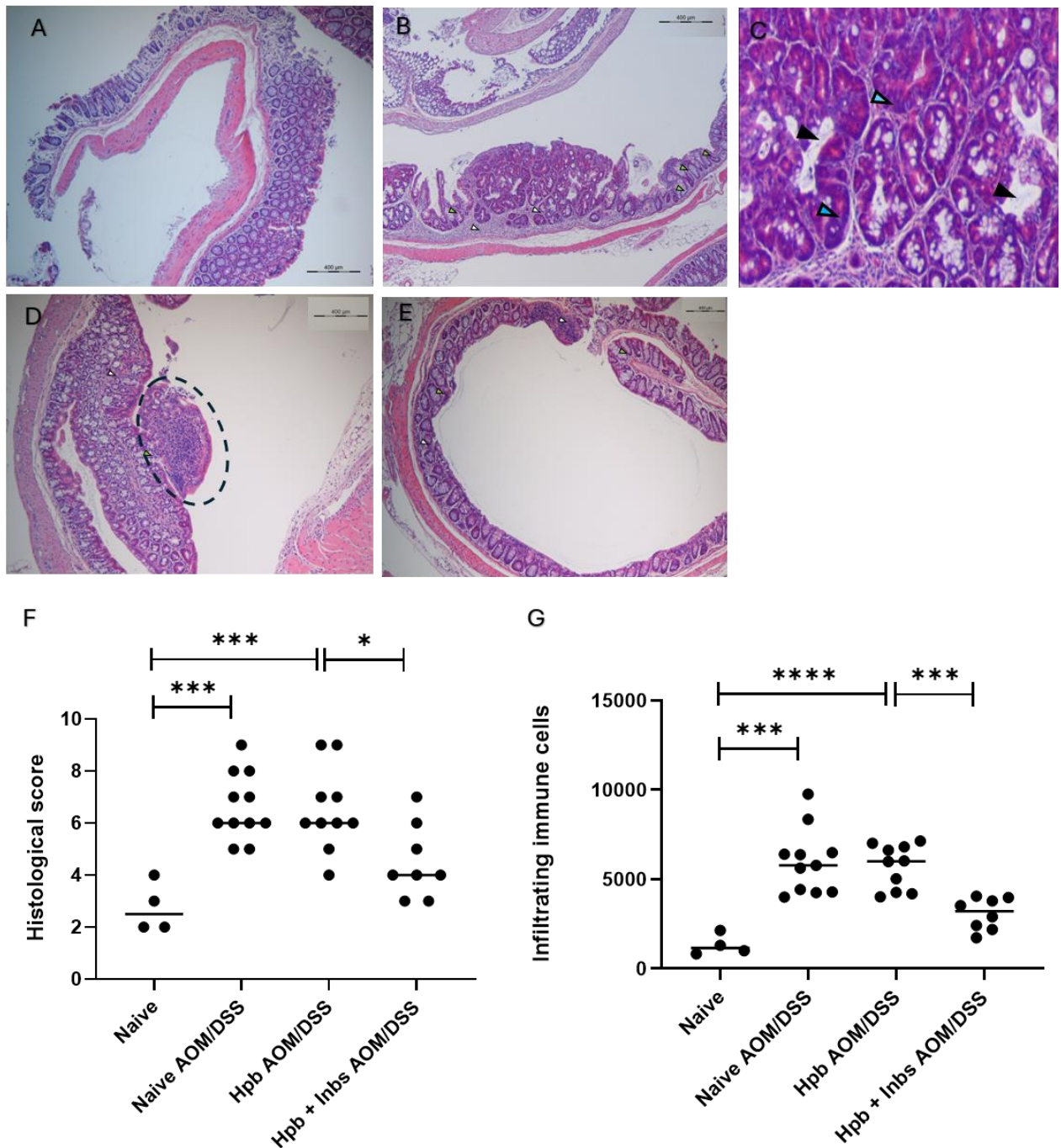


Figure 7. EP2/EP4 antagonist treatment reduces histological score and infiltrating immune cells during AOM/DSS in *H. polygyrus* infected colon. (A-E) Mice from each group were euthanised at day 64 post-administration of AOM and colon sections taken for H&E histological staining. (D, Naive n = 4; E, Naive AOM/DSS n = 11; F, Hpb AOM/DSS n = 10; G, Hpb + Inbs AOM/DSS n = 8). Representative H&E stained colon sections (100x magnification) are shown for each group. Arrows indicate infiltrating immune cells (white), goblet cell hyperplasia (green), intratumoural abscess (black), and hyperchromatic nuclei (blue). Polyps are highlighted with a black dotted circle. From the H&E stained slides, **(F)** the histological score was estimated and **(G)** infiltrating immune cells quantified using ImageJ. Data shown represents one experiment (Naive, n = 3; Naive AOM/DSS, n = 5; Hpb AOM/DSS, n = 4; Hpb + Inb AOM/DSS, n = 4). Unpaired T-test, * p ≤ 0.05, *** p ≤ 0.005, **** p ≤ 0.001, error bars Mean ± SD.

3.4.6 *H. polygyrus* infection results in a significant increase in intestinal inflammation which is reduced with EP2/EP4 inhibitors

Despite the lack of clinical signs and visible tumours in the AOM/DSS model, the increased histology severity score indicates there is a degree of intestinal pathology. Given the relationship between EP2/EP4 signalling and intestinal inflammation as indicated by increased faecal calprotectin, this marker was chosen in order to quantify the intestinal pathology with *H. polygyrus* infection. Stool samples were collected from all mice on the final day of each DSS cycle. The concentration of faecal calprotectin showed a trend of increasing throughout the DSS cycles in the naïve and infected cohort, reaching significance at cycle 3 (**Figure 8A**). There was a significant reduction in the concentration of calprotectin during all cycles of DSS in helminth infected mice given EP2 and EP4 inhibitors, reaching levels similar to those observed in uninfected naïve mice in the no AOM/DSS group, suggesting the ability of *H. polygyrus* to increase intestinal inflammation is dependent on EP2/EP4 signalling (**Figure 8A**).

To establish the effect of *H. polygyrus* activation of EP2/EP4 receptors on intestinal inflammation, faecal calprotectin was measured at different points in the lifecycle with and without inhibitors. Stool samples were collected at day 0, 4, 7, 10, and 14 post-infection with and without inhibitors, as well as from uninfected mice at the same timepoints. Calprotectin concentrations showed no significant change up to day 7 post-infection, whereas at day 10 and 14 there was an significant increase observed compared to uninfected (**Figure 8B**). Interestingly, the inhibitors treated group showed a significant decrease at these same timepoints compared to the infected group, with calprotectin concentrations returning to those observed in the naïve uninfected group (**Figure 8B**). Given there is little difference in the concentrations of calprotectin in the AOM/DSS model compared to *H. polygyrus* alone, it cannot be concluded whether *H. polygyrus* increases intestinal inflammation during the AOM/DSS model.

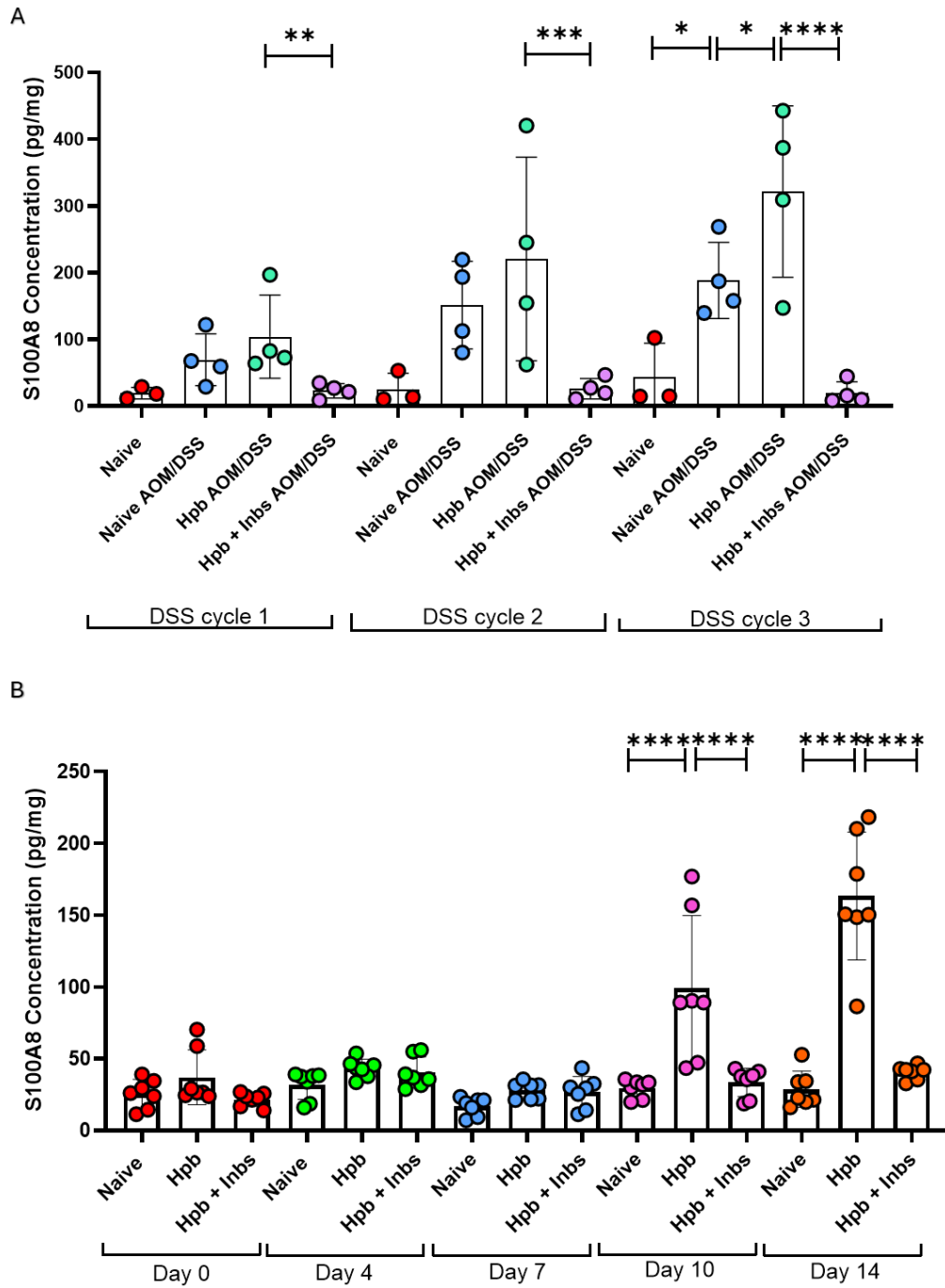


Figure 8. Impact of *H. polygyrus* infection on faecal calprotectin concentrations. (A) Stool samples were collected from all mice from different treatment conditions on the final day of each DSS cycle. **(B)** Stool samples were collected from all mice from different treatment conditions at day 0, 4, 7, 10, and 14 post-infection. Data shown is the average of one independent experiment performed in duplicate (Naïve, n = 3; Naïve AOM/DSS, n = 4; Hpb AOM/DSS, n = 4; Hpb + Inbs AOM/DSS, n = 4). Unpaired T-test, * p ≤ 0.05, ** p ≤ 0.01, *** p ≤ 0.005, **** p ≤ 0.001, error bars Mean ± SD.

3.4.7 HES causes an increase in *in vitro* intestinal cell permeability in a similar manner to a PGE₂ receptor agonist

Data shown so far in this chapter has increased PGE₂ EP2/EP4 receptor signalling in the colon following helminth infection *in vivo* which is then responsible for a downregulation in E-cadherin expression, suggestive of a “leaky-gut” phenotype. Although infection has been shown to modulate intestinal permeability, ESPs can also promote increased cellular permeability. Whether this is mediated through PGE₂-dependent activation of EP2 and EP4 is not known. As the colon is at a distant site to where *H. polygyrus* resides, *H. polygyrus* may be able to activate PGE₂ receptor signalling in the colon via the release of its secretions (HES). The effect of HES on cell permeability was investigated by developing a well-established fluorescein isothiocyanate (FITC)-dextran 4kDa (FD4) trans-well assay using two murine colorectal cancer cell lines. Following 3-5 days of culture, CMT-93 were able to form an impermeable monolayer, as indicated by a lack of FD4 in the basolateral chamber of the assay, whereas CT26 were not able to form an impermeable monolayer (**Figure 9**). 1uM Trypsin is known to increase cell permeability by cleaving proteins involved in maintaining cell-cell junctions, including E-cadherin (284, 285) and was included as a positive control, whilst a trans-well containing only CMT93 cells and no FD4 was used as a negative control.

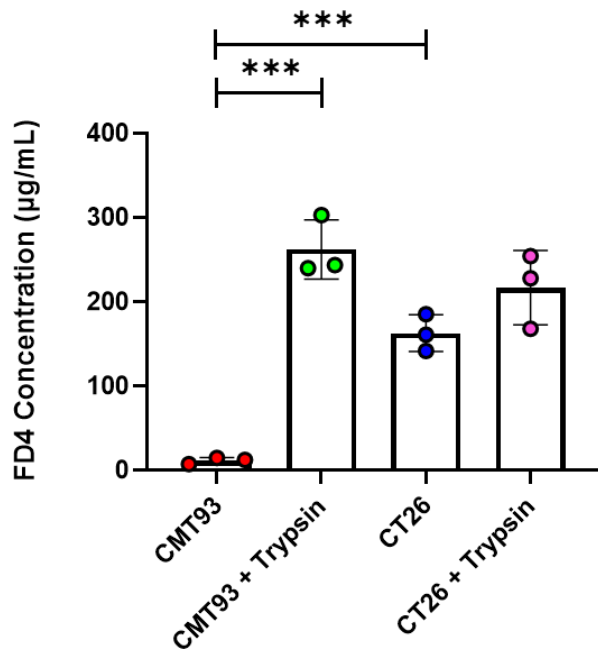


Figure 9. Comparison of the ability of two murine colorectal cancer cell lines to form a monolayer. FD4 in the basolateral chamber was quantified after CMT93 and CT26 cells were cultured for 3-5 days. Data shown is the mean of three independent experiments with n = 3 per group. Unpaired T-test, *** p ≤ 0.005, error bars Mean ± SD.

Permeability of a CMT-93 cell monolayer was quantified by determining the FD4 concentration in the basolateral chamber of the assay at 18 hours following addition of a 10-fold dilution series of HES (0.01 – 10 µg/mL). The positive control trypsin increased cellular permeability, reflected by an increase in FD4 concentration to 323.399 SD±/µg/mL. The addition of 0.01 µg/mL HES resulted in an average increase in FD4 concentration of 1.414 µg/mL, whereas 10 µg/mL of HES lead to a 209.410 µg/mL increase (**Figure 10A**). As the fold-change in FD4 concentration compared to the untreated control did not increase by factors of 10, it can be concluded that this observed effect is not dose-dependent (**Figure 10B**).

The ability of 10µg/ml HES to increase permeability was compared to a known agonist of EP receptor signalling, 16,16-dimethyl PGE₂ (dmPGE₂). Two concentrations of dmPGE₂ were chosen, 2ng/mL as this was the physiological concentration of PGE₂ observed in the murine colon by Smith *et al* (190), whereas 200ng/mL was previously shown to activate EP signalling *in vitro* (286). Addition of 2 or 200ng/mL dmPGE₂ led to a significant increase in cell permeability, with an average increase in FD4 concentration of 86.65 µg/mL and 222.89 µg/mL respectively (**Figure 10C**). Increased permeability following addition of 10µg/ml HES was equivalent to that seen following addition of 200ng/mL dmPGE₂ (**Figure 10C**). These experiments suggest that 10µg/ml HES correlates with an increase in cell permeability by promoting PGE₂ receptor activation.

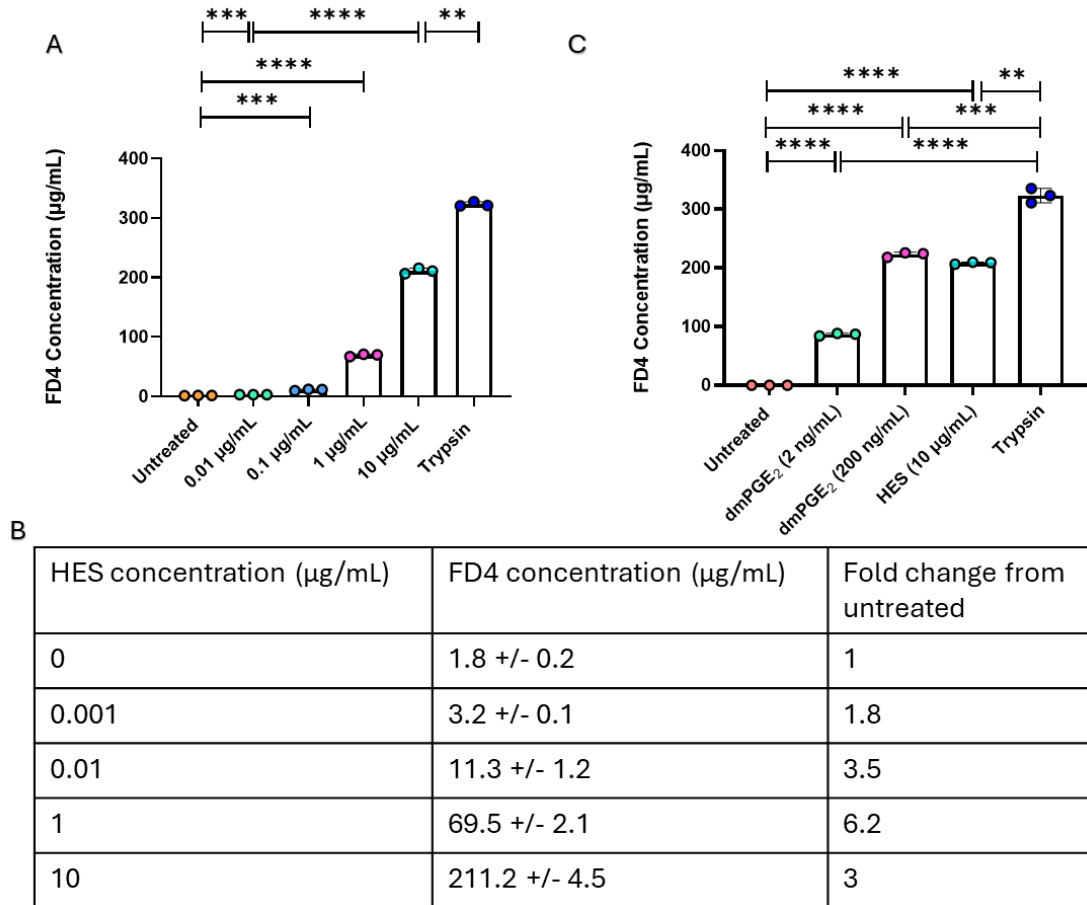


Figure 10. The addition of HES correlates with an increase in intestinal cell permeability *in vitro* to a similar degree than a PGE₂ receptor agonist. (A) FD4 in the basolateral chamber quantified after addition of dmPGE₂ at 2 ng/mL and 200 ng/mL. **(B)** Table showing the FD4 concentration and fold change from untreated with each concentration of HES. Mean +/- SD = +/- . **(C)** FD4 in the basolateral chamber quantified after the addition of HES in a 1/10 dilution series (0.01 – 10 µg/mL). Data shown is the mean of three independent experiments with n = 3 per group. Unpaired T-test, ** p ≤ 0.01, *** p ≤ 0.005, **** p ≤ 0.001, error bars Mean ± SD.

3.4.8 The ability of HES to increase *in vitro* intestinal cell permeability is mediated primarily through EP2 receptor signalling

My *in vivo* experiments suggested that helminth infection activated PGE₂ receptor signalling via EP2 and EP4. To determine whether HES increases cell permeability by promoting PGE₂ receptor activation through EP2 and EP4, expression of *PTGER2* and *PTGER4* by CMT-93 cells was first confirmed by PCR (Figure 11).

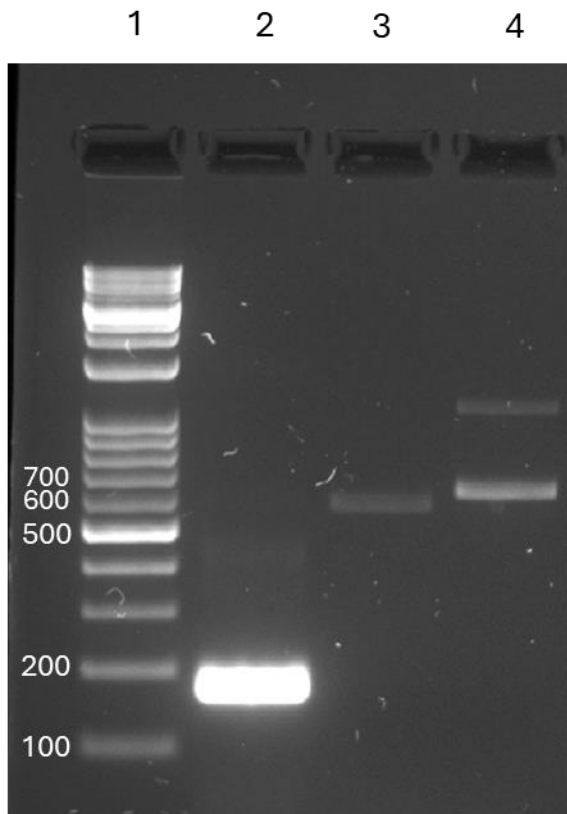
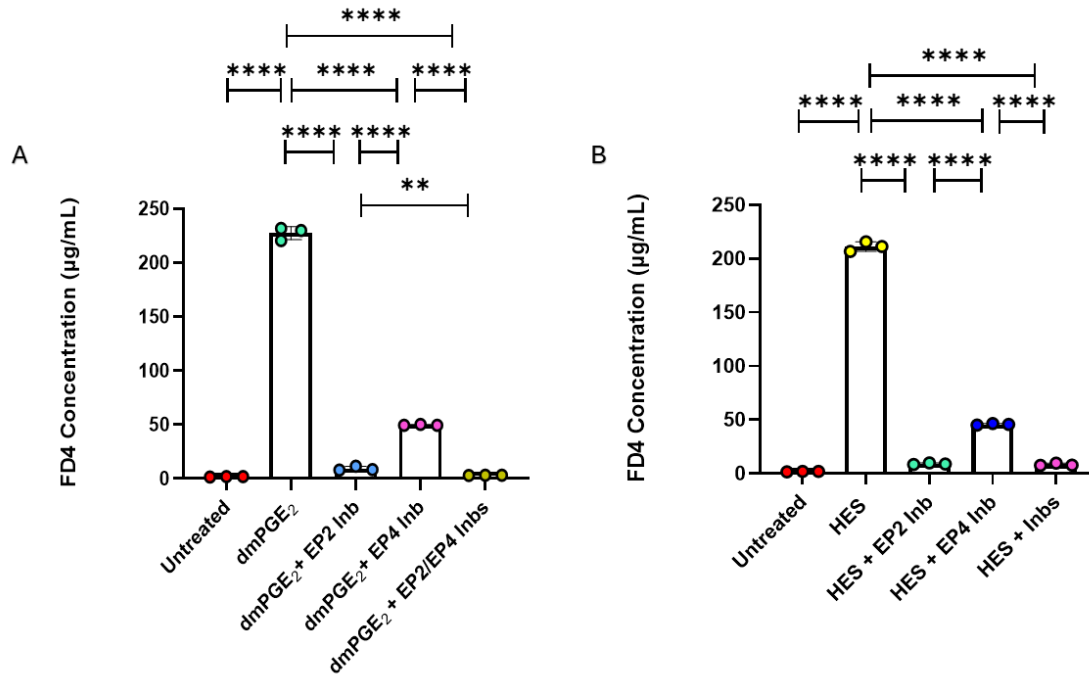


Figure 11. Expression of EP2 and EP4 in CMT93 cells. (1) 100 base pair (bp) DNA ladder, (2) GAPDH predicted size 180bp, (3) EP2 predicted size 569bp, (4) EP4 predicted size 612bp. Data shown is representative of one independent experiment.

I then established whether inhibition of EP2 and EP4 could prevent dmPGE₂-dependent increases in cellular permeability. Adding both EP2 and EP4 inhibitor significantly decreased dmPGE₂-dependent increases in permeability (**Figure 12A**). Addition of either the EP2 or EP4 inhibitor alone significantly reduced dmPGE₂-dependent increases in permeability, however an EP2 inhibitor was more effective, resulting in a final FD4 concentration of 9 µg/mL vs 45.8 µg/mL (**Figure 12A&C**). I then determined that addition of both EP2 and EP4 inhibitors significantly decreased HES-dependent increases in permeability, again with the EP2 inhibitor being significantly more effective (**Figure 12B&D**). My findings suggest that although dmPGE₂ drives permeability through EP2 and EP4 receptor activation, the effect of HES is mainly due to a preference for EP2.



C

Treatment	FD4 concentration (µg/mL)	Fold change from untreated
Untreated	1.8 +/- 0.2	1
dmPGE ₂	222.9 +/- 4.0	123.8
dmPGE ₂ + EP2 Inb	9.0 +/- 0.8	5
dmPGE ₂ + EP4 Inb	45.77 +/- 0.8	25.4
dmPGE ₂ + EP2/EP4 Inb	0.8 +/- 0.09	0.4

D

Treatment	FD4 concentration ($\mu\text{g}/\text{mL}$)	Fold change from untreated
Untreated	1.8 +/- 0.2	1
HES	211.2 +/- 4.5	117.4
HES + EP2 <u>Inb</u>	9.3 +/- 2.0	5.2
HES + EP4 <u>Inb</u>	49.7 +/- 0.4	27.6
HES + EP2/EP4 <u>Inb</u>	0.5 +/- 0.1	0.3

Figure 12. HES favourably signals through the EP2 receptor to increase cell permeability. The addition of EP2 and EP4 inhibitors were tested both individually (1 μM) and in combination to assess impact on **(A)** dmPGE₂ and **(B)** HES-induced increase in cell permeability. **(C&D)** Tables showing the FD4 concentration in the basolateral chamber following inhibitor treatment and fold change from untreated. Mean +/- SD = +/- . Data shown is the mean of three independent experiments (n = 9). Unpaired T-test, ** $p \leq 0.01$, **** $p \leq 0.0001$, error bars Mean \pm SD.

3.4.9 HES causes an increase in phosphorylation of β -catenin Ser⁵⁵² *in vitro* which is significantly reduced with EP2 & EP4 inhibitors

Previously in this chapter, I showed that *H. polygyrus* infection dependent increases in β -catenin Ser⁵⁵² were mediated through EP2 and EP4 *in vivo* (**Figure 3**). Results shown in **Figure 12** show that HES-dependent increases in cellular permeability can be mediated by EP2 and EP4 signalling. I therefore aimed to determine whether HES-dependent increases in cellular permeability via EP2/EP4 were associated with increased β -catenin Ser⁵⁵². Having shown that dmPGE₂ increases β -catenin Ser⁵⁵² I next established whether inhibition of EP2 and EP4 could prevent dmPGE₂-dependent increases in β -catenin Ser⁵⁵². Addition of these inhibitors resulted in a significant decrease in β -catenin Ser⁵⁵² compared to dmPGE₂ treatment alone (**Figure 13**).

The same strategy was adopted to investigate whether addition of HES to CMT93 cells increases activation of PGE₂ receptor signalling *in vitro* in a similar manner to dmPGE₂. Addition of 10 $\mu\text{g}/\text{mL}$ HES resulted in a significant 4.8 fold increase in β -catenin Ser⁵⁵² in comparison to the untreated group (**Figure 13**). This significant increase demonstrates that the HES is able to activate PGE₂ receptor signalling (**Figure 13**). β -catenin Ser⁵⁵² can occur as a consequence of several activated signalling pathways (287-289). Therefore, to determine the extent to which PGE₂ receptors are activated with the addition of HES, CMT93 cells were treated with a combination of EP2 and EP4 inhibitors alongside

HES and quantified p β -catenin Ser⁵⁵². The addition of EP2 and EP4 receptor inhibitors resulted in a significant 2.15 fold decrease in p β -catenin Ser⁵⁵² compared to HES treatment alone. (**Figure 13**). This result suggests that the HES is able to activate PGE₂ EP2/EP4 receptor signalling in CMT93 cells in a similar manner to dmPGE₂.

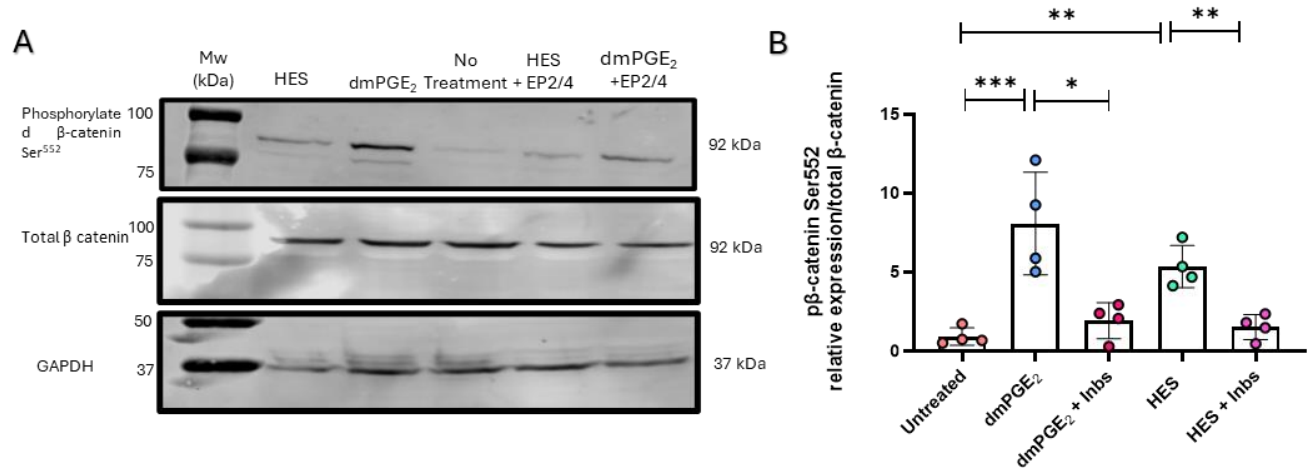


Figure 13. The addition of EP2 & EP4 inhibitors significantly reduces the ability of HES to increase phosphorylation of β -catenin Ser⁵⁵² *in vitro*. (A) Example western blot of p β -catenin Ser⁵⁵² and total β -catenin (both 92 kDa) compared to GAPDH (37 kDa) from CMT93 cells treated with HES (10 μ g/mL) or dmPGE₂ (200 ng/mL) +/- EP2/EP4 inhibitors (Inbs) (1 μ M). (B) Graphical summary of the ratio of β -catenin Ser⁵⁵² normalised to total β -catenin and expressed as a fold change relative to control wells. Data shown represents four independent experiments (n = 4). Unpaired T-test, * p \leq 0.05, ** \leq 0.01, *** \leq 0.005, error bars Mean \pm SD.

3.4.10 HES causes a decrease in expression of E-cadherin *in vitro* which is rescued with EP2 & EP4 inhibitors

To validate *in vivo* findings observed with *H. polygyrus* infection in mice with CAC, E-cadherin expression was investigated after treating the CMT93 monolayer with HES (10 μ g/mL) or dmPGE₂ (200 ng/mL). As was found *in vivo* in mice with CAC, a significant decrease in E-cadherin expression in the HES treated monolayer was observed (**Figure 14**). Finally, it was shown that this decrease in E-cadherin expression is mediated by PGE₂ receptor signalling, as cells treated with a combination of EP2 and EP4 inhibitors show a significant increase in E-cadherin expression near to untreated levels (**Figure 14**). Together, this data suggests that the decrease in E-cadherin expression observed during *H. polygyrus* infection *in vivo* is mediated by HES activation of PGE₂ EP2/EP4 receptor signalling.

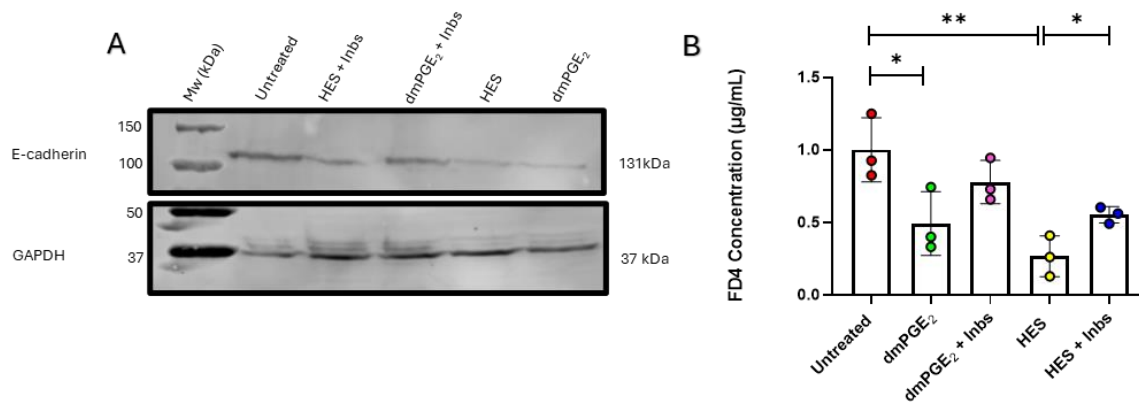


Figure 14. The addition of EP2 & EP4 inhibitors significantly increased the expression of E-cadherin following HES treatment. (A) Example western blot of E-cadherin (131 kDa) and GAPDH (37 kDa) from CMT93 cells treated with HES (10 µg/mL) or dmPGE₂ (200 ng/mL) +/- EP2/EP4 inhibitors (Inbs) (1 µM). **(B)** Graphical summary of the ratio of E-cadherin normalised to GAPDH and expressed as a fold change relative to control wells. Data shown represents four independent experiments (n = 4). Unpaired T-test, * p ≤ 0.05, ** ≤ 0.01, error bars Mean ± SD.

3.5 Discussion

To summarise, this chapter was crucial in following on from findings from Smith *et al*, who point to a role for PGE₂ in driving the mechanism for exacerbation of CAC by *H. polygyrus* infection (190). EP2/EP4 receptor activation following helminth infection mediated a decrease in E-cadherin expression in the colon. Findings *in vivo* were corroborated using an *in vitro* CMT93 cell monolayer culture, with HES treatment replicating the increase in dmPGE₂ EP2/EP4 receptor signalling and decrease in E-cadherin expression. Taken together, these findings demonstrate a role for the release of HES during *H. polygyrus* infection in increasing PGE₂ receptor signalling in the colon, leading to a decrease in E-cadherin expression.

To begin, this chapter investigates levels of PGE₂ receptor activation in the colon at day 14 post-infection, coinciding with when CAC was induced in the AOM/DSS model, and finds a significant increase of pβ-catenin Ser⁵⁵². This report is the first to describe the ability of *H. polygyrus* to increase pβ-catenin Ser⁵⁵² in the colon. In fact, this ability to increase pβ-catenin Ser⁵⁵² has only been described for one other parasite; *Toxoplasma gondii*, which modulates pβ-catenin Ser⁵⁵² to promote its replication and infection in host cells (290).

Levels of pβ-catenin Ser⁵⁵² have been shown to be associated with worsened disease progression in the AOM/DSS model (274). Analysis of *in vivo* colon samples taken from mice 64 days post-AOM administration showed significantly increased pβ-catenin Ser⁵⁵² observed with *H. polygyrus* infection.

Despite p β -catenin Ser⁵⁵² being noted as a key molecular event downstream of EP2/EP4 activation (269, 271, 272), it is important to acknowledge that p β -catenin Ser⁵⁵² can occur downstream of several receptors, including the glucagon receptor, low-density lipoprotein receptors (LDLR), and the epidermal growth factor receptor (EGFR) (287-289). Given how the administration of a combination of EP2/EP4 receptor inhibitors resulted in a significant reduction in p β -catenin Ser⁵⁵², it demonstrates how *H. polygyrus* infection is causing increased p β -catenin Ser⁵⁵² downstream of EP2/EP4 activation. However, levels of p β -catenin Ser⁵⁵² did not change in the AOM/DSS model which contradicts findings from Brudvik *et al* (273), who show a significant increase in p β -catenin Ser⁵⁵² during the AOM/DSS model. Therefore, results shown in this chapter are suggestive of the significant increase in p β -catenin Ser⁵⁵² being due to *H. polygyrus* infection, and not the induction of CAC.

PGE₂-EP2/EP4 receptor signalling has previously been shown to increase intestinal inflammation by increasing inflammatory cytokine production and immune cell recruitment (291, 292). Therefore, to investigate if *H. polygyrus* activation of EP2/EP4 receptors mediated intestinal inflammation, faecal calprotectin was utilised as a biomarker for intestinal inflammation, due to its high sensitivity and specificity and regular use in the clinic (293). Knowledge of the different points of the *H. polygyrus* lifecycle were used to choose timepoints post-infection whereby significant events occur (217), and so may influence inflammation. No significant changes were observed until day 10, where concentrations of calprotectin significantly increased, with a further increase seen at day 14. As expected based on previous findings (280), concentrations of calprotectin increased with each cycle of DSS. Additionally, concentrations of calprotectin were further increased with *H. polygyrus* infection. Finally, concentrations of calprotectin were found to be significantly decreased with the addition of EP2/EP4 inhibitors, both during the *H. polygyrus* lifecycle and AOM/DSS model, returning to levels observed in the naïve group. However, with the concentrations observed, it cannot be concluded that *H. polygyrus* is exacerbating intestinal inflammation during the AOM/DSS model. The concentrations observed are; significantly lower than what is observed in the literature (280), and not significantly different than the lifecycle.

Along with increased intestinal inflammation, a further key feature of the pathogenesis of colitis is an increase in intestinal barrier permeability (61). The cell-cell adhesion protein E-cadherin was chosen to investigate effects of *H. polygyrus* on the integrity of the intestinal barrier, as it is an essential protein for barrier function (294). E-cadherin expression is shown to not change at day 14 post-infection in the colon, which is contradictory to results observed in the literature (165). However, it is important to note that Su *et al* performed experiments using a different strain of mouse (BALB/c) and took samples at day 7 post-infection, indicating that results may differ depending on strain and also time post-infection. Furthermore, the sample size in this report was low (n = 3), and therefore an increased

sample size may reveal significance. Analysis of *in vivo* colon samples taken from mice 64 days post-AOM administration showed a significant decrease in E-cadherin expression, which was restored to naïve levels with the administration of EP2/EP4 receptor inhibitors. As E-cadherin did not change with *H. polygyrus* infection alone, it is concluded that the decrease in E-cadherin expression is due to the induction of AOM/DSS CAC, which supports the literature (274). It is important to acknowledge that E-cadherin is not only a marker of cell-cell adhesion, but also epithelial-mesenchymal transition (EMT), with the loss of its expression occurring frequently during tumour metastasis (295). Therefore, despite this report showing a significant decrease in E-cadherin expression in the colon with *H. polygyrus* infection during the AOM/DSS model, it is not possible to conclude this leads to a more “leaky-gut”. However, it is more likely that this is an indication of increased permeability as opposed to EMT as there was little visual evidence of cancer in these mice.

Next, histologically stained colon tissue samples were analysed for disease severity score and colon length/weight ratios measured. The length/weight ratios of the colon are used as a marker of hyperplasia of the mucosa and of the severity of chronic colitis; because DSS induces shortening of the colon, this can be used as a visual index and to quantitate levels of colitis (158). Histologically, no significant difference between the naïve and *H. polygyrus* infected mice in the AOM/DSS group was observed. Given results from Pastille *et al* who show *H. polygyrus* exacerbation of pathology in the colonic histology (151), this result was a surprise and suggests the model may not have worked as expected. This may be due to a lack of appropriate controls, such as a naïve group plus the EP2/EP4 inhibitors, and a *H. polygyrus* group without induction of AOM/DSS CAC plus the EP2/EP4 inhibitors. Further surprising observations included the lack of visible tumours in the colon, no differences in colon/weight ratios, (190) and no differences in weight loss throughout the AOM/DSS model compared to the vehicle group. It is well documented in the literature that the AOM/DSS model results in a significant number of visible tumours, significant weight loss, and colon shortening (158, 296, 297). Despite no visible tumours, one tumour was detected in the histology for both the naïve and helminth infected group, however this is significantly less than what is reported in this model (158). Therefore, despite the inhibitors significantly reducing the histology severity score and number of infiltrating immune cells, it is difficult to draw conclusions from this experiment due to the lack of clinical signs in the naïve AOM/DSS group.

As described in **Introduction section 1.5.2** excretory/secretory products (HES) are released when the parasite emerges into the lumen as an adult (144, 298). Treating the CMT93 cell monolayer with HES did result in a significant increase in cell permeability, as indicated by the increased FD4 concentration. Similar findings with other excretory/secretory products (ES) have been observed by Hiemstra *et al*, who show that the ES from the nematode *T. suis* dose-dependently increased flux of FD4 in treated

CMT93 monolayers, which was accompanied with a decrease in tight junction expression (170). This increase in FD4 flux observed in this chapter was also associated with a decrease in E-cadherin expression in the HES-treated monolayers, which was dependent on EP2/EP4 receptor signalling. Furthermore, HES treatment resulted in a significant increase in p β -catenin Ser⁵⁵² which was inhibited with EP2/EP4 inhibitors. These results suggest that the HES is mediating E-cadherin expression via activation of EP2/EP4 receptors. This is believed to be the first evidence detailing the ability of HES to activate EP2/EP4 receptors. This result has previously only been shown for the antigens from *Taenia solium* larval cysts, which have been shown to stimulate PGE₂ production from monocytes, which then triggers Treg cell expansion via EP2/EP4 receptor activation as an immunomodulation strategy (203).

As EP2/EP4 signalling has been implicated in increasing cell permeability (108, 264), it was investigated whether the HES exhibits preferential receptor activation by adding EP2/EP4 inhibitors separately. Evidence for preferential receptor activation comes from Lejeune *et al*, who show the ability of the protozoan parasite *Entamoeba histolytica* to preferentially signal via the EP4 receptor to alter cell permeability (299). The inhibitors in combination resulted in significant amelioration in the ability of the HES to increase cellular permeability, with a significant restoration in E-cadherin expression also observed. The addition of EP2 antagonist alone resulted in a significant decrease in FD4 concentration, with little additive effect being observed with the addition of the EP4 inhibitor. This is suggestive of the HES having a preference for EP2 receptor signalling over EP4. Interestingly, data from Ma *et al* indicate that the PGE₂-EP2 signalling axis dominates in the colon tumour microenvironment due to a higher affinity for the EP2 receptor in the colonic environment, promoting the production of inflammatory cytokines (300). Therefore, this ability of HES to preferentially signal through EP2 may give a clue as to how *H. polygyrus* can mediate intestinal inflammation.

Finally, it is important to note a major criticism of this chapter, and that is the use of a murine CRC cell line. The CMT-93 cell line has been shown to exhibit chromosomal instability and is replicative of human late-stage CRC (301), therefore may respond differently to *H. polygyrus* antigen compared to non-cancerous cells. Despite this, in the absence of an *in vivo* model, the use of a CRC cell line does provide some evidence of *H. polygyrus* effecting cell permeability and E-cadherin expression in cancer epithelial cells, providing scope to investigate this further *in vivo*.

The original objectives of this chapter were met to a certain extent. During this chapter, it was established that helminth secretions promote EP receptor-dependent increases in intestinal permeability *in vitro*, and helminth infection *in vivo* is associated with increased PGE₂ signalling and decreased colonic E-cadherin expression. However, whether the increase in PGE₂ EP2/EP4 signalling is linked to exacerbation of CAC was not determined due to the AOM/DSS model not working as

expected. Therefore, it remains inconclusive from this chapter that *H. polygyrus* exacerbation of CAC is mediated through prostaglandin signalling-dependent increases in intestinal permeability.

Chapter 4: Analysis of the HES to determine what is driving the increase in cellular permeability

4.1 Introduction

In the previous chapter, I revealed the ability of HES to increase cell permeability *in vitro* through EP2/EP4 activation, however it is currently unknown what molecule within the HES is responsible for this effect. Therefore, this chapter adopts several *in vitro* and bioinformatic techniques in an attempt to identify the molecule within the HES enabling the increase in cell permeability.

The excretory/secretory products (ESPs) of *Trichuris muris* and *T. spiralis* have been shown to contain a serine protease. The ability of these ESPs to increase cell permeability was demonstrated to be dependent on the activity of the serine protease, as shown by experiments involving heat inactivation and the addition of protease inhibitors (168, 169). Hewitson *et al* demonstrated that the HES contains several serine proteases, as well as other protease families such as matrix metalloproteases (MMPs) (145). Whether these proteases in the HES contribute to the increase in cell permeability remains unknown and will be investigated in this chapter.

The HES contains several immune-modulatory proteins, with both heat-stable and heat-labile molecules modulating the effect on the immune response (298). I aim to investigate whether the HES-induced increases in cell permeability are reliant on a heat-labile protein. Furthermore, both Hewitson *et al* and McSorely *et al* utilised size fractionation to identify active immune-modulatory molecules from 100's of proteins (298, 302). I will utilise size fractionation columns to identify active molecules within the HES that lead to the increase in cell permeability.

Interestingly, ESPs of other helminths have been shown to contain PGE₂, with *T. suis* being one example (**Figure 1**) (194). Furthermore, it was revealed that *T. suis* PGE₂ was responsible for modulating dendritic cell function partly via EP2 and EP4 signalling (194), demonstrating how a helminth secreted PGE₂ is able to activate EP2/EP4 receptors. Therefore, given results in Chapter 3 pointing to a role for PGE₂ signalling via EP2/EP4 receptors to increase cell permeability, this evidence provides a rationale for screening the HES to investigate if a PGE₂ molecule is present.

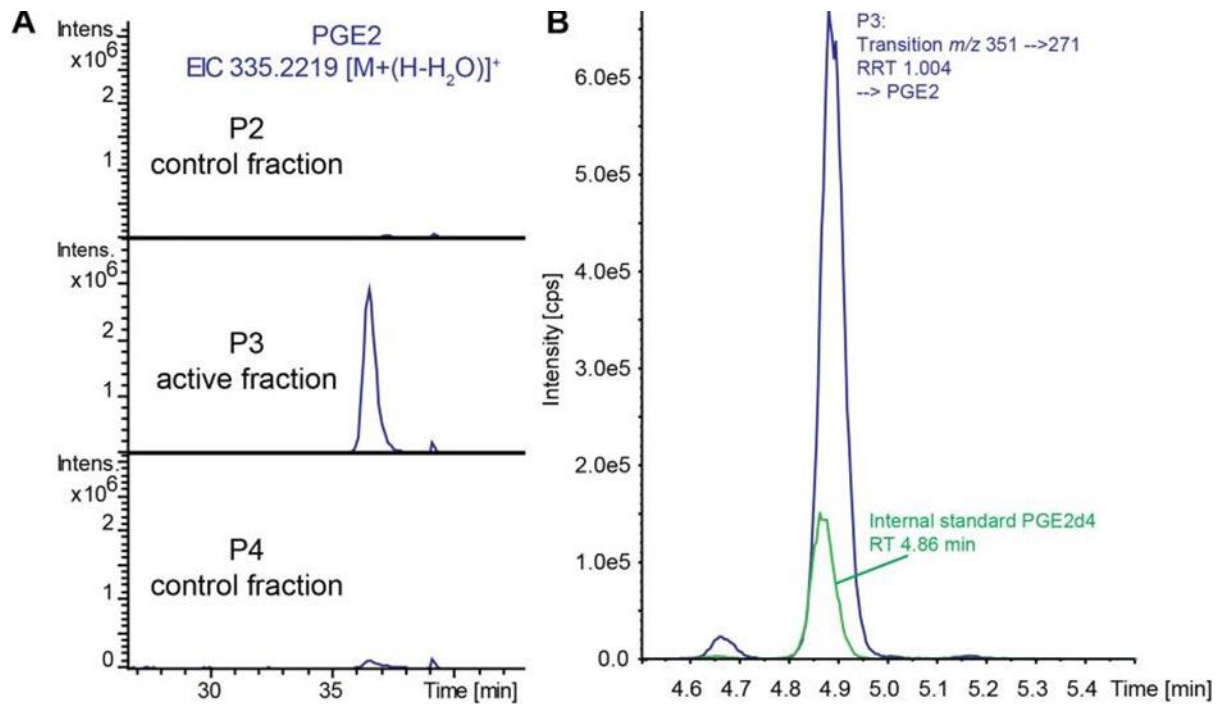


Figure 1. Identification of PGE₂ in sample P3 by LC-MS/MS. (A) Extracted ion chromatograms from two control fractions (P2 and P4) and one active fraction (P3) showing one discriminative peak between the active fraction and control fractions. **(B)** SRM transition of the active fraction showed a high-intensity peak at a relative retention time corresponding to the internal standard PGE₂. Data from Laan *et al.*, 2017.

Several novel proteins have also been identified using a variety of bioinformatic approaches (211, 303-305), and I aim to utilise these approaches to investigate whether *H. polygyrus* encodes metabolic enzymes that may contribute to downstream PGE₂ synthesis, and contribute to increased EP2/EP4 activation as observed in Chapter 3. For example, McSorely *et al* identified transforming growth factor- β (TGF- β) homologues in *H. polygyrus* and another laboratory model nematode *N. brasiliensis*, as well as two major parasites of ruminant livestock; *Haemonchus contortus* and *Teladorsagia circumcincta*, by utilising sequence analysis of the parasitic genome to identify sequences of significant homology (304). Marcus *et al* also used this bioinformatic analysis approach when identifying novel C-type lectin proteins in *H. polygyrus* and *N. brasiliensis* (211). Production of PGE₂ has been shown by helminth-derived glutamate dehydrogenase (203, 306), however it is not yet known whether adult *H. polygyrus* can encode enzymes which can promote PGE₂ production *in vivo*. Using the publicly available *H. polygyrus* genome accessed via WormBase Parasite (PRJEB15396), I adopted the same strategy to perform sequence analysis searching for enzyme homologues which may contribute to downstream PGE₂ synthesis and subsequent increase EP2/EP4 signalling.

With the evidence presented in Chapter 3 detailing the HES being able to increase cell permeability through activation of PGE₂ EP2/EP4 receptor signalling, the overall aims of this chapter are to 1.

determine if the proteases within HES contribute to its ability to increase cell permeability, 2. investigate the presence of PGE₂ in the HES and, 3. analyse the *H. polygyrus* genome for sequences bearing significant homology to human and murine metabolic enzymes which contribute to PGE₂ synthesis. This will be address through the following objectives:

4.2 Chapter Aims

1. Determine if the ability of HES to increase cell permeability is due to the presence of proteases
2. Investigate if the HES contains PGE₂ or any other oxylipins
3. Investigate if the HES contains metabolic enzymes which contribute to synthesis of PGE₂ and therefore increased EP2/EP4 receptor signalling

4.3 Hypothesis

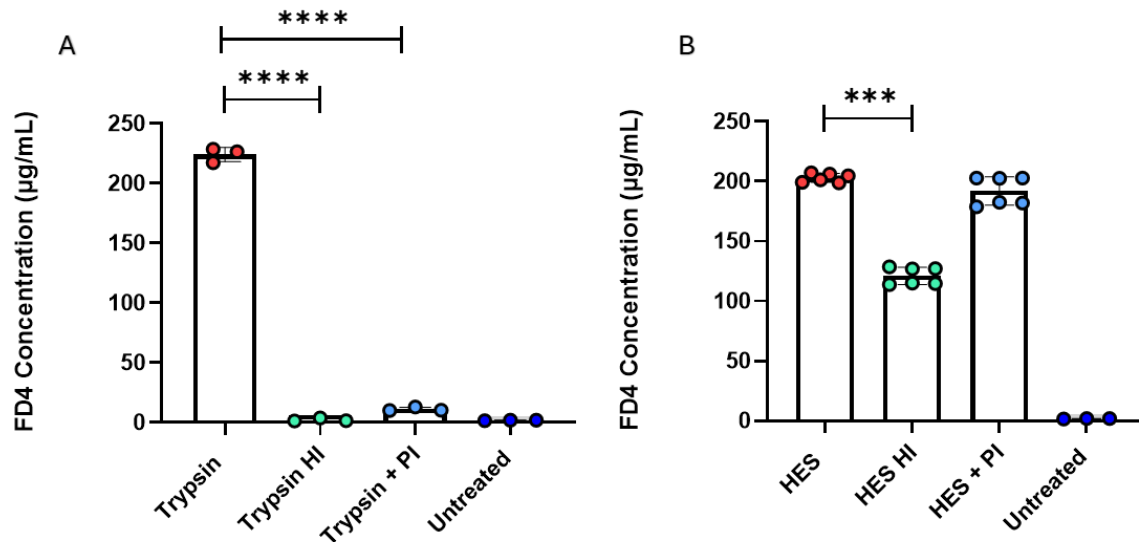
1. The HES contains PGE₂ which can lead to increased signalling through EP2/EP4 receptors and subsequent increase in cell permeability
2. The HES contains metabolic enzymes which contribute to the downstream synthesis of PGE₂, leading to increased signalling through EP2/EP4 receptors and subsequent increase in cell permeability

4.4 Results

4.4.1 Protease inhibition had no significant impact on the ability of HES to increase cellular permeability

Given the abundance of proteases in HES and established evidence that helminth-derived proteases can increase cell permeability (145, 169), initial investigations focussed on establishing a role for proteases with the HES in increasing cell permeability. Confirming the ability of a bovine pancreatic protease to disrupt epithelial integrity, addition of 1 μ M of trypsin significantly increased permeability of the CMT-93 monolayer (**Figure 2A**). As the ability of trypsin to increase cell permeability has been shown to be inhibited by both heat and the addition of protease inhibitors (307), I tested the efficiency of the heat-inactivation protocol and protease inhibitor cocktail on trypsin. Addition of a protease inhibitor cocktail significantly decreased this trypsin-dependent increase in permeability, reducing FD4 concentration in the basolateral chamber by 95.1% based on the average value (**Figure 2A**). Similarly, heat-inactivation of trypsin prevented the ability of trypsin to increase permeability of these cells (**Figure 2A**). Addition of the protease inhibitor had no significant impact on the increased permeability of the CMT-93 monolayer seen following exposure to 10ug/ml HES (**Figure 2B**). Heat-inactivation of

HES did result in a significant reduction in permeability when compared to HES however, this reduction was not complete and there was still an 63% increase in permeability with heat-inactivation of HES, when compared to a 0.9% increase with heat-inactivated trypsin based on the average values (**Figure 2A-C**).



C

Treatment	FD4 concentration (µg/mL)	% increase from untreated
Untreated	1.8 +/- 0.2	-
Trypsin	227.4 +/- 6.1	100
Trypsin + PI	11.1 +/- 1.7	4.9
Trypsin HI	2.2 +/- 1.3	0.9
HES	202.7 +/- 0.1	100
HES + PI	199.8 +/- 1.3	98
HES HI	127.6 +/- 0.9	63

Figure 2. The ability of HES to increase cell permeability is dependent on a molecule(s) that is not a protease. Effects of heat-inactivation (HI) and addition of protease inhibitor (PI) on the ability of (A) HES and (B) Trypsin to increase cell permeability. (C) Table showing FD4 concentrations with trypsin and HES alone, with PI or HI, and the % increase compared to untreated. Data shown is the mean of (A) three (B) or six independent experiments. Unpaired T-test, *** $p \leq 0.005$, **** $p \leq 0.001$, error bars Mean \pm SD.

4.4.2 Size fractionation of HES reveals a predicted molecular weight of molecule(s) responsible for increasing cellular permeability

As HES is estimated to contain 374 of proteins of various molecular weights (145), I performed size fractionation using 10,000 and 50,000 molecular weight cut-off (MWCO) filters to see if I could determine the fraction of molecular weight (MW) containing the molecule responsible for the observed increase in cell permeability. Data shown in **Figure 3A** shows that the ability of HES to increase permeability is due to a molecule below 50,000 MW, with activity being maintained in the filtrate (< 50,000 MW) and lost in the concentrate (> 50,000 MW). The 50,000 MW HES filtrate was then put through a 10,000 MWCO filter which showed activity being lost in the filtrate (< 10,000 MW) and maintained in the concentrate (> 10,000 MW) (**Figure 3B**). It is important to note that there is still a significant loss in the ability to increase cell permeability within the concentrate of the 50,000 MWCO filter and the filtrate of the 10,000 MWCO filter (**Figure 3A&B**), suggesting that there are molecules within the HES > 50,000 MW and < 10,000 MW that may contribute to the ability of HES to increase cell permeability.

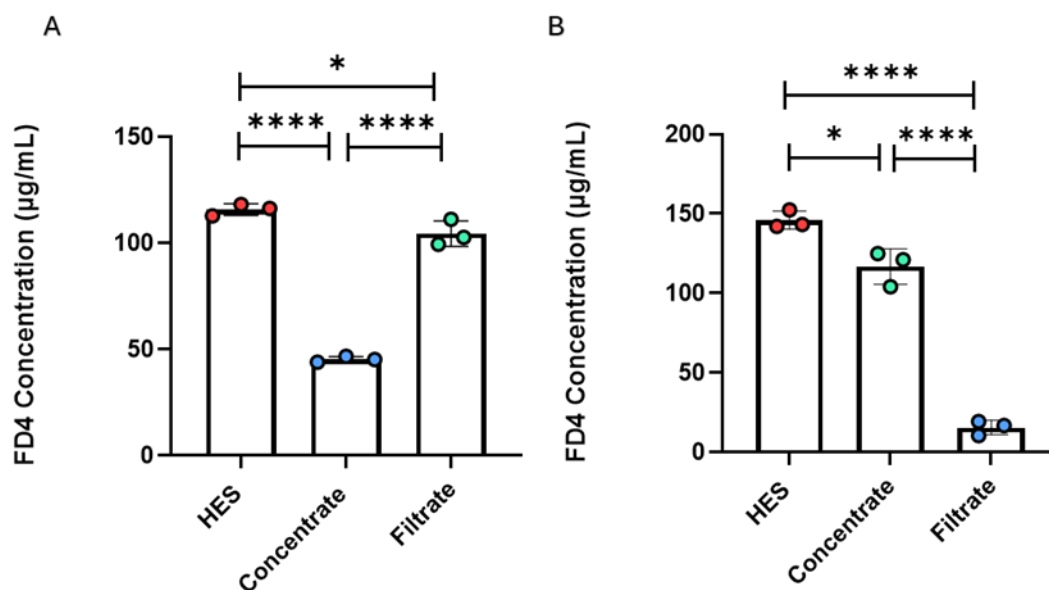


Figure 3. The active molecule(s) in the HES that are driving the increase in cellular permeability are between 10,000 and 50,000 molecular weight. Size-fractionation of the HES using (A) 50,000 MWCO filter and (B) 10,000 MWCO filter with FD4 concentrations quantified using a standard curve. Data shown is the mean of three independent experiments. Unpaired T-test, * $p \leq 0.05$, **** $p \leq 0.001$, error bars Mean \pm SD.

4.4.3 Oxylipins were below the level of detection in HES using LC/MS

Based on the evidence from the previous chapter, which shows that HES can enhance PGE₂ receptor signalling in vitro and that its ability to increase cell permeability depends on this signalling, 100 µL of HES was screened for the presence of PGE₂ and other oxylipins known to increase during *H. polygyrus* infection using LC/MS (194). Internal standards were detected (details in Materials and Methods) but as shown in **Figure 4**, it is clear that there is no PGE₂ or any other oxylipins present in the HES.

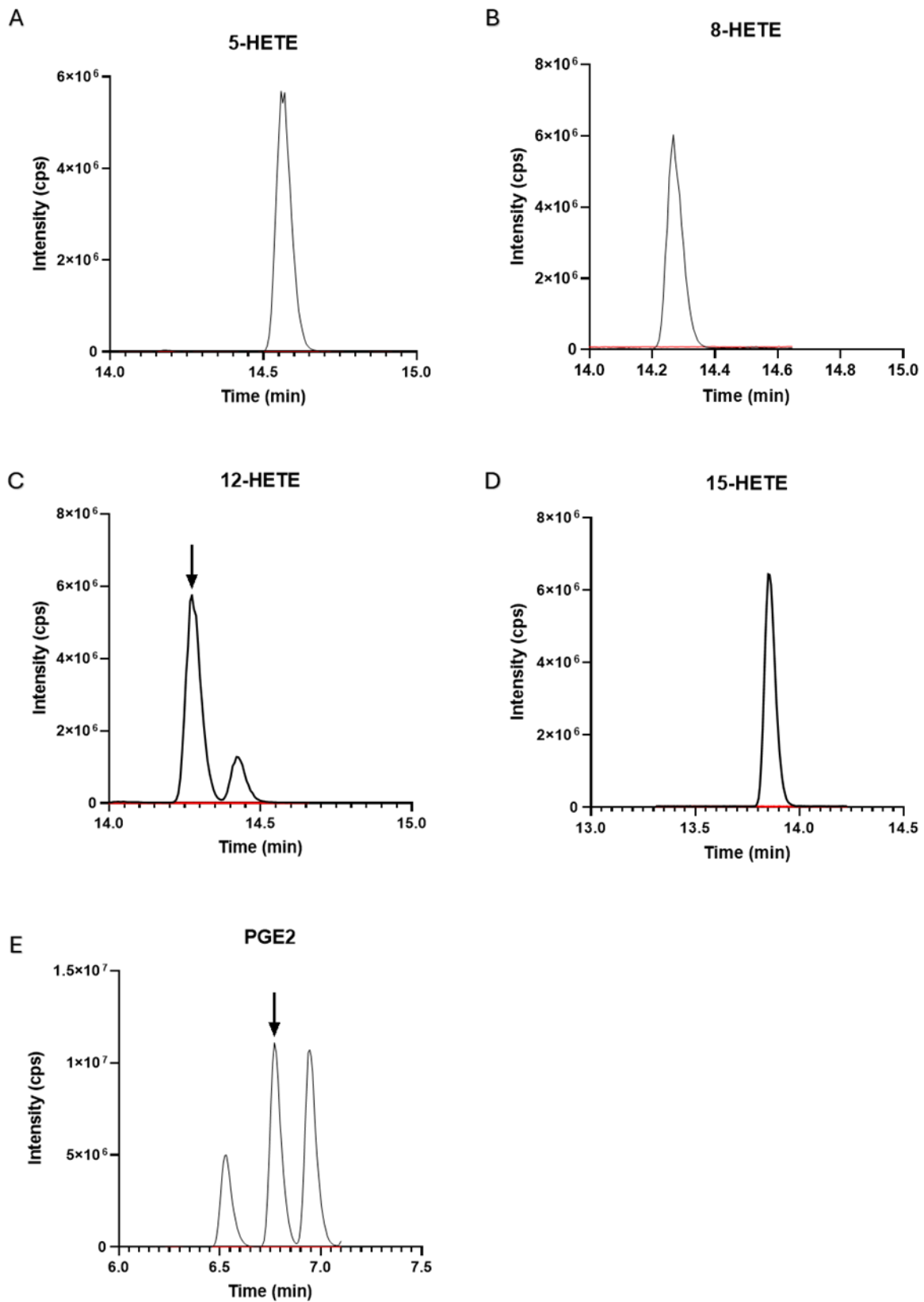


Figure 4. LC/MS analysis of HES. Extracted ion chromatograms showing peaks for internal standards (black) and overlay of corresponding intensity of sample at the same retention time in 100 μ L HES (red).

4.4.4 HES contains three homologues of secreted phospholipase A₂

To investigate the composition of the 10,000 – 50,000 MW fraction of HES, a sample was sent for proteomic analysis. The raw data files obtained from LC/MS were run against the *H. polygyrus* database found in Uniprot using the SEQUEST HT algorithm, with 1,198 proteins being identified and the top 100 most abundant based on the sum of the scores of the individual peptides shown in **Appendix Table 1**. The full list of proteins can be found in **Appendix Table 2**. It is interesting to note the difference in detected proteins in this analysis (1,198) compared to that of Hewitson *et al* (374) (145), highlighting the advancements of proteomic technologies in the last decade (308).

Amongst the proteins identified in this fraction of HES were a selection of proteases, particularly metalloproteases (zinc metalloproteases) metalloendopeptidases, and cysteine proteases, as well as other classes of enzymes such as apyrases, chitinases, and lysozymes. A large number of proteins were detected which belong to the family of Venom Allergen-Like (VAL) proteins, supporting the findings of Hewitson *et al* (145).

By inputting the gene IDs into g:Profiler, GO annotations of the HES 10,000 – 50,000 molecular weight fraction (**Figure 4** and **Appendix Table 3**) were obtained. The GO analysis indicated that catalytic activity (GO: 0003824) was the most common “molecular function” term (**Figure 4A**), and metabolic process (GO: 0008152) was the most common “biological process” term (**Figure 4B**).

Of the 1,198 proteins identified, 470 (56.29%) contained a predicted N-terminal signal peptide (SP) (**Figure 4D**) suggesting the majority of proteins are secreted. To support this, extracellular (GO: 0005615) was the most common “cellular compartment” term (**Figure 4D**). In addition, 203 (17.4%) were novel proteins to *H. polygyrus* (**Figure 4E**), which was determined by comparing them to known secreted proteins identified by Hewitson *et al* (145). When these 203 secreted proteins of unknown function were examined for the presence of a SP, 119 (58.6%) were SP positive, indicating that an important set of novel secreted proteins are present in this fraction of HES.

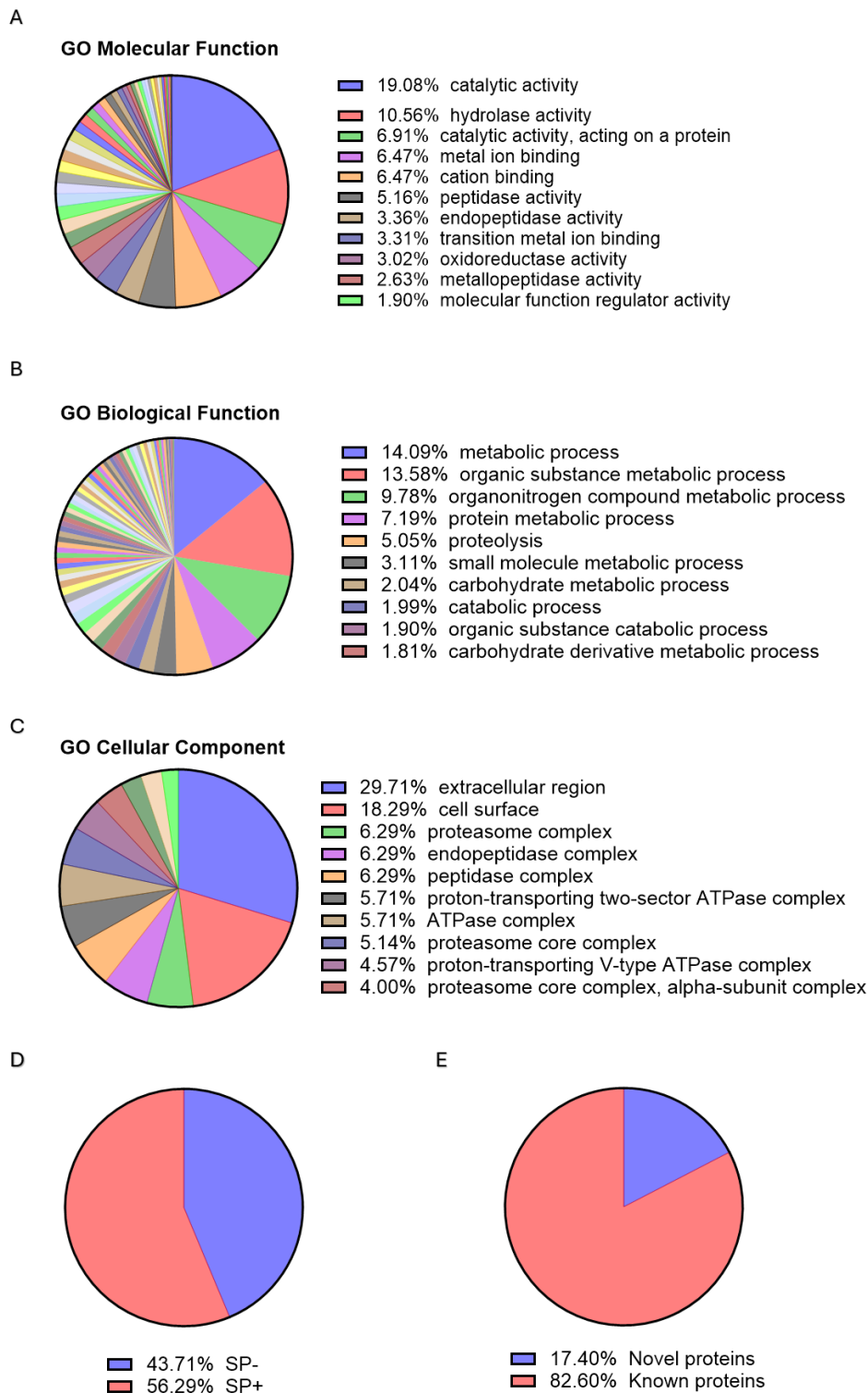


Figure 4. GO distribution of the proteins in the 10,000 – 50,000 molecular weight fraction of HES. All identified proteins in the 10,000 – 50,000 molecular weight fraction of HES were analysed by Gene Ontology and categorized into **(A)** molecular function, **(B)** biological process and **(C)** cellular component. Within each category, the top 10 enriched terms are listed. Gene Ontology analysis performed using g:Profiler. **(D)** Proportion of signal peptide (SP)-containing protein sequences. **(E)** Proportions of novel and characterized proteins containing signal peptides. Signal peptide analysis conducted using SignalP-6.0.

4.4.5 HES-dependent increases in cell permeability are cyclooxygenase-dependent

With no PGE₂ present and evidence from Chapter 3 suggesting the importance of EP2/EP4 signalling in increasing permeability, I utilised acetylsalicylic acid (aspirin), a non-selective cyclooxygenase (COX) inhibitor to assess the contribution of COX activity to the HES-induced increase in EP2/EP4 signalling. Using dmPGE₂, an EP receptor agonist and product of COX activity, I found that addition of increasing doses of aspirin significantly reduced the permeability of a CMT-93 monolayer (**Figure 5A**). Administration of 10 mM aspirin to 10µg/mL HES significantly reduced cell permeability to the levels seen with 10 mM aspirin alone (**Figure 5A&B**). This implies that the addition of HES results in the activation of COX2 and a subsequent increase in the production of PGE₂ which can then activate EP2/EP4 receptors.

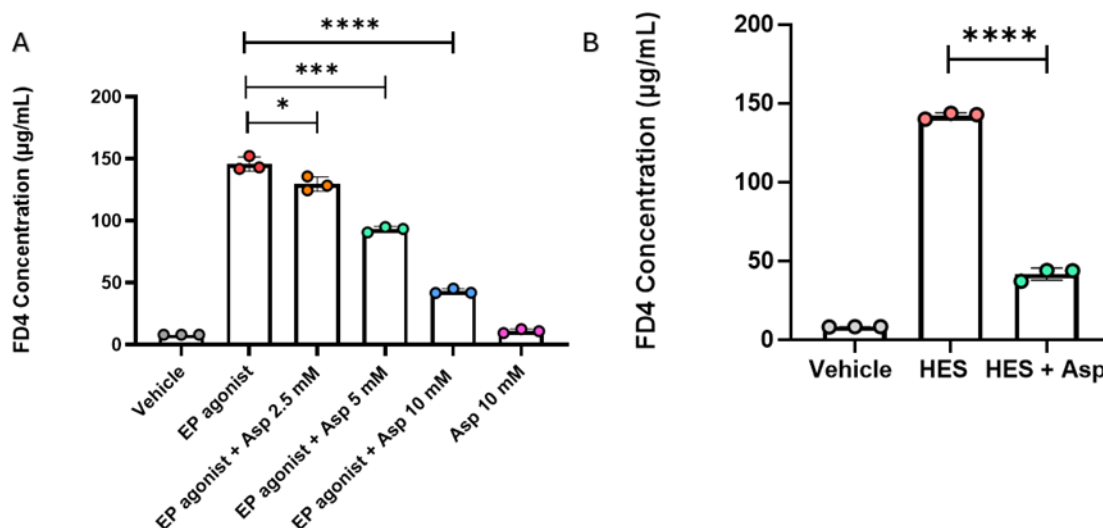


Figure 5. The ability of aspirin treatment to inhibit HES-induced increase in cell permeability. (A) dmPGE₂ was added at 200 ng/mL with different concentrations of aspirin to determine optimum dose that caused most significant decrease in FD4 concentration. **(B)** The effect of the addition of aspirin (10 mM) to HES (10 µg/mL) treated cells on FD4 concentration in the basolateral chamber. Data shown is the mean of three independent experiments. Unpaired T-test, * $p \leq 0.05$, *** $p \leq 0.005$, **** $p \leq 0.001$, error bars Mean \pm SD.

4.4.6 HES encodes several homologues of metabolic enzymes

Evidence in this chapter has shown no PGE₂ in the HES, however Chapter 3 points towards HES being able to increase EP2/EP4 activation leading to increased cell permeability. I have shown that there may be an increase in paracrine or autocrine EP2/EP4 signalling with HES, however what is enabling this remains unknown. Therefore, I next investigated whether any metabolic enzymes which contribute to

PGE₂ synthesis are encoded in the genome, and could be secreted in the HES to increase PGE₂ production from the cells, leading to increased paracrine or autocrine EP2/EP4 signalling. Using the publicly available *H. polygyrus* genome (PRJEB18396) in Wormbase Parasite, I used a variety of search terms corresponding to important enzymes in producing arachidonic acid, as well as enzymes which use this substrate to produce PGE₂ (**Figure 6**). The results are shown in **Table 1**, with several hits revealed in the *H. polygyrus* genome corresponding to some of the enzymes of interest, suggesting metabolic enzymes corresponding to PGE₂ synthesis may be encoded in the *H. polygyrus* genome. To see if any of these are secreted in the 10,000 – 50,000 MW fraction of HES, I mapped the gene IDs from WormBase Parasite back to the proteomics data discussed earlier in the chapter. The proteomics confirmed hits against *PTGS2*, prostaglandin E synthase (PGES), and fatty acid desaturase are not present in the 10,000 – 50,000 MW fraction of HES. Interestingly, the proteomics revealed the presence of HPOL_0000384601 encoding a known orthologue of several human PLA₂ enzymes (PLA₂G2D, PLA₂G5, PLA₂G2F, PLA₂G2C, PLA₂G2A, PLA₂G2E), HPOL_0000928401 encoding a known orthologue of the human PLA₂G15, and HPOL_0001491401 which doesn't have a known orthologue but appeared using the search term "Phospholipase A₂" in WormBase Parasite (**Table 1**). These results suggest the presence of three homologues of sPLA₂ within the 10,000 – 50,000 MW fraction of HES.

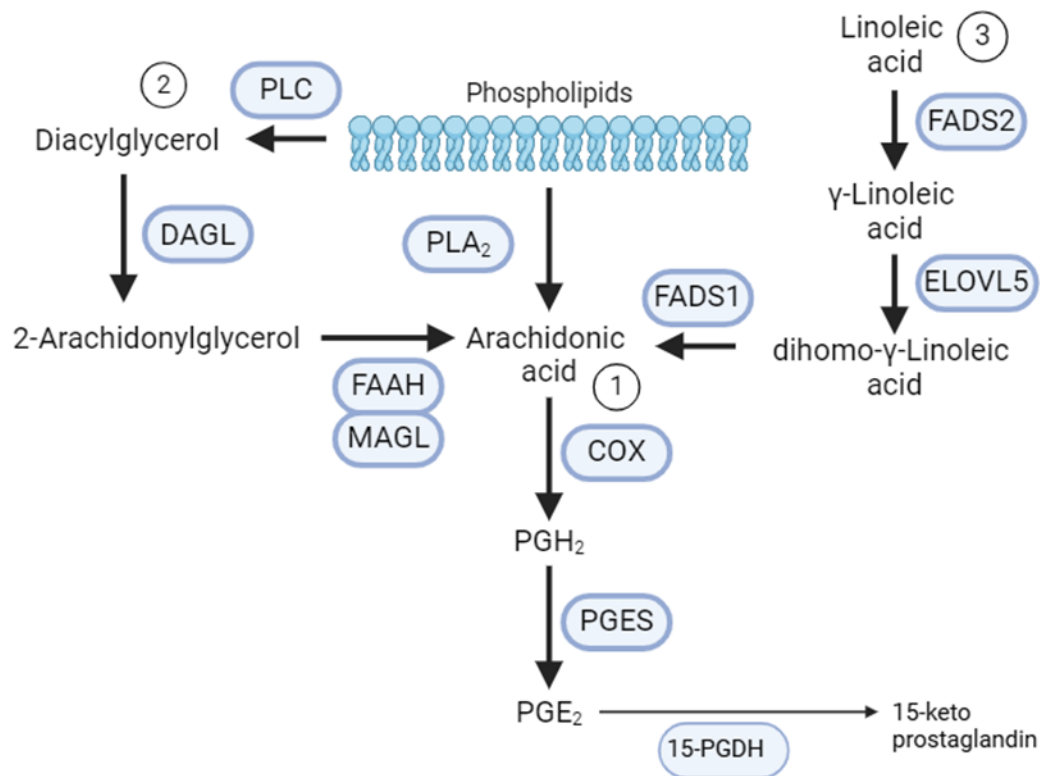


Figure 6. A schematic summary of how arachidonic acid is synthesised and how it is converted to PGE₂. Arachidonic acid is synthesised via 3 main pathways: **1.** Phospholipase A₂ (PLA₂) liberates arachidonic acid which is metabolised by cyclooxygenase (COX) to prostaglandin H₂ (PGH₂) which is metabolised to PGE₂ via prostaglandin E synthase (PGES), **2.** Phospholipase C (PLC) releases diacylglycerol (DAG) from phospholipids, which is metabolised to 2-arachidonylglycerol by DAG lipase (DAGL) and then to arachidonic acid by monoacylglycerol lipase (MAGL) or Fatty acid amidohydrolase (FAAH), **3.** Linoleic acid is metabolised to γ-linoleic acid by fatty acid desaturase 2 (FADS2), then metabolised to dihomo- γ-linoleic acid by fatty acid elongase 5 (ELOVL5), before metabolism to arachidonic acid by fatty acid desaturase 1 (FADS1). PGE₂ is inactivated by 15-prostaglandin dehydrogenase and converted to 15-keto prostaglandin. Image generated in Biorender.com

Table 1. Enzymes with hits against *H. polygyrus* genome. Search terms used in WormBase Parasite to identify hits, with Gene IDs listed. Whether genes were mapped to proteome is indicated by being coloured in black.

Search term	Hits	Gene ID	Mapped to proteome
Phospholipase A₂	17	HPOL_0000928401	YES
		HPOL_0000384601	YES
		HPOL_0002120101	NO
		HPOL_0001789301	NO
		HPOL_0001544401	NO
		HPOL_0002294901	NO
		HPOL_0000225901	NO
		HPOL_0002142601	NO
		HPOL_0001237801	NO
		HPOL_0000739901	NO
		HPOL_0000740001	NO
		HPOL_0001491401	YES
		HPOL_0000043801	NO
		HPOL_0000559401	NO
		HPOL_0001391701	NO
		HPOL_0000274901	NO
		HPOL_0001319601	NO
Cyclooxygenase, Prostaglandin-endoperoxide synthase, COX	1	HPOL_0000753101	NO
Prostaglandin E synthase	1	HPOL_0000513601	NO
Fatty acid desaturase 1	4	HPOL_0001982101	NO
		HPOL_0001800801	NO
		HPOL_0000711501	NO
		HPOL_0001929101	NO
Fatty acid desaturase 2	2	HPOL_0000711501	NO
		HPOL_0001929101	NO
Fatty acid elongase	0	-	-
Diacylglycerol lipase	1	HPOL_000612301	NO
Monoacylglycerol lipase	0	-	-
Fatty acid amidohydrolase	0	-	-
Phospholipase C	0	-	-
Hydroxyprostaglandin dehydrogenase 15, 15-prostaglandin dehydrogenase	0	-	-

4.4.7 PGES2 gene is expressed in the adult life-stage of *H. polygyrus*

To investigate gene expression of PGES2 at different points in the lifecycle of *H. polygyrus*, PCR was employed with cDNA prepared from larval (free-living), adult (intestinal) and eggs, with gene-specific primers designed for the *PGES2* (HPOL_0000513601) cDNA sequence. To ensure the cDNA in each lifecycle amplified, primers for *H. polygyrus actin* were used as a housekeeping gene as it has been shown to be equally expressed in all lifecycle stages (211). The results show that the *PGES2* gene expression appears to be restricted to the adult, intestinal-dwelling, stage of *H. polygyrus* (**Figure 6A**).

However, it should be noted that the *H. polygyrus actin* expression observed in the egg cDNA is significantly lower than expected (211), therefore it cannot be concluded from this experiment alone that PGES2 is not expressed in the egg lifecycle stage.

A phylogenetic tree for the *PGES2 H. polygyrus* gene was generated using WormBase Parasite and is shown in **Figure 6B**. The *H. polygyrus PGES2* gene is shown to have highly related gene IDs in the rodent nematode *N. brasiliensis*, as well as highly related gene IDs in ruminant and human nematodes, including *Haemonchus contortus* and *Necator americanus* (**Figure 6B**) suggesting conservation across species.

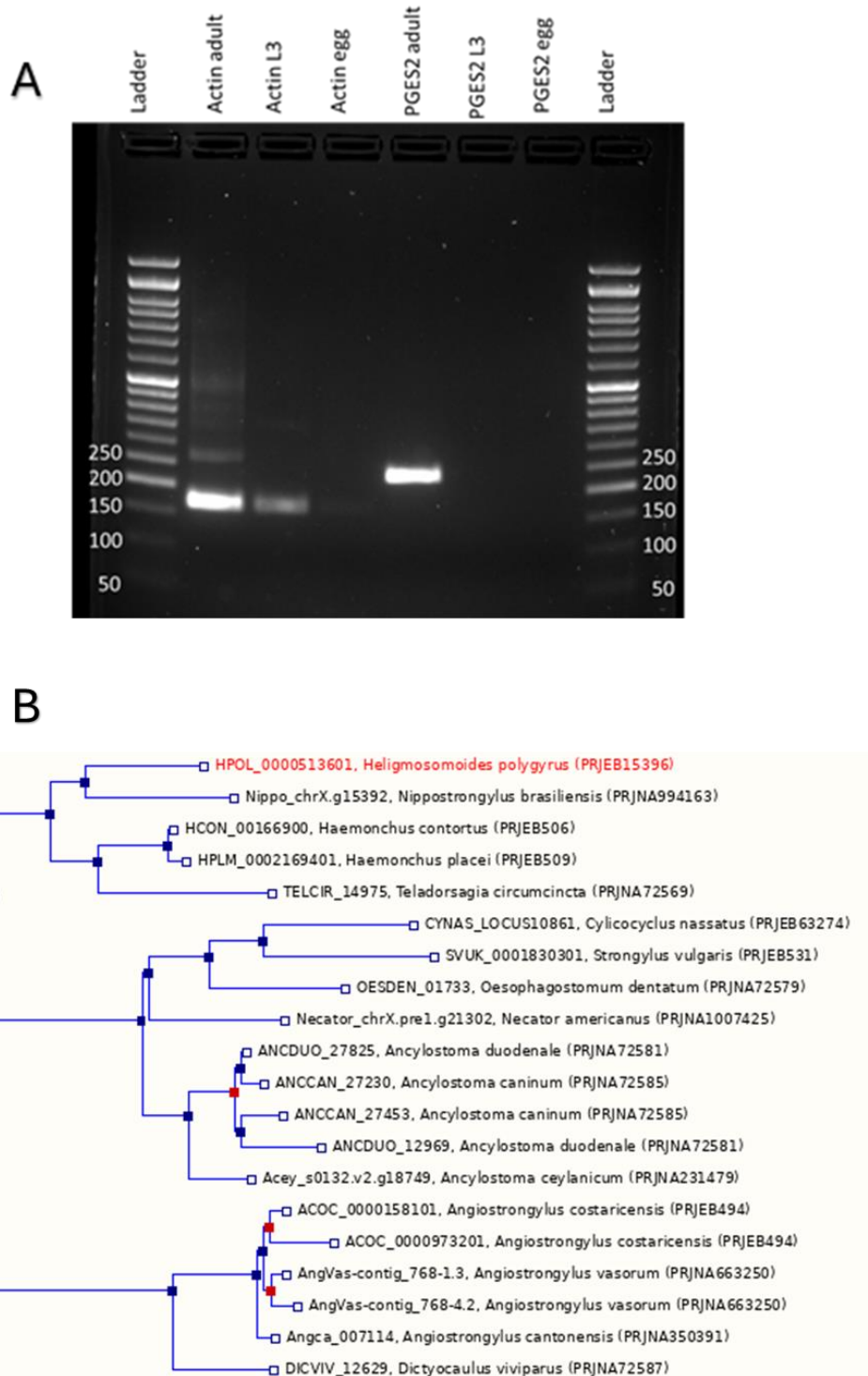


Figure 6. Gel electrophoresis showing gene expression of *H. polygyrus* *PGES2* at different lifecycle stages. (A) Adult, L3 larvae, and egg cDNA with primers designed against the HPOL_0000513601 *H. polygyrus* sequence. Actin was run as the housekeeping gene. Predicted product sizes: Actin – 180 base pairs (bp); HPOL_0000513601 – 235 bp. (B) Phylogeny trees showing high conservation of HPOL_0000513601 in other species of nematodes. Phylogeny trees generated in WormBase Parasite. Blue square – speciation node, red square – duplication node, clear square – gene node.

4.4.8 *H. polygyrus* PGES2 enzyme homologue shows highly conserved primary and tertiary amino acid structures to human and murine enzyme

The HPOL_0000513601 gene is predicted to encode a protein 346 amino acids in length with a predicted molecular weight of 39 kDa. Clustal Omega alignment of the predicted primary amino acid structure of HPOL_0000513601 with the human and murine PGES2 amino acid sequence (Uniprot ID: Q9H7Z7) revealed 41.94% identity, as well as 100% conservation of active site residues (**Figure 7A**). The 3D tertiary structure of the *H. polygyrus* PGES2 protein generated in Swiss-prot and the human PGES2 protein (Uniprot ID: Q9H7Z7) were aligned using Pymol software (**Figure 7B**). The alignment revealed a high degree of similarity, including active sites with similar configurations, with the only exception being the presence of an additional alpha helix in the human PGES2 structure.

A

HPOL_0000513601	EFYGFYSYIIVEVNPVTKSQLSFSRDYKIPVWTSSEGT---FVESLIISELATYLRRP	135
Homo_sapien	DFHALPYQVVEVNPVRRAEIKFS-SYRKIPILVAQEGESSQLNDSVIISALKTYLVS-	178
Mus_musculus	DFHSLPYQVVEVNPVRRTEIKFS-SYRKIPILVAQEGDSLQLNDSVIISALKTYLVS-	177
	:*::: *::***** ::::.* .*:***:..:.* : :***:* * **	
HPOL_0000513601	DRNFLFEIGDMYPSIDAINDEGKRVKCCPNMYFIMKGNDDDD-----LGAEREERKREWV	190
Homo_sapien	GQPLEEIITYYPAMKAVNEQGKEVTEFGNKYWLMLNEKAQQVYGGKEARTEEMKWRQWA	238
Mus_musculus	GQPLEEVITYYPPMKAMNDQGKEVTEFCNKYWLMLDEKAQQMYGGKEARTEEMKWRQWA	237
	.. * * : ** :.*:***.*. * *::* :.: : * . ** ***:..	
HPOL_0000513601	DDHFIHLISPNIYRSLTESFQTFEFWSHYGEWDVHFSTWSRLLAKYVGFVMMVAKRLK	250
Homo_sapien	DDWLVHLISPNVYRTPTEALASFDYIVREGKF---GAVEGAVAKYMGAAAYLISKRLK	294
Mus_musculus	DDWLVHLISPNVYRTPAEALASFDYIVREGKF---GAVEAAMAKYVGAAAYLISKRLK	293
	** :*****:**: :*: :*::: : *:: :. : :***:** .*:::**	
HPOL_0000513601	RRHNITDE-RKALTDAFNDWMNAIGPNRKYMGGDAPNLADLAMYGAMIAFAGCSAFNEAV	309
Homo_sapien	SRHRLQDNVREDLYEAADKWVAAVGKDRPFMGGQKPNLADLAVYGVLRVMEGLDAFDDLM	354
Mus_musculus	SRHHLQDDVRVDLYEAANKWVTAVGKDRPFMGGQKPNLADLAVYGVLRVMEGLEAFDDLM	353
	.: * : * * :* :.* :* * :*: *****:**: .: * .**:: :	
HPOL_0000513601	VNNPIERWFSMRRRAVQNHDRAMIARTKNLPIQAN	346
Homo_sapien	QHTHIQPWYLRVERAITEASPAH-----	377
Mus_musculus	RHSHIQPWYLRMERAIEEAPSVHHVNPCKD-----	384
	.. * : * : :***: :	

B

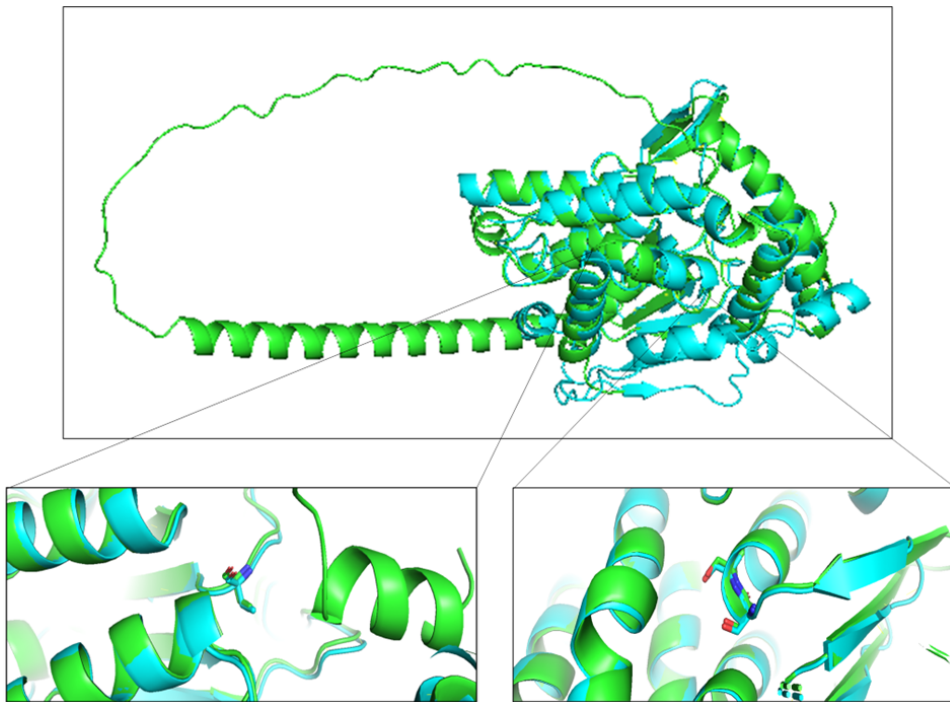
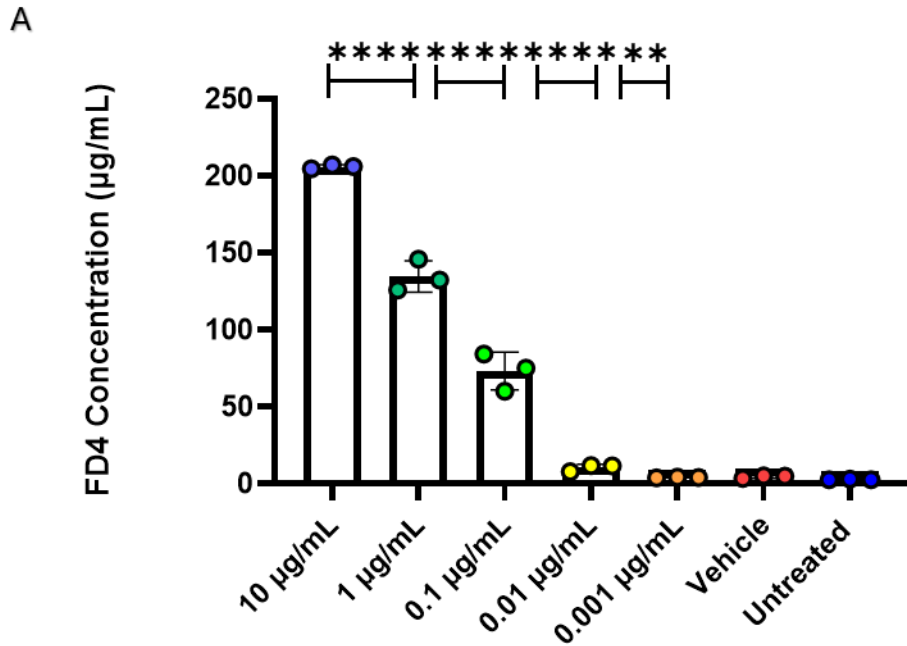


Figure 7. Amino acid sequence and tertiary structure alignment of *H. polygyrus* sequence HPOL_0000513601 against human and murine PGES2. (A) Amino acid alignment of HPOL_0000513601 to the human and murine PGES2. Active sites (green) are indicated. Symbols under each alignment indicate the degree of conservation between the sequences, with an asterisk (*) indicating positions which have a single, fully conserved residue, a colon (:) indicating conservation between groups of strongly similar properties and a period (.) indicating conservation between groups of weakly similar properties. *H. polygyrus* sequences obtained using WormBase ParaSite, human and murine sequences obtained using Uniprot. Alignment performed using Clustal Omega. **(B)** Alignment of the predicted tertiary structure of sequence ‘HPOL_0000513601’ (blue) and known human PGES2 crystal structure (green). Active site residues of the human PGES2 were marked on the alignment to identify homology at these sites. Alignment performed using PyMol (Version 2.5.2).

4.4.9 Addition of a recombinant human PGES2 increases cellular permeability

As PGES2 is one of the key enzymes involved in PGE₂ synthesis, it was hypothesized that it may be present in HES and contribute to increased PGE₂ production by the cells, subsequently enhancing cell permeability through EP2/EP4 receptor signalling. To investigate whether PGES2 increases cellular permeability, I added a recombinant human PGES2 in a 10 fold dilution series (0.001 – 10 µg/mL) to a CMT93 cell monolayer and measured FD4 concentration in the basolateral chamber after 20 hrs. As shown in **Figure 8A**, the addition of PGES2 resulted in a significant increase in cell permeability, with the addition of 0.001 µg/mL resulting in an average increase of 2.2415 µg/mL and the addition of 10 µg/mL resulting in an average increase of 204.196 µg/mL (**Figure 8B**). As the fold-change in FD4 concentration compared to the untreated control did not increase by factors of 10, it can be concluded that this observed effect is not dose-dependent. This data suggests that if *H. polygyrus* PGES2 is expressed, it may be one of the responsible molecules in the HES which increase cell permeability if it has the same activity as the human recombinant PGES2 used.



B

PGES2 concentration (µg/mL)	FD4 concentration (µg/mL)	Fold change from untreated
0	1.8 +/- 0.2	1
0.001	4.1 +/- 0.2	2.28
0.01	10.4 +/- 2.2	2.54
0.1	73.2 +/- 12.3	7.04
1	134.7 +/- 10.2	1.84
10	206 +/- 1.3	1.53

Figure 8. The addition of recombinant human PGES2 (rPGES2) causes a significant increase in cell permeability. (A) Titration of the human rPGES2 in a 1/10 dilution series (0.001 – 10 µg/mL) with FD4 concentrations being calculated from a standard curve. **(B)** Table showing the FD4 concentration and fold change from untreated with each concentration of PGES2. Mean +/- SD = +/- . Data shown is the mean of three independent experiments performed in triplicate. Unpaired T-test, **** p ≤ 0.001, error bars Mean ± SD.

4.4.10 *H. polygyrus* PGES2 is not predicted to be secreted

Having established that human recombinant PGES2 does increase cell permeability, it was investigated whether the *H. polygyrus* PGES2 sequence contains a signal peptide, to further confirm findings from the proteomics of *H. polygyrus* PGES2 not being secreted. Using SignalP software, HPOL_0000513601 was not predicted to contain a signal peptide (**Figure 9A**). Deeploc software predicted it is processed via a non-secretory pathway and expressed in the mitochondria (**Figure 9B**). In addition to utilising this prediction software, attempts to clone and express the *H. polygyrus* PGES2 protein proved

unsuccessful (details of the cloning strategy in Materials & Methods), as expression was only successful in the insoluble fraction (**Figure 9C**). These data demonstrate that the secretion of this homologue is unlikely to be responsible for HES-mediated increases in permeability of a CMT-93 cell line.

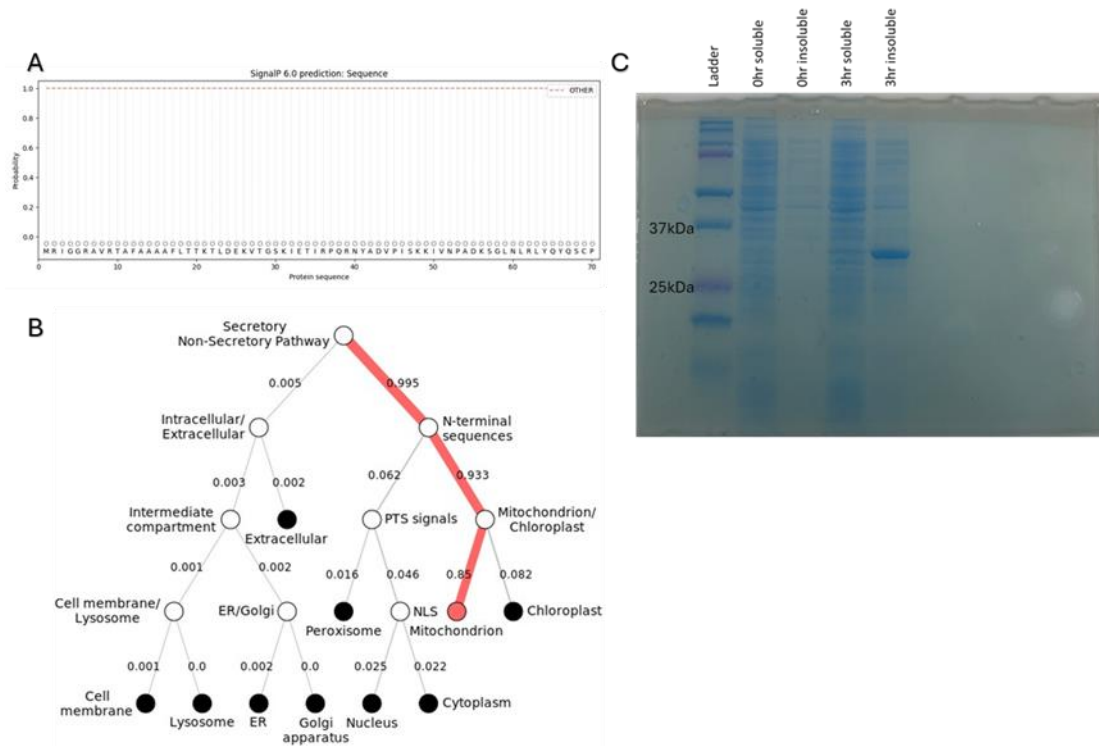


Figure 9. Evidence that the *H. polygyrus* HPOL_0000513601 sequence is predicted not to be secreted. (A) Signal peptide and **(B)** subcellular processing analysis performed using SignalP 6.0. and DeepLoc prediction software respectively. **(C)** SDS-PAGE gel stained with Instant Blue stain to detect expression of HPOL_0000513601 protein. Expected band size of expressed HPOL_0000513601 protein is 28kDa.

4.4.11 *H. polygyrus* has PLA₂ activity in the HES and adult antigen

Earlier in the chapter, bioinformatic analysis of the *H. polygyrus* genome revealed the presence of three PLA₂ homologue sequences; HPOL_0000384601, HPOL_0000928401, and HPOL_0001491401. The presence of all three proteins were confirmed with proteomic analysis, therefore I performed a colorimetric PLA₂ assay to investigate if the HES or *H. polygyrus* adult antigen has PLA₂ activity. The assay confirmed PLA₂ activity in both the HES and adult antigen (**Table 2**). This suggests that HPOL_0000384601, HPOL_0000928401, and HPOL_0001491401 may encode functional PLA₂ enzymes that are secreted into the HES.

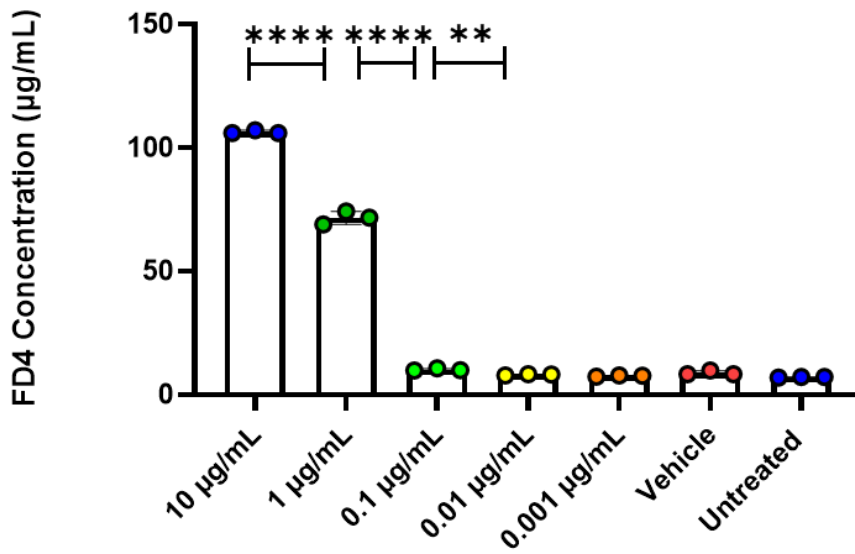
Table 2. Quantification of PLA₂ activity in the HES and adult supernatant

Sample	Fluorescent reading (460/515 nm)		Activity (U/mL)	Activity (U/μg)
HES	648.5	572.5	0.303	0.06
Adult supernatant	11206.5	11010.5	2.14	0.002

4.4.12 Addition of recombinant PLA₂ increases cellular permeability

A recombinant *Apis mellifera* PLA₂ was used to assess whether this enzyme causes an effect on cell permeability, as it has previously been demonstrated to do so (309). As with the recombinant human PGES2, I observed a significant increase in cell permeability with the addition of bee venom sPLA₂ (**Figure 10A**). Similarly, this effect was shown not to be dose-dependent (**Figure 10B**). This data suggests that the PLA₂ activity seen in the HES may contribute to its ability to increase cell permeability.

A



B

PLA ₂ concentration (µg/mL)	FD4 concentration (µg/mL)	Fold change from control
0	1.8 +/- 0.2	1
0.001	7.6 +/- 0.2	4.22
0.01	8.1 +/- 0.3	1.10
0.1	10.1 +/- 0.5	1.25
1	71.6 +/- 2.6	7.09
10	106.3 +/- 0.7	1.48

Figure 10. The addition of recombinant bee venom PLA₂ causes a significant increase in cell permeability. Titration of bee venom PLA₂ in a 1/10 dilution series (0.001 – 10 µg/mL) with FD4 concentrations being calculated from a standard curve. **(B)** Table showing the concentration and fold change from untreated with each concentration of PLA₂. Mean +/- SD = +/- . All values are corrected for background fluorescence. Data shown is the mean of three independent experiments. Significance was analysed using GraphPad Prism 10.2.0 and an unpaired T-test performed, where $p \leq 0.01$, **** $p \leq 0.001$. Where no statistical comparison is shown the result was not significant. Data presented as Mean ± SD.

4.4.13 *H. polygyrus* PLA₂ enzyme homologues show highly conserved primary and tertiary structures to human enzymes

With 10 catalytically active isoforms of human secretory PLA₂ (sPLA₂) known, I performed a percentage identity matrix to determine whether HPOL_0000384601, HPOL_0000928401, and HPOL_0001491401 share significant identity to a specific isoform of sPLA₂. As shown in **Figure 11** HPOL_0000384601 shares most significant identity to human PLA₂G1B (36.36%), HPOL_0000928401 to PLA₂G15 (44.99%), and HPOL_0001491401 to PLA₂G2A (26.26%).

Having confirmed which human isoforms the three *H. polygyrus* PLA₂ sequences share the most significant homology with, I compared the amino acid structures looking for conservation in active and binding sites (**Figure 12**). Alignment of the HPOL_0000384601 sequence with the human PLA₂G1B revealed 100% conservation of calcium binding sites and active sites (**Figure 12A**), suggesting HPOL_0000384601 may be an active homologue of the human PLA₂G1B enzyme. Despite HPOL_0000928401 showing conservation in the active sites of the human PLA₂G15, 50% of the zinc binding sites are not conserved (**Figure 12B**). Zinc can be used to inhibit activity in human PLA₂G15 (310), so although this does not rule out this enzyme being functional, it suggests the worm protein may not be inhibited in the same way. Similarly, HPOL_0001491401 shows conservation in the active site of the human PLA₂G2A, but the calcium binding sites are not conserved (**Figure 12C**), suggesting HPOL_0001491401 may not encode a functional PLA₂G2A.

Finally, as the amino acid alignments suggest HPOL_0000384601 may be the most likely homologue to possess PLA₂ activity, I compared the predicted tertiary structure of HPOL_0000384601 with the known tertiary structure of human PLA₂G1B, to analyse the configuration of the active sites. The tertiary structures show significant similarities in the overall structure, as well as highly identical configurations of active site residues (**Figure 13**). Together, this data suggests that HPOL_0000384601 encodes a functional PLA₂G1B enzyme, and may be the responsible molecule for the PLA₂ activity detected in the HES and adult antigen.

A

1: PLA2G15	100.00	13.58	18.61	11.51	9.02	16.78	16.45	16.94	10.77	9.30	9.45
2: PLA2G12A	13.58	100.00	20.41	20.62	29.13	28.04	20.00	21.57	26.47	23.53	21.00
3: PLA2G3	18.61	20.41	100.00	22.22	17.50	20.00	23.85	20.51	19.83	18.18	21.85
4: HPOL_0000384601	11.51	20.62	22.22	100.00	36.36	30.28	29.50	27.13	29.41	30.37	30.08
5: PLA2G1B	9.02	29.13	17.50	36.36	100.00	33.09	32.59	33.08	38.52	38.06	39.85
6: PLA2G10	16.78	28.04	20.00	30.28	33.09	100.00	32.17	37.78	38.03	35.46	37.41
7: PLA2G2F	16.45	20.00	23.85	29.50	32.59	32.17	100.00	38.97	44.06	40.14	40.00
8: PLA2G5	16.94	21.57	20.51	27.13	33.08	37.78	38.97	100.00	42.03	44.93	44.12
9: PLA2G2D	10.77	26.47	19.83	29.41	38.52	38.03	44.06	42.03	100.00	46.53	37.32
10: PLA2G2A	9.30	23.53	18.18	30.37	38.06	35.46	40.14	44.93	46.53	100.00	51.41
11: PLA2G2E	9.45	21.00	21.85	30.08	39.85	37.41	40.00	44.12	37.32	51.41	100.00

B

1: HPOL_0000928401	100.00	44.99	13.82	16.56	18.18	14.17	17.78	14.41	14.66	13.79	14.91
2: PLA2G15	44.99	100.00	11.26	15.76	12.84	19.84	16.42	20.18	18.42	15.79	15.18
3: PLA2G12A	13.82	11.26	100.00	18.71	30.19	25.86	19.66	20.95	26.36	21.82	19.44
4: PLA2G3	16.56	15.76	18.71	100.00	16.67	20.55	25.33	21.95	19.38	15.50	18.11
5: PLA2G1B	18.18	12.84	30.19	16.67	100.00	33.09	32.59	33.08	38.52	38.06	39.85
6: PLA2G10	14.17	19.84	25.86	20.55	33.09	100.00	32.17	37.78	38.03	35.46	37.41
7: PLA2G2F	17.78	16.42	19.66	25.33	32.59	32.17	100.00	38.97	44.06	40.14	40.00
8: PLA2G5	14.41	20.18	20.95	21.95	33.08	37.78	38.97	100.00	42.03	44.93	44.12
9: PLA2G2D	14.66	18.42	26.36	19.38	38.52	38.03	44.06	42.03	100.00	46.53	37.32
10: PLA2G2A	13.79	15.79	21.82	15.50	38.06	35.46	40.14	44.93	46.53	100.00	51.41
11: PLA2G2E	14.91	15.18	19.44	18.11	39.85	37.41	40.00	44.12	37.32	51.41	100.00

C

1: HPOL_0001491401	100.00	15.23	22.96	11.68	19.44	18.92	17.92	19.39	15.15	26.26	16.49
2: PLA2G15	15.23	100.00	13.25	17.68	12.20	15.83	14.58	16.24	13.82	12.20	9.92
3: PLA2G12A	22.96	13.25	100.00	18.71	30.19	25.86	19.66	20.95	26.36	21.82	19.44
4: PLA2G3	11.68	17.68	18.71	100.00	16.67	20.55	25.33	21.95	19.38	15.50	18.11
5: PLA2G1B	19.44	12.20	30.19	16.67	100.00	33.09	32.59	33.08	38.52	38.06	39.85
6: PLA2G10	18.92	15.83	25.86	20.55	33.09	100.00	32.17	37.78	38.03	35.46	37.41
7: PLA2G2F	17.92	14.58	19.66	25.33	32.59	32.17	100.00	38.97	44.06	40.14	40.00
8: PLA2G5	19.39	16.24	20.95	21.95	33.08	37.78	38.97	100.00	42.03	44.93	44.12
9: PLA2G2D	15.15	13.82	26.36	19.38	38.52	38.03	44.06	42.03	100.00	46.53	37.32
10: PLA2G2A	26.26	12.20	21.82	15.50	38.06	35.46	40.14	44.93	46.53	100.00	51.41
11: PLA2G2E	16.49	9.92	19.44	18.11	39.85	37.41	40.00	44.12	37.32	51.41	100.00

Figure 11. Percentage identity matrix *H. polygyrus* PLA₂ sequences to human sPLA₂ enzymes. The % identity of the amino acid sequences of (A) HPOL_0000384601, (B) HPOL_0000928401, and (C) HPOL_0001491401 were compared to the 10 isoforms of human sPLA₂. Analysis performed in Clustal Omega.

A

HPOL_0000384601 PLA2G1B	MHRAILLGLIPQLLSV-TVVPKQV GALWNFGEVAECVLHY--NALVYNNYGCWCGVGG --MKLLVL---AVLLTVAADSGISPRAVWQFRKMIKCVIPGSDPFLEYNNYGCYCLGG :*** **:* . . *:* * : : ** : * *****:**:**	57 55
HPOL_0000384601 PLA2G1B	SHEPVDEIDRCMHHDKCYDAAVDKKVC-FDVAWEYIDSYKWKINSTAICTETSDNCKA SGTPVDELKCCQTHDNCYDQAKKLDSCFKLLDNPHYHTYSYSCSGSAITCSSKNKECEA * *****:** **:** * . . * * : * .:*.:. * .*: * :.....:**	116 115
HPOL_0000384601 PLA2G1B	ALCAGVAVVNCWSQYGKPKRRAKCNRTPTKTRFLH- 155 FICCDRNAAICFSKAPYNKAHKNL-----DTKKYCQS 148 :* ** .. *:* : : : .*.: :	

B

HPOL_0000928401 PLA2G15	LIETTYRYNAHTRIIITVGHSMGNPMMLYFFNKIVDQEWKDKYIESHVSLAAPWGGSMQIV MIEEMYQLYGG-PVVLVAHSMGNMYTLYFLQR-QPQAWKDKYIRAFVSLGAPWGGVAKTL :** * : . : : *.***** ***: : * *****.:.***.***** : :	217 237
HPOL_0000928401 PLA2G15	RLFASGYNMNYRIVLPPSKLRGMQRSFTSSAF LFPSNGVWNSTEVLASTVEKNYTVANV RVLASGDNNR--IPVIGPLKIREQQRSAVSTSWLLPYNWTSPEKVFVQTPPTINYLDRDY *::*** * . : : * *:* *** .*: : * * * .*: : * * * : * * * : :	277 295
HPOL_0000928401 PLA2G15	QEFFQDINMTGWEQYVAAQLNGKLDPPGVKVVHICIYSGSLSTPEQFNWAKGYFPDYQPA RKFFQDIGFEDGWLMRQDTEGLVEATMPPGVQLHCLYGTGVPTPDSFYFE--SFPDRDPK :*****.: ** * : * *****:**:**:** **:* : *** :*	337 353
HPOL_0000928401 PLA2G15	VVYGDGDGTGNKRSAEVCLNWNKNNNGKPVTTHEVPNAEHMGILQSPVAIEIVRKAIVG ICFGDGDGTGNLKSALQCAWQSRQEH--QVLLQELPGSEHIEMLANATTLAYLKRVLG : ***** ** * * : : : : * : * : * : * : * . : : : : * *	397 411
HPOL_0000928401 PLA2G15	LL 399 P- 412	

C

HPOL_0001491401 PLA2G2A	ECRLKNRETTFHFTCKDGLWYDSDNVYDGG LPAHLSCSATPIDFIGNGTWE CGTTPFVK -----EAALSYGFYGC HCGVGG-----R----- : : : : * : *	115 53
HPOL_0001491401 PLA2G2A	QLFLAPVSLFCPSLRNDLNACCNQHDQCYTDQKGRE-----K -----GSPKDATDRCCVTHDCCYKRLKRGCGTKFLSYKFSNSGSRITCAKQDS * : : : ** ** * . : *	152 102
HPOL_0001491401 PLA2G2A	CDGIYCRCLTRVTKHSNWGCRVLYSKAYCALVKAFGGSAYEASKDYVPPEKKD----- CRSRLCECDKAAAT-----CF-----ARNKTTYNKKYQYYSNKHCRGSTPRC * . *. * . . . * * . : * : * : *	205 144

Figure 12. Amino acid alignment of *H. polygyrus* PLA₂ homologues to human PLA₂ enzymes. Amino alignment of (A) HPOL_0000384601 to human PLA₂G1B, (B) HPOL_0000928401 to human PLA₂G15, and (C) HPOL_0001491401 to human PLA₂G2A. In all alignments active site residues are coloured in blue. In alignment (A) and (C) calcium binding sites are highlighted in yellow, whereas in (C) zinc binding sites are highlighted in yellow. Symbols under each alignment indicate the degree of conservation between the sequences, with an asterisk (*) indicating positions which have a single, fully conserved residue, a colon (:) indicating conservation between groups of strongly similar properties and a period (.) indicating conservation between groups of weakly similar properties. Alignment performed using Clustal Omega

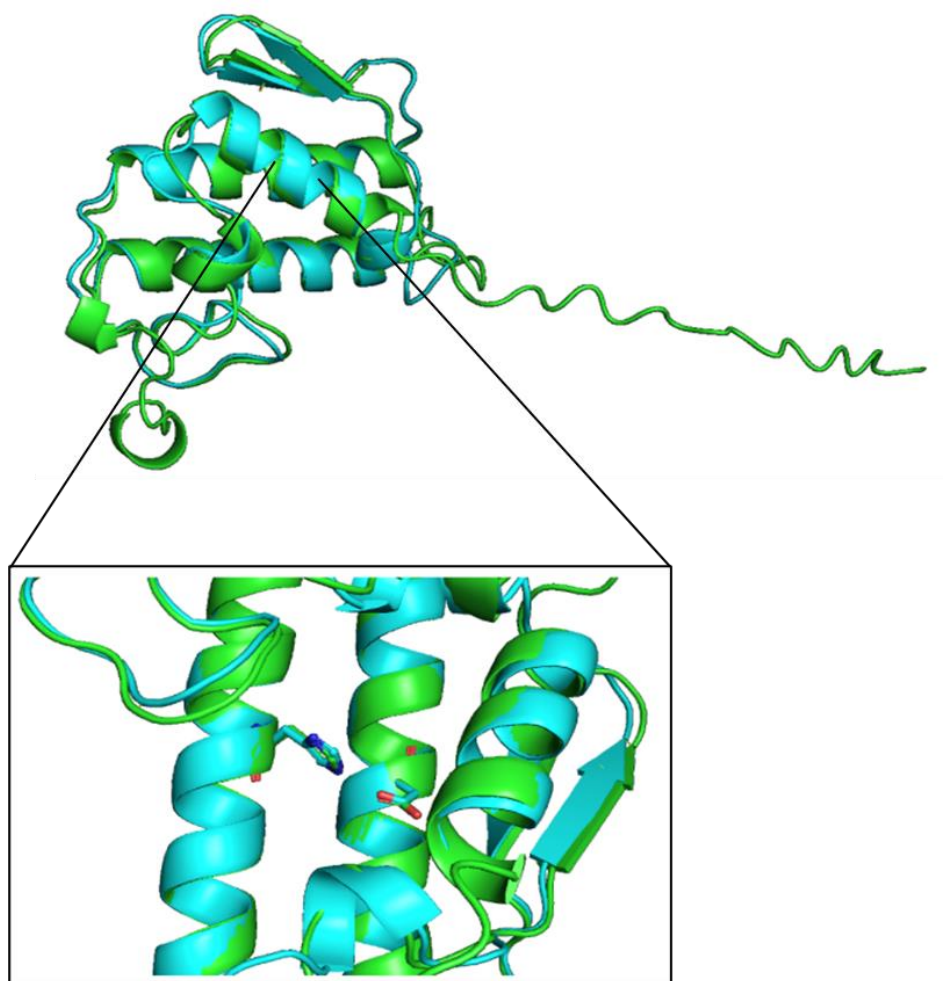


Figure 13. Tertiary structure alignment of HPOL_0000384601 to human PLA₂G1B. The predicted tertiary structure of HPOL_0000384601 (blue) is aligned to the known human PLA₂G1B tertiary structure (green). Known active residues of human PLA₂G1B at His70 and Asp121 are highlighted. Alignment performed using PyMol (Version 2.5.2).

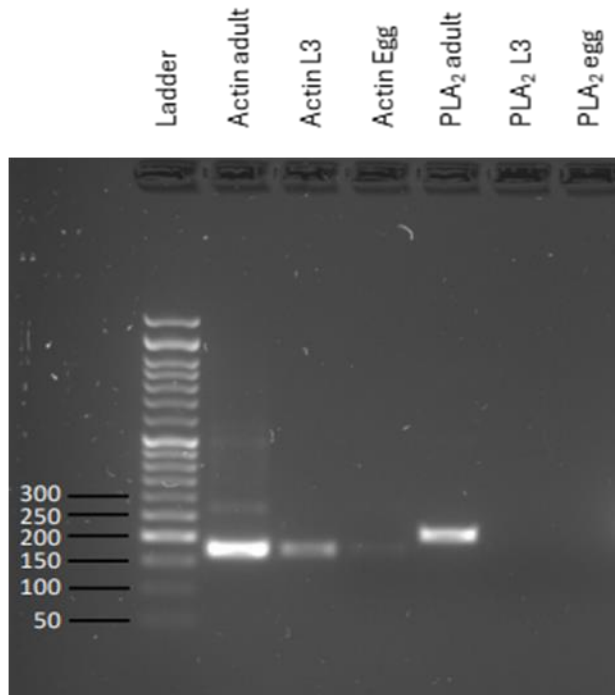
4.4.14 *sPLA₂* gene is expressed in the adult life-stage of *H. polygyrus*

With HPOL_0000384601 being suggested to encode a functional PLA₂G1B, I designed primers for the *H. polygyrus sPLA₂* (Gene ID: HPOL_0000384601) cDNA sequence and investigated gene expression at different points in the lifecycle of *H. polygyrus*. The results show that the *sPLA₂* gene expression appears to be restricted to the adult, intestinal-dwelling, stage of *H. polygyrus* (**Figure 14A**) as was the case with the *PGES2* gene earlier in the chapter. Again, the *H. polygyrus actin* expression observed in the egg cDNA is significantly lower than expected (211), therefore it cannot be concluded from this experiment alone that *sPLA₂* is not expressed in the egg lifecycle stage.

A phylogenetic tree for the *sPLA₂* *H. polygyrus* gene was generated using WormBase Parasite and is shown in **Figure 14B** respectively. The *H. polygyrus sPLA₂* gene is shown to have highly related gene

IDs in the rodent nematode *N. brasiliensis*, as well as highly related gene IDs in canine and human nematodes, including *Ancylostoma caninum* and *Necator americanus* (**Figure 14B**) suggesting conservation between species.

A



B

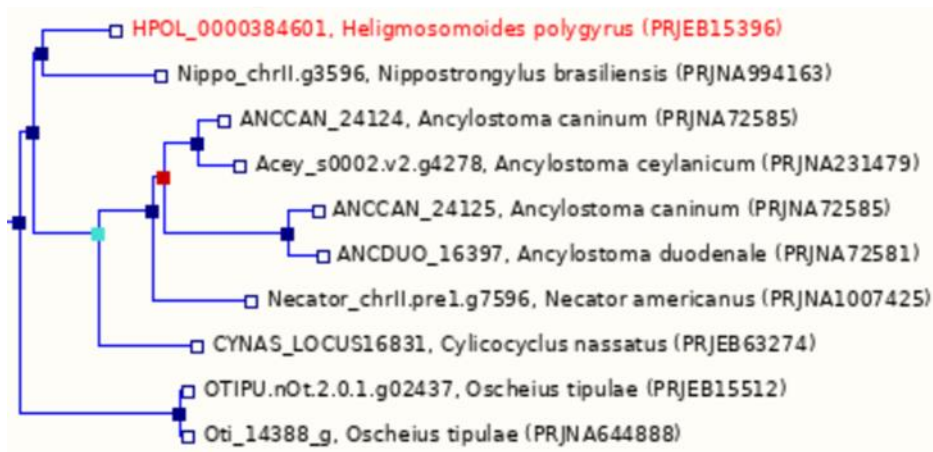


Figure 14. Gel electrophoresis showing gene expression of *H. polygyrus* *sPLA*₂ at different lifecycle stages. (A) Adult, L3 larvae, and egg cDNA with primers designed against the HPOL_0000384601 *H. polygyrus* sequence. Actin was run as the housekeeping gene. Predicted product sizes: Actin – 180 base pairs (bp); HPOL_0000384601 – 205 bp. **(B)** Phylogeny trees showing high conservation of HPOL_0000384601 in other species of nematodes. Phylogeny trees generated in WormBase Parasite. Blue square – speciation node, red square – duplication node, clear square – gene node.

4.4.15 *H. polygyrus* sPLA₂ is predicted to be secreted

Having shown HPOL_0000384601 as being the most likely candidate for encoding a functional sPLA₂ enzyme homologue, and how it shows preferential expression for the adult-stage of *H. polygyrus*, I finally wanted to investigate whether HPOL_0000384601 is predicted to be secreted. The HPOL_0000384601 sequence is predicted to contain a signal peptide sequence (**Figure 15A**), and is processed via a secretory pathway into the extracellular domain (**Figure 15B**). Furthermore, proteomic analysis of the 10-50,000 MW fraction confirmed the presence of HPOL_0000384601, indicating it is secreted in the HES. Therefore, this data suggests that HPOL_0000384601 may encode a functional sPLA₂ enzyme, enabling an increase in the amount of arachidonic acid available to the cells to convert to PGE₂, leading to enhanced EP2/EP4 activation and subsequent cell permeability.

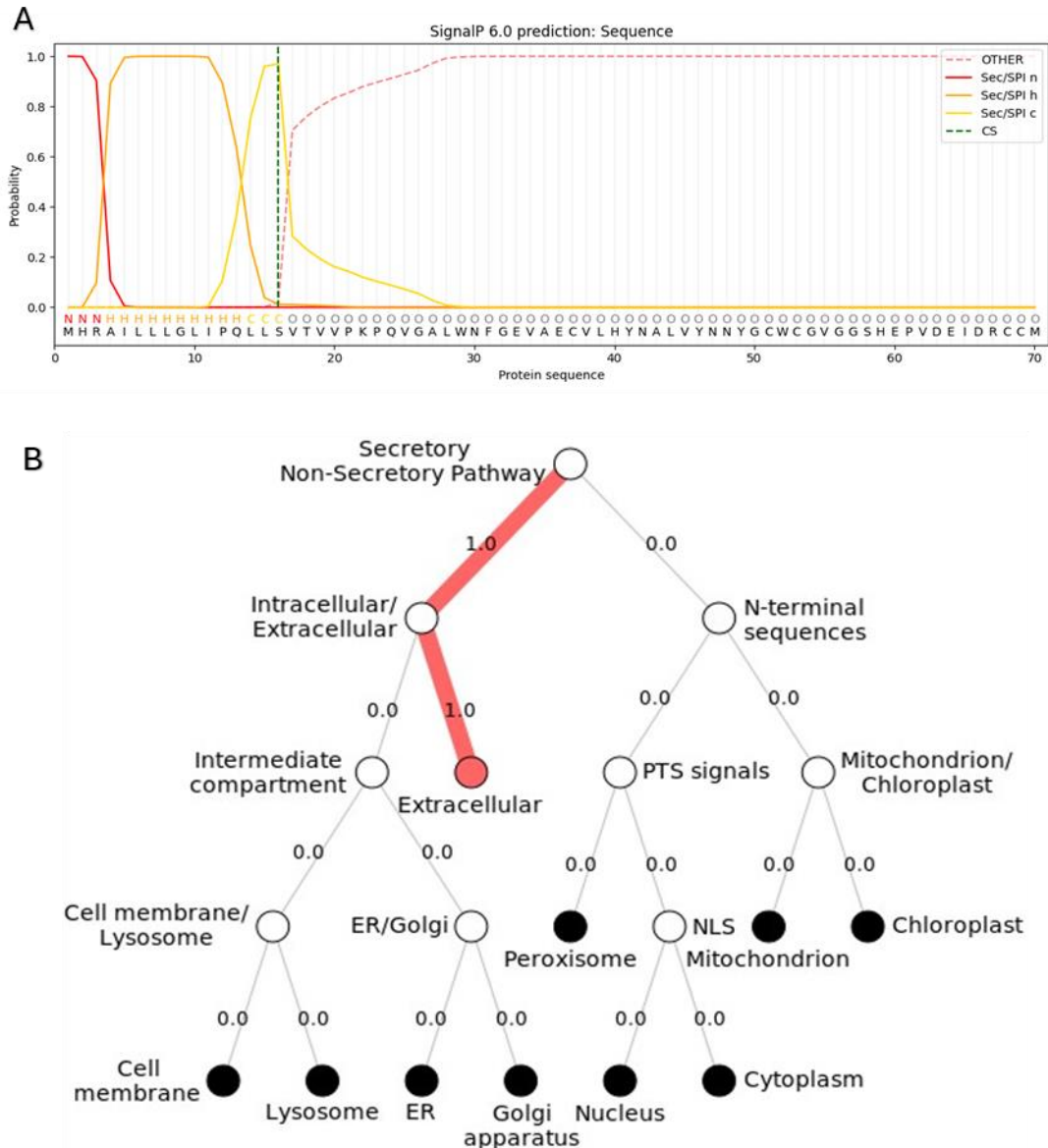


Figure 15. Evidence that the *H. polygyrus* HPOL_0000513601 sequence is predicted to be secreted. (A) Signal peptide and (B) subcellular processing analysis performed using SignalP 6.0. and DeepLoc prediction software respectively.

4.5 Discussion

To summarise, this chapter follows on from findings in Chapter 3, whereby the ability of HES to increase permeability via EP2/EP4 signalling was uncovered, but the molecule responsible remains unknown. Biochemical characteristics of the molecule(s) are revealed, with it not being a protease, heat-stable, and between 10,000 – 50,000 molecular weight. The possibility of HES containing PGE₂ or any other oxylipin was eliminated using LC/MS, with the genome analysis identifying sequences bearing significant identity to PGES2 and several members of the sPLA₂ family. It was demonstrated using predictive software that HPOL_0000384601 is predicted to be secreted, with proteomics confirming it

is secreted into the 10,000 – 50,000 molecular weight HES fraction. Along with existing literature showing that sPLA₂ can increase cellular permeability, and the evidence presented in this chapter, it is suggested that *H. polygyrus* sPLA₂ may play a key role in increasing PGE₂ synthesis and subsequent EP2/EP4 signalling, ultimately leading to increased cell permeability.

Within the HES mixture, Hewitson *et al* profiled several examples of enzymes belonging to the protease family (145). Proteases are naturally occurring in the intestine in low levels to maintain gut homeostasis, however they are significantly upregulated during inflammatory disorders, and are associated with a loss in integrity of the intestinal barrier (69, 74, 75). Furthermore, the ESPs mechanism of *T. suis* and *T. spiralis* have been shown to contain serine proteases, and it is the release of these serine proteases which enables them to breakdown the intestinal barrier, the proposed by which they establish their respective lifecycles (168, 169). By adopting similar methods of heat-inactivation and protease inhibition used by Hasnain *et al* and Song *et al* (168, 169), the possibility of a protease being responsible for the ability of HES to increase cell permeability is unlikely. The use of a broad range protease inhibitor cocktail is a robust method of inhibiting proteases, however it is a possibility that *H. polygyrus* proteases may have significant structural discrepancies deeming the inhibitor ineffective against them (311, 312). It is also important to acknowledge the existence of proteases whereby activity can still remain despite the high temperature, such as certain isoforms of matrix metalloproteases (MMPs) (313), which cannot be conclusively ruled out.

Evidence from Chapter 3 strongly suggests that the HES is acting through PGE₂ receptors EP2 and EP4 to increase cell permeability. The initial hypothesis was that the HES may contain PGE₂ which is then able to activate EP2 and EP4 receptor signalling in the CMT93 cell monolayers. Using LC/MS, PGE₂ has been detected in *T. suis* ES (35,945 pg/mL +/- 516.2) as well as different lifecycle stages of *S. mansoni* as a proposed immunomodulatory oxylipin (194, 196). Given that lipidomic analysis has never been performed on the HES, LC/MS was performed in an attempt to identify if PGE₂, or any other oxylipins are present. It was shown that HES doesn't contain PGE₂ or any other oxylipins, however this experiment is limited by the level of detection, and it is possible HES contains oxylipins at concentrations beyond the level of detection used.

As the HES doesn't contain high amounts of PGE₂ compared to *T. suis*, it was investigated whether HES is stimulating the CMT93 cell monolayer to produce PGE₂, enabling increased paracrine or autocrine signalling through the EP2 and EP4 receptors. Activation of EP2 signalling in neutrophils is linked to stimulation of cAMP production, increased expression of pro-inflammatory genes, including the prostaglandin endoperoxide synthase-2 (*Ptgs2*) gene encoding COX-2 and thus increased production of PGE₂ (300). Similarly in human colorectal cancer cell line, activation of EP4 receptor signalling was

also shown to elevate cAMP levels via COX-dependent PGE₂ synthesis (314). Following exposure of human monocyte derived macrophages to the larval products of *H. polygyrus*, increased PGE₂ production was associated with increased *Ptgs2* expression, which could be inhibited by the non-selective COX inhibitor (indomethacin) and a selective COX-2 inhibitor (CAY10404) (306). In this chapter, it was shown that aspirin treatment inhibits the ability of HES to increase cell permeability in a similar manner to dmPGE₂, suggesting that the ability of HES to increase cell permeability is both COX-dependent as well as EP2 and EP4 receptor signalling. However, whether CMT93 cells increase PGE₂ synthesis upon HES stimulation in this assay would need to be determined.

A possible mechanism for HES increasing PGE₂ autocrine or paracrine signalling is by secreting enzymes which contribute to PGE₂ synthesis, and therefore leading to increased EP2/EP4 activation. Of particular importance was the identification HPOL_0000513601 bearing significant amino acid identity to PGES2, and HPOL_0000384601, HPOL_0000928401, and HPOL_0001491401 showing identity to isoforms of the sPLA₂ enzyme family. These are believed to be significant findings as both PGES2 and sPLA₂ enzymes are critical for the synthesis of PGE₂.

Proteomic analysis of the 10-50,000 MW HES fraction revealed the secretion of HPOL_0000384601, HPOL_0000928401, and HPOL_0001491401 but not HPOL_0000513601. Further analysis revealed a lack of conservation of the HPOL_0000928401 and HPOL_0001491401 amino acid sequences with the zinc and calcium binding domains of the human PLA₂G15 and PLA₂G2A enzymes respectively. This is believed to be a significant discrepancy, as PLA₂G2A is known to be calcium-dependent (315), and so the inability of HPOL_0001491401 to bind calcium may deem the enzyme inactive. In contrast, HPOL_0000384601 was shown to have conservation within the calcium binding sites of human PLA₂G1B, therefore HPOL_0000384601 was pursued as a potential active enzyme homologue.

Further evidence for HPOL_0000384601 being secreted in the HES was provided by utilising a PLA₂ colorimetric assay, showing PLA₂ activity in the HES. It is believed that this is the first description of PLA₂ activity in the HES, but the presence of a sPLA₂ enzyme has been shown in the ESPs of other species of helminths, such as *Trypanosoma cruzi* and *Trypanosoma brucei* (316, 317). The PLA₂ enzyme produced by *T. brucei* is shown to be important in releasing arachidonic acid and increasing the release of eicosanoid products that modulate the host immune response (318). Additionally, sPLA₂ in the products of *Steinernema carpocapsae* was shown by Parks *et al* to possess immunosuppressive properties, such as downregulation of the production of anti-microbial peptides (199). Phylogenetic analysis revealed high conservation of HPOL_0000384601 with other species of helminths such as *N. americanus* and *H. contortus*, suggesting this may be a highly conserved component of helminth ESPs.

The activity of sPLA₂ enzymes results in the release of bioactive oxylipins which are involved in several biological functions such as immunomodulation and inflammation, and is crucial for the liberation of arachidonic acid, a key precursor in the biosynthesis of PGE₂ (319-321). The discovery of sPLA₂ activity in the HES is exciting, however the benefit of *H. polygyrus* encoding such an enzyme currently remains unclear. In order to gather more information as to how *H. polygyrus* might exploit the presence of this enzyme, the cDNA of three different lifecycle stages of *H. polygyrus* was analysed: the infective L3 larvae, the tissue-dwelling adult, and the egg to see if its expression was unique to one or more lifecycle stage. The gene expression of the sPLA₂ homologue sequence HPOL_0000384601 was discovered in the adult tissue-dwelling stage, however it is acknowledged that the expression of the housekeeping gene actin is significantly lower in the L3 and egg cDNA than what would be expected based on previous publications (211, 304), therefore it cannot be concluded that it is not expressed in L3 or egg *H. polygyrus* cDNA without replication. Nonetheless, the discovery of adult expression is interesting, as this suggests that *H. polygyrus* may utilise this enzyme as an immunomodulation strategy. Another function could be to liberate polyunsaturated fatty acids from the phospholipid bilayer as a source of nutrition, as *H. polygyrus* has been shown to feed on epithelial cells as opposed to blood (322). These speculative functions of HPOL_0000384601, and whether its function is important in *H. polygyrus* survival, require further investigation.

Finally in this chapter, it is eluded that the PLA₂ activity seen in the HES is key in explaining how HES treatment of a cellular monolayer results in an increase in permeability. It was first demonstrated how the addition of a secretory sPLA₂ isolated from *A. mellifera* is able to increase cell permeability, which corroborates evidence in the literature of PLA₂ enzymes being able to disrupt cellular barriers (323-325). The levels of PLA₂ are shown to be elevated in the sera of ulcerative colitis patients, where a compromised intestinal barrier is a key characteristic of disease (326). PLA₂ mediates hydrolysis of phosphatidylcholine (PC) to lysophosphatidylcholine (L-PC), and when both are applied to the apical surface of a murine intestinal cell monolayer an increase in permeability is observed (325), suggesting the implications of helminth-secreted PLA₂ on human epithelial barriers.

Together, evidence presented in this chapter suggests the ability of HES to increase cell permeability may be due to an active homologue of human PLA₂G1B, which enable an increase in PGE₂ synthesis and EP2/EP4 activation.

The aims of this chapter were achieved successfully, with the ability of HES to increase permeability shown not to be due to proteases, the lipidomic profile of HES screened for oxylipins, and the presence of a potential PLA₂G1B homologue discovered. The first hypothesis of this chapter, that the HES contains PGE₂, was disproven with LC/MS analysis. The second hypothesis that the HES contains

metabolic enzymes that may contribute to PGE₂ synthesis was proved to an extent, with the discovery of *H. polygyrus* PLA₂G1B. However it still remains unknown from this chapter whether there is increased PGE₂ production from CMT93 cells treated with HES.

Chapter 5: *H. polygyrus* secretory phospholipase A₂ drug development and linking its activity to increased cell permeability

5.1 Introduction

In the previous chapter, screening of the *H. polygyrus* genome revealed three potential homologues to the human PLA₂ enzyme family. Alignment of the amino acid sequences using Clustal Omega, and superimposition of the tertiary structures using PyMol revealed sequence HPOL_0000384601 as showing the most conservation between active and binding sites of the human PLA₂G1B enzyme.

Several PLA₂ enzymes have been shown to influence inflammatory diseases in the gastrointestinal tract (GIT), with PLA₂G4A shown to exacerbate DSS colitis and decrease E-cadherin expression *in vivo* (327). Interestingly, inactivation of PLA₂G4A using barberine, a natural benzylisoquinoline alkaloid found in a wide variety of plants such as *Coptis chinensis* Franch. (Chinese goldthread), was shown to be beneficial in suppressing disease (328). PLA₂G1B is one of the most abundant PLA₂ in the GIT, and genetic inactivation of PLA₂G1B has been shown to protect against DSS-induced colitis by restoring expression of zonula occludens 1 (ZO1) and E-cadherin (329). Furthermore, increased PLA₂ activity is proposed to trigger PGE₂ biosynthesis, and is associated with increased EP signalling (330), leading to subsequent increase in cell permeability (108) (**Figure 1**). Evidence from previous chapters has shown that the ability of HES to increase cell permeability is dependent on EP2/EP4 signalling and COX activity. In this chapter, the proposed mechanism summarised in **Figure 1** will be investigated, whereby it is proposed that the *H. polygyrus* PLA₂G1B secreted in the HES increases biosynthesis of PGE₂ in the cell monolayer, leading to increased autocrine or paracrine EP2/EP4 signalling and decreased E-cadherin expression.

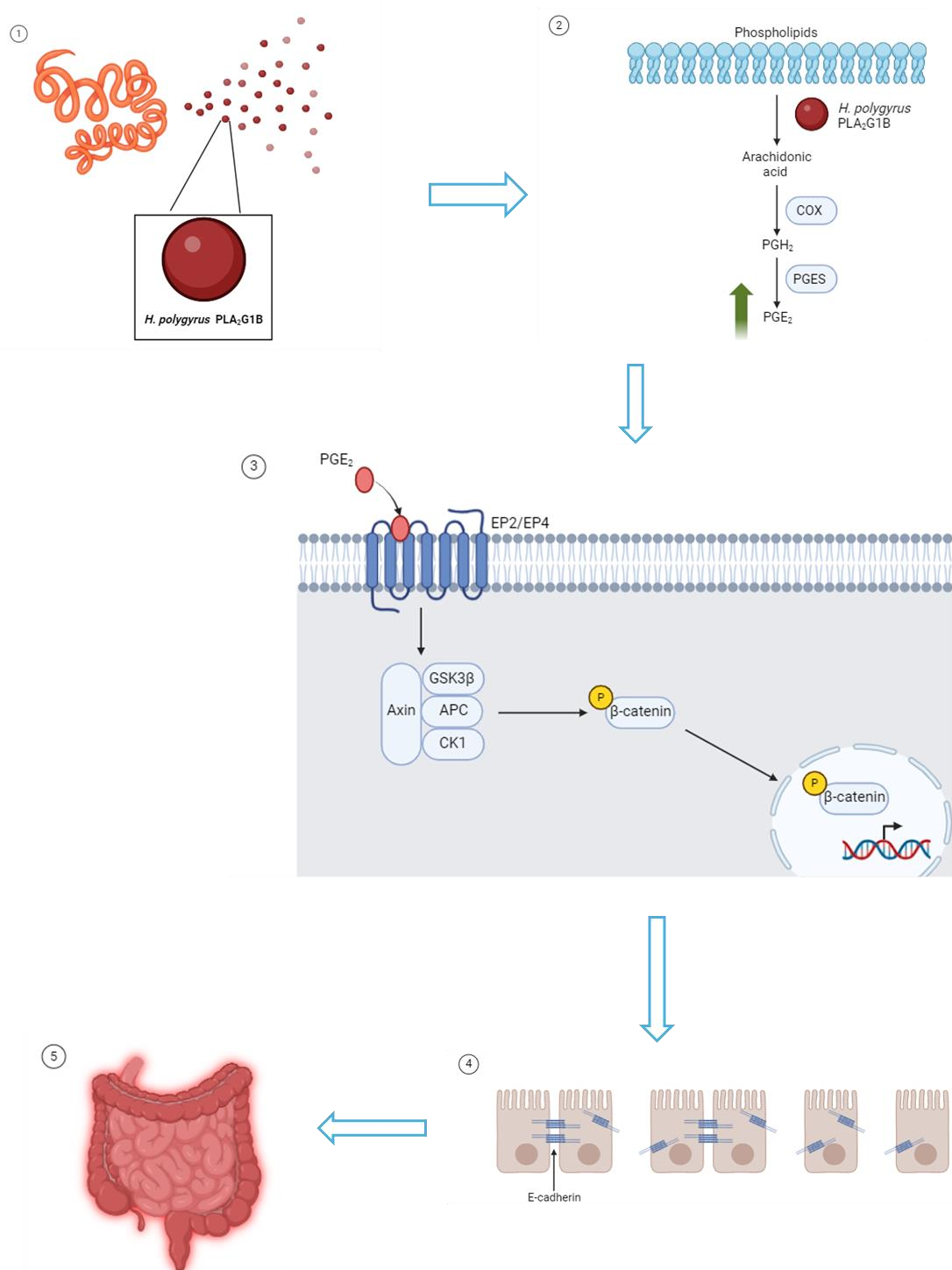


Figure 1. Schematic showing the proposed mechanism by which *H. polygyrus* phospholipase A₂ exacerbates cell permeability. **1.** Adult *H. polygyrus* releases HES once it emerges into the intestinal lumen, and within the HES is a secreted PLA₂G1B homologue ("*H. polygyrus* PLA₂G1B"). **2.** *H. polygyrus* PLA₂G1B results in the release of arachidonic acid from the phospholipid bilayer, which then promotes the increased production of prostaglandin E₂ (PGE₂). **3.** The PGE₂ binds to EP2/EP4 receptors, thereby increasing phosphorylation of β -catenin Ser⁵⁵². **4.** The increased EP2/EP4 receptor signalling results in disassembly of E-cadherin and an increase in cell permeability. **5.** The increase in cell permeability results in an increase in intestinal inflammation. Image created in Biorender.

With the involvement of sPLA₂s in the development and progression of inflammatory diseases coming to light, several small-molecule synthetic inhibitors have been developed (331, 332). One of the most well-known sPLA₂ inhibitors is varespladib, which shows high-level inhibition of snake venom sPLA₂ at nano- and picomolar concentrations (333). Another potent sPLA₂ inhibitor is manoalide, designed against cobra venom PLA₂, and known to inhibit rodent sPLA₂ in an irreversible manner (334). Both these drugs have been used to inhibit human and rodent sPLA₂ enzymes (335, 336), but have not been tested against helminth PLA₂ activity. Interestingly, neither of these drugs have been used in permeability assays, therefore their effect is unknown. Experiments conducted by Mazvydas Koveckis showed that these two commercial inhibitors could effectively inhibit *Apis mellifera* PLA₂ activity (**Figure 2A&B**), with 100 μM manoalide inhibiting activity by 87.1% and 100 μM varespladib inhibiting activity by 92.5%. However, these concentrations did not significantly alter PLA₂ activity in the somatic antigen isolated from *H. polygyrus*, with 100 μM manoalide resulting in an agonistic effect, whereas 500 μM of varespladib was required to see significance (**Figure 2C&D**).

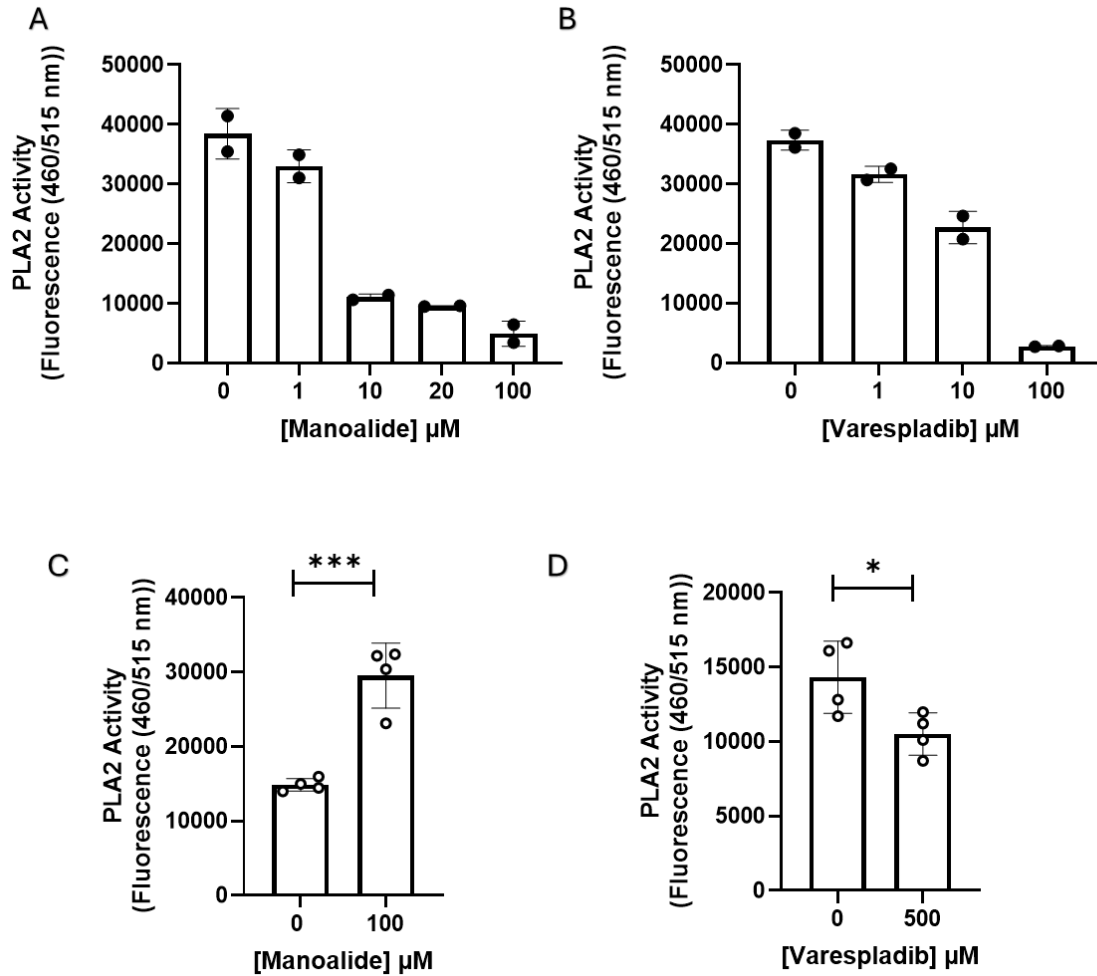


Figure 2. The commercially available PLA₂ inhibitors manoalide and varespladib effectively inhibit bee venom PLA₂ activity, however are ineffective against *H. polygyrus* PLA₂. Data re-plotted from experiments performed by M Koveckis, *A. mellifera* PLA₂ activity measured after treatment with titration of (A) manoalide or (B) varespladib. PLA₂ activity measured in *H. polygyrus* somatic antigen after treatment with titration of (C) manoalide or (D) varespladib. Data shown represents (A&B) two (n = 2) or (C&D) four (n = 4) technical replicates. Error bars Mean \pm SD.

As the commercially available sPLA₂ inhibitors were ineffective on the *H. polygyrus* PLA₂G1B homologue, an *in silico* structure-based methodology was utilised in an attempt to design molecules to be specific for the *H. polygyrus* PLA₂G1B. This proposed strategy has been successfully used to design novel helminth-specific inhibitors, for example, Zheng *et al* successfully developed an inhibitor specific for *S. mansoni* cyclic nucleotide phosphodiesterase 4A (337).

By using inhibitors designed using *in silico* structure-based drug design, this chapter aims to define a role for *H. polygyrus* PLA₂G1B in increasing cell permeability.

5.2 Chapter Aims

1. Screen for effective inhibitors of the *H. polygyrus* PLA₂G1B homologue, using *in silico* structure-based drug design
2. Determine whether inhibition of *H. polygyrus* PLA₂G1B activity prevents HES-dependent increases in cell permeability

5.3 Hypothesis

1. A helminth-derived PLA₂G1B homologue increases cell permeability

5.4 Results

5.4.1 Structure-based identification of potential *H. polygyrus* secretory phospholipase A₂ inhibitors and molecular docking studies

With the use of two commercial PLA₂ inhibitors proven to be unsuccessful, a well characterised *in silico* structure-based virtual screening approach (338-340) was adopted to identify novel inhibitors of *H. polygyrus* PLA₂G1B. As there is no 3D crystal structure for *H. polygyrus* PLA₂G1B, one first had to be generated using the Iterative Threading ASSEmbly Refinement (I-TASSER) protein threading technique (254). The high-resolution crystallographic structure of human sPLA₂ complexed with a highly potent inhibitor (FPL67047XX) (Protein Data Bank (341) accession code PDB ID: 1KVO (342)) was selected for a template for the protein threading. Having the inhibitor complexed with the *H. polygyrus* PLA₂G1B protein threading model allows us to see the important ligand interactions in the binding pocket (**Figure 2**), therefore allowing the identification of potential inhibitors which interact with these residues.

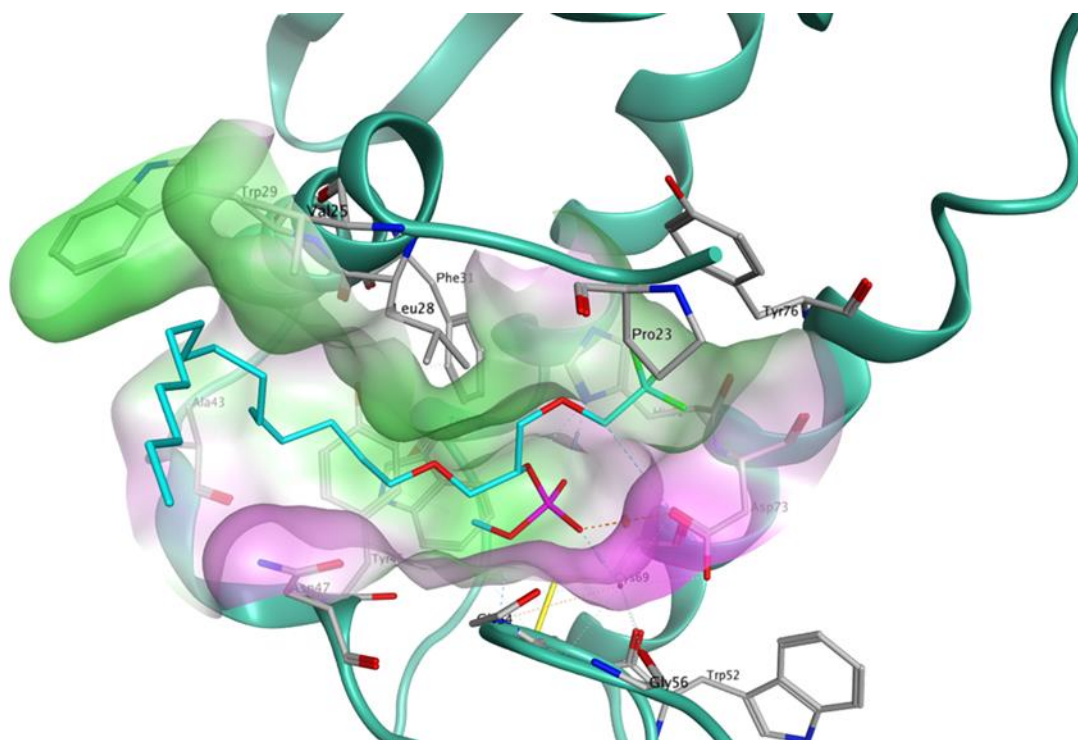


Figure 3. Predicted 3-D structure of the *H. polygyrus* secretory phospholipase A₂ in complex with the substrate analogue 4-(s)-[(1-oxo-7-phenylheptyl)amino]-5-[4-(phenylmethyl)phenylthio]pentanoic acid. The *H. polygyrus* sPLA₂ is represented with a green ribbon with the inhibitor shown in blue. The binding site area is represented as a molecular surface. Predicted binding with amino acids in the binding pocket is shown (dotted blue and orange).

Virtual screening was aimed at identifying small molecule inhibitors that might interact with important residues in the *H. polygyrus* sPLA₂ binding pocket, within a library of commercially available, drug-like small molecules. The substrate analogue from the template structure 1KVO, included in the model generation for induced fit, revealed Aspartic acid 102 (Asp102), Glycine 56 (Gly56), and Histidine 72 (His72) as key residues that the inhibitor may interact with (**Figure 3**). These residues are also predicted to have hydrophobic interactions with the inhibitor, as shown with ligand interaction prediction software in MOE, suggesting higher binding affinity (343). Furthermore, the histidine/aspartic acid dyad present in the binding pocket has been shown to be critical for human PLA₂ enzymatic activity (344). Therefore, molecules were selected from the virtual screening exercise based on their predicted ability to interact with all three of these residues to enable disruption of enzymatic activity.

Using Clustal Omega, an amino acid alignment of these residues to the other 3 sPLA₂ homologues secreted in the HES discovered in chapter 4 revealed no conservation (**Figure 4**), suggesting that this inhibitor may be specific for *H. polygyrus* PLA₂G1B. Interestingly, the proposed drug binding sites are 100% conserved with homologues in canine and human pathogenic species, *A. caninum*

of the *H. polygyrus* PLA₂G1B protein threading model are shown in **Figure 6A**, whilst their skeletal structures can be seen in **Figure 6B**.

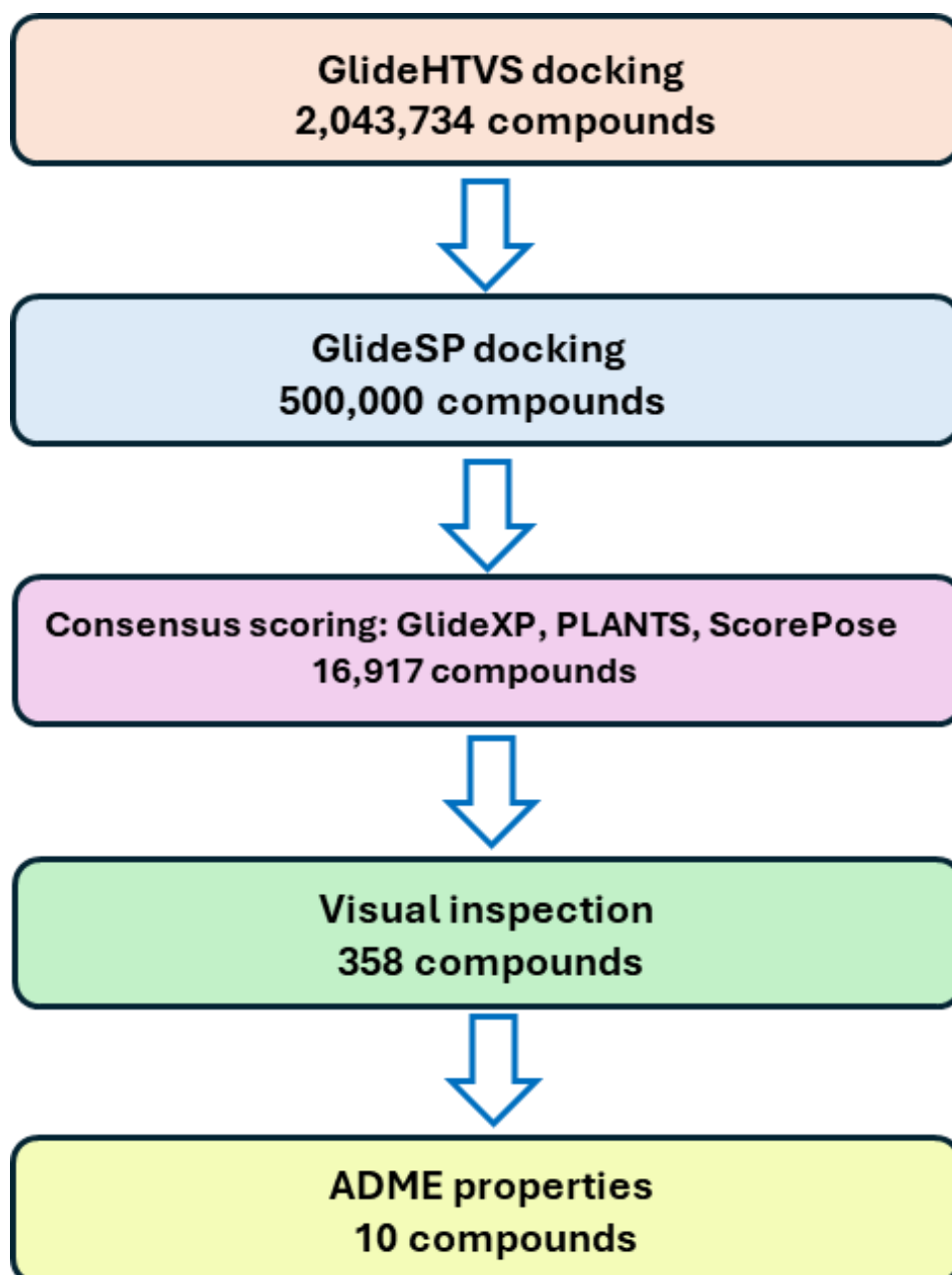
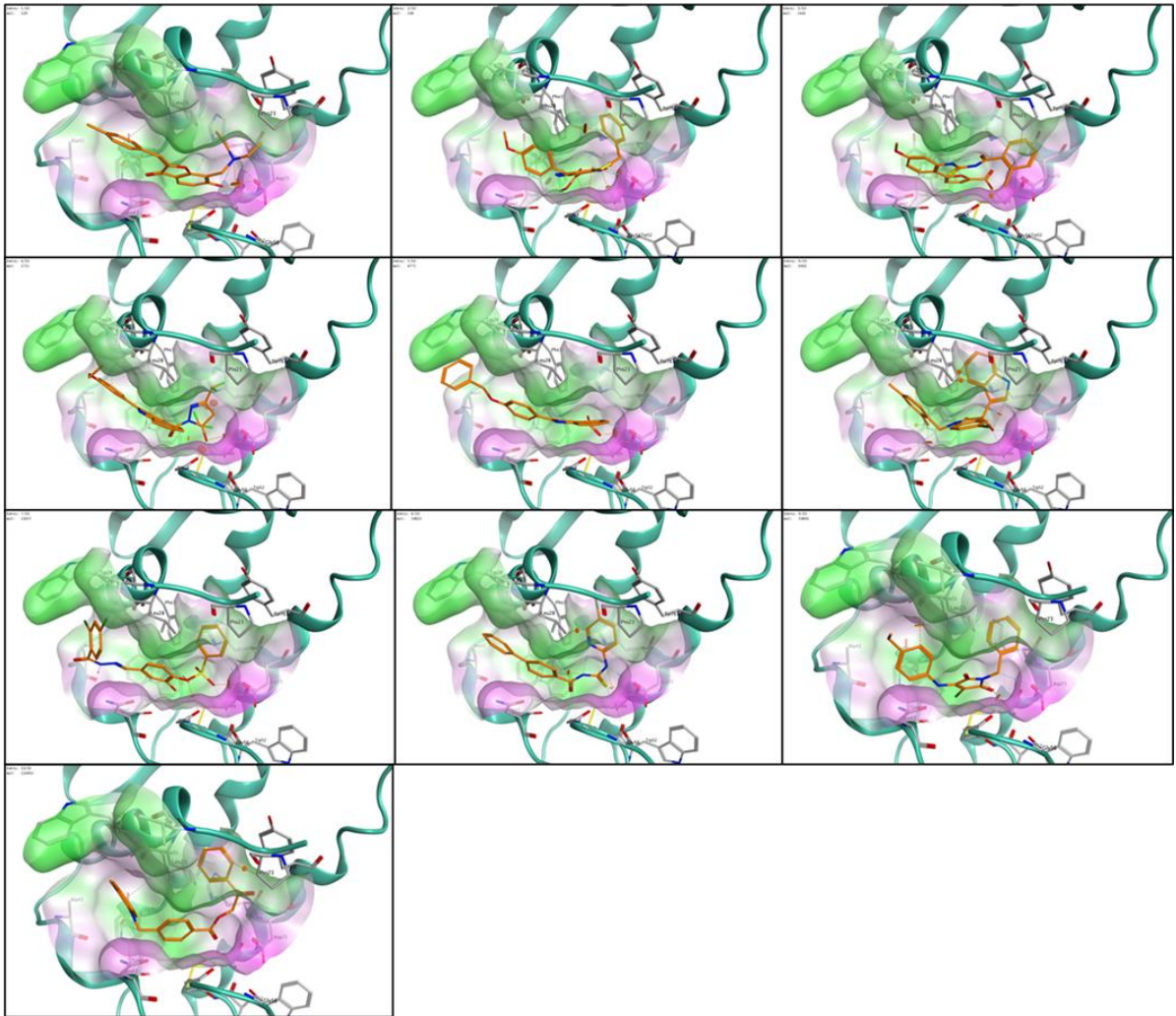


Figure 5. The screening workflow that was applied to discern novel *H. polygyrus* sPLA₂ inhibitors. Each number represents the number of unique entries at each stage, not the total number of poses. Glide high-throughput screening (HTVS), Glide standard precision (SP), Glide extra precision (XP), Protein-Ligand ANTSsystem (PLANTS), Absorption Distribution Metabolism Excretion (ADME).

A



B

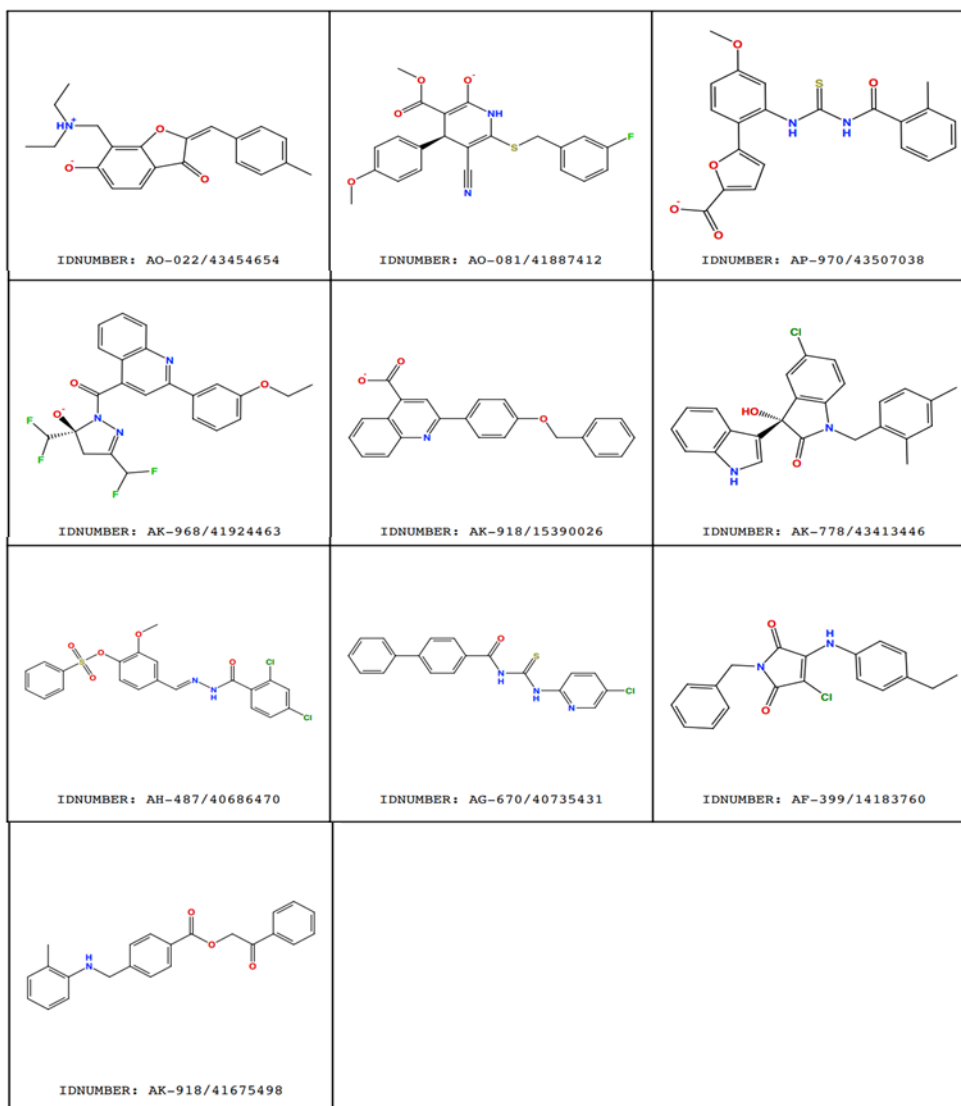


Figure 6. Structure of the 10 compounds selected from the ligand-based screening. (A) 3-D structure of compound visualized in the binding pocket of the *H. polygyrus* PLA₂G1B and **(B)** the 2-D skeletal structures of each compound. All the selected compounds are associated with an optimum predicted occupation of the main binding site, with an ideal overall fitting of the binding pocket, and the potential of forming direct contacts with Asp102, Gly56, and His72.

5.4.2 Selected inhibitors of *H. polygyrus* secretory phospholipase A₂ show activity against *H. polygyrus* adult supernatant

Having identified 10 virtual hit compounds, further investigation aimed to quantify their effect on PLA₂ activity in the adult *H. polygyrus* adult supernatant. The compounds were screened against the supernatant and not the HES as a higher signal was detected in the PLA₂ enzymatic assay detailed in Chapter 4. Each compound was initially tested at 100 μM, an initial concentration used commonly in the literature when testing novel compounds for activity (339, 340, 348, 349). All compounds except compound AO-022/43454654 were shown to exhibit 85-95% inhibition of PLA₂ activity (**Figure 7A&B**). For studies to determine the IC₅₀, four compounds were selected based on highest % inhibition (AK-968/41924463, AK-918/15390026, AK-778/43413446 and AF-399/14183760) (**Figure 7B**). The IC₅₀ is defined as the concentration of the drug at which 50% inhibition of the target activity (e.g., enzyme activity, receptor binding, cell viability) is observed (350). To determine their IC₅₀ values, a dose-response titration (0.1 – 30 μM) was conducted on adult *H. polygyrus* supernatant (**Figure 7C**). The calculated IC₅₀ values are shown in **Figure 7D**, revealing AF-399/14183760 as having the highest potency with the lowest IC₅₀ value (IC₅₀ = 0.72 μM).

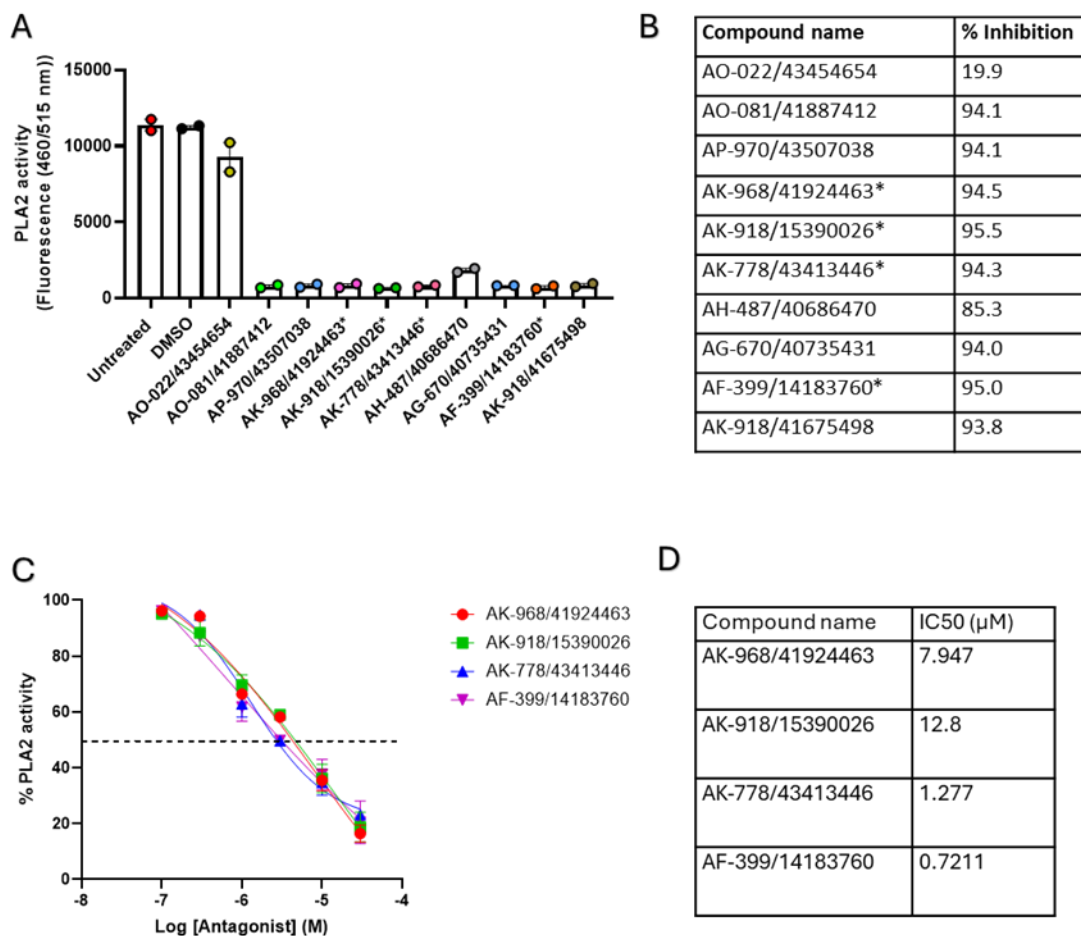


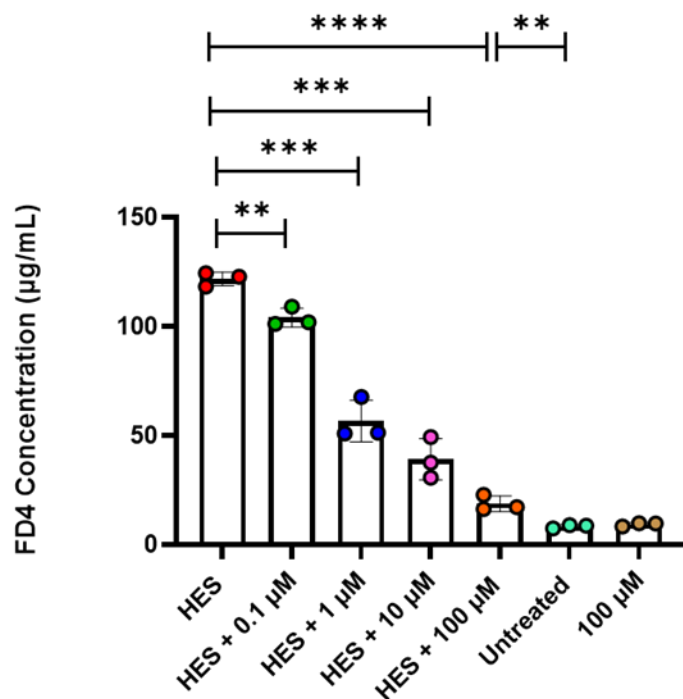
Figure 7. The novel *H. polygyrus* secretory phospholipase A₂ inhibitors successfully inhibit activity in the adult supernatant. (A) The 10 *H. polygyrus* secretory PLA₂ inhibitors were screened in duplicate against the adult supernatant at 100 μM. The top four compounds are indicated with a star (*). **(B)** Table detailing the % inhibition of all 10 of the compounds. **(C)** The top four compounds based on % inhibition were titrated (30 – 0.1 μM) and screened against the adult supernatant in triplicate to determine IC₅₀ values. **(D)** Table showing the IC₅₀ values for the top four compounds. Data shown represents **(A)** two n = 2 or **(B)** three n = 3 technical replicates. Error bars Mean ± SD.

5.4.3 Inhibiting the *H. polygyrus* secretory phospholipase A₂ significantly reduces the ability of *H. polygyrus* excretory/secretory products from increasing intestinal cell permeability

To determine whether the ability of HES to increase cell permeability is dependent on the PLA₂ activity, the compound determined to have the highest potency (AF-399/14183760) was tested in a dose-response titration (0.1 – 100 μM) and FD4 basolateral concentration measured after 18 hrs. Addition of AF-399/14183760 to the apical chamber along with HES resulted in a significant reduction in FD4 concentration in the basal chamber (**Figure 8A**). The addition of 0.1 μM resulted in a final FD4 concentration of 104.1 μg/mL, whereas 100 μM resulted in a final FD4 concentration of

18.8 µg/mL (**Figure 8B**). As the fold change of FD4 concentration does not decrease by a factor of 10 (**Figure 8B**), this effect cannot be concluded to be dose-dependent.

To assess the contribution of *H. polygyrus* PLA₂ in the ability of HES to increase cell permeability, I used the dose-response curve in **Figure 7C** was used to calculate the inhibitory concentration (IC) of AF-399/14183760 at 0.1, 1, 10 and 100 µM. The IC can then be compared to the % decrease in FD4 concentration, to determine the contribution of PLA₂ activity in increasing cell permeability. At 1 µM the IC is 38.35 whereas a 53.5% decrease in FD4 was observed (**Figure 8B**). This data is suggestive that the ability of HES to increase cell permeability is largely due to PLA₂ activity.



B

Concentration (µM)	FD4 concentration (µg/mL)	Fold change	Predicted IC	% decrease [FD4]
0	121.9 +/- 3.1	1	-	-
0.1	104.1 +/- 4.3	1.2	3.78	14.6 +/- 3.8
1	56.6 +/- 9.5	1.8	38.35	53.5 +/- 9.1
10	39.2 +/- 9.4	1.4	62.39	67.9 +/- 7.8
100	18.8 +/- 3.5	2.1	95.04	84.6 +/- 2.6

Figure 8. The addition of a *H. polygyrus* secretory phospholipase A₂ inhibitor significantly reduces the ability of the excretory/secretory products to increase cellular permeability. (A) Cells were treated with HES (10 µg/mL) alongside a 10-fold increasing concentration of compound AF-399/14183760 (0.1 – 100 µM). **(B)** Table showing the FD4 concentration and fold change from HES alone, alongside the predicted inhibitory concentration (IC) of each concentration of drug using the IC₅₀ curve, with the observed % decrease in [FD4] also shown. Data shown represents 3 biological replicates with 9 technical replicates. Unpaired T-test performed, where ** p ≤ 0.01, *** p ≤ 0.001, **** p ≤ 0.0001, error bars Mean ± SD.

5.4.4 Off-target effects of *H. polygyrus* PLA₂G1B inhibitor AF-399/14183760

Finally, potential off-target effects of AF-399/14183760 were investigated by performing an amino acid alignment of all human sPLA₂ isoforms to *H. polygyrus* PLA₂G1B using Clustal Omega and evaluating the potential conservation of key amino acids identified in the model binding site. As shown in **Figure**

9, the Gly56, His72, and Asp102 residues are conserved in the murine PLA₂G10 and PLA₂G2F isoforms, suggesting that AF-399/14183760 may have off-target effects if used *in vivo*.

PLA2G15	LNLELLLPVIIDCWIDNIRLVYNKTSRATQFPDGVDRVPGFGKTFSLFLDPSKSSVGS	136
PLA2G12A	YKPS----PPNGCGSPLFGVHL---N--I-GIPSLTKCCNOHRCY--ETCG-----	118
PLA2G3	T-----MPGTLWCGVGD SAGNSSE--LGVFQGPLCCREHRCY--QNISPLQ-----	195
HPOL_0000384601	Y-----NNGYGCWCGVGSHEPV-----DEIDRCCMHHDKCY--DAAVDKKVC---	85
PLA2G1B	Y-----NNGYGCYGLGGSGTPV-----DELDKCCQTHDNCY--DQAKKLDSC---	83
PLA2G10	Y-----MKYGCFCGLGGHGQPR-----DAIDWCCCHGHGCCY--TRAE EAG-----	99
PLA2G2F	F-----VGYGCYCYGLGGRGQPK-----DEVDWCCCHAHGCCY--QELFDQG-----	78
PLA2G5	Y-----GFYGCYCYGLGGRGTPK-----DGTDWCCWAHDHCY--GRLEEKG-----	78
PLA2G2D	Y-----WPYGCCHCGLGGRGQPK-----DATDWCCQTHDCCY--DHLKTQG-----	78
PLA2G2A	Y-----GFYGCYCYGLGGRGSPK-----DATDRCCVTHDCCY--KRLEKRG-----	78
PLA2G2E	Y-----NDYGCYCYGLGSHWPV-----DQTDWCCCHAHGCCY--GRLEKLG-----	76
	..	
PLA2G15	YFHTMVESLVGWGYTRGEDVIRGAPYDWRRAFNENGPYFLALREMI EEMYQLYGGPVV LVA	196
PLA2G12A	-----	120
PLA2G3	-----YN-----YGIRNYR FHT-----	209
HPOL_0000384601	-F-----DVAW-----EYIDSYKWK CINS-T---AICT-E-----TSDNCKAA	117
PLA2G1B	KF-----LLDN-----PYTHTYSYSCSGS-A---ITCS-S-----KNKECEAF	116
PLA2G10	-----CS-----PKTERYSWQCVNQ-S---VLCG-P-----AENKQCEL	128
PLA2G2F	-----CH-----PYVDHYDHTIENNTE---IVCS-D-----LNKTECDKQ	109
PLA2G5	-----CN-----IRTQSYKYRFAWG-V---VTCE-P-----G-PFCHVN	106
PLA2G2D	-----CS-----IYKDYRYRNF SQ-N---IHCS-D-----KGSWCEQQ	107
PLA2G2A	-----CG-----TKFLSYKFSNSGS-R---ITCA-K-----Q-DSCRSQ	106
PLA2G2E	-----CE-----PKLEKYLFSVSE R-G---IFCA-G-----R-TTCQRL	104

Figure 9. Amino acid alignment of human PLA₂ isoforms with *H. polygyrus* PLA₂G1B homologue. The drug binding sites Gly56, His72, and Asp102 are highlighted in yellow. The two murine isoforms with full conservation with drug binding sites are highlighted in blue. Alignment performed using clustal omega.

5.5 Discussion

To summarise, this chapter focusses on identifying a novel inhibitor of *H. polygyrus* PLA₂G1B, and elucidating the contribution of *H. polygyrus* PLA₂G1B in the ability of HES to increase cell permeability. The use of two commercially available PLA₂ inhibitors failed to inhibit PLA₂ activity in *H. polygyrus* adult supernatant, therefore a well-established structure-based virtual screening approach was utilised to identify *H. polygyrus* PLA₂ specific inhibitors. Ten molecules were selected with this computational exercise, with eight found to inhibit *H. polygyrus* PLA₂ activity of the adult antigen by >90%. Most notably, inhibition of *H. polygyrus* PLA₂ activity significantly reduces the increased cell permeability induced by HES, implicating phospholipase activity from the secreted protein encoded by HPOL_0000384601 as having a key role in HES-induced increase in cell permeability.

This structure-based virtual screening approach has been successful in the literature at identifying specific inhibitors for helminth-specific enzymes (337, 351). It is important to acknowledge that this method of virtual screening has its advantages and disadvantages, most notably the use of a predictive structural model of the target enzyme, which enables this screening to be performed without a known

crystal structure (352, 353). However, the reliance on a model made with protein threading and not a known crystal structure can have implications for reliability of the predicted ligand interactions, such as not accounting for conformational changes upon enzyme-substrate binding (354).

From the virtual screening, the top 10 compounds were purchased and tested for activity against the *H. polygyrus* PLA₂ in the adult supernatant. Excitingly, eight out of the 10 compounds exhibited 85-95% inhibition of PLA₂ activity, with the top four also showing low IC₅₀ values; indicative of high potency (355). The compound with the lowest IC₅₀ (highest potency) was AF-399/14183760 (1-benzyl-3-chloro-4-(4-ethylanilino)-1H-pyrrole-2,5-dione). A literature search of the published use of the compound revealed that it has been shown to possess strong antifungal activities against a panel of clinically important fungi including yeasts, *Aspergillus* species and dermatophytes due to the presence of an intact maleimido ring (356). The compound is not known to target PLA₂ enzymes, therefore the antifungal activity suggests off-target effects.

As a final proof of principle experiment to link *H. polygyrus* PLA₂ activity to the increase in cell permeability following HES treatment, compound AF-399/14183760 was added with HES to the cell monolayer and FD4 concentration in the basolateral chamber quantified. Addition of AF-399/14183760 was shown to significantly reduce the ability of HES to increase cell permeability. At the highest concentration of 100 µM, there is still a significant increase in FD4 concentration (18.8 µg/mL) compared to untreated (1.8 µg/mL), therefore suggesting that the ability of HES to increase cell permeability is not solely due to PLA₂G1B activity. As discussed in Chapter 4, HES contains three potential sPLA₂ homologues. Sequence alignment revealed that the drug binding sites are not conserved, suggesting that compound AF-399/14183760 is specific for HPOL_0000384601 and is not predicted to react with the other *H. polygyrus* isoforms. However, amino acid alignment with murine sPLA₂ isoforms revealed conservation of the predicted binding sites with PLA₂G10 and PLA₂G2F, suggesting the possibility for off-target effects if used *in vivo*, although this suggestion is limited without a tertiary alignment. Therefore, if compound AF-399/14183760 were to be used *in vivo*, there may be implications for lipid metabolism and cell function.

Overall, sPLA₂ expression in colon adenocarcinoma tissue sections was strongly associated with tumour diameter (357), with PLA₂G1B gene overexpression shown by Abbenhardt *et al* to be associated with CRC (358). Furthermore, Haller *et al* reveal how PLA₂G1B may be a target for colitis management, with PLA₂G1B^{-/-} mice treated with DSS showing a reduction in weight loss and colitis pathology compared to wild-type mice (329). Given the findings of this chapter implementing *H. polygyrus* PLA₂G1B in exacerbation of CAC, and the knowledge of PLA₂G1B overexpression in CRC, the

development of a novel *H. polygyrus* PLA₂G1B inhibitor could be beneficial in the treatment of helminth-exacerbation of cancer, or could be modified to target the human isoform.

Interestingly, recent literature has shown the importance of PLA₂ enzymes in parasite survival, given their role in immunomodulation (199, 359) and enabling tissue invasion to establish infection (360, 361); therefore suggesting their importance as novel anthelmintics. For example, Saffer *et al* showed the importance of PLA₂ in invasion of *Toxoplasma gondii* (361). Exogenous PLA₂ from snake venom (*Naja naja*) increased the penetration of fibroblasts by *T. gondii*, while horse antiserum to *Ophiophagus hannah* venom inhibited penetration (361). An irreversible PLA₂ inhibitor, p-bromophenacyl bromide, blocked penetration without metabolically disabling the parasite (361). Given the significant rise in anthelmintic resistance (362, 363), and a shift in focus towards host metabolism when designing novel anthelmintics (364), it is proposed that compound AF-399/14183760 should be investigated further for anthelmintic potential.

Chapter 6: Profiling the colonic transcriptome of *H. polygyrus* infected mice

6.1 Introduction

Previous chapters in this thesis have implicated a role for HES-induced EP2/EP4 receptor signalling in the increase in cell permeability *in vitro*, and propose that this may be a mechanism by which *H. polygyrus* exacerbates tumour formation in CAC *in vivo*. To study the multifaceted nature of CAC initiation involving several pathways (365, 366), this chapter details the profiling of the colonic transcriptome of *H. polygyrus* infected mice. Transcriptome analysis is particularly well-suited for this context, as it allows for the comprehensive examination of gene expression patterns and pathway interactions (367), offering a holistic view of the biological processes influenced by *H. polygyrus* infection. This approach can uncover novel insights that may not be evident through targeted studies, thereby enhancing our understanding of CAC development.

It has been observed that an increase in *Ptgs2* expression, one of the key enzymes in the PGE₂ synthetic pathway, is observed in CRC tumours and correlated with metastasis and poor prognosis in patients (104, 368, 369). Furthermore, an overexpression of PGE₂ synthases (*Ptges*, *Ptgs2*, and *Ptgs3*) was observed in CRC tumours (370), demonstrating an abnormal behaviour of genes in the PGE₂ synthetic pathway in CRC tumours. Given findings in previous chapters implicating PGE₂-EP2/EP4 activation in HES-induced increase in cell permeability, I will investigate PGE₂ synthetic enzyme expression, as well as EP2/EP4 receptor expression, to determine if this pathway is altered in the colonic transcriptome as a consequence of *H. polygyrus* infection.

Previous work has shown how the immune cell population is altered in response to helminth infection, with an expansion of M2 macrophages, T regulatory cells (Treg), and increase in mast cell degranulation seen (144, 371, 372). This results an immunosuppressive environment to allow parasite survival, however this may create a favourable environment for tumour growth by limiting the host anti-tumour immune response (373, 374). In this chapter, I will combine my transcriptomic data with the *in silico* flow cytometry software CIBERSORTx (245) is utilised to estimate the immune cell population of the colon with *H. polygyrus* infection, to analyse if infection is creating a favourable immunosuppressive environment for tumour growth.

As described in section 1.2.2.1 in Chapter 1, altered intestinal stem cell (ISC) differentiation is one of the key initiating events of CRC development, resulting in the uncontrolled proliferation and expansion of progenitor cells accumulating into a tumour growth (50, 51, 54, 375). Colonic cancer stem cells are characterised as being Leucine-rich repeat-containing G-protein coupled receptor 5 (*Lgr5*) positive

(376). Infection with *H. polygyrus* has been shown by Nusse *et al* to decrease *Lgr5* expression in the crypts overlying the site where *H. polygyrus* larvae reside in the small intestine (177). Nusse *et al* reported the increase in Sca-1 (*Ly6a*) in these crypts, indicative of *Ly6a* being a useful marker of crypt cells responding to *H. polygyrus*-driven epithelial disruption (177, 183). Whether *H. polygyrus* is able to alter the expression of ISC markers within the colonic crypt is currently unknown. Research from Drurey *et al* show similar findings with HES-treated small intestinal organoids, with a loss of *Lgr5* and gain of *Ly6a* expression (377). Drurey *et al* also report an expansion of tuft cells in the small intestine *in vivo* (377). Again, it is currently unknown whether *H. polygyrus* alters ISC differentiation in the colon.

To date, how the colonic transcriptome is altered with helminth infection has not been investigated. Therefore, the main aim of this chapter is to profile the colonic transcriptome of infected and uninfected mice, and utilise this data to investigate multiple facets of CRC: 1. alterations in gene expression, 2. immune cell population, and 3. intestinal stem cell differentiation.

6.2 Chapter Aims

1. To compare the colonic transcriptome profiles of infected and uninfected mice two weeks post-infection, and identify significant changes in gene expression
2. To use the colonic transcriptome profiles of infected and uninfected mice to predict the immune cell population
3. To compare the expression of genes relating to intestinal stem cell differentiation and identify differences with *H. polygyrus* infection

6.3 Hypothesis

1. Infection with *H. polygyrus* alters cell signalling pathways in the colon, potentially exacerbating CAC
2. Infection with *H. polygyrus* alters the immune cell population in the colon, resulting in an immunosuppressive environment
3. Infection with *H. polygyrus* alters the colonic stem cell compartment to represent epithelial dysfunction as seen in the small intestine

6.4 Results

6.4.1 RNA extraction quality control results

Proper quality control measures, such as assessing RNA integrity (RIN) and purity (260/280), help identify and eliminate degraded samples with impurities, thereby minimizing the risk of sequencing

artifacts and optimizing the success of downstream applications (378). As shown in **Table 1** and **Figure 1**, all 10 samples showed high integrity and purity, with RIN between 8-10 and 260/280 ratios being ~2 (379, 380), and so all samples were used for transcriptomic sequencing. Interestingly, though no significant differences were observed in the total number of unique mapped reads, a notable difference in detected transcripts with reads ≥ 1 was seen in sample 4 from both conditions (**Table 1**). This suggests a significantly lower amount of genes were successfully mapped to the genome in these samples.

Principal component analysis (PCA) was performed to identify similarities in the gene expression levels between conditions, and reveal the presence of any outliers in the dataset (381). As shown in **Figure 2A**, a significant variation in the dataset of sample 4 in both conditions compared to the other samples was identified. We believe this is due to the discrepancy in total detected transcripts as detailed in **Table 1**. The decision was made to remove sample 4 from both conditions as it was concluded that the inclusion of this sample could skew the dataset to not be representative of the transcriptome. After removing sample 4 from both conditions, a second PCA analysis was performed showing no extreme outliers and separate clustering between the two experimental conditions (**Figure 2B**).

Table 1. Quality control results from the RNA extractions and sequencing. (A) Table detailing DNA and RNA concentrations which were used to calculate the % DNA contamination. The 260/280 and 260/230 ratios were obtained using a Nanodrop. TapeStation was used to quantify the ribosomal integrity number (RIN). Numbers are highlighted in green as they meet the requirements for high quality RNA (RNA concentration > 180 ng/μL; % DNA contamination < 5%; 260/280 > 2; 260/230 > 1.8; RIN > 4). Total number of uniquely mapped reads and total number of detected transcripts ≥ 1 are also detailed.

Sample	DNA (ng/μL)	RNA (ng/μL)	Total nucleic acid	% DNA	260/280	260/230	RIN	Total number of uniquely mapped reads	Total number of detected transcripts with reads ≥ 1
Naïve 1	4.74	276.3	281.04	1.686593	2.18	2.33	8.8	59,455,532	21,574
Naïve 2	4.8	202.1	206.9	2.319961	2.07	1.97	8.4	58,746,877	21,603
Naïve 3	3.2	185.9	189.1	1.692226	2.04	2.18	9.5	55,219,077	21,558
Naïve 4	4.56	251	255.56	1.784317	2.1	2.16	9.4	56,876,118	18,172
Naïve 5	3.68	211.8	215.48	1.707815	2.08	2.14	9	52,441,493	23,003
Hpb 1	3.86	206.1	209.96	1.838445	2.1	2.07	9.4	64,509,544	22,686
Hpb 2	4.36	289.3	293.66	1.48471	2.09	2.17	8.6	57,456,581	21,993
Hpb 3	4	214.8	218.8	1.828154	2.08	2.11	9.4	56,181,780	23,162
Hpb 4	5	211.7	216.7	2.307337	2.1	2.08	8.3	77,506,389	17,982
Hpb 5	4.22	234.8	239.02	1.765543	2.11	2.22	8.8	62,846,757	21,887

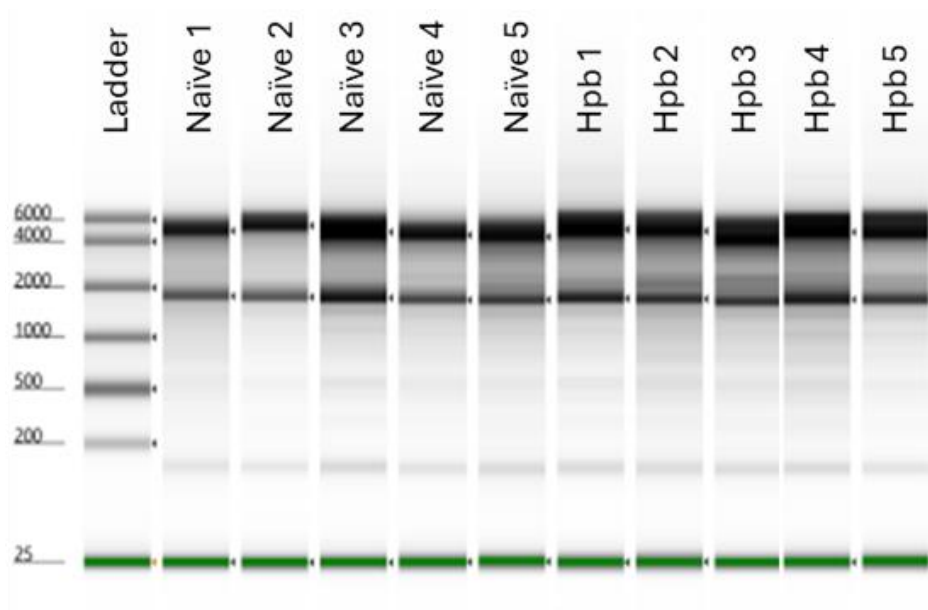
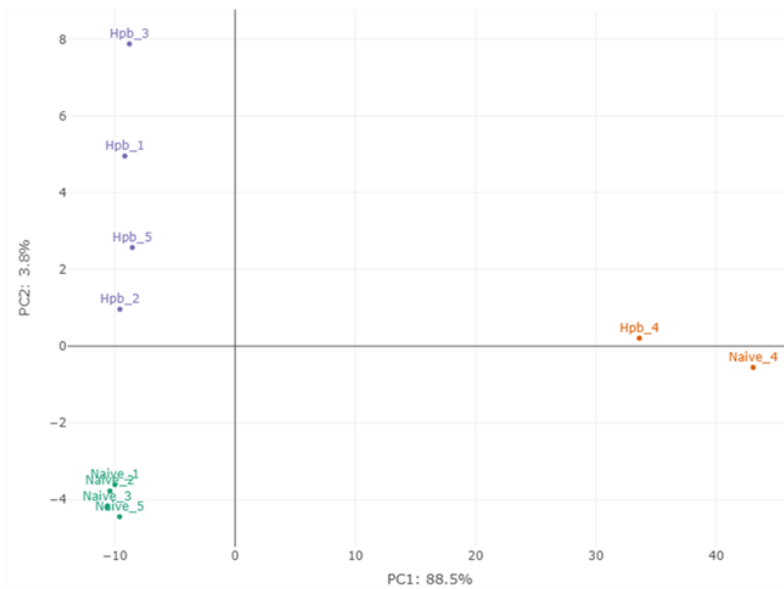


Figure 1. Quality control results from the RNA extractions and sequencing. The resulting gel electrophoresis from the TapeStation showing intact 18S (1.5 kb) and 28S (4.5 kb) rRNA bands.

A



B

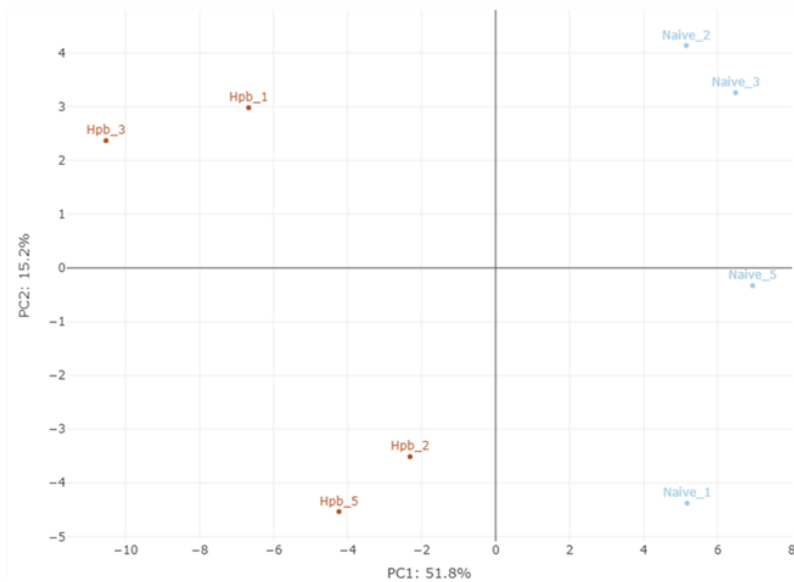


Figure 2. Pearson correlation analysis and principle component analysis (PCA) of all samples reveals sample 4 has high variance within its dataset. (A) PCA plot shows 88.5% variation between wild type (WT) and *H. polygyrus* (Hpb) groups and 3.8% variation in the datasets of the individual samples in the same conditions. **(B)** PCA plot showing the reduction in variance between conditions (51.8%) and an increase in variance between the individual samples (15.2%) after the exclusion of sample 4 from both conditions.

6.4.2 Differential gene expression in the colon of *H. polygyrus* infected mice vs un-infected

To identify genes that were altered in the colon with *H. polygyrus* infection, differential gene expression (DEG) analysis was performed with samples 1, 2, 3, and 5 from each condition using the nf-core/rnaseq pipeline (228, 382). Input was a matrix of 56,941 genes for 8 samples, reduced to 29,110 genes after filtering for low abundance (total read count from all samples < 1). From 29,110 genes which showed abundant expression levels, 163 genes were differentially expressed between naive and *H. polygyrus* infected mice (**Appendix table 4**) using two criteria: a greater than 1.5 fold expression level change and p-value (FDR) ≤ 0.05 from Wald test with Benjamini-Hochberg correction. These 163 genes included 151 upregulated genes and 12 downregulated genes as shown in the volcano plot in **Figure 3A**, with the top 10 being labelled. The heat map of the whole set of DEG in colon tissue (**Figure 3B**) confirms the expression pattern shown in the volcano plot where most genes are significantly upregulated with *H. polygyrus* infection, even if there are some inconsistencies between replicates.

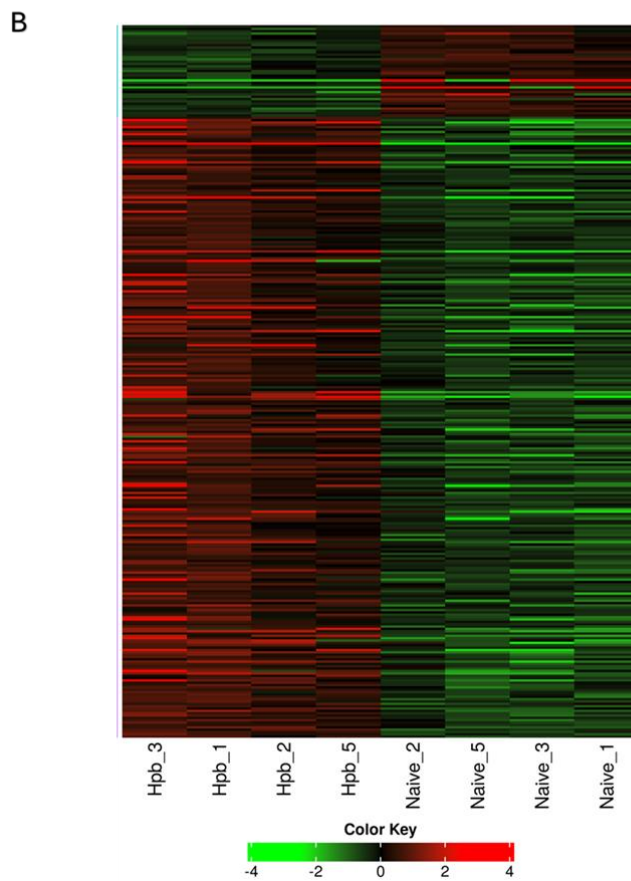
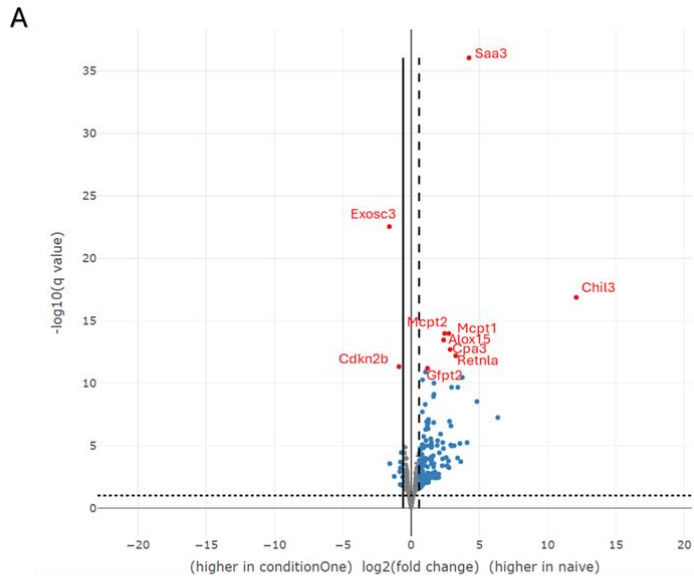


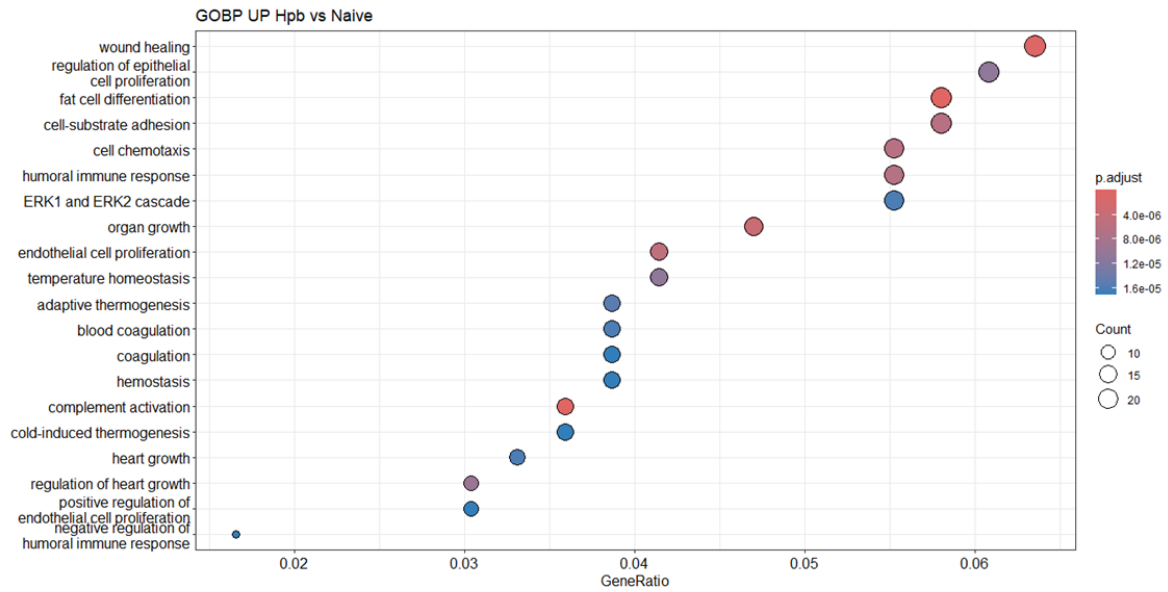
Figure 3. Differential gene expression analysis. (A) Volcano plot showing 29,110 differentially expressed genes, with 163 being significant ($\text{Log}_2\text{FoldChange} > 0.58$ or < 0.58 , $\text{padj} < 0.05$). Each circle corresponds to one gene. The x-axis represents \log_2 fold change (Hpb / WT) and the y-axis represents \log_{10} p-adjusted value calculated using the Wald test followed by Benjamini/Hochberg correction between Hpb and WT groups. The top 10 significantly differentially expressed genes are shown with red dots and labelled. **(B)** Heatmap showing the \log_2 fold change of all significantly changed genes -4 (green) = downregulated, 4 (red) = upregulated.

6.4.3 Upregulated genes and their corresponding biological process and molecular function

Using the clusterProfiler R package, gene ontology (GO) analysis of the upregulated DEGs revealed the top 20 enriched biological process terms (**Figure 4A**) and 20 molecular function terms (**Figure 4B**) as defined by the PANTHER classification system (383).

These results suggest that *H. polygyrus* infection in mice leads to significant enrichment of biological processes related to the humoral immune response, regulation of epithelial cell proliferation, and wound healing (**Figure 4A**), alongside molecular functions involving carbohydrate binding and serine hydrolase activity (**Figure 4B**). The highly significant enrichment of complement binding activities and humoral immune responses suggests genes associated with an immune response are activated in the colon in response to *H. polygyrus* infection.

A



B

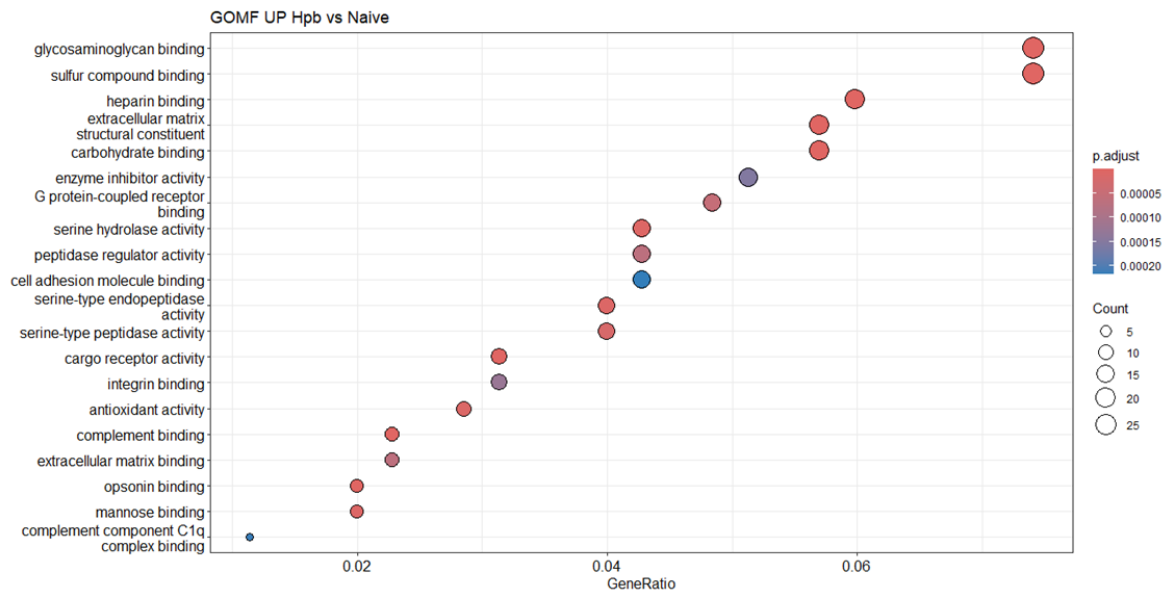


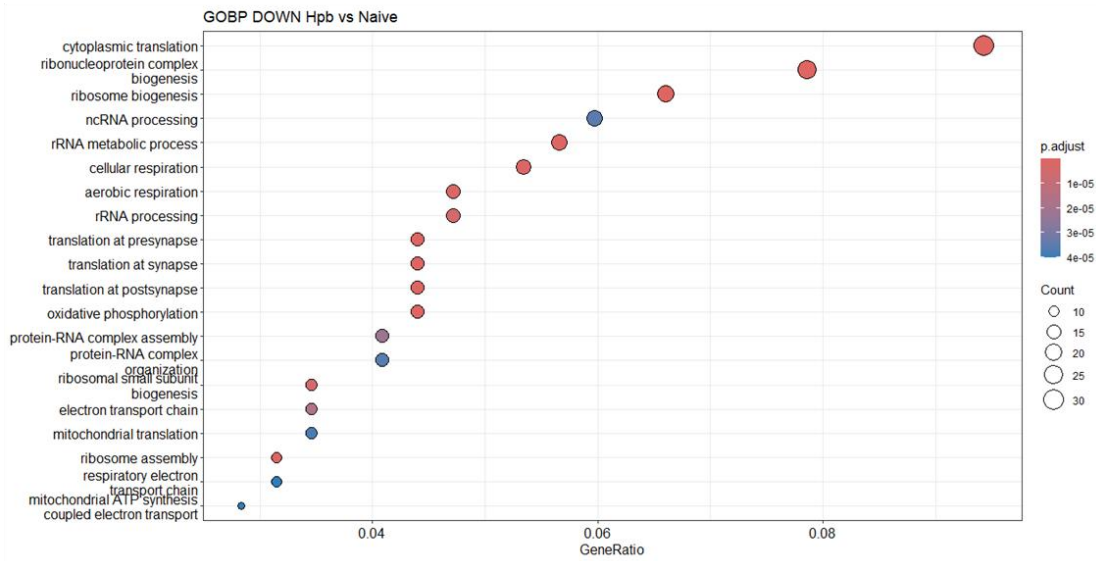
Figure 4. Gene ontology (GO) annotation of the upregulated genes. Transcriptome annotation classification reporting the top 20 most abundant GO terms for **(A)** Biological Process and **(B)** Molecular Function groups in the *H. polygyrus* infected group compared to the uninfected group for the upregulated genes. The size of the dots represent the number of genes in the significantly differentially expressed gene list associated with the GO term and the colour of the dots represent the p-adjusted values. The gene ratio is the number of genes in the input list associated with the GO term.

6.4.4 Downregulated genes and their corresponding biological process and molecular function

Gene ontology (GO) analysis of the downregulated DEGs revealed the top 20 enriched biological process terms (**Figure 5A**) and 20 molecular function terms (**Figure 5B**) as defined by the PANTHER classification system (383).

Among the top terms are biological processes related to cytoplasmic translation, ribosome biogenesis, and ribonucleoprotein complex biogenesis, all of which are critical for protein synthesis and ribosome assembly (**Figure 5A**). Other notable processes include non-coding RNA (ncRNA) processing and ribosomal RNA (rRNA) metabolic processes, which further support the notion that *H. polygyrus* infection negatively impacts core ribosomal and RNA processing pathways (384). The downregulation of rRNA transcription is a mechanism that is involved in the response to various types of stress (385, 386), and it induces various processes, such as cell cycle arrest, apoptosis, or autophagy (387, 388). These results suggest that *H. polygyrus* may induce cell stress in the colon.

A



B

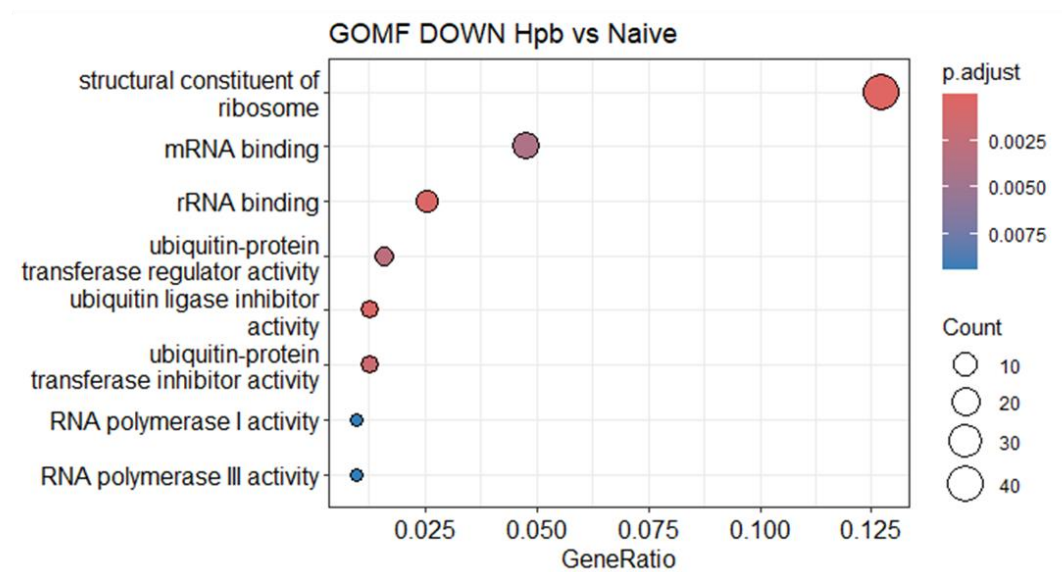


Figure 5. Gene ontology (GO) annotation of the downregulated genes. Transcriptome annotation classification reporting the top 20 most abundant GO terms for **(A)** Biological Process and **(B)** Molecular Function groups in the *H. polygyrus* infected group compared to the uninfected group for the downregulated genes. The size of the dots represent the number of genes in the significantly differentially expressed gene list associated with the GO term and the colour of the dots represent the P-adjusted values. The gene ratio is the number of genes in the input list associated with the GO term.

6.4.5 Gene set enrichment analysis reveals significantly enriched pathways in the colon of *H. polygyrus* infected mice

To explore the biological pathways enriched in the dataset, Gene Set Enrichment Analysis (GSEA) was performed using the significantly altered genes and the mouse-orthologue hallmark gene sets from the Molecular Signatures Database (MSigDB) (389). GSEA is often used in conjunction with GO analysis, with GSEA providing information on how the significantly altered genes may work together in different cellular processes. The analysis revealed several significantly enriched pathways, as shown in **Figure 6**.

Coagulation and complement pathways were highly enriched (**Figure 6A&B**), with positive enrichment scores (ES) peaking at approximately 0.55 and 0.45, respectively, suggesting *H. polygyrus* influences the immune response in the colon. Epithelial-Mesenchymal Transition (EMT), a critical process involved in cancer metastasis, also demonstrated significant enrichment (**Figure 6C**), with ES peaks near 0.5. Genes associated with increased KRAS Signalling (**Figure 6D**) also showed positive enrichment (ES 0.5). This indicates that genes involved in KRAS signalling are upregulated in the colon of *H. polygyrus* infected mice, potentially pointing towards activated oncogenic signalling pathways (390).

G2/M Checkpoint and p53 Pathway (**Figure 6E&F**) displayed negative enrichment scores, with ES values around -0.4 and -0.6, respectively. This negative enrichment suggests that genes involved in the G2/M cell cycle checkpoint and p53 tumour suppressor pathway are downregulated in the colon of *H. polygyrus* infected mice. This may imply a disruption in cell cycle control and apoptosis mechanisms in the colon, which are crucial hallmarks of cancer progression.

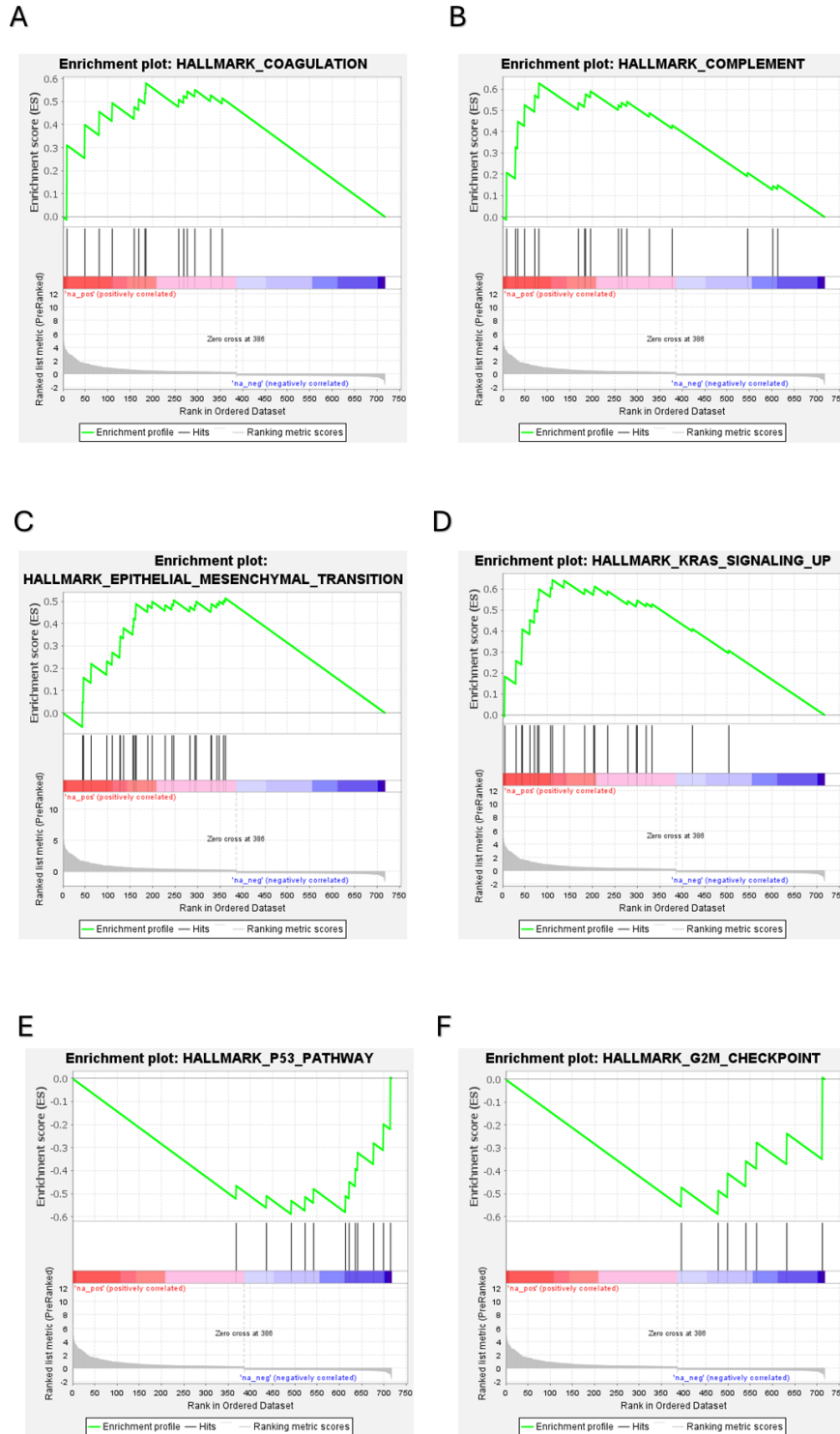


Figure 6. Gene set enrichment analysis in the colon of *H. polygyrus* infected mice compared to uninfected. The running enrichment score for each gene set is represented by the green line. The vertical lines show where the members of the gene appear in the ranked list of genes. **(A-D)** Enrichment plots showing the four most positively enriched pathways being complement, coagulation, epithelial-to-mesenchymal transition, and KRAS signalling in the colon *H. polygyrus* mice. **(E&F)** Enrichment plots showing the two negatively enriched pathways being p53 pathway and G2M checkpoint pathways in the colon of *H. polygyrus* infected mice. Analysis performed using Gene Set Enrichment Analysis (GSEA).

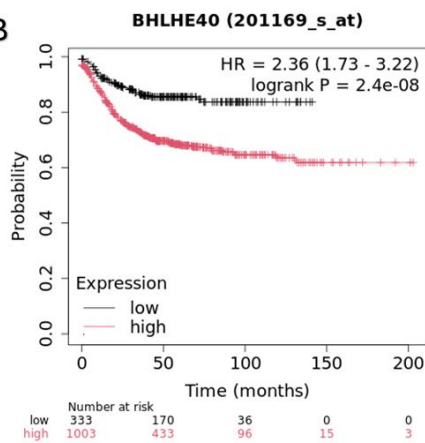
To expand on the GSEA, leading edge analysis was used to identify the subset of genes within the enriched gene set that are the most responsible for driving the enrichment signal. Out of the 49 enriched gene sets, *Bhlhe40*, *Me1*, and *Cd44* were the most enriched genes, being found in five gene sets (**Figure 7A**). Genes *Angptl4*, *Cfh*, *Thy1*, *C3*, *Il15*, and *Serpib2* were enriched in four gene sets, whilst *Irs2* was enriched in three gene sets (**Figure 7A**).

To assess the significance of this enriched subset of genes, Kaplan-Meier plots were used to analyse CRC survival data based on expression of these genes (**Figure 7B-G**). Interestingly, high expression levels of six of the genes, *Bhlhe40*, *Cd44*, *Cfh*, *Thy1*, *C3*, and *Serpib2* (**Figure 7B-G**), were all significantly associated with poorer survival outcomes in human CRC, with the hazard ratio (HR) > 1 and p value < 0.05. These results highlight the potential prognostic value of specific gene expressions in predicting how helminth infection may prime the colon environment for cancer development, and suggest that some genes may serve as potential biomarkers (391).

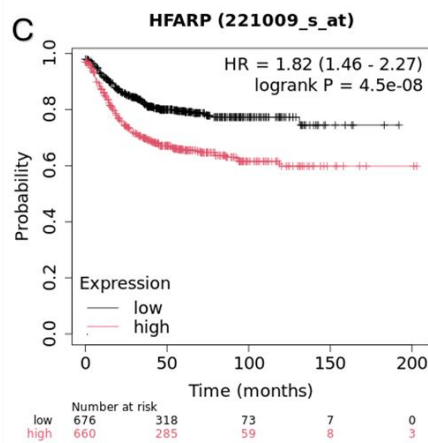
A

Gene Symbol	Gene Name	Number of Gene Sets
Bhlhe40	Basic helix-loop-helix family member E40	5
Me1	Malic enzyme 1	5
Cd44	Cluster of differentiation 44	5
Angptl1	Angiopoietin-like protein 1	4
Cfh	Complement factor H	4
Thy1	Thy-1 cell surface antigen	4
C3	Complement component 3	4
Il15	Interleukin-15	4
Serpib2	Serpin family B member 2	4
Irs2	Insulin receptor substrate 2	3

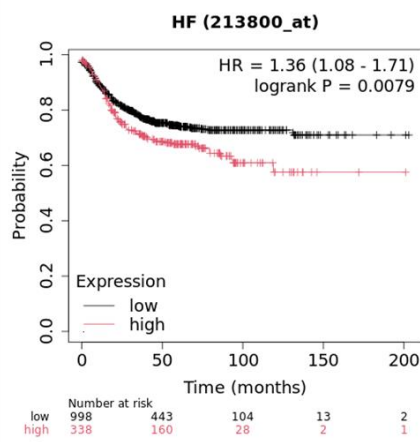
B



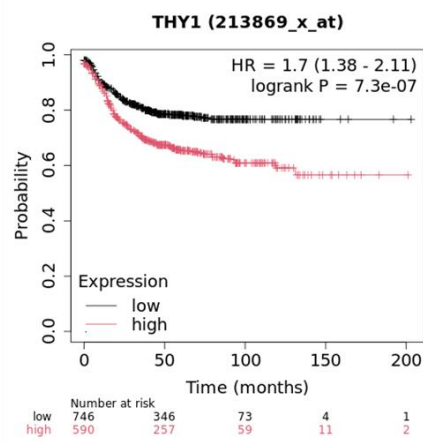
C



D



E



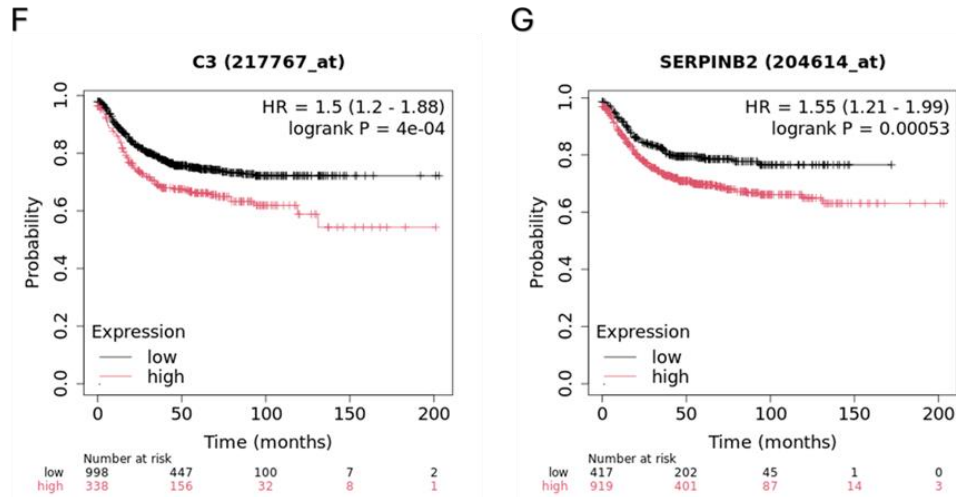


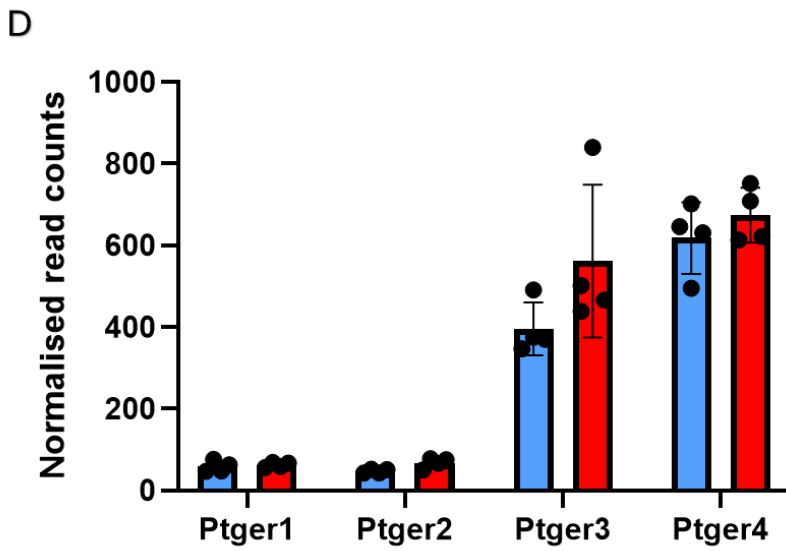
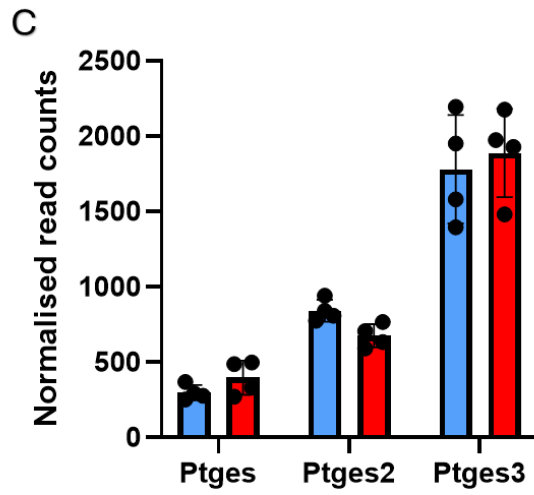
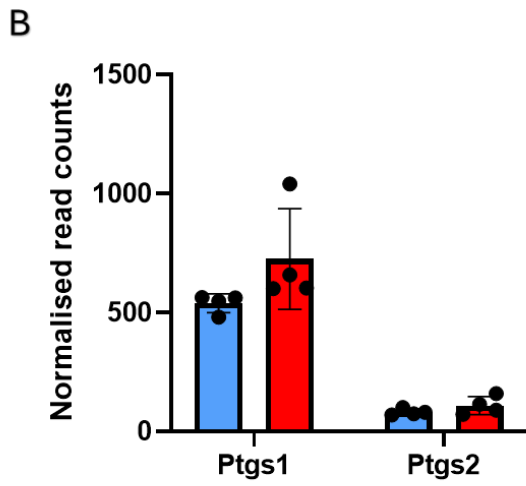
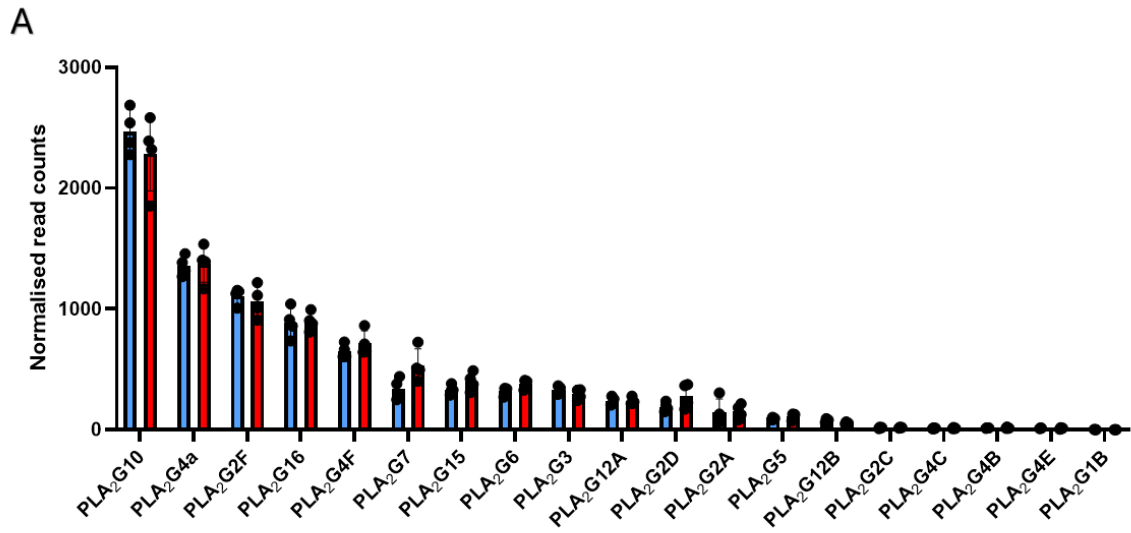
Figure 7. Leading edge analysis identifies a subset of genes in the colon of *H. polygyrus* infected mice responsible for enriched pathways. (A) Table showing the results of the leading edge analysis, showing the top 10 enriched genes from the gene set enrichment analysis. **(B-G)** Corresponding Kaplan-Meier plots for the six enriched genes showing unfavourable survival with high expression. For all figures, the red curves represent the survival probability of individuals with highly expressed genes/gene combinations, while the black curves represent the survival probability of individuals with non-highly expressed genes/gene combinations. A p value < 0.05 is considered a statistically significant correlation. HR – hazard ratio. Figures generated using Kaplan-Meier plotter.

6.4.6 Expression profiling of the PGE₂ synthetic and signalling pathway in the colon of *H. polygyrus* infected mice

Given the upregulation of the PGE₂ synthetic pathway in human CRC tumour samples, and the suggestion from previous chapters that increased PGE₂-EP/EP4 is occurring in the colon of *H. polygyrus* infected mice, I analysed the colonic transcriptome of mice infected with *H. polygyrus* and compared expression levels of significant genes in PGE₂ synthesis. The Log₂ fold change values for these enzymes are shown in **Figure 8A-C**, with no significant difference between naïve and *H. polygyrus* infected mice seen. Expression of the EP receptors was also shown not to be significant between the two conditions (**Figure 8D**).

Despite no change in EP receptor expression, I next analysed the expression of transcription factors known to be activated downstream of EP2/EP4 activation (392-397). Again, no significant change in peroxisome proliferator-activated receptor gamma (*Pparg*), vascular endothelial growth factor A (*Vegfa*), laminin subunit alpha 1 (*Lama1*), matrix metalloprotease 7 (*Mmp7*), cellular myelocytomatosis oncogene (*c-myc*), or cyclin D1 (*Ccnd1*) expression were observed between naïve and *H. polygyrus* infected mice (**Figure 8E**).

Together, these data demonstrate that there is no change in the expression of enzymes involved in PGE₂ synthesis and suggest no increase in EP2/EP4 activation in the colon as a consequence of *H. polygyrus* infection.



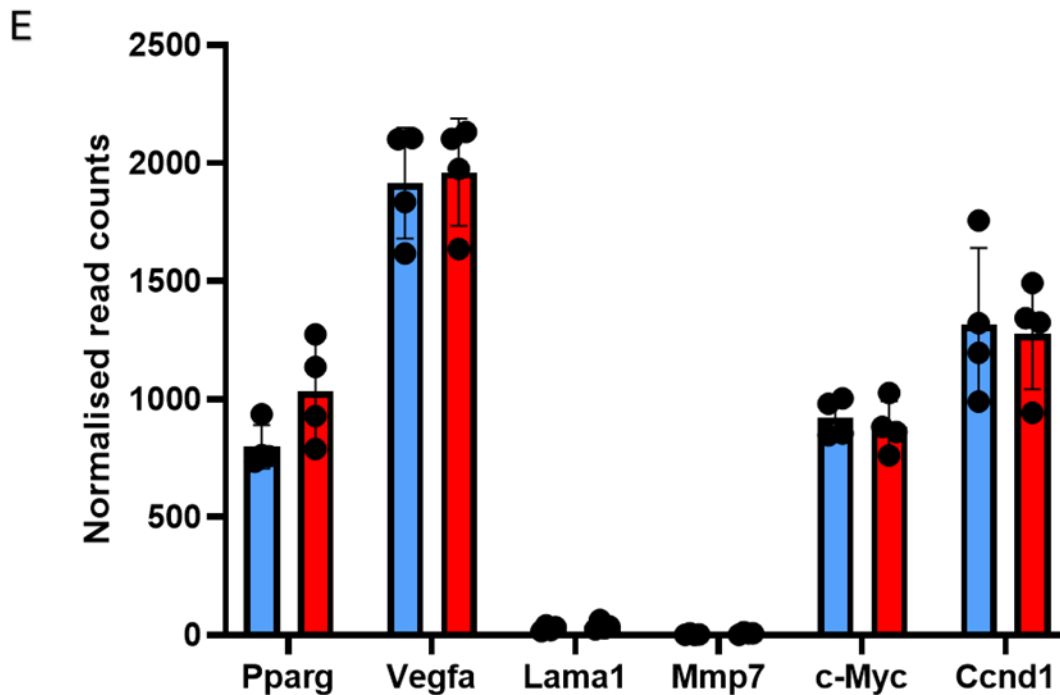


Figure 8. Expression of PGE₂ synthetic enzymes and receptors. (A-D) Graphs showing normalised read count values for synthetic enzymes involved in the synthesis of PGE₂ as well as the receptors PGE₂ activates. Naïve (blue) and *H. polygyrus* (red). **(E)** Graphs showing normalised read count values for transcription factors activated downstream of EP2/EP4 signalling.

6.4.7 Differential immune cell content in the colon of *H. polygyrus* infected mice

The immune cell population of the colon has been shown by Hang *et al* and Pastille *et al* to be altered with *H. polygyrus* infection, with an expansion of Tregs seen (398, 399). This is suggestive of an immunosuppressive environment, which may be favourable for tumour growth by limiting the beneficial effects of the anti-tumour adaptive immune response (400, 401). With the gene signature suggesting activation of immune cells, we explored this further using CIBERSORTx to estimate immune cell populations from the gene expression data. The CIBERSORTx software is utilised as an *in silico* flow cytometry analysis, whereby the immune cell populations are defined by the expression of certain genes. The data obtained from CIBERSORTx has been validated in the literature by flow cytometry (402, 403), therefore we believe this analysis gives an accurate estimation of the immune cell population. The population of immune cells was shown to change with *H. polygyrus* infection, with an increase in M2 macrophages, plasma cells, and activated mast cells (**Figure 9**), supporting results from Weng *et al* who also show an expansion of M2 macrophages in the colon post-infection (404). Despite the variation between conditions seen in **Figure 9A**, the heatmap in **Figure 9B** suggests that an increase in immune cells associated with helminth infection is seen.

An important observation to note is the presence of certain immune cell types in the naïve group that was unexpected. The naïve 5 sample includes a high percentage of activated dendritic cells (**Figure 9A**), whilst naïve 2 contains a signature relating to plasma cells and naïve 1 containing activated mast cells (**Figure 9B**). These signatures are indicative of an activated type-2 immune response (405), suggesting these mice may not be truly naïve, possibly due to an unrelated infection transmitted in the housing facility.

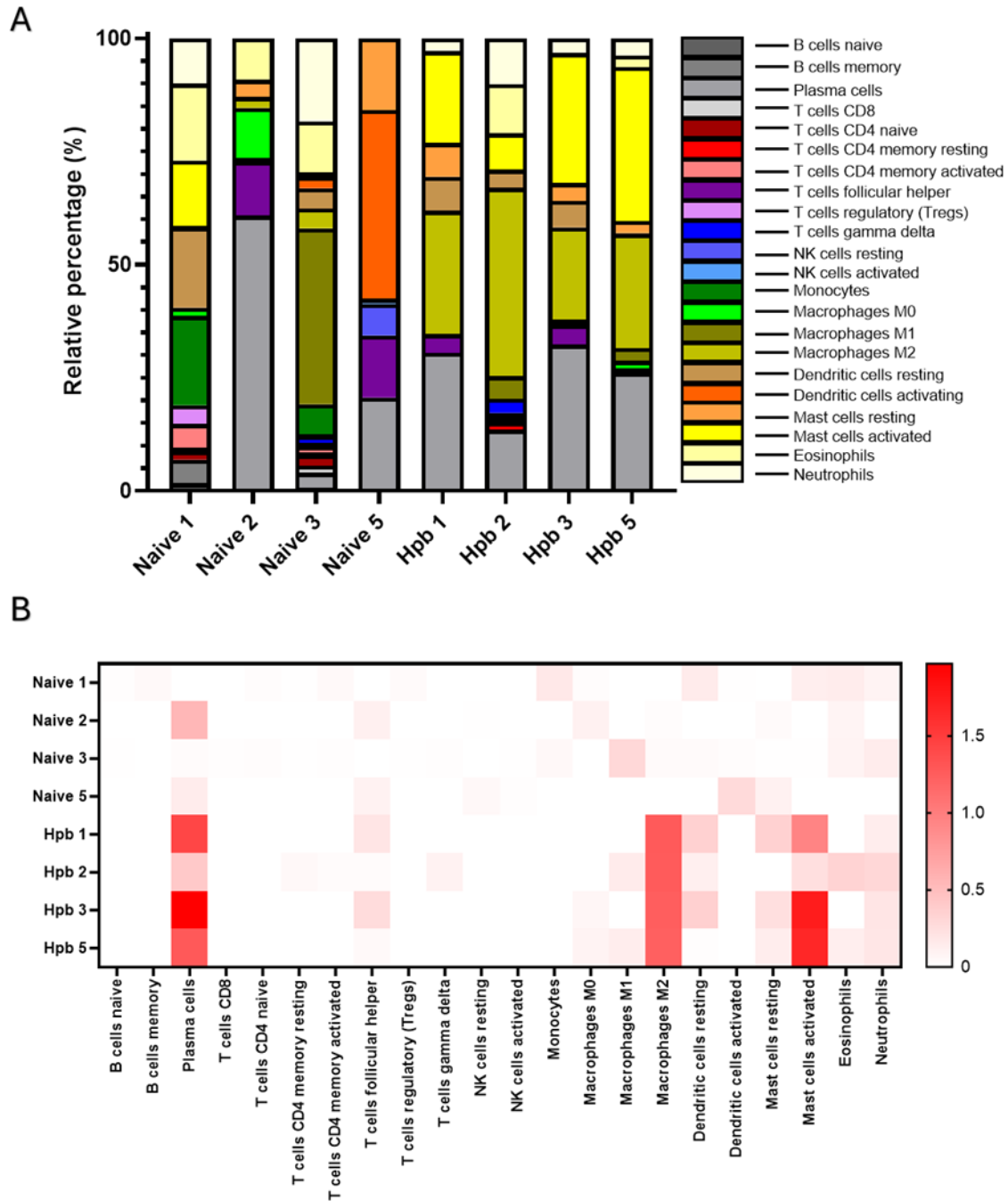


Figure 9. Different immune cell profiles in the colon of *H. polygyrus* infected mice compared to uninfected. (A) Relative immune cell percentages in the naive and *H. polygyrus* (Hpb) infected groups estimated with CIBERSORTx based on a publicly available bulk RNA-seq dataset containing markers for 178 cell types obtained from C57BL/6 as part of the Immunological genome project. **(B)** Heat map showing the log₂ fold change of differential immune cell fractions between the *H. polygyrus* and naive groups (padj < 0.05).

6.4.8 Effect of *H. polygyrus* infection on the colonic stem cell compartment

With the ISC compartment of the small intestine shown to be altered with *H. polygyrus* infection (177, 377), and the established role for an altered ISC in CRC (51), expression of ISC markers in the colonic transcriptome were analysed.

Markers of ISC proliferation in the colonic crypt *Lgr5*, *Ly6a*, and *Olfm4* were chosen from the literature (49, 177, 406), and show no significant change between naïve and *H. polygyrus* conditions (**Figure 10A**), suggesting no change in the colonic ISCs within the crypt as a consequence of *H. polygyrus* infection. As shown in **Figure 10B**, there are significant increases in markers of tuft cell differentiation (*Dclk1* and *Pou2f3*) in response to *H. polygyrus* infection, suggesting an increase in tuft cell expansion in the colon.

Following results from Nusse *et al* showing how helminth-associated crypts acquire a foetal-like programme associated with crypt injury (177), we investigated this panel of foetal epithelial markers to investigate if this same phenotype is observed in the colon. The gene expression of *Il33* and *Vsig1* were significantly increased in response to *H. polygyrus* infection, whereas *Chga* significantly decreased (**Figure 10C**). The rest of the markers were unchanged (**Figure 10D**).

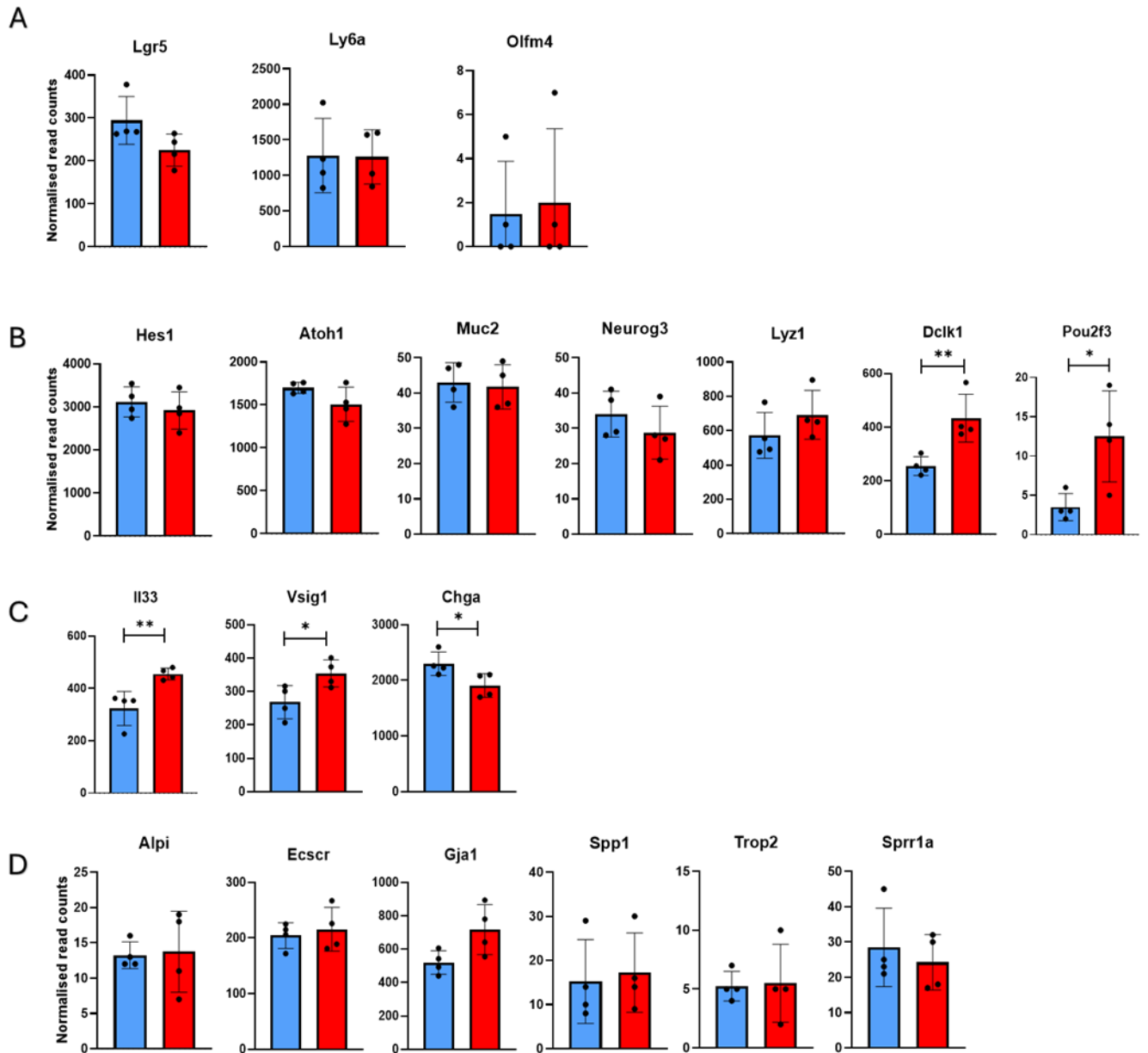


Figure 10. Impact of *H. polygyrus* infection on colonic stem cell markers. Normalised read counts shown to investigate the impact of *H. polygyrus* on (A) colonic stem cell markers in the crypt, (B) stem cell differentiation, and a panel of foetal stem cell markers as described by Nusse *et al*, 2018 with (C) significant change and (D) no significant change. Naïve (blue) and *H. polygyrus* (red). Unpaired T-test followed by Benjamini and Hochberg's correction for multiple testing was used to adjust the p-value, * $p < 0.05$, ** $p < 0.01$, error bars SEM.

6.5 Discussion

To conclude, this chapter describes the first study profiling the colonic transcriptome of *H. polygyrus* infected mice, providing a comprehensive gene expression analysis. Correlation analysis revealed sample 4 from both the *H. polygyrus* and naïve groups showed significant variability compared to the other samples. The sample quality control (QC) performed before sequencing did not highlight any clear discrepancies in RNA quality or quantity, however there is a significant difference in the total number of transcripts with reads ≥ 1 . This suggests variation in the sequencing depth or the library preparation, or could be a consequence of biological variation.

This study highlights the multifaceted host response to *H. polygyrus* infection, characterized by a gene signature associated with colonic inflammation, immune modulation, and potential oncogenic signalling. A gene signature associated with inflammatory pathways, coagulation, complement activation, and wound healing align with observed increases in faecal calprotectin and MMP expression, suggesting tissue damage. Protease dysregulation, enriched hydrolase and peptidase activity, and epithelial-mesenchymal transition (EMT) pathway activation indicate risks of tumorigenesis, with KRAS signalling enrichment and p53 pathway suppression further implicating oncogenic processes. Despite no significant changes in PGE2 synthesis or downstream EP2/EP4 signalling, mast cell activation and M2 macrophage expansion point to immune modulation that aids parasite clearance but may promote tumor growth. Additionally, alterations in stem cell signatures, including potential tuft cell differentiation, suggest adaptive responses to infection and tissue injury. Overall, *H. polygyrus* infection presents a "double-edged sword," balancing anti-inflammatory mechanisms and immune activation with increased tumorigenic potential in the colon.

The upregulated acute inflammatory and humoral immune response, as well as wound healing, coagulation, and complement activation demonstrate that colonic inflammation may be a feature of the host response to *H. polygyrus* infection. This supports findings from Pastille *et al* and Ariyaratne *et al* (151, 407), and aligns with results seen in Chapter 3, whereby an increase in faecal calprotectin is seen with *H. polygyrus* infection suggesting an increase in colonic inflammation. An increase in colonic inflammation with *H. polygyrus* was also observed by Ariyaratne *et al*, who show an increase in MMP expression in the host response to infection resulting in tissue damage (407). In this analysis, we observed hydrolase, endopeptidase, and peptidase molecular function terms enriched. As previously discussed in Chapter 4, protease dysregulation, especially their overexpression, is often linked to cancer progression, as they can influence various key processes in tumour development, including tumour invasion, growth, and metastasis (408).

The EMT pathway's positive enrichment indicates a potential shift in cellular characteristics from epithelial to mesenchymal states, which is commonly associated with increased cellular motility and invasive potential. This transition is significant in processes like cancer progression (409), hinting that such mechanisms might be active in *H. polygyrus* infection. Importantly, live infection and *in vivo* and *in vitro* treatments with HES, have previously been shown to alter the expression of EMT markers (410-412). The enrichment of KRAS signalling suggests an upregulation of proliferative signals, likely impacting cell growth and survival. KRAS signalling activation is common in various cancers and plays a crucial role in maintaining proliferative signals (413). The downregulation of the p53 pathway suggests a potential suppression of tumour-suppressive mechanisms, which may enhance cell survival and reduce apoptosis (414). Given p53's role in DNA damage repair and apoptosis (414), its decreased activity could enable genomic instability, promoting unchecked cell proliferation in the colon of *H. polygyrus* infected mice upon administration of AOM. Finally, the negative enrichment in the G2/M checkpoint pathway indicates potential dysregulation in cell cycle control, specifically in the transition from G2 to mitosis. This checkpoint ensures DNA is correctly replicated before cell division, and its suppression could lead to aberrant cell cycle progression, a hallmark in many proliferative disorders, including cancers (415). Overall, these findings highlight significant dysregulation in both oncogenic signalling and tumour suppressor pathways, which may contribute to the exacerbation of CAC as a result of *H. polygyrus* infection. Interestingly, this analysis contradicts *in vitro* findings from Jacobs *et al*, who treat a different CRC murine cell line CT26.WT with HES and see an increase in p53 expression and a decrease in cellular proliferation (410). This discrepancy highlights how the effect of HES on cell behaviour differs from cancer cells to healthy epithelial cells, and also the differences in an *in vivo* model.

The leading edge analysis revealed *Bhlhe40*, *Me1*, and *Cd44* as being the most significantly enriched subset of genes in the colonic transcriptome following *H. polygyrus* infection. *Bhlhe40* regulates pro-inflammatory cytokines and immune responses, which may exacerbate chronic inflammation and contribute to a tumour-promoting microenvironment (416). *Me1* supports metabolic reprogramming by generating NADPH for lipid biosynthesis and redox balance, fuelling the rapid proliferation of cells and enhancing their resistance to apoptosis (417). *Cd44* promotes cancer stem cell properties, cell migration, and extracellular matrix remodelling, facilitating tumour growth and invasion (418). Interestingly, all three of these genes show upregulated expression in CRC patients and have been suggested to have pro-tumorigenic roles (419-421). Together, these genes suggest a convergence of inflammatory signaling, metabolic adaptation, and stemness, providing a potential mechanistic link between *H. polygyrus* infection, chronic inflammation, and CAC development

Data presented in this thesis has implicated a role for HES-dependent activation of EP2/EP4 signalling in increasing cell permeability, following on from results by Smith *et al* who show how PGE₂ signalling may contribute to exacerbation of tumour formation during CAC (190). Therefore, the colonic transcriptome was used to determine if expression of enzymes contributing to the synthesis of PGE₂ or levels of EP2/EP4 signalling are increased with *H. polygyrus* infection. It was revealed that there are no significant alterations in gene expression of enzymes contributing to PGE₂ synthesis, therefore suggesting that *H. polygyrus* infection does not alter PGE₂ production in the colon. Evidence from Smith *et al* supports these findings, as they show using LC/MS that the concentration of PGE₂ is not altered at day 14 post-infection.

We next looked at EP2/EP4 receptor signalling, and found no change in the gene expression of transcription factors that are activated downstream of EP2/EP4 activation. Interestingly, PGE₂-EP2/EP4 signalling has been shown to regulate proliferation and type 2 cytokine production from activated type 2 innate lymphoid cells (ILC2) (422), the migration and release of inflammatory mediators in eosinophils (423, 424), degranulation of mast cells (425, 426), and immunomodulatory effects in dendritic cells (194). The transcriptome analysis showed significant increases in the gene expression of mast cell protease 1 (*Mcpt1*), mast cell protease 4 (*Mcpt4*), and chymase 2 (*Cma2*), suggesting an increase in mast cell degranulation. An *in silico* flow cytometry also predicts an increase in mast cell activation in response to *H. polygyrus* infection. Mast cells are frequently activated in the tumour microenvironment in CRC (427) as well as in response to helminth infection (428). The activation of mast cells results in the release of proteases, leading to an increase in intestinal permeability to facilitate the expulsion of parasites (162), which may have consequences for CAC.

Analysis of the immune cell population also revealed the increase in alternatively activated macrophages, otherwise known as M2 macrophages seen with *H. polygyrus* infection. This was indicated by the increase in M2 macrophage markers, such as chitinase-like 3 (*Chil3*), arginase 1 (*Arg1*), and secreted frizzled-related protein 4 (*Sfrp4*) (429). M2 macrophages are activated by exposure to certain cytokines, notably IL-4 or IL-13 which are released as part of the type 2 immune response to infection (430). M2 macrophages have been shown to play a crucial role in the clearance of parasites, where they contribute to trapping helminth larvae in tissues to make them accessible to infiltrating immune cells (372). However, M2 macrophages are also known as tumour-associated macrophages (TAMs) and constitute an essential component of the tumour microenvironment (374). During the initial phases of tumour development, M2 macrophages have been shown to accumulate and distribute around tumour tissue to induce regulatory T-cell responses, promote tumour cell immune escape, provoke epithelial-mesenchymal transition (EMT), and enhance tumour cell infiltration and

spread (431). Therefore, despite their ability to clear parasite infections, the expansion of the M2 macrophage population in the colon may contribute to exacerbation of CAC.

Finally, we investigated whether *H. polygyrus* leads to an alteration in ISC differentiation in the colon. Infection with *H. polygyrus* has been shown to alter the Lgr5⁺ population, with Nusse *et al* showing that in the small intestine there is loss of Lgr5⁺ cells and an up-regulation of Sca-1 (*Ly6a*) in the crypt epithelium overlying the granuloma 6 days post-infection (177). Drurey *et al* reveal similar findings *in vitro* where small intestinal organoids treated with HES show an increase in Sca-1 expression (377). The expansion of the Sca-1⁺ ISC population is suggested to be indicative of an increase in cell proliferation in response to crypt damage, with Lgr5⁺ ISC increasing day 10 post-infection, indicating resolution of crypt damage (177). The colonic transcriptome showed no change in *Lgr5* or *Ly6a* gene expression, suggesting that *H. polygyrus* doesn't alter the population of stem cells within the colonic crypt. The adoption of a foetal gene signature in the small intestine is indicative of an infection-mediated alteration in response to injury, whereby foetal development pathways are used to regenerate tissue when there is injury (177). A significant change in three foetal gene signatures was observed, with the increase in *Il33* and *Vsig1* suggesting the development of a foetal-like programme in the colonic crypt. The *Vsig1* gene encodes the V-set and Immunoglobulin domain containing 1 (VSIG1) protein, a transmembrane protein possessing immunosuppressive and anti-proliferative properties in response to tissue injury (432, 433). *Il33* encodes for interleukin-33 (IL-33) which is expressed by intestinal epithelial cells in response to tissue injury to recruit immune cells, behaving as an alarmin (434). However, it cannot be concluded from the alteration of two genes in the panel that a foetal-like programme is acquired in the colonic crypt.

Further RNA-seq performed by Nusse *et al* and Drurey *et al* revealed the signatures of tuft cells, *Dclk1* and *Pou2f3*, were upregulated in the small intestine and on HES-treated organoids (177, 377). Upregulation of *Dclk1* and *Pou2f3* was also seen in the colonic transcriptome of *H. polygyrus* infected mice, suggesting an increase in ISC differentiation to tuft cells in the colon. Tuft cells have recently emerged as having a critical function in initiating mucosal type 2 immune responses following helminth infection through interleukin-25 (IL-25) secretion, which activates ILC2s to initiate the anti-helminth immune response through type 2 CD4⁺ helper T cells (15, 16, 435). However, CIBERSORTx analysis showed no expansion of type 2 CD4⁺ helper T cells, highlighting the need for future investigations to confirm if tuft cell expansion does occur in the colon as a consequence of *H. polygyrus* infection.

The overall aims of this chapter were successfully met, with the colonic transcriptome profiled and effects of *H. polygyrus* on gene expression, immune cell population, and intestinal stem cell differentiation investigated. The first hypothesis was proven to be correct, with GSEA analysis revealing

KRAS signalling enrichment which may exacerbate CAC. Additionally the second hypothesis was also proven, with profiling of the immune cell population revealing an enrichment of M2 macrophages which may promote an immunosuppressive environment. Lastly, the third hypothesis was disproven, with analysis of markers in the ISC compartment revealing few are significantly altered unlike what is seen in the small intestine, suggesting little epithelial dysfunction.

Chapter 7: Final Discussion

7.1 Summary of results

This thesis has focussed on identifying a mechanism by which *H. polygyrus* is able to exacerbate tumour formation in an *in vivo* model of CAC with a high ω -6 diet via PGE₂ signalling. Both *in vitro* and *in vivo* evidence suggests the ability of *H. polygyrus* live infection and secretions (HES) to increase EP2/EP4 signalling, accompanied with a decrease in E-cadherin expression in the colon, suggesting a mechanism for increase in cell permeability. This decrease in E-cadherin expression both *in vitro* and *in vivo* was shown to be dependent on EP2/EP4 activation, with a combination of EP2/EP4 inhibitors partially restoring E-cadherin expression. Using a bioinformatic approach, I identified homologues of the sPLA₂ family of enzymes in the *H. polygyrus* genome, with proteomic evidence presented in this thesis suggesting they may be secreted into the HES. Preliminary investigations using novel inhibitors I identified by *in silico* drug identification suggest that it is the secretion of a helminth homologue of sPLA₂ which mediates the increase in cell permeability seen *in vitro*.

Initial experiments focussed on utilising p β -catenin Ser⁵⁵² as a marker for EP2/EP4 activation, and showed a significant increase in the colon with *H. polygyrus* infection. With an established role for EP2/EP4 activation and increased cell permeability (267, 268), expression of E-cadherin in the colon was investigated *in vivo* as it is a marker of colonic epithelial tight junctions, and was shown to significantly decrease with *H. polygyrus* infection, supporting findings from Su *et al* (165). Interestingly, Su *et al* showed the decrease in E-cadherin at a different time point (day 7) and in a different strain of mouse (C57BL/6). Using a combination of EP2/EP4 antagonists, I show this decrease in E-cadherin to be dependent on EP2/EP4 activation, although a lack of clinical signs questions the clinical relevance of this result. Results of the impact of EP2/EP4 antagonists on Hpb-exacerbation of tumour burden were inconclusive, due to a lack of clinical signs of disease in all treatment groups, therefore repetition is needed. As the colon is at a distant site to where *H. polygyrus* resides, I focussed on the ability of HES to increase permeability. HES has been shown to cause systemic effects during helminth infection, such as during a model of airway allergy (306). Therefore, I optimised an FD4 *in vitro* permeability assay using two murine CRC cell lines; CMT-93 and CT26, to assess the effect of HES on cell permeability. Having optimised the assay with CMT-93, I then demonstrated the ability of HES to significantly increase cell permeability, and that this is dependent on EP2/EP4 activation with a suggested preference for EP2. However, it is important to acknowledge that the inhibitors used show affinity to other EP receptor subtypes, therefore non-specific effects due to binding of other subtypes are possible. However, as other subtypes are not highly expressed in the colon, we don't believe this

to be a concern to the validity of the data. This is believed to be a novel finding, as the ability of HES to permeabilise a cell monolayer has not been investigated, whereas this has been performed for ESPs of other helminths (168, 169). Aligning with findings *in vivo*, HES was shown to activate EP2/EP4 receptors with an increase in p β -catenin Ser⁵⁵², which was associated with a decrease in E-cadherin expression. Interestingly, similar findings are observed with a PGE₂ receptor agonist (dmPGE₂). This suggests that the HES may possess a similar mechanism of action to dmPGE₂ to increase cell permeability.

Further investigation into the mechanism by which HES is able to activate EP2/EP4 receptor signalling and increase cell permeability was performed, involving various *in vitro* and bioinformatic approaches. Since EP2/EP4 are PGE₂ receptors and Laan *et al* demonstrated the presence of PGE₂ in the ESPs of *T. suis* (194), I conducted a lipidomic analysis of the HES to search for PGE₂ but conclusively ruled out its presence. I ruled out the possibility of a protease in the HES increasing permeability, which contradicts findings with *T. spiralis* ESPs (169), and that the activity of the molecule is not impacted by heat which again contradicts findings with *T. spiralis* ESPs (169). The molecule was further narrowed down to the 10-50,000 MW fraction of HES. Proteomic analysis of the 10-50,000 MW fraction revealed the presence of three sequences (HPOL_0000384601, HPOL_0000928401, and HPOL_0001491401) bearing significant identity to human sPLA₂ isoforms, with an *in vitro* assay confirmed PLA₂ activity in the HES and helminth adult antigen. I confirmed the ability of a PLA₂ enzyme to increase cell permeability by using *A. mellifera* PLA₂ on the FD4 assay, which supports evidence in the literature of PLA₂ increasing cell permeability (323-325). Despite sPLA₂ being identified in other ESPs of helminths (199, 316, 317), I believe this is the first functional characterisation of sPLA₂ activity in the HES, which may contribute to its ability to increase cell permeability. As to why *H. polygyrus* encodes a sPLA₂ enzyme, this remains unknown from this project, but it could be linked to a mechanism of obtaining nutrients from the host or to invade the host epithelium to establish chronic infection.

For the purpose of this thesis, HPOL_0000384601 was pursued as the most promising candidate for encoding a functional sPLA₂, as HPOL_0000928401 and HPOL_0001491401 have not got conservation in the zinc and calcium binding sites respectively, which are critical for PLA₂ function (310, 315). HPOL_0000384601 is hypothesised to encode a homologue for the human PLA₂G1B enzyme, with significant tertiary and secondary similarities shown in this thesis. Interestingly, HPOL_0000384601 is shown to be conserved with other species of helminths that lack abrasive structures to invade host epithelium. Furthermore, sPLA₂ secreted by other helminths has been shown to have immunomodulatory effects (199, 318), therefore suggesting a further survival advantage to helminths for secreting a functional sPLA₂. This immunomodulation likely contributes to creating a more favourable environment for the helminths' persistence and survival within the host. These findings

suggest that the secretion of functional sPLA₂ by helminths could be a strategic adaptation to evade immune detection and suppression. Consequently, understanding the mechanisms and pathways through which sPLA₂ mediates these effects could provide valuable insights into helminth biology and host-parasite interactions, potentially unveiling new therapeutic targets or strategies to mitigate parasitic infections.

Chapter 5 aimed to link sPLA₂ activity to the HES-induced increase in cell permeability, with existing evidence in the lab using commercially available PLA₂ inhibitors, manoalide and varespladib, showing minimal inhibition at high concentrations against the *H. polygyrus* somatic antigen. Initially this result was surprising, however further research into the mechanism of action of these inhibitors revealed the binding sites of the inhibitors were not conserved in the *H. polygyrus* PLA₂G1B amino acid sequence. Therefore, I utilised an established *in silico* ligand-based molecular docking workflow to design inhibitors specific for HPOL_0000384601. A homology model was first developed for HPOL_0000384601, with a known ligand for human PLA₂ docked to identify significant interactions in the binding pocket. Compounds passing computational and visual scoring were ordered, with the compound displaying the highest affinity (lowest IC₅₀) for PLA₂ activity in the somatic antigen chosen for *in vitro* testing. Compound AF-399/14183760 was added alongside HES, and significantly inhibited HES-induced increase in cell permeability. It is important to acknowledge how the compounds were screened against the somatic antigen, but then tested against the HES. This approach was chosen as the somatic antigen gave the strongest signal in the PLA₂ activity assay, however it is possible that the compounds could have reacted differently if they were screened against the HES. The data presented in chapter 5 suggests that the ability of HES to increase cell permeability is dependent on activity of *H. polygyrus* PLA₂G1B, however whether this increases PGE₂ concentration in the cell monolayer, leading to paracrine or autocrine EP2/EP4 signalling and increased permeability, remains unknown. Additionally, the importance of *H. polygyrus* encoding a homologue of PLA₂G1B *in vivo* also remains unknown and warrants further investigation.

Chapter 6 details the analysis of the colonic transcriptome in mice infected with *H. polygyrus* fed a high ω -6 diet. The transcriptomics revealed the inflammatory response and wound healing as being enriched functional processes, with protease activity also increased following helminth infection. Given findings described in this thesis, an increase in protease activity could be significant in dysregulating the colonic epithelial barrier (68). Work in this thesis also describes activation of the PGE₂-EP2/EP4 signalling pathway by HES as being crucial for increasing cell permeability *in vitro*. Transcriptomic data showed that the gene expression of enzymes involved in synthesising PGE₂ are not altered *in vivo*, nor are the transcription factors downstream of PGE₂-EP2/EP4 activation. This data supports findings from Smith *et al* who show no alteration in PGE₂ concentration in the colon of *H.*

polygyrus infected mice at the same time-point (190). Pathway enrichment analysis revealed the increase in inflammatory and oncogenic pathways, whilst cell cycle regulation and tumour suppressor pathways. Specifically, the upregulation of inflammatory pathways likely promotes a pro-tumorigenic microenvironment, characterized by the release of cytokines and chemokines that can stimulate angiogenesis, immune cell recruitment, and epithelial cell proliferation (436-440). Concurrently, the activation of oncogenic pathways could enhance tumour cell survival, proliferation, and metastasis (441). On the other hand, the suppression of cell cycle regulation and tumour suppressor pathways likely impairs critical cellular checkpoints, reducing the ability of cells to halt uncontrolled growth or undergo apoptosis in response to DNA damage (442). Together, these changes create an imbalance favouring tumour initiation and progression, amplifying the severity of CAC under the influence of *H. polygyrus* infection. Finally, we reveal the immune cell phenotype in the colon as having a high abundance of M2 macrophages and activated mast cells, indicating an anti-helminthic response but also an environment favourable for cancer development (374).

7.2 Limitations

While the data presented in this thesis explore the mechanism by which *H. polygyrus* can exacerbate CAC, there are limitations to this study.

The transcriptomics performed as part of chapter 6 was performed with a read depth of 30 million reads per sample, which is the minimum that is accepted in the literature as enabling information on a global view of gene expression between conditions (443). The sequencing identified 80.33% of the genes in the mouse genome, with missing genes not abundant enough to be picked up with the read depth, therefore a higher read depth may identify missing genes of a lower abundance which could still reveal crucial findings (444-446). Furthermore, the initial sample size of $n = 5$ was reduced to $n = 4$ due to high sample heterogeneity. The original sample size of $n = 5$ was chosen due to G*Power analysis which gave $n = 5$, but reliability could be improved by increasing the number of replicates to >6 (447), therefore this analysis requires more replicates to increase reliability of results.

There are also several limitations associated with the use of Gene Set Enrichment Analysis (GSEA) used in Chapter 6. These include its dependence on the quality and relevance of gene set databases, which may be outdated, incomplete, or overly generalized, potentially leading to less accurate or misleading insights (448). Additionally, GSEA assumes coordinated expression changes across genes within a set, which may oversimplify the complexity of biological pathways, as not all genes in a pathway respond uniformly to biological stimuli (448). The method is also sensitive to noise, particularly in datasets with small sample sizes or high variability, which can obscure meaningful patterns or introduce false positives (448). Furthermore, GSEA does not account for interactions or hierarchical relationships

between pathways, limiting its ability to provide nuanced, context-specific insights (448). Lastly, the scoring mechanism used in GSEA may favour larger gene sets, potentially underrepresenting smaller but biologically significant pathways (448). These limitations highlight the need for careful interpretation and integration of GSEA results with experimental validation (details in Future Work section).

7.3 Future work

The data presented in this thesis suggesting a mechanism by which *H. polygyrus* can exacerbate CAC leaves much to be explored.

The AOM/DSS model detailed in chapter 3 lacks appropriate controls, with a group of *H. polygyrus* infected mice without AOM/DSS and a group of naïve mice given EP2/EP4 inhibitors not included.. It was inconclusive from the H&E staining whether tumours were present, therefore these would need to be confirmed with β -catenin staining, used as its abnormal activity is commonly associated with cancerous cells (449-451), to have further confidence in these results.

One key finding from this thesis is that the addition of HES may lead to autocrine or paracrine PGE₂-EP2/EP4 activation, leading to the observed increase in cell permeability *in vitro*. To investigate this mechanism, LC/MS could be performed on cell supernatants and lysates after treatment with HES to measure if PGE₂ is produced following the stimulus, in a similar manner to the experiments detailed by Pozzi *et al* (452). Jimenez *et al* performed a similar experiment with bone marrow-derived macrophages, showing increased PGE₂ production after 24 hrs of stimulation with *H. polygyrus* larval products (306), suggesting the increase in PGE₂ occurs quickly after stimulation. Therefore, our experiment would involve collecting cell supernatant and lysates every 2 hrs post-stimulation. Furthermore, the only measure of tight junction integrity used in this thesis was E-cadherin, whilst it is a widely used marker for tight junction integrity there are disadvantages as discussed in chapter 3. Therefore, to strengthen this evidence, other tight junction proteins such as claudin-1 and occludin should be investigated, with both also showing evidence of being regulated by EP2/EP4 receptor activation (109, 314). The FD4 assay can also be replicated *in vivo*, by administering FD4 via oral gavage alongside the EP2/EP4 inhibitors and measuring concentrations in the serum, to assess if findings *in vitro* are replicated *in vivo*.

As previously mentioned, *in vitro* assays were performed with a CRC cell line which represents a major limitation to this thesis. To gain insight into what may be happening in “normal” physiological conditions, the use of primary colonic cells or organoids should be considered as these won’t harbour the mutations in the cancerous cell line.

The discovery of the “*H. polygyrus* PLA₂G1B” is regarded as one of the most exciting findings of this thesis. Further work can be conducted to establish the importance of this enzyme for *H. polygyrus* survival, by culturing worms *in vitro* with the AF-399/14183760 compound and worm viability measured, or by administering AF-399/14183760 *in vivo* and measuring egg burden as well as levels of EP2/EP4 signalling which I’ve shown to be upregulated with helminth infection in Chapter 3. Performing these experiments would allow the significance of *H. polygyrus* PLA₂G1B to the helminths’ survival to be investigated. However, as discussed in chapter 5, the drug binding sites of AF-399/14183760 are conserved with three isoforms of murine sPLA₂ suggesting non-specific binding to other sPLA₂ isoforms. It would first need to be determined if the inhibitor inhibits these other isoforms, which can be predicted using *in silico* modelling of the inhibitor into the active sites of the isoform structures. This could then be tested *in vitro* by expressing these isoforms using a lipofectamine transfection and His-tag expression, followed by a PLA₂ activity assay following addition of the inhibitor. If the inhibitor is shown to interact with the other isoforms, it would next be important to characterise other sites in the binding pocket of *H. polygyrus* PLA₂G1B that are important for its function and not conserved in murine isoforms. To do this, residues can be mutated to probe the role of individual residues in the stability, abundance and function of a protein (453).

It is important to validate the transcriptomic findings using qPCR before looking at the functional implications of the changes. Furthermore, to get a more robust overview of the effects of *H. polygyrus* infection in the colon, the transcriptomic data can be combined with proteomic analysis, as some genes may not be detected at transcriptome level due to post-translational modifications (454). At the cellular level, expression and localisation of specific genes can be confirmed using RNA *in situ* hybridisation. Functional assays to confirm the altered biological processes and signalling pathways can be performed to investigate the biological relevance of the transcriptomic findings. For example, cell proliferation assays such as MTT or BrdU incorporation can measure changes in cell growth rates, reflecting pathways related to cell cycle regulation. Migration and invasion assays, including scratch wound healing assays or Transwell chamber assays, can assess the impact on pathways influencing cellular motility and invasiveness, often tied to EMT processes. Apoptosis assays, such as flow cytometry-based annexin V/propidium iodide staining or caspase activity assays, can validate disruptions in survival signaling. Furthermore, immunoblotting or immunofluorescence can be used to monitor the expression of pathway-specific proteins, such as E-cadherin and KRAS, providing direct evidence of altered signaling.

Flow cytometry can be performed to confirm findings from the CIBERSORTx analysis, with single cell RNAseq providing a further avenue to identify the immune cell populations (455). To perform this experiment, the immune cells would be isolated from the colon tissue using appropriate markers, such

as CD45 for leukocytes or specific markers for subpopulations like T cells (CD3), macrophages (CD11b), or dendritic cells (CD11c) (456). These cells would then be stained with fluorescently tagged antibodies against surface markers relevant to the immune populations identified in the CIBERSORTx analysis. The samples would be analyzed on a flow cytometer, enabling the quantification and characterization of distinct immune subsets based on their fluorescence profiles. Additionally, scRNA-seq can be employed to provide a more granular view of immune cell diversity. After isolating single cells, RNA would be extracted, sequenced, and mapped to a reference genome. The resulting data can be used to identify gene expression signatures of different immune populations, validate the proportions identified by CIBERSORTx, and uncover novel subsets that may not be detected by bulk RNA sequencing.

7.4 Overall implications

The findings presented in this thesis significantly enhance our understanding of how *H. polygyrus* can activate colonic PGE₂ signalling to increase intestinal cell permeability. By revealing that *H. polygyrus* secretions (HES) increase cell permeability through EP2/EP4 signaling *in vitro*, this work provides new insights into how helminth infections can disrupt epithelial integrity. The identification of a helminth homologue of PLA₂G1B in HES, which is shown to be functionally active and linked to increased cell permeability, is a novel contribution to the field. This discovery suggests that *H. polygyrus* PLA₂G1B activity may not only facilitate parasite invasion but also modulate the host's immune environment to favour chronic infection, and possibly have an impact on cancer development. Furthermore, the transcriptomic analysis highlights how *H. polygyrus* infection enriches inflammatory and oncogenic pathways, contributing to a microenvironment which may favour tumour development. While the findings offer promising directions for future research, particularly regarding the functional characterization of the *H. polygyrus* PLA₂G1B enzyme and the broader implications of PGE₂ signaling, the study also acknowledges limitations, such as the use of a cancer cell line and incomplete transcriptomic data. These findings underscore the need for further *in vivo* studies and more comprehensive cell-based models to fully elucidate the parasite-host interactions in the context of cancer. Ultimately, this thesis opens avenues for exploring therapeutic strategies targeting *H. polygyrus* PLA₂G1B or EP2/EP4 signaling, potentially mitigating the adverse effects of helminth infections on cancer progression.

References

1. Sulaiman S, Marciani L. MRI of the Colon in the Pharmaceutical Field: The Future before us. *Pharmaceutics*. 2019;11(4).
2. Hamilton SR. Structure of the colon. *Scand J Gastroenterol Suppl*. 1984;93:13-23.
3. Vancamelbeke M, Vermeire S. The intestinal barrier: a fundamental role in health and disease. *Expert Rev Gastroenterol Hepatol*. 2017;11(9):821-34.
4. Helander HF, Fändriks L. Surface area of the digestive tract - revisited. *Scand J Gastroenterol*. 2014;49(6):681-9.
5. Turner JR. Intestinal mucosal barrier function in health and disease. *Nat Rev Immunol*. 2009;9(11):799-809.
6. Pelaseyed T, Bergström JH, Gustafsson JK, Ermund A, Birchenough GM, Schütte A, et al. The mucus and mucins of the goblet cells and enterocytes provide the first defense line of the gastrointestinal tract and interact with the immune system. *Immunol Rev*. 2014;260(1):8-20.
7. Van der Sluis M, De Koning BA, De Bruijn AC, Velcich A, Meijerink JP, Van Goudoever JB, et al. Muc2-deficient mice spontaneously develop colitis, indicating that MUC2 is critical for colonic protection. *Gastroenterology*. 2006;131(1):117-29.
8. Pietrzak B, Tomela K, Olejnik-Schmidt A, Mackiewicz A, Schmidt M. Secretory IgA in Intestinal Mucosal Secretions as an Adaptive Barrier against Microbial Cells. *Int J Mol Sci*. 2020;21(23).
9. Groschwitz KR, Hogan SP. Intestinal barrier function: molecular regulation and disease pathogenesis. *J Allergy Clin Immunol*. 2009;124(1):3-20; quiz 1-2.
10. Kolios G, Moodley Y. Introduction to stem cells and regenerative medicine. *Respiration*. 2013;85(1):3-10.
11. Umar S. Intestinal stem cells. *Curr Gastroenterol Rep*. 2010;12(5):340-8.
12. Miron N, Cristea V. Enterocytes: active cells in tolerance to food and microbial antigens in the gut. *Clin Exp Immunol*. 2012;167(3):405-12.
13. Snoeck V, Goddeeris B, Cox E. The role of enterocytes in the intestinal barrier function and antigen uptake. *Microbes Infect*. 2005;7(7-8):997-1004.
14. Gribble FM, Reimann F. Function and mechanisms of enteroendocrine cells and gut hormones in metabolism. *Nat Rev Endocrinol*. 2019;15(4):226-37.
15. Howitt MR, Lavoie S, Michaud M, Blum AM, Tran SV, Weinstock JV, et al. Tuft cells, taste-chemosensory cells, orchestrate parasite type 2 immunity in the gut. *Science*. 2016;351(6279):1329-33.
16. Gerbe F, Sidot E, Smyth DJ, Ohmoto M, Matsumoto I, Dardalhon V, et al. Intestinal epithelial tuft cells initiate type 2 mucosal immunity to helminth parasites. *Nature*. 2016;529(7585):226-30.
17. Lueschow SR, McElroy SJ. The Paneth Cell: The Curator and Defender of the Immature Small Intestine. *Front Immunol*. 2020;11:587.
18. Cheng H, Leblond CP. Origin, differentiation and renewal of the four main epithelial cell types in the mouse small intestine. V. Unitarian Theory of the origin of the four epithelial cell types. *Am J Anat*. 1974;141(4):537-61.
19. Reya T, Clevers H. Wnt signalling in stem cells and cancer. *Nature*. 2005;434(7035):843-50.
20. Shah K, Kazi JU. Phosphorylation-Dependent Regulation of WNT/Beta-Catenin Signaling. *Front Oncol*. 2022;12:858782.
21. Kai Y. Intestinal villus structure contributes to even shedding of epithelial cells. *Biophys J*. 2021;120(4):699-710.
22. Schneikert J, Behrens J. The canonical Wnt signalling pathway and its APC partner in colon cancer development. *Gut*. 2007;56(3):417-25.
23. Zhan T, Rindtorff N, Boutros M. Wnt signaling in cancer. *Oncogene*. 2017;36(11):1461-73.

24. Bray F, Ferlay J, Soerjomataram I, Siegel RL, Torre LA, Jemal A. Global cancer statistics 2018: GLOBOCAN estimates of incidence and mortality worldwide for 36 cancers in 185 countries. *CA Cancer J Clin.* 2018;68(6):394-424.
25. Durko L, Malecka-Panas E. Lifestyle Modifications and Colorectal Cancer. *Curr Colorectal Cancer Rep.* 102014. p. 45-54.
26. Sato Y, Tsujinaka S, Miura T, Kitamura Y, Suzuki H, Shibata C. Inflammatory Bowel Disease and Colorectal Cancer: Epidemiology, Etiology, Surveillance, and Management. *Cancers (Basel).* 2023;15(16).
27. Chatila WK, Walch H, Hechtman JF, Moyer SM, Sgambati V, Faleck DM, et al. Integrated clinical and genomic analysis identifies driver events and molecular evolution of colitis-associated cancers. *Nat Commun.* 2023;14(1):110.
28. Steele SR, Park GE, Johnson EK, Martin MJ, Stojadinovic A, Maykel JA, et al. The impact of age on colorectal cancer incidence, treatment, and outcomes in an equal-access health care system. *Dis Colon Rectum.* 2014;57(3):303-10.
29. Jasperson KW, Tuohy TM, Neklason DW, Burt RW. Hereditary and familial colon cancer. *Gastroenterology.* 2010;138(6):2044-58.
30. Solomon E, Voss R, Hall V, Bodmer WF, Jass JR, Jeffreys AJ, et al. Chromosome 5 allele loss in human colorectal carcinomas. *Nature.* 1987;328(6131):616-9.
31. Dang CV, Le A, Gao P. MYC-induced cancer cell energy metabolism and therapeutic opportunities. *Clin Cancer Res.* 2009;15(21):6479-83.
32. Eilers M, Eisenman RN. Myc's broad reach. *Genes Dev.* 2008;22(20):2755-66.
33. Hall M, Peters G. Genetic alterations of cyclins, cyclin-dependent kinases, and Cdk inhibitors in human cancer. *Adv Cancer Res.* 1996;68:67-108.
34. Olave MC, Graham RP. Mismatch repair deficiency: The what, how and why it is important. *Genes Chromosomes Cancer.* 2022;61(6):314-21.
35. Rustgi AK. The genetics of hereditary colon cancer. *Genes Dev.* 2007;21(20):2525-38.
36. Smith D, Ballal M, Hodder R, Soin G, Selvachandran SN, Cade D. Symptomatic presentation of early colorectal cancer. *Ann R Coll Surg Engl.* 2006;88(2):185-90.
37. Majumdar SR, Fletcher RH, Evans AT. How does colorectal cancer present? Symptoms, duration, and clues to location. *Am J Gastroenterol.* 1999;94(10):3039-45.
38. Meza R, Jeon J, Renehan AG, Luebeck EG. Colorectal cancer incidence trends in the United States and United Kingdom: evidence of right- to left-sided biological gradients with implications for screening. *Cancer Res.* 2010;70(13):5419-29.
39. Pretzsch E, Bösch F, Neumann J, Ganschow P, Bazhin A, Guba M, et al. Mechanisms of Metastasis in Colorectal Cancer and Metastatic Organotropism: Hematogenous versus Peritoneal Spread. *J Oncol.* 2019;2019:7407190.
40. Adebayo AS, Agbaje K, Adesina SK, Olajubutu O. Colorectal Cancer: Disease Process, Current Treatment Options, and Future Perspectives. *Pharmaceutics.* 2023;15(11).
41. Tofthagen C. Surviving chemotherapy for colon cancer and living with the consequences. *J Palliat Med.* 2010;13(11):1389-91.
42. Wang Q, Shen X, Chen G, Du J. Drug Resistance in Colorectal Cancer: From Mechanism to Clinic. *Cancers (Basel).* 2022;14(12).
43. Vogelstein B, Fearon ER, Hamilton SR, Kern SE, Preisinger AC, Leppert M, et al. Genetic alterations during colorectal-tumor development. *N Engl J Med.* 1988;319(9):525-32.
44. Armaghany T, Wilson JD, Chu Q, Mills G. Genetic alterations in colorectal cancer. *Gastrointest Cancer Res.* 2012;5(1):19-27.
45. Abdul Khalek FJ, Gallicano GI, Mishra L. Colon cancer stem cells. *Gastrointest Cancer Res.* 2010(Suppl 1):S16-23.
46. Barker N, van Es JH, Kuipers J, Kujala P, van den Born M, Cozijnsen M, et al. Identification of stem cells in small intestine and colon by marker gene Lgr5. *Nature.* 2007;449(7165):1003-7.

47. Zheng L, Duan SL. Molecular regulation mechanism of intestinal stem cells in mucosal injury and repair in ulcerative colitis. *World J Gastroenterol.* 2023;29(16):2380-96.
48. Van der Flier LG, Sabates-Bellver J, Oving I, Haegebarth A, De Palo M, Anti M, et al. The Intestinal Wnt/TCF Signature. *Gastroenterology.* 2007;132(2):628-32.
49. Barker N, Clevers H. Leucine-rich repeat-containing G-protein-coupled receptors as markers of adult stem cells. *Gastroenterology.* 2010;138(5):1681-96.
50. Puglisi MA, Tesori V, Lattanzi W, Gasbarrini GB, Gasbarrini A. Colon cancer stem cells: controversies and perspectives. *World J Gastroenterol.* 2013;19(20):2997-3006.
51. O'Brien CA, Pollett A, Gallinger S, Dick JE. A human colon cancer cell capable of initiating tumour growth in immunodeficient mice. *Nature.* 2007;445(7123):106-10.
52. Maenhaut C, Dumont JE, Roger PP, van Staveren WC. Cancer stem cells: a reality, a myth, a fuzzy concept or a misnomer? An analysis. *Carcinogenesis.* 2010;31(2):149-58.
53. Huang JL, Oshi M, Endo I, Takabe K. Clinical relevance of stem cell surface markers CD133, CD24, and CD44 in colorectal cancer. *Am J Cancer Res.* 2021;11(10):5141-54.
54. Botchkina G. Colon cancer stem cells--from basic to clinical application. *Cancer Lett.* 2013;338(1):127-40.
55. Pantic I. Cancer stem cell hypotheses: impact on modern molecular physiology and pharmacology research. *J Biosci.* 2011;36(5):957-61.
56. Vicente-Dueñas C, Gutiérrez de Diego J, Rodríguez FD, Jiménez R, Cobaleda C. The role of cellular plasticity in cancer development. *Curr Med Chem.* 2009;16(28):3676-85.
57. Preston SL, Wong WM, Chan AO, Poulsom R, Jeffery R, Goodlad RA, et al. Bottom-up histogenesis of colorectal adenomas: origin in the monocryptal adenoma and initial expansion by crypt fission. *Cancer Res.* 2003;63(13):3819-25.
58. Martin ML, Zeng Z, Adileh M, Jacobo A, Li C, Vakiani E, et al. Logarithmic expansion of LGR5(+) cells in human colorectal cancer. *Cell Signal.* 2018;42:97-105.
59. Shih IM, Wang TL, Traverso G, Romans K, Hamilton SR, Ben-Sasson S, et al. Top-down morphogenesis of colorectal tumors. *Proc Natl Acad Sci U S A.* 2001;98(5):2640-5.
60. de Souza HS, Fiocchi C. Immunopathogenesis of IBD: current state of the art. *Nat Rev Gastroenterol Hepatol.* 2016;13(1):13-27.
61. Michielan A, D'Inca R. Intestinal Permeability in Inflammatory Bowel Disease: Pathogenesis, Clinical Evaluation, and Therapy of Leaky Gut. *Mediators Inflamm.* 2015;2015:628157.
62. Salim SY, Söderholm JD. Importance of disrupted intestinal barrier in inflammatory bowel diseases. *Inflamm Bowel Dis.* 2011;17(1):362-81.
63. Wang F, Graham WV, Wang Y, Witkowski ED, Schwarz BT, Turner JR. Interferon-gamma and tumor necrosis factor-alpha synergize to induce intestinal epithelial barrier dysfunction by up-regulating myosin light chain kinase expression. *Am J Pathol.* 2005;166(2):409-19.
64. Noth R, Stüber E, Häslér R, Nikolaus S, Kühbacher T, Hampe J, et al. Anti-TNF- α antibodies improve intestinal barrier function in Crohn's disease. *J Crohns Colitis.* 2012;6(4):464-9.
65. Desai A, Zator ZA, de Silva P, Nguyen DD, Korzenik J, Yajnik V, et al. Older age is associated with higher rate of discontinuation of anti-TNF therapy in patients with inflammatory bowel disease. *Inflamm Bowel Dis.* 2013;19(2):309-15.
66. Colombel JF, Loftus EV, Jr., Tremaine WJ, Egan LJ, Harmsen WS, Schleck CD, et al. The safety profile of infliximab in patients with Crohn's disease: the Mayo clinic experience in 500 patients. *Gastroenterology.* 2004;126(1):19-31.
67. Asscher VER, van der Vliet Q, van der Aalst K, van der Aalst A, Brand EC, van der Meulen-de Jong AE, et al. Anti-tumor necrosis factor therapy in patients with inflammatory bowel disease; comorbidity, not patient age, is a predictor of severe adverse events. *Int J Colorectal Dis.* 2020;35(12):2331-8.

68. Van Spaendonk H, Ceuleers H, Witters L, Patteet E, Joossens J, Augustyns K, et al. Regulation of intestinal permeability: The role of proteases. *World J Gastroenterol.* 2017;23(12):2106-23.
69. Biancheri P, Di Sabatino A, Corazza GR, MacDonald TT. Proteases and the gut barrier. *Cell Tissue Res.* 2013;351(2):269-80.
70. Caminero A, Guzman M, Libertucci J, Lomax AE. The emerging roles of bacterial proteases in intestinal diseases. *Gut Microbes.* 2023;15(1):2181922.
71. López-Otín C, Bond JS. Proteases: multifunctional enzymes in life and disease. *J Biol Chem.* 2008;283(45):30433-7.
72. Kleiner DE, Stetler-Stevenson WG. Matrix metalloproteinases and metastasis. *Cancer Chemother Pharmacol.* 1999;43 Suppl:S42-51.
73. Marônek M, Marafini I, Gardlík R, Link R, Troncone E, Monteleone G. Metalloproteinases in Inflammatory Bowel Diseases. *J Inflamm Res.* 2021;14:1029-41.
74. Jablaoui A, Kriaa A, Mkaouar H, Akermi N, Soussou S, Wysocka M, et al. Fecal Serine Protease Profiling in Inflammatory Bowel Diseases. *Front Cell Infect Microbiol.* 2020;10:21.
75. Denadai-Souza A, Bonnart C, Tapias NS, Marcellin M, Gilmore B, Alric L, et al. Functional Proteomic Profiling of Secreted Serine Proteases in Health and Inflammatory Bowel Disease. *Sci Rep.* 2018;8(1):7834.
76. Edogawa S, Edwinston AL, Peters SA, Chikkamenahalli LL, Sundt W, Graves S, et al. Serine proteases as luminal mediators of intestinal barrier dysfunction and symptom severity in IBS. *Gut.* 2020;69(1):62-73.
77. Johansson ME, Gustafsson JK, Holmén-Larsson J, Jabbar KS, Xia L, Xu H, et al. Bacteria penetrate the normally impenetrable inner colon mucus layer in both murine colitis models and patients with ulcerative colitis. *Gut.* 2014;63(2):281-91.
78. Eichele DD, Kharbanda KK. Dextran sodium sulfate colitis murine model: An indispensable tool for advancing our understanding of inflammatory bowel diseases pathogenesis. *World J Gastroenterol.* 2017;23(33):6016-29.
79. Schultz C, Van Den Berg FM, Ten Kate FW, Tytgat GN, Dankert J. The intestinal mucus layer from patients with inflammatory bowel disease harbors high numbers of bacteria compared with controls. *Gastroenterology.* 1999;117(5):1089-97.
80. Zolotarevsky Y, Hecht G, Koutsouris A, Gonzalez DE, Quan C, Tom J, et al. A membrane-permeant peptide that inhibits MLC kinase restores barrier function in in vitro models of intestinal disease. *Gastroenterology.* 2002;123(1):163-72.
81. de Waal GM, de Villiers WJS, Pretorius E. The Link Between Bacterial Inflammagens, Leaky Gut Syndrome and Colorectal Cancer. *Curr Med Chem.* 2021;28(41):8534-48.
82. Chakaroun RM, Massier L, Kovacs P. Gut Microbiome, Intestinal Permeability, and Tissue Bacteria in Metabolic Disease: Perpetrators or Bystanders? *Nutrients.* 2020;12(4).
83. Stolfi C, Maresca C, Monteleone G, Laudisi F. Implication of Intestinal Barrier Dysfunction in Gut Dysbiosis and Diseases. *Biomedicines.* 2022;10(2).
84. Sung H, Ferlay J, Siegel RL, Laversanne M, Soerjomataram I, Jemal A, et al. Global Cancer Statistics 2020: GLOBOCAN Estimates of Incidence and Mortality Worldwide for 36 Cancers in 185 Countries. *CA Cancer J Clin.* 2021;71(3):209-49.
85. Shin A, Cho S, Sandin S, Lof M, Oh MY, Weiderpass E. Omega-3 and -6 Fatty Acid Intake and Colorectal Cancer Risk in Swedish Women's Lifestyle and Health Cohort. *Cancer Res Treat.* 2020;52(3):848-54.
86. Hanson S, Thorpe G, Winstanley L, Abdelhamid AS, Hooper L. Omega-3, omega-6 and total dietary polyunsaturated fat on cancer incidence: systematic review and meta-analysis of randomised trials. *Br J Cancer.* 2020;122(8):1260-70.
87. Song M, Chan AT, Fuchs CS, Ogino S, Hu FB, Mozaffarian D, et al. Dietary intake of fish, ω -3 and ω -6 fatty acids and risk of colorectal cancer: A prospective study in U.S. men and women. *Int J Cancer.* 2014;135(10):2413-23.

88. Tojjari A, Choucair K, Sadeghipour A, Saeed A, Saeed A. Anti-Inflammatory and Immune Properties of Polyunsaturated Fatty Acids (PUFAs) and Their Impact on Colorectal Cancer (CRC) Prevention and Treatment. *Cancers (Basel)*. 2023;15(17).
89. D'Angelo S, Motti ML, Meccariello R. ω -3 and ω -6 Polyunsaturated Fatty Acids, Obesity and Cancer. *Nutrients*. 2020;12(9).
90. Simopoulos AP. The importance of the ratio of omega-6/omega-3 essential fatty acids. *Biomed Pharmacother*. 2002;56(8):365-79.
91. Gabbs M, Leng S, Devassy JG, Monirujjaman M, Aukema HM. Advances in Our Understanding of Oxylipins Derived from Dietary PUFAs. *Adv Nutr*. 2015;6(5):513-40.
92. Scher JU, Pillinger MH. The anti-inflammatory effects of prostaglandins. *J Investig Med*. 2009;57(6):703-8.
93. Ricciotti E, FitzGerald GA. Prostaglandins and inflammation. *Arterioscler Thromb Vasc Biol*. 2011;31(5):986-1000.
94. Investigators IBDiES, Tjonneland A, Overvad K, Bergmann MM, Nagel G, Linseisen J, et al. Linoleic acid, a dietary n-6 polyunsaturated fatty acid, and the aetiology of ulcerative colitis: a nested case-control study within a European prospective cohort study. *Gut*. 2009;58(12):1606-11.
95. Lu Y, Li D, Wang L, Zhang H, Jiang F, Zhang R, et al. Comprehensive Investigation on Associations between Dietary Intake and Blood Levels of Fatty Acids and Colorectal Cancer Risk. *Nutrients*. 2023;15(3).
96. Hudert CA, Weylandt KH, Lu Y, Wang J, Hong S, Dignass A, et al. Transgenic mice rich in endogenous omega-3 fatty acids are protected from colitis. *Proc Natl Acad Sci U S A*. 2006;103(30):11276-81.
97. Whelan J, McEntee MF. Dietary (n-6) PUFA and intestinal tumorigenesis. *J Nutr*. 2004;134(12 Suppl):3421S-6S.
98. Nowak J, Weylandt KH, Habbel P, Wang J, Dignass A, Glickman JN, et al. Colitis-associated colon tumorigenesis is suppressed in transgenic mice rich in endogenous n-3 fatty acids. *Carcinogenesis*. 2007;28(9):1991-5.
99. Rohwer N, Kuhl AA, Ostermann AI, Hartung NM, Schebb NH, Zopf D, et al. Effects of chronic low-dose aspirin treatment on tumor prevention in three mouse models of intestinal tumorigenesis. *Cancer Med*. 2020;9(7):2535-50.
100. Figueiredo JC, Jacobs EJ, Newton CC, Guinter MA, Cance WG, Campbell PT. Associations of Aspirin and Non-Aspirin Non-Steroidal Anti-Inflammatory Drugs With Colorectal Cancer Mortality After Diagnosis. *J Natl Cancer Inst*. 2021;113(7):833-40.
101. Coleman RA, Smith WL, Narumiya S. International Union of Pharmacology classification of prostanoid receptors: properties, distribution, and structure of the receptors and their subtypes. *Pharmacol Rev*. 1994;46(2):205-29.
102. Wang D, DuBois RN. An inflammatory mediator, prostaglandin E2, in colorectal cancer. *Cancer J*. 2013;19(6):502-10.
103. Finetti F, Travelli C, Ercoli J, Colombo G, Buoso E, Trabalzini L. Prostaglandin E2 and Cancer: Insight into Tumor Progression and Immunity. *Biology (Basel)*. 2020;9(12).
104. Rigas B, Goldman IS, Levine L. Altered eicosanoid levels in human colon cancer. *J Lab Clin Med*. 1993;122(5):518-23.
105. Konya V, Marsche G, Schuligoi R, Heinemann A. E-type prostanoid receptor 4 (EP4) in disease and therapy. *Pharmacol Ther*. 2013;138(3):485-502.
106. Yang L, Huang Y, Porta R, Yanagisawa K, Gonzalez A, Segi E, et al. Host and direct antitumor effects and profound reduction in tumor metastasis with selective EP4 receptor antagonism. *Cancer Res*. 2006;66(19):9665-72.
107. Mutoh M, Watanabe K, Kitamura T, Shoji Y, Takahashi M, Kawamori T, et al. Involvement of prostaglandin E receptor subtype EP(4) in colon carcinogenesis. *Cancer Res*. 2002;62(1):28-32.

108. Rodríguez-Lagunas MJ, Martín-Venegas R, Moreno JJ, Ferrer R. PGE2 promotes Ca²⁺-mediated epithelial barrier disruption through EP1 and EP4 receptors in Caco-2 cell monolayers. *Am J Physiol Cell Physiol*. 2010;299(2):C324-34.
109. Tanaka MN, Diaz BL, de Souza W, Morgado-Diaz JA. Prostaglandin E2-EP1 and EP2 receptor signaling promotes apical junctional complex disassembly of Caco-2 human colorectal cancer cells. *BMC Cell Biol*. 2008;9:63.
110. Zhang Y, Daaka Y. PGE2 promotes angiogenesis through EP4 and PKA Cy pathway. *Blood*. 2011;118(19):5355-64.
111. Günzel D, Yu AS. Claudins and the modulation of tight junction permeability. *Physiol Rev*. 2013;93(2):525-69.
112. Spiering D, Hodgson L. Dynamics of the Rho-family small GTPases in actin regulation and motility. *Cell Adh Migr*. 2011;5(2):170-80.
113. Boutaud O, Sosa IR, Amin T, Oram D, Adler D, Hwang HS, et al. Inhibition of the Biosynthesis of Prostaglandin E2 By Low-Dose Aspirin: Implications for Adenocarcinoma Metastasis. *Cancer Prev Res (Phila)*. 2016;9(11):855-65.
114. Vane JR, Botting RM. The mechanism of action of aspirin. *Thromb Res*. 2003;110(5-6):255-8.
115. Drew DA, Schuck MM, Magicheva-Gupta MV, Stewart KO, Gilpin KK, Miller P, et al. Effect of Low-dose and Standard-dose Aspirin on PGE(2) Biosynthesis Among Individuals with Colorectal Adenomas: A Randomized Clinical Trial. *Cancer Prev Res (Phila)*. 2020;13(10):877-88.
116. Chan AT, Giovannucci EL, Meyerhardt JA, Schernhammer ES, Curhan GC, Fuchs CS. Long-term use of aspirin and nonsteroidal anti-inflammatory drugs and risk of colorectal cancer. *Jama*. 2005;294(8):914-23.
117. Rothwell PM, Fowkes FG, Belch JF, Ogawa H, Warlow CP, Meade TW. Effect of daily aspirin on long-term risk of death due to cancer: analysis of individual patient data from randomised trials. *Lancet*. 2011;377(9759):31-41.
118. Schreinemachers DM, Everson RB. Aspirin use and lung, colon, and breast cancer incidence in a prospective study. *Epidemiology*. 1994;5(2):138-46.
119. Dubé C, Rostom A, Lewin G, Tsertsvadze A, Barrowman N, Code C, et al. The use of aspirin for primary prevention of colorectal cancer: a systematic review prepared for the U.S. Preventive Services Task Force. *Ann Intern Med*. 2007;146(5):365-75.
120. Logan RF, Grainge MJ, Shepherd VC, Armitage NC, Muir KR. Aspirin and folic acid for the prevention of recurrent colorectal adenomas. *Gastroenterology*. 2008;134(1):29-38.
121. Baron JA, Cole BF, Sandler RS, Haile RW, Ahnen D, Bresalier R, et al. A randomized trial of aspirin to prevent colorectal adenomas. *N Engl J Med*. 2003;348(10):891-9.
122. Sandler RS, Halabi S, Baron JA, Budinger S, Paskett E, Keresztes R, et al. A randomized trial of aspirin to prevent colorectal adenomas in patients with previous colorectal cancer. *N Engl J Med*. 2003;348(10):883-90.
123. Benamouzig R, Deyra J, Martin A, Girard B, Jullian E, Piednoir B, et al. Daily soluble aspirin and prevention of colorectal adenoma recurrence: one-year results of the APACC trial. *Gastroenterology*. 2003;125(2):328-36.
124. Huang ES, Strate LL, Ho WW, Lee SS, Chan AT. Long-term use of aspirin and the risk of gastrointestinal bleeding. *Am J Med*. 2011;124(5):426-33.
125. Cloud GC, Williamson JD, Thao LTP, Tran C, Eaton CB, Wolfe R, et al. Low-Dose Aspirin and the Risk of Stroke and Intracerebral Bleeding in Healthy Older People: Secondary Analysis of a Randomized Clinical Trial. *JAMA Netw Open*. 2023;6(7):e2325803.
126. Jourdan PM, Lamberton PHL, Fenwick A, Addiss DG. Soil-transmitted helminth infections. *Lancet*. 2018;391(10117):252-65.
127. Barry MA, Simon GG, Mistry N, Hotez PJ. Global trends in neglected tropical disease control and elimination: impact on child health. *Arch Dis Child*. 2013;98(8):635-41.

128. Bethony J, Brooker S, Albonico M, Geiger SM, Loukas A, Diemert D, et al. Soil-transmitted helminth infections: ascariasis, trichuriasis, and hookworm. *Lancet*. 2006;367(9521):1521-32.
129. Sartorius B, Cano J, Simpson H, Tusting LS, Marczak LB, Miller-Petrie MK, et al. Prevalence and intensity of soil-transmitted helminth infections of children in sub-Saharan Africa, 2000-18: a geospatial analysis. *Lancet Glob Health*. 2021;9(1):e52-e60.
130. Pullan RL, Smith JL, Jasrasaria R, Brooker SJ. Global numbers of infection and disease burden of soil transmitted helminth infections in 2010. *Parasit Vectors*. 2014;7:37.
131. Murray CJ, Acharya AK. Understanding DALYs (disability-adjusted life years). *J Health Econ*. 1997;16(6):703-30.
132. Tian X, Chen J, Wang X, Xie Y, Zhang X, Han D, et al. Global, regional, and national HIV/AIDS disease burden levels and trends in 1990-2019: A systematic analysis for the global burden of disease 2019 study. *Front Public Health*. 2023;11:1068664.
133. Shi D, Wei L, Liang H, Yan D, Zhang J, Wang Z. Trends of the Global, Regional and National Incidence, Mortality, and Disability-Adjusted Life Years of Malaria, 1990-2019: An Analysis of the Global Burden of Disease Study 2019. *Risk Manag Healthc Policy*. 2023;16:1187-201.
134. Holland CV. The long and winding road of *Ascaris* larval migration: the role of mouse models. *Parasitology*. 2021;148(14):1-9.
135. Brooker S, Bethony J, Hotez PJ. Human hookworm infection in the 21st century. *Adv Parasitol*. 2004;58:197-288.
136. Khurana S, Sethi S. Laboratory diagnosis of soil transmitted helminthiasis. *Trop Parasitol*. 2017;7(2):86-91.
137. O'Connell EM, Nutman TB. Molecular Diagnostics for Soil-Transmitted Helminths. *Am J Trop Med Hyg*. 2016;95(3):508-13.
138. Chai JY, Jung BK, Hong SJ. Albendazole and Mebendazole as Anti-Parasitic and Anti-Cancer Agents: an Update. *Korean J Parasitol*. 2021;59(3):189-225.
139. Moser W, Schindler C, Keiser J. Efficacy of recommended drugs against soil transmitted helminths: systematic review and network meta-analysis. *Bmj*. 2017;358:j4307.
140. Krücken J, Fraundorfer K, Mugisha JC, Ramünke S, Sift KC, Geus D, et al. Reduced efficacy of albendazole against *Ascaris lumbricoides* in Rwandan schoolchildren. *Int J Parasitol Drugs Drug Resist*. 2017;7(3):262-71.
141. Diemert DJ, Zumer M, Campbell D, Grahek S, Li G, Peng J, et al. Safety and immunogenicity of the Na-APR-1 hookworm vaccine in infection-naïve adults. *Vaccine*. 2022;40(42):6084-92.
142. Behnke JM, Menge DM, Noyes H. *Heligmosomoides bakeri*: a model for exploring the biology and genetics of resistance to chronic gastrointestinal nematode infections. *Parasitology*. 2009;136(12):1565-80.
143. Filbey KJ, Grainger JR, Smith KA, Boon L, van Rooijen N, Harcus Y, et al. Innate and adaptive type 2 immune cell responses in genetically controlled resistance to intestinal helminth infection. *Immunol Cell Biol*. 2014;92(5):436-48.
144. Maizels RM, Hewitson JP, Murray J, Harcus YM, Dayer B, Filbey KJ, et al. Immune modulation and modulators in *Heligmosomoides polygyrus* infection. *Exp Parasitol*. 2012;132(1):76-89.
145. Hewitson JP, Harcus Y, Murray J, van Agtmaal M, Filbey KJ, Grainger JR, et al. Proteomic analysis of secretory products from the model gastrointestinal nematode *Heligmosomoides polygyrus* reveals dominance of venom allergen-like (VAL) proteins. *J Proteomics*. 2011;74(9):1573-94.
146. Grainger JR, Smith KA, Hewitson JP, McSorley HJ, Harcus Y, Filbey KJ, et al. Helminth secretions induce de novo T cell Foxp3 expression and regulatory function through the TGF- β pathway. *J Exp Med*. 2010;207(11):2331-41.
147. Osbourn M, Soares DC, Vacca F, Cohen ES, Scott IC, Gregory WF, et al. HpARI Protein Secreted by a Helminth Parasite Suppresses Interleukin-33. *Immunity*. 2017;47(4):739-51.e5.

148. de Martel C, Ferlay J, Franceschi S, Vignat J, Bray F, Forman D, et al. Global burden of cancers attributable to infections in 2008: a review and synthetic analysis. *Lancet Oncol.* 2012;13(6):607-15.
149. Madbouly KM, Senagore AJ, Mukerjee A, Hussien AM, Shehata MA, Navine P, et al. Colorectal cancer in a population with endemic *Schistosoma mansoni*: is this an at-risk population? *Int J Colorectal Dis.* 2007;22(2):175-81.
150. Hayes KS, Cliffe LJ, Bancroft AJ, Forman SP, Thompson S, Booth C, et al. Chronic *Trichuris muris* infection causes neoplastic change in the intestine and exacerbates tumour formation in APC min/+ mice. *PLoS Negl Trop Dis.* 2017;11(6):e0005708.
151. Pastille E, Frede A, McSorley HJ, Grab J, Adamczyk A, Kollenda S, et al. Intestinal helminth infection drives carcinogenesis in colitis-associated colon cancer. *PLoS Pathog.* 2017;13(9):e1006649.
152. Katsidzira L, Gangaidzo IT, Makunike-Mutasa R, Manyanga T, Matsena-Zingoni Z, Thomson S, et al. A case-control study of risk factors for colorectal cancer in an African population. *Eur J Cancer Prev.* 2019;28(3):145-50.
153. Elliott DE, Li J, Blum A, Metwali A, Qadir K, Urban JF, Jr., et al. Exposure to schistosome eggs protects mice from TNBS-induced colitis. *Am J Physiol Gastrointest Liver Physiol.* 2003;284(3):G385-91.
154. Varyani F, Fleming JO, Maizels RM. Helminths in the gastrointestinal tract as modulators of immunity and pathology. *Am J Physiol Gastrointest Liver Physiol.* 2017;312(6):G537-g49.
155. Khan WI, Blennerhasset PA, Varghese AK, Chowdhury SK, Omsted P, Deng Y, et al. Intestinal nematode infection ameliorates experimental colitis in mice. *Infect Immun.* 2002;70(11):5931-7.
156. Heylen M, Ruysers NE, Gielis EM, Vanhomwegen E, Pelckmans PA, Moreels TG, et al. Of worms, mice and man: an overview of experimental and clinical helminth-based therapy for inflammatory bowel disease. *Pharmacol Ther.* 2014;143(2):153-67.
157. Chu KM, Watermeyer G, Shelly L, Janssen J, May TD, Brink K, et al. Childhood helminth exposure is protective against inflammatory bowel disease: a case control study in South Africa. *Inflamm Bowel Dis.* 2013;19(3):614-20.
158. Parang B, Barrett CW, Williams CS. AOM/DSS Model of Colitis-Associated Cancer. *Methods Mol Biol.* 2016;1422:297-307.
159. Sohn OS, Fiala ES, Requeijo SP, Weisburger JH, Gonzalez FJ. Differential effects of CYP2E1 status on the metabolic activation of the colon carcinogens azoxymethane and methylazoxymethanol. *Cancer Res.* 2001;61(23):8435-40.
160. Okayasu I, Hatakeyama S, Yamada M, Ohkusa T, Inagaki Y, Nakaya R. A novel method in the induction of reliable experimental acute and chronic ulcerative colitis in mice. *Gastroenterology.* 1990;98(3):694-702.
161. Waldner MJ, Foersch S, Neurath MF. Interleukin-6--a key regulator of colorectal cancer development. *Int J Biol Sci.* 2012;8(9):1248-53.
162. McDermott JR, Bartram RE, Knight PA, Miller HR, Garrod DR, Grecis RK. Mast cells disrupt epithelial barrier function during enteric nematode infection. *Proc Natl Acad Sci U S A.* 2003;100(13):7761-6.
163. Hyoh Y, Nishida M, Tegoshi T, Yamada M, Uchikawa R, Matsuda S, et al. Enhancement of apoptosis with loss of cellular adherence in the villus epithelium of the small intestine after infection with the nematode *Nippostrongylus brasiliensis* in rats. *Parasitology.* 1999;119 (Pt 2):199-207.
164. Shea-Donohue T, Sullivan C, Finkelman FD, Madden KB, Morris SC, Goldhill J, et al. The role of IL-4 in *Heligmosomoides polygyrus*-induced alterations in murine intestinal epithelial cell function. *J Immunol.* 2001;167(4):2234-9.

165. Su CW, Cao Y, Kaplan J, Zhang M, Li W, Conroy M, et al. Duodenal helminth infection alters barrier function of the colonic epithelium via adaptive immune activation. *Infect Immun*. 2011;79(6):2285-94.
166. Kanai T, Watanabe M, Hayashi A, Nakazawa A, Yajima T, Okazawa A, et al. Regulatory effect of interleukin-4 and interleukin-13 on colon cancer cell adhesion. *Br J Cancer*. 2000;82(10):1717-23.
167. Fujii-Maeda S, Kajiwara K, Ikizawa K, Shinazawa M, Yu B, Koga T, et al. Reciprocal regulation of thymus and activation-regulated chemokine/macrophage-derived chemokine production by interleukin (IL)-4/IL-13 and interferon-gamma in HaCaT keratinocytes is mediated by alternations in E-cadherin distribution. *J Invest Dermatol*. 2004;122(1):20-8.
168. Hasnain SZ, McGuckin MA, Grecis RK, Thornton DJ. Serine protease(s) secreted by the nematode *Trichuris muris* degrade the mucus barrier. *PLoS Negl Trop Dis*. 2012;6(10):e1856.
169. Song YY, Zhang XZ, Wang BN, Cheng YK, Guo X, Zhang X, et al. A novel *Trichinella spiralis* serine proteinase disrupted gut epithelial barrier and mediated larval invasion through binding to RACK1 and activating MAPK/ERK1/2 pathway. *PLoS Negl Trop Dis*. 2024;18(1):e0011872.
170. Hiemstra IH, Klaver EJ, Vrijland K, Kringel H, Andreasen A, Bouma G, et al. Excreted/secreted *Trichuris suis* products reduce barrier function and suppress inflammatory cytokine production of intestinal epithelial cells. *Mol Immunol*. 2014;60(1):1-7.
171. Sorobetea D, Holm JB, Henningson H, Kristiansen K, Svensson-Frej M. Acute infection with the intestinal parasite *Trichuris muris* has long-term consequences on mucosal mast cell homeostasis and epithelial integrity. *Eur J Immunol*. 2017;47(2):257-68.
172. Lawrence CE, Paterson YY, Wright SH, Knight PA, Miller HR. Mouse mast cell protease-1 is required for the enteropathy induced by gastrointestinal helminth infection in the mouse. *Gastroenterology*. 2004;127(1):155-65.
173. Hepworth MR, Danitowicz-Luebert E, Rausch S, Metz M, Klotz C, Maurer M, et al. Mast cells orchestrate type 2 immunity to helminths through regulation of tissue-derived cytokines. *Proc Natl Acad Sci U S A*. 2012;109(17):6644-9.
174. Yasuda K, Nakanishi K. Host responses to intestinal nematodes. *Int Immunol*. 2018;30(3):93-102.
175. Kamal M, Dehlawi MS, Brunet LR, Wakelin D. Paneth and intermediate cell hyperplasia induced in mice by helminth infections. *Parasitology*. 2002;125(Pt 3):275-81.
176. Sharpe C, Thornton DJ, Grecis RK. A sticky end for gastrointestinal helminths; the role of the mucus barrier. *Parasite Immunol*. 2018;40(4):e12517.
177. Nusse YM, Savage AK, Marangoni P, Rosendahl-Huber AKM, Landman TA, de Sauvage FJ, et al. Parasitic helminths induce fetal-like reversion in the intestinal stem cell niche. *Nature*. 2018;559(7712):109-13.
178. Sato T, van Es JH, Snippert HJ, Stange DE, Vries RG, van den Born M, et al. Paneth cells constitute the niche for Lgr5 stem cells in intestinal crypts. *Nature*. 2011;469(7330):415-8.
179. Drurey C, Lindholm HT, Coakley G, Poveda MC, Loser S, Doolan R, et al. Intestinal epithelial tuft cell induction is negated by a murine helminth and its secreted products. *J Exp Med*. 2022;219(1).
180. Yang Q, Bermingham NA, Finegold MJ, Zoghbi HY. Requirement of Math1 for secretory cell lineage commitment in the mouse intestine. *Science*. 2001;294(5549):2155-8.
181. Jenny M, Uhl C, Roche C, Duluc I, Guillermin V, Guillemot F, et al. Neurogenin3 is differentially required for endocrine cell fate specification in the intestinal and gastric epithelium. *Embo j*. 2002;21(23):6338-47.
182. Jensen J, Pedersen EE, Galante P, Hald J, Heller RS, Ishibashi M, et al. Control of endodermal endocrine development by Hes-1. *Nat Genet*. 2000;24(1):36-44.
183. Karo-Atar D, Ouladan S, Javkar T, Joumier L, Matheson MK, Merritt S, et al. Helminth-induced reprogramming of the stem cell compartment inhibits type 2 immunity. *J Exp Med*. 2022;219(9).

184. Vasquez EG, Nasreddin N, Valbuena GN, Mulholland EJ, Belnoue-Davis HL, Eggington HR, et al. Dynamic and adaptive cancer stem cell population admixture in colorectal neoplasia. *Cell Stem Cell*. 2022;29(8):1213-28.e8.
185. Krotenberg Garcia A, Fumagalli A, Le HQ, Jackstadt R, Lannagan TRM, Sansom OJ, et al. Active elimination of intestinal cells drives oncogenic growth in organoids. *Cell Rep*. 2021;36(1):109307.
186. Upadhyay G. Emerging Role of Lymphocyte Antigen-6 Family of Genes in Cancer and Immune Cells. *Front Immunol*. 2019;10:819.
187. Lin B, Coleman JH, Peterson JN, Zunitch MJ, Jang W, Herrick DB, et al. Injury Induces Endogenous Reprogramming and Dedifferentiation of Neuronal Progenitors to Multipotency. *Cell Stem Cell*. 2017;21(6):761-74.e5.
188. Henkel FDR, Friedl A, Haid M, Thomas D, Bouchery T, Haimerl P, et al. House dust mite drives proinflammatory eicosanoid reprogramming and macrophage effector functions. *Allergy*. 2019;74(6):1090-101.
189. de Los Reyes Jimenez M, Lechner A, Alessandrini F, Bohnacker S, Schindela S, Trompette A, et al. An anti-inflammatory eicosanoid switch mediates the suppression of type-2 inflammation by helminth larval products. *Sci Transl Med*. 2020;12(540).
190. Katherine A Smith EKR, Victoria J Tyrrell, Claire Butters, Matthew G Darby, Brunette Katsandegwaza, Alisha Chetty, William GC Horsnell, Valerie B O'Donnell, Awen Gallimore. Helminth-induced prostaglandin signalling and dietary shifts in PUFA metabolism promote colitis-associated cancer. *Journal of Lipid Research*. 2025.
191. Oyesola OO, Tait Wojno ED. Prostaglandin regulation of type 2 inflammation: From basic biology to therapeutic interventions. *Eur J Immunol*. 2021;51(10):2399-416.
192. Salafsky B, Fusco AC. *Schistosoma mansoni*: a comparison of secreted vs nonsecreted eicosanoids in developing schistosomulae and adults. *Exp Parasitol*. 1987;64(3):361-7.
193. Brattig NW, Schwohl A, Rickert R, Büttner DW. The filarial parasite *Onchocerca volvulus* generates the lipid mediator prostaglandin E(2). *Microbes Infect*. 2006;8(3):873-9.
194. Laan LC, Williams AR, Stavenhagen K, Giera M, Kooij G, Vlasakov I, et al. The whipworm (*Trichuris suis*) secretes prostaglandin E2 to suppress proinflammatory properties in human dendritic cells. *Faseb j*. 2017;31(2):719-31.
195. Ramaswamy K, Kumar P, He YX. A role for parasite-induced PGE2 in IL-10-mediated host immunoregulation by skin stage schistosomula of *Schistosoma mansoni*. *J Immunol*. 2000;165(8):4567-74.
196. Giera M, Kaisar MMM, Derks RJE, Steenvoorden E, Kruize YCM, Hokke CH, et al. The *Schistosoma mansoni* lipidome: Leads for immunomodulation. *Anal Chim Acta*. 2018;1037:107-18.
197. Liu LX, Buhlmann JE, Weller PF. Release of prostaglandin E2 by microfilariae of *Wuchereria bancrofti* and *Brugia malayi*. *Am J Trop Med Hyg*. 1992;46(5):520-3.
198. Liu LX, Weller PF. Intravascular filarial parasites inhibit platelet aggregation. Role of parasite-derived prostanoids. *J Clin Invest*. 1992;89(4):1113-20.
199. Parks SC, Okakpu OK, Azizpor P, Nguyen S, Martinez-Beltran S, Claudio I, et al. Parasitic nematode secreted phospholipase A(2) suppresses cellular and humoral immunity by targeting hemocytes in *Drosophila melanogaster*. *Front Immunol*. 2023;14:1122451.
200. Lu D, Macchietto M, Chang D, Barros MM, Baldwin J, Mortazavi A, et al. Activated entomopathogenic nematode infective juveniles release lethal venom proteins. *PLoS Pathog*. 2017;13(4):e1006302.
201. Wu Y, Li Y, Shang M, Jian Y, Wang C, Bardeesi AS, et al. Secreted phospholipase A2 of *Clonorchis sinensis* activates hepatic stellate cells through a pathway involving JNK signalling. *Parasit Vectors*. 2017;10(1):147.

202. Sheppe AEF, Edelmann MJ. Roles of Eicosanoids in Regulating Inflammation and Neutrophil Migration as an Innate Host Response to Bacterial Infections. *Infect Immun*. 2021;89(8):e0009521.
203. Prodjinotho UF, Gres V, Henkel F, Lacorcia M, Dandl R, Haslbeck M, et al. Helminthic dehydrogenase drives PGE(2) and IL-10 production in monocytes to potentiate Treg induction. *EMBO Rep*. 2022;23(5):e54096.
204. Franks LM, Hemmings VJ. A cell line from an induced carcinoma of mouse rectum. *J Pathol*. 1978;124(1):35-8.
205. Kennel KB, Burmeister J, Radhakrishnan P, Giese NA, Giese T, Salfenmoser M, et al. The HIF-prolyl hydroxylases have distinct and nonredundant roles in colitis-associated cancer. *JCI Insight*. 2022;7(22).
206. Zhu L, Andersen-Civil AIS, Myhill LJ, Thamsborg SM, Kot W, Krych L, et al. The phytonutrient cinnamaldehyde limits intestinal inflammation and enteric parasite infection. *J Nutr Biochem*. 2022;100:108887.
207. Geraghty RJ, Capes-Davis A, Davis JM, Downward J, Freshney RI, Knezevic I, et al. Guidelines for the use of cell lines in biomedical research. *Br J Cancer*. 2014;111(6):1021-46.
208. Li BR, Wu J, Li HS, Jiang ZH, Zhou XM, Xu CH, et al. In Vitro and In Vivo Approaches to Determine Intestinal Epithelial Cell Permeability. *J Vis Exp*. 2018(140).
209. Mahmood T, Yang PC. Western blot: technique, theory, and trouble shooting. *N Am J Med Sci*. 2012;4(9):429-34.
210. Schneider CA, Rasband WS, Eliceiri KW. NIH Image to ImageJ: 25 years of image analysis. *Nat Methods*. 2012;9(7):671-5.
211. Harcus Y, Nicoll G, Murray J, Filbey K, Gomez-Escobar N, Maizels RM. C-type lectins from the nematode parasites *Heligmosomoides polygyrus* and *Nippostrongylus brasiliensis*. *Parasitol Int*. 2009;58(4):461-70.
212. Ye J, Coulouris G, Zaretskaya I, Cutcutache I, Rozen S, Madden TL. Primer-BLAST: a tool to design target-specific primers for polymerase chain reaction. *BMC Bioinformatics*. 2012;13:134.
213. Corpet F. Multiple sequence alignment with hierarchical clustering. *Nucleic Acids Res*. 1988;16(22):10881-90.
214. Stothard P. The sequence manipulation suite: JavaScript programs for analyzing and formatting protein and DNA sequences. *Biotechniques*. 2000;28(6):1102, 4.
215. Gibson DG, Young L, Chuang RY, Venter JC, Hutchison CA, 3rd, Smith HO. Enzymatic assembly of DNA molecules up to several hundred kilobases. *Nat Methods*. 2009;6(5):343-5.
216. Tabor S. Expression using the T7 RNA polymerase/promoter system. *Curr Protoc Mol Biol*. 2001;Chapter 16:Unit16.2.
217. Johnston CJ, Robertson E, Harcus Y, Grainger JR, Coakley G, Smyth DJ, et al. Cultivation of *Heligmosomoides polygyrus*: an immunomodulatory nematode parasite and its secreted products. *J Vis Exp*. 2015(98):e52412.
218. Kolberg L, Raudvere U, Kuzmin I, Adler P, Vilo J, Peterson H. g:Profiler-interoperable web service for functional enrichment analysis and gene identifier mapping (2023 update). *Nucleic Acids Res*. 2023;51(W1):W207-w12.
219. Teufel F, Almagro Armenteros JJ, Johansen AR, Gíslason MH, Pihl SI, Tsirigos KD, et al. SignalP 6.0 predicts all five types of signal peptides using protein language models. *Nat Biotechnol*. 2022;40(7):1023-5.
220. Tanaka T, Kohno H, Suzuki R, Yamada Y, Sugie S, Mori H. A novel inflammation-related mouse colon carcinogenesis model induced by azoxymethane and dextran sodium sulfate. *Cancer Sci*. 2003;94(11):965-73.
221. Busserolles J, Rock E, Gueux E, Mazur A, Grolier P, Rayssiguier Y. Short-term consumption of a high-sucrose diet has a pro-oxidant effect in rats. *Br J Nutr*. 2002;87(4):337-42.

222. O'Brien J, Hayder H, Peng C. Automated Quantification and Analysis of Cell Counting Procedures Using ImageJ Plugins. *J Vis Exp*. 2016(117).
223. Kanehara K, Ohnuma S, Kanazawa Y, Sato K, Kokubo S, Suzuki H, et al. The indole compound MA-35 attenuates tumorigenesis in an inflammation-induced colon cancer model. *Sci Rep*. 2019;9(1):12739.
224. Hopkins EGD, Roumeliotis TI, Mullineaux-Sanders C, Choudhary JS, Frankel G. Intestinal Epithelial Cells and the Microbiome Undergo Swift Reprogramming at the Inception of Colonic *Citrobacter rodentium* Infection. *mBio*. 2019;10(2).
225. Barry R, Ruano-Gallego D, Radhakrishnan ST, Lovell S, Yu L, Kotik O, et al. Faecal neutrophil elastase-antiprotease balance reflects colitis severity. *Mucosal Immunol*. 2020;13(2):322-33.
226. Parkhomchuk D, Borodina T, Amstislavskiy V, Banaru M, Hallen L, Krobitch S, et al. Transcriptome analysis by strand-specific sequencing of complementary DNA. *Nucleic Acids Res*. 2009;37(18):e123.
227. Haque A, Engel J, Teichmann SA, Lönnberg T. A practical guide to single-cell RNA-sequencing for biomedical research and clinical applications. *Genome Med*. 2017;9(1):75.
228. Ewels PA, Peltzer A, Fillinger S, Patel H, Alneberg J, Wilm A, et al. The nf-core framework for community-curated bioinformatics pipelines. *Nat Biotechnol*. 2020;38(3):276-8.
229. S A. FastQC: a quality control tool for high throughput sequence data 2010 [Available from: <http://www.bioinformatics.babraham.ac.uk/projects/fastqc>].
230. Smith T, Heger A, Sudbery I. UMI-tools: modeling sequencing errors in Unique Molecular Identifiers to improve quantification accuracy. *Genome Res*. 2017;27(3):491-9.
231. Felix Krueger FJ, Phil Ewels, Ebrahim Afyounian, Michael Weinstein, Benjamin Schuster-Boeckler, Gert Hulselmans. FelixKrueger/TrimGalore: v0.6.10 - add default decompression path 0.6.10 ed: Zenodo; 2023.
232. Bushnell B. BBSplit 2018 [Available from: <https://github.com/BioInfoTools/BBMap/blob/master/sh/bbsplit.sh>].
233. Kopylova E, Noé L, Touzet H. SortMeRNA: fast and accurate filtering of ribosomal RNAs in metatranscriptomic data. *Bioinformatics*. 2012;28(24):3211-7.
234. Dobin A, Davis CA, Schlesinger F, Drenkow J, Zaleski C, Jha S, et al. STAR: ultrafast universal RNA-seq aligner. *Bioinformatics*. 2013;29(1):15-21.
235. Patro R, Duggal G, Love MI, Irizarry RA, Kingsford C. Salmon provides fast and bias-aware quantification of transcript expression. *Nat Methods*. 2017;14(4):417-9.
236. Li H, Handsaker B, Wysoker A, Fennell T, Ruan J, Homer N, et al. The Sequence Alignment/Map format and SAMtools. *Bioinformatics*. 2009;25(16):2078-9.
237. Picard toolkit Broad institute, GitHub repository Broad Institute 2019 [Available from: <https://broadinstitute.github.io/picard/>].
238. Pertea M, Kim D, Pertea GM, Leek JT, Salzberg SL. Transcript-level expression analysis of RNA-seq experiments with HISAT, StringTie and Ballgown. *Nat Protoc*. 2016;11(9):1650-67.
239. Love MI, Huber W, Anders S. Moderated estimation of fold change and dispersion for RNA-seq data with DESeq2. *Genome Biol*. 2014;15(12):550.
240. Anders S, Huber W. Differential expression analysis for sequence count data. *Genome Biol*. 2010;11(10):R106.
241. Young MD, Wakefield MJ, Smyth GK, Oshlack A. Gene ontology analysis for RNA-seq: accounting for selection bias. *Genome Biol*. 2010;11(2):R14.
242. Gaudet P, Škunca N, Hu JC, Dessimoz C. Primer on the Gene Ontology. *Methods Mol Biol*. 2017;1446:25-37.
243. Liberzon A, Birger C, Thorvaldsdóttir H, Ghandi M, Mesirov JP, Tamayo P. The Molecular Signatures Database (MSigDB) hallmark gene set collection. *Cell Syst*. 2015;1(6):417-25.

244. Györfy B, Lanczky A, Eklund AC, Denkert C, Budczies J, Li Q, et al. An online survival analysis tool to rapidly assess the effect of 22,277 genes on breast cancer prognosis using microarray data of 1,809 patients. *Breast Cancer Res Treat.* 2010;123(3):725-31.
245. Newman AM, Steen CB, Liu CL, Gentles AJ, Chaudhuri AA, Scherer F, et al. Determining cell type abundance and expression from bulk tissues with digital cytometry. *Nat Biotechnol.* 2019;37(7):773-82.
246. Painter MW, Davis S, Hardy RR, Mathis D, Benoist C. Transcriptomes of the B and T lineages compared by multiplatform microarray profiling. *J Immunol.* 2011;186(5):3047-57.
247. Gautier EL, Shay T, Miller J, Greter M, Jakubzick C, Ivanov S, et al. Gene-expression profiles and transcriptional regulatory pathways that underlie the identity and diversity of mouse tissue macrophages. *Nat Immunol.* 2012;13(11):1118-28.
248. Pandey G, Cohain A, Miller J, Merad M. Decoding dendritic cell function through module and network analysis. *J Immunol Methods.* 2013;387(1-2):71-80.
249. Bezman NA, Kim CC, Sun JC, Min-Oo G, Hendricks DW, Kamimura Y, et al. Molecular definition of the identity and activation of natural killer cells. *Nat Immunol.* 2012;13(10):1000-9.
250. Miller JC, Brown BD, Shay T, Gautier EL, Jovic V, Cohain A, et al. Deciphering the transcriptional network of the dendritic cell lineage. *Nat Immunol.* 2012;13(9):888-99.
251. Narayan K, Sylvia KE, Malhotra N, Yin CC, Martens G, Vallerskog T, et al. Intrathymic programming of effector fates in three molecularly distinct $\gamma\delta$ T cell subtypes. *Nat Immunol.* 2012;13(5):511-8.
252. ULC CCG. Molecular Operating Environment (MOE). 910-1010 Sherbrooke St. W., Montreal, QC H3A 2R7, Canada2023.
253. 2023-4 SR. BioLuminate, Schrödinger, LLC, New York, NY2023.
254. Zhou X, Zheng W, Li Y, Pearce R, Zhang C, Bell EW, et al. I-TASSER-MTD: a deep-learning-based platform for multi-domain protein structure and function prediction. *Nat Protoc.* 2022;17(10):2326-53.
255. Korb O, Stütze T, Exner TE. Empirical scoring functions for advanced protein-ligand docking with PLANTS. *J Chem Inf Model.* 2009;49(1):84-96.
256. Software OSSOOS. Santa Fe, NM, USA2023.
257. Daina A, Michielin O, Zoete V. SwissADME: a free web tool to evaluate pharmacokinetics, drug-likeness and medicinal chemistry friendliness of small molecules. *Sci Rep.* 2017;7:42717.
258. Altschul SF, Gish W, Miller W, Myers EW, Lipman DJ. Basic local alignment search tool. *J Mol Biol.* 1990;215(3):403-10.
259. Madeira F, Pearce M, Tivey ARN, Basutkar P, Lee J, Edbali O, et al. Search and sequence analysis tools services from EMBL-EBI in 2022. *Nucleic Acids Res.* 2022;50(W1):W276-w9.
260. UniProt: the Universal Protein Knowledgebase in 2023. *Nucleic Acids Res.* 2023;51(D1):D523-d31.
261. The PyMOL Molecular Graphics System VS, LLC.
262. Thumulari V, Almagro Armenteros JJ, Johansen AR, Nielsen H, Winther O. DeepLoc 2.0: multi-label subcellular localization prediction using protein language models. *Nucleic Acids Res.* 2022;50(W1):W228-w34.
263. Peterson LW, Artis D. Intestinal epithelial cells: regulators of barrier function and immune homeostasis. *Nat Rev Immunol.* 2014;14(3):141-53.
264. Lejeune M, Leung P, Beck PL, Chadee K. Role of EP4 receptor and prostaglandin transporter in prostaglandin E2-induced alteration in colonic epithelial barrier integrity. *Am J Physiol Gastrointest Liver Physiol.* 2010;299(5):G1097-105.
265. Dong Y, Johnson BA, Ruan L, Zeineldin M, Liu AZ, Raychaudhuri S, et al. Disruption of Epithelium Integrity by Inflammation-Associated Fibroblasts through Prostaglandin Signaling: IAFs disrupt colon epithelium via PGE2-EP4. *bioRxiv.* 2023.
266. Aoki T, Narumiya S. Prostaglandin E(2)-EP2 signaling as a node of chronic inflammation in the colon tumor microenvironment. *Inflamm Regen.* 2017;37:4.

267. Brouxhon S, Kyrkanides S, O'Banion MK, Johnson R, Pearce DA, Centola GM, et al. Sequential down-regulation of E-cadherin with squamous cell carcinoma progression: loss of E-cadherin via a prostaglandin E2-EP2 dependent posttranslational mechanism. *Cancer Res.* 2007;67(16):7654-64.
268. Watanabe Y, Imanishi Y, Ozawa H, Sakamoto K, Fujii R, Shigetomi S, et al. Selective EP2 and Cox-2 inhibition suppresses cell migration by reversing epithelial-to-mesenchymal transition and Cox-2 overexpression and E-cadherin downregulation are implicated in neck metastasis of hypopharyngeal cancer. *Am J Transl Res.* 2020;12(3):1096-113.
269. Wang D, Dubois RN. Eicosanoids and cancer. *Nat Rev Cancer.* 2010;10(3):181-93.
270. Chang J, Vacher J, Yao B, Fan X, Zhang B, Harris RC, et al. Prostaglandin E receptor 4 (EP4) promotes colonic tumorigenesis. *Oncotarget.* 2015;6(32):33500-11.
271. Shao J, Jung C, Liu C, Sheng H. Prostaglandin E2 Stimulates the beta-catenin/T cell factor-dependent transcription in colon cancer. *J Biol Chem.* 2005;280(28):26565-72.
272. Castellone MD, Teramoto H, Williams BO, Druey KM, Gutkind JS. Prostaglandin E2 promotes colon cancer cell growth through a Gs-axin-beta-catenin signaling axis. *Science.* 2005;310(5753):1504-10.
273. Brudvik KW, Paulsen JE, Aandahl EM, Roald B, Taskén K. Protein kinase A antagonist inhibits β -catenin nuclear translocation, c-Myc and COX-2 expression and tumor promotion in Apc(Min/+) mice. *Mol Cancer.* 2011;10:149.
274. Tanimura Y, Fukui T, Horitani S, Matsumoto Y, Miyamoto S, Suzuki R, et al. Long-term model of colitis-associated colorectal cancer suggests tumor spread mechanism and nature of cancer stem cells. *Oncol Lett.* 2021;21(1):7.
275. Wallace JL. Prostaglandin biology in inflammatory bowel disease. *Gastroenterol Clin North Am.* 2001;30(4):971-80.
276. Montrose DC, Nakanishi M, Murphy RC, Zarini S, McAleer JP, Vella AT, et al. The role of PGE2 in intestinal inflammation and tumorigenesis. *Prostaglandins Other Lipid Mediat.* 2015;116-117:26-36.
277. Walsham NE, Sherwood RA. Fecal calprotectin in inflammatory bowel disease. *Clin Exp Gastroenterol.* 2016;9:21-9.
278. Fukunaga S, Kuwaki K, Mitsuyama K, Takedatsu H, Yoshioka S, Yamasaki H, et al. Detection of calprotectin in inflammatory bowel disease: Fecal and serum levels and immunohistochemical localization. *Int J Mol Med.* 2018;41(1):107-18.
279. Schoepfer AM, Beglinger C, Straumann A, Safroneeva E, Romero Y, Armstrong D, et al. Fecal calprotectin more accurately reflects endoscopic activity of ulcerative colitis than the Lichtiger Index, C-reactive protein, platelets, hemoglobin, and blood leukocytes. *Inflamm Bowel Dis.* 2013;19(2):332-41.
280. Rafique A, Ali I, Kim S, Farooq A, Manzoor U, Moon J, et al. Toll-like receptor 13-mediated signaling protects against the development of colon cancer. *Int J Cancer.* 2024.
281. Mizuno R, Kawada K, Sakai Y. Prostaglandin E2/EP Signaling in the Tumor Microenvironment of Colorectal Cancer. *Int J Mol Sci.* 2019;20(24).
282. Barber RD, Harmer DW, Coleman RA, Clark BJ. GAPDH as a housekeeping gene: analysis of GAPDH mRNA expression in a panel of 72 human tissues. *Physiol Genomics.* 2005;21(3):389-95.
283. Karpishev V, Joshi N, Zekiy AO, Beyzai B, Hojjat-Farsangi M, Namdar A, et al. EP4 receptor as a novel promising therapeutic target in colon cancer. *Pathol Res Pract.* 2020;216(12):153247.
284. He SH. Key role of mast cells and their major secretory products in inflammatory bowel disease. *World J Gastroenterol.* 2004;10(3):309-18.
285. González-Mariscal L, Betanzos A, Nava P, Jaramillo BE. Tight junction proteins. *Prog Biophys Mol Biol.* 2003;81(1):1-44.

286. Iizuka Y, Kuwahara A, Karaki S. Role of PGE2 in the colonic motility: PGE2 generates and enhances spontaneous contractions of longitudinal smooth muscle in the rat colon. *J Physiol Sci*. 2014;64(2):85-96.
287. Chowdhury MK, Montgomery MK, Morris MJ, Cognard E, Shepherd PR, Smith GC. Glucagon phosphorylates serine 552 of β -catenin leading to increased expression of cyclin D1 and c-Myc in the isolated rat liver. *Arch Physiol Biochem*. 2015;121(3):88-96.
288. Sorrenson B, Dissanayake WC, Hu F, Lee KL, Shepherd PR. A role for PAK1 mediated phosphorylation of β -catenin Ser552 in the regulation of insulin secretion. *Biochem J*. 2021;478(8):1605-15.
289. Wu S, Wang S, Zheng S, Verhaak R, Koul D, Yung WK. MSK1-Mediated β -Catenin Phosphorylation Confers Resistance to PI3K/mTOR Inhibitors in Glioblastoma. *Mol Cancer Ther*. 2016;15(7):1656-68.
290. Majumdar T, Sharma S, Kumar M, Hussain MA, Chauhan N, Kalia I, et al. Tryptophan-kynurenine pathway attenuates β -catenin-dependent pro-parasitic role of STING-TICAM2-IRF3-IDO1 signalosome in *Toxoplasma gondii* infection. *Cell Death Dis*. 2019;10(3):161.
291. Yao C, Sakata D, Esaki Y, Li Y, Matsuoka T, Kuroiwa K, et al. Prostaglandin E2-EP4 signaling promotes immune inflammation through Th1 cell differentiation and Th17 cell expansion. *Nat Med*. 2009;15(6):633-40.
292. Lee J, Aoki T, Thumkeo D, Siriwach R, Yao C, Narumiya S. T cell-intrinsic prostaglandin E(2)-EP2/EP4 signaling is critical in pathogenic T(H)17 cell-driven inflammation. *J Allergy Clin Immunol*. 2019;143(2):631-43.
293. Pathirana GW, Chubb SP, Gillett MJ, Vasikaran SD. Faecal Calprotectin. *Clin Biochem Rev*. 2018;39(3):77-90.
294. Tunggal JA, Helfrich I, Schmitz A, Schwarz H, Günzel D, Fromm M, et al. E-cadherin is essential for in vivo epidermal barrier function by regulating tight junctions. *Embo j*. 2005;24(6):1146-56.
295. Loh CY, Chai JY, Tang TF, Wong WF, Sethi G, Shanmugam MK, et al. The E-Cadherin and N-Cadherin Switch in Epithelial-to-Mesenchymal Transition: Signaling, Therapeutic Implications, and Challenges. *Cells*. 2019;8(10).
296. De Robertis M, Massi E, Poeta ML, Carotti S, Morini S, Cecchetelli L, et al. The AOM/DSS murine model for the study of colon carcinogenesis: From pathways to diagnosis and therapy studies. *J Carcinog*. 2011;10:9.
297. Wang M, Zhou B, Cong W, Zhang M, Li Z, Li Y, et al. Amelioration of AOM/DSS-Induced Murine Colitis-Associated Cancer by Evodiamine Intervention is Primarily Associated with Gut Microbiota-Metabolism-Inflammatory Signaling Axis. *Front Pharmacol*. 2021;12:797605.
298. McSorley HJ, O'Gorman MT, Blair N, Sutherland TE, Filbey KJ, Maizels RM. Suppression of type 2 immunity and allergic airway inflammation by secreted products of the helminth *Heligmosomoides polygyrus*. *Eur J Immunol*. 2012;42(10):2667-82.
299. Lejeune M, Moreau F, Chadee K. Prostaglandin E2 produced by *Entamoeba histolytica* signals via EP4 receptor and alters claudin-4 to increase ion permeability of tight junctions. *Am J Pathol*. 2011;179(2):807-18.
300. Ma X, Aoki T, Tsuruyama T, Narumiya S. Definition of Prostaglandin E2-EP2 Signals in the Colon Tumor Microenvironment That Amplify Inflammation and Tumor Growth. *Cancer Res*. 2015;75(14):2822-32.
301. Inai T, Sengoku A, Hirose E, Iida H, Shibata Y. Comparative characterization of mouse rectum CMT93-I and -II cells by expression of claudin isoforms and tight junction morphology and function. *Histochem Cell Biol*. 2008;129(2):223-32.
302. Hewitson JP, Filbey KJ, Grainger JR, Dowle AA, Pearson M, Murray J, et al. *Heligmosomoides polygyrus* elicits a dominant nonprotective antibody response directed against restricted glycan and peptide epitopes. *J Immunol*. 2011;187(9):4764-77.

303. Hoselton S, Piche L, Gustad T, Robinson M. Production of a recombinant version of a *Heligmosomoides polygyrus* antigen that is preferentially recognized by resistant mouse strains. *Parasite Immunol.* 2002;24(8):429-35.
304. McSorley HJ, Grainger JR, Harcus Y, Murray J, Nisbet AJ, Knox DP, et al. daf-7-related TGF-beta homologues from *Trichostrongyloid* nematodes show contrasting life-cycle expression patterns. *Parasitology.* 2010;137(1):159-71.
305. Rzepecka J, Rausch S, Klotz C, Schnöller C, Kornprobst T, Hagen J, et al. Calreticulin from the intestinal nematode *Heligmosomoides polygyrus* is a Th2-skewing protein and interacts with murine scavenger receptor-A. *Mol Immunol.* 2009;46(6):1109-19.
306. de Los Reyes Jiménez M, Lechner A, Alessandrini F, Bohnacker S, Schindela S, Trompette A, et al. An anti-inflammatory eicosanoid switch mediates the suppression of type-2 inflammation by helminth larval products. *Sci Transl Med.* 2020;12(540).
307. Enjoji S, Ohama T, Sato K. Regulation of epithelial cell tight junctions by protease-activated receptor 2. *J Vet Med Sci.* 2014;76(9):1225-9.
308. Pino LK, Rose J, O'Broin A, Shah S, Schilling B. Emerging mass spectrometry-based proteomics methodologies for novel biomedical applications. *Biochem Soc Trans.* 2020;48(5):1953-66.
309. Tilinca M, Florea A. Ultrastructural analysis of early toxic effects produced by bee venom phospholipase A2 and melittin in Sertoli cells in rats. *Toxicol.* 2018;141:94-103.
310. Bouley RA, Hinkovska-Galcheva V, Shayman JA, Tesmer JGG. Structural Basis of Lysosomal Phospholipase A(2) Inhibition by Zn(2). *Biochemistry.* 2019;58(13):1709-17.
311. Caffrey CR, Mathieu MA, Gaffney AM, Salter JP, Sajid M, Lucas KD, et al. Identification of a cDNA encoding an active asparaginyl endopeptidase of *Schistosoma mansoni* and its expression in *Pichia pastoris*. *FEBS Lett.* 2000;466(2-3):244-8.
312. Sajid M, McKerrow JH. Cysteine proteases of parasitic organisms. *Mol Biochem Parasitol.* 2002;120(1):1-21.
313. Meraz-Cruz N, Vadillo-Ortega F, Jiménez-Garduño AM, Ortega A. Thermal stability of human matrix metalloproteinases. *Heliyon.* 2020;6(5):e03865.
314. Hawcroft G, Ko CW, Hull MA. Prostaglandin E2-EP4 receptor signalling promotes tumorigenic behaviour of HT-29 human colorectal cancer cells. *Oncogene.* 2007;26(21):3006-19.
315. Six DA, Dennis EA. The expanding superfamily of phospholipase A(2) enzymes: classification and characterization. *Biochim Biophys Acta.* 2000;1488(1-2):1-19.
316. Connelly MC, Kierszenbaum F. Modulation of macrophage interaction with *Trypanosoma cruzi* by phospholipase A2-sensitive components of the parasite membrane. *Biochem Biophys Res Commun.* 1984;121(3):931-9.
317. Ridgley EL, Ruben L. Phospholipase from *Trypanosoma brucei* releases arachidonic acid by sequential sn-1, sn-2 deacylation of phospholipids. *Mol Biochem Parasitol.* 2001;114(1):29-40.
318. Eintracht J, Maathai R, Mellors A, Ruben L. Calcium entry in *Trypanosoma brucei* is regulated by phospholipase A2 and arachidonic acid. *Biochem J.* 1998;336 (Pt 3)(Pt 3):659-66.
319. Murakami M, Taketomi Y, Girard C, Yamamoto K, Lambeau G. Emerging roles of secreted phospholipase A2 enzymes: Lessons from transgenic and knockout mice. *Biochimie.* 2010;92(6):561-82.
320. Murakami M, Taketomi Y, Sato H, Yamamoto K. Secreted phospholipase A2 revisited. *J Biochem.* 2011;150(3):233-55.
321. Murakami M, Yamamoto K, Miki Y, Murase R, Sato H, Taketomi Y. The Roles of the Secreted Phospholipase A(2) Gene Family in Immunology. *Adv Immunol.* 2016;132:91-134.
322. Bansemir AD, Sukhdeo MV. The food resource of adult *Heligmosomoides polygyrus* in the small intestine. *J Parasitol.* 1994;80(1):24-8.
323. Putz T, Ramoner R, Gander H, Rahm A, Bartsch G, Bernardo K, et al. Bee venom secretory phospholipase A2 and phosphatidylinositol-homologues cooperatively disrupt membrane

integrity, abrogate signal transduction and inhibit proliferation of renal cancer cells. *Cancer Immunol Immunother.* 2007;56(5):627-40.

324. Muñoz NM, Desai A, Meliton LN, Meliton AY, Zhou T, Leff AR, et al. Group V phospholipase A(2) increases pulmonary endothelial permeability through direct hydrolysis of the cell membrane. *Pulm Circ.* 2012;2(2):182-92.

325. Sawai T, Drongowski RA, Lampman RW, Coran AG, Harmon CM. The effect of phospholipids and fatty acids on tight-junction permeability and bacterial translocation. *Pediatr Surg Int.* 2001;17(4):269-74.

326. Minami T, Tojo H, Shinomura Y, Komatsubara T, Matsuzawa Y, Okamoto M. Elevation of phospholipase A2 protein in sera of patients with Crohn's disease and ulcerative colitis. *Am J Gastroenterol.* 1993;88(7):1076-80.

327. Rosengarten M, Hadad N, Solomonov Y, Lamprecht S, Levy R. Cytosolic phospholipase A2 α has a crucial role in the pathogenesis of DSS-induced colitis in mice. *Eur J Immunol.* 2016;46(2):400-8.

328. Zhai L, Huang T, Xiao HT, Wu PG, Lin CY, Ning ZW, et al. Berberine Suppresses Colonic Inflammation in Dextran Sulfate Sodium-Induced Murine Colitis Through Inhibition of Cytosolic Phospholipase A2 Activity. *Front Pharmacol.* 2020;11:576496.

329. Haller AM, Wolfkiel PR, Jaeschke A, Hui DY. Inactivation of Group 1B Phospholipase A(2) Enhances Disease Recovery and Reduces Experimental Colitis in Mice. *Int J Mol Sci.* 2023;24(22).

330. Schewe M, Franken PF, Sacchetti A, Schmitt M, Joosten R, Böttcher R, et al. Secreted Phospholipases A2 Are Intestinal Stem Cell Niche Factors with Distinct Roles in Homeostasis, Inflammation, and Cancer. *Cell Stem Cell.* 2016;19(1):38-51.

331. Dennis EA, Cao J, Hsu YH, Magrioti V, Kokotos G. Phospholipase A2 enzymes: physical structure, biological function, disease implication, chemical inhibition, and therapeutic intervention. *Chem Rev.* 2011;111(10):6130-85.

332. Tomita Y, Jyoyama H, Kobayashi M, Kuwabara K, Furue S, Ueno M, et al. Role of group IIA phospholipase A2 in rat colitis induced by dextran sulfate sodium. *Eur J Pharmacol.* 2003;472(1-2):147-58.

333. Lewin M, Samuel S, Merkel J, Bickler P. Varespladib (LY315920) Appears to Be a Potent, Broad-Spectrum, Inhibitor of Snake Venom Phospholipase A2 and a Possible Pre-Referral Treatment for Envenomation. *Toxins (Basel).* 2016;8(9).

334. Glaser KB, de Carvalho MS, Jacobs RS, Kernan MR, Faulkner DJ. Manoalide: structure-activity studies and definition of the pharmacophore for phospholipase A2 inactivation. *Mol Pharmacol.* 1989;36(5):782-8.

335. Li C, Lin H, He H, Ma M, Jiang W, Zhou R. Inhibition of the NLRP3 Inflammasome Activation by Manoalide Ameliorates Experimental Autoimmune Encephalomyelitis Pathogenesis. *Front Cell Dev Biol.* 2022;10:822236.

336. Wang HR, Tang JY, Wang YY, Farooqi AA, Yen CY, Yuan SF, et al. Manoalide Preferentially Provides Antiproliferation of Oral Cancer Cells by Oxidative Stress-Mediated Apoptosis and DNA Damage. *Cancers (Basel).* 2019;11(9).

337. Zheng Y, Schroeder S, Kanev GK, Botros SS, William S, Sabra AA, et al. To Target or Not to Target *Schistosoma mansoni* Cyclic Nucleotide Phosphodiesterase 4A? *Int J Mol Sci.* 2023;24(7).

338. Queirós-Reis L, Mesquita JR, Brancale A, Bassetto M. Exploring the Fatty Acid Binding Pocket in the SARS-CoV-2 Spike Protein - Confirmed and Potential Ligands. *J Chem Inf Model.* 2023;63(23):7282-98.

339. Giancotti G, Nannetti G, Padalino G, Landini M, Santos-Ferreira N, Van Dycke J, et al. Structural Investigations on Novel Non-Nucleoside Inhibitors of Human Norovirus Polymerase. *Viruses.* 2022;15(1).

340. Picarazzi F, Zuanon M, Pasqualetto G, Cammarone S, Romeo I, Young MT, et al. Identification of Small Molecular Chaperones Binding P23H Mutant Opsin through an In Silico Structure-Based Approach. *J Chem Inf Model.* 2022;62(22):5794-805.

341. Berman HM, Westbrook J, Feng Z, Gilliland G, Bhat TN, Weissig H, et al. The Protein Data Bank. *Nucleic Acids Res.* 2000;28(1):235-42.
342. Cha SS, Lee D, Adams J, Kurdyla JT, Jones CS, Marshall LA, et al. High-resolution X-ray crystallography reveals precise binding interactions between human nonpancreatic secreted phospholipase A2 and a highly potent inhibitor (FPL67047XX). *J Med Chem.* 1996;39(20):3878-81.
343. Patil R, Das S, Stanley A, Yadav L, Sudhakar A, Varma AK. Optimized hydrophobic interactions and hydrogen bonding at the target-ligand interface leads the pathways of drug-designing. *PLoS One.* 2010;5(8):e12029.
344. Burke JE, Dennis EA. Phospholipase A2 biochemistry. *Cardiovasc Drugs Ther.* 2009;23(1):49-59.
345. Wu MR, Nissim L, Stupp D, Pery E, Binder-Nissim A, Weisinger K, et al. A high-throughput screening and computation platform for identifying synthetic promoters with enhanced cell-state specificity (SPECS). *Nat Commun.* 2019;10(1):2880.
346. Friesner RA, Banks JL, Murphy RB, Halgren TA, Klicic JJ, Mainz DT, et al. Glide: a new approach for rapid, accurate docking and scoring. 1. Method and assessment of docking accuracy. *J Med Chem.* 2004;47(7):1739-49.
347. Hawkins PC, Skillman AG, Nicholls A. Comparison of shape-matching and docking as virtual screening tools. *J Med Chem.* 2007;50(1):74-82.
348. Bassetto M, De Burghgraeve T, Delang L, Massarotti A, Coluccia A, Zonta N, et al. Computer-aided identification, design and synthesis of a novel series of compounds with selective antiviral activity against chikungunya virus. *Antiviral Res.* 2013;98(1):12-8.
349. Cancellieri M, Bassetto M, Widjaja I, van Kuppeveld F, de Haan CA, Brancale A. In silico structure-based design and synthesis of novel anti-RSV compounds. *Antiviral Res.* 2015;122:46-50.
350. Aykul S, Martinez-Hackert E. Determination of half-maximal inhibitory concentration using biosensor-based protein interaction analysis. *Anal Biochem.* 2016;508:97-103.
351. Padalino G, El-Sakkary N, Liu LJ, Liu C, Harte DSG, Barnes RE, et al. Anti-schistosomal activities of quinoxaline-containing compounds: From hit identification to lead optimisation. *Eur J Med Chem.* 2021;226:113823.
352. Lionta E, Spyrou G, Vassilatis DK, Cournia Z. Structure-based virtual screening for drug discovery: principles, applications and recent advances. *Curr Top Med Chem.* 2014;14(16):1923-38.
353. Cavasotto CN, Orry AJ. Ligand docking and structure-based virtual screening in drug discovery. *Curr Top Med Chem.* 2007;7(10):1006-14.
354. Gimeno A, Ojeda-Montes MJ, Tomás-Hernández S, Cereto-Massagué A, Beltrán-Debón R, Mulero M, et al. The Light and Dark Sides of Virtual Screening: What Is There to Know? *Int J Mol Sci.* 2019;20(6).
355. Chou TC. Theoretical basis, experimental design, and computerized simulation of synergism and antagonism in drug combination studies. *Pharmacol Rev.* 2006;58(3):621-81.
356. Sortino M, Garibotto F, Cechinel Filho V, Gupta M, Enriz R, Zacchino S. Antifungal, cytotoxic and SAR studies of a series of N-alkyl, N-aryl and N-alkylphenyl-1,4-pyrrolediones and related compounds. *Bioorg Med Chem.* 2011;19(9):2823-34.
357. Falidas E, Kitsioulis E, Spyropoulou D, Tsiambas E, Kalogirou A, Tsouvelas G, et al. Secretory Phospholipase A2 Digital Expression Analysis in Colon Adenocarcinoma. *In Vivo.* 2022;36(2):738-42.
358. Abbenhardt C, Poole EM, Kulmacz RJ, Xiao L, Curtin K, Galbraith RL, et al. Phospholipase A2G1B polymorphisms and risk of colorectal neoplasia. *Int J Mol Epidemiol Genet.* 2013;4(3):140-9.

359. Entwistle LJ, Pelly VS, Coomes SM, Kannan Y, Perez-Lloret J, Czieso S, et al. Epithelial-Cell-Derived Phospholipase A(2) Group 1B Is an Endogenous Anthelmintic. *Cell Host Microbe*. 2017;22(4):484-93.e5.
360. Passero LF, Laurenti MD, Tomokane TY, Corbett CE, Toyama MH. The effect of phospholipase A2 from *Crotalus durissus collilineatus* on *Leishmania (Leishmania) amazonensis* infection. *Parasitol Res*. 2008;102(5):1025-33.
361. Saffer LD, Long Krug SA, Schwartzman JD. The role of phospholipase in host cell penetration by *Toxoplasma gondii*. *Am J Trop Med Hyg*. 1989;40(2):145-9.
362. Fissiha W, Kinde MZ. Anthelmintic Resistance and Its Mechanism: A Review. *Infect Drug Resist*. 2021;14:5403-10.
363. Kapo N, Omeragić J, Goletić Š, Šabić E, Softić A, Smajlović A, et al. First Report of Benzimidazole Resistance in Field Population of *Haemonchus contortus* from Sheep, Goats and Cattle in Bosnia and Herzegovina. *Pathogens*. 2024;13(1).
364. Reed EK, Smith KA. Using our understanding of interactions between helminth metabolism and host immunity to target worm survival. *Trends Parasitol*. 2024;40(7):549-61.
365. Pira G, Uva P, Scanu AM, Rocca PC, Murgia L, Uleri E, et al. Landscape of transcriptome variations uncovering known and novel driver events in colorectal carcinoma. *Sci Rep*. 2020;10(1):432.
366. Rajamäki K, Taira A, Katainen R, Välimäki N, Kuosmanen A, Plaketti RM, et al. Genetic and Epigenetic Characteristics of Inflammatory Bowel Disease-Associated Colorectal Cancer. *Gastroenterology*. 2021;161(2):592-607.
367. Wang Z, Gerstein M, Snyder M. RNA-Seq: a revolutionary tool for transcriptomics. *Nat Rev Genet*. 2009;10(1):57-63.
368. Ogino S, Kirkner GJ, Nosho K, Irahara N, Kure S, Shima K, et al. Cyclooxygenase-2 expression is an independent predictor of poor prognosis in colon cancer. *Clin Cancer Res*. 2008;14(24):8221-7.
369. Tsujii M, Kawano S, DuBois RN. Cyclooxygenase-2 expression in human colon cancer cells increases metastatic potential. *Proc Natl Acad Sci U S A*. 1997;94(7):3336-40.
370. Cebola I, Custodio J, Muñoz M, Díez-Villanueva A, Paré L, Prieto P, et al. Epigenetics override pro-inflammatory PTGS transcriptomic signature towards selective hyperactivation of PGE2 in colorectal cancer. *Clin Epigenetics*. 2015;7(1):74.
371. Maizels RM, Hewitson JP, Smith KA. Susceptibility and immunity to helminth parasites. *Curr Opin Immunol*. 2012;24(4):459-66.
372. Kreider T, Anthony RM, Urban JF, Jr., Gause WC. Alternatively activated macrophages in helminth infections. *Curr Opin Immunol*. 2007;19(4):448-53.
373. Ha TY. The role of regulatory T cells in cancer. *Immune Netw*. 2009;9(6):209-35.
374. Yang Q, Guo N, Zhou Y, Chen J, Wei Q, Han M. The role of tumor-associated macrophages (TAMs) in tumor progression and relevant advance in targeted therapy. *Acta Pharm Sin B*. 2020;10(11):2156-70.
375. Boman BM, Wicha MS, Fields JZ, Runquist OA. Symmetric division of cancer stem cells--a key mechanism in tumor growth that should be targeted in future therapeutic approaches. *Clin Pharmacol Ther*. 2007;81(6):893-8.
376. Shekarriz R, Montazer F, Alizadeh-Navaei R. Overexpression of cancer stem cell marker *Lgr5* in colorectal cancer patients and association with clinicopathological findings. *Caspian J Intern Med*. 2019;10(4):412-6.
377. Drurey C, Lindholm HT, Coakley G, Poveda MC, Löser S, Doolan R, et al. Intestinal epithelial tuft cell induction is negated by a murine helminth and its secreted products. *J Exp Med*. 2022;219(1).
378. Fleige S, Pfaffl MW. RNA integrity and the effect on the real-time qRT-PCR performance. *Mol Aspects Med*. 2006;27(2-3):126-39.

379. Schroeder A, Mueller O, Stocker S, Salowsky R, Leiber M, Gassmann M, et al. The RIN: an RNA integrity number for assigning integrity values to RNA measurements. *BMC Mol Biol.* 2006;7:3.
380. Chong GO, Han HS, Lee SD, Lee YH. Improvement in RNA quantity and quality in cervico-vaginal cytology. *Virology.* 2020;17(1):8.
381. Chen X, Zhang B, Wang T, Bonni A, Zhao G. Robust principal component analysis for accurate outlier sample detection in RNA-Seq data. *BMC Bioinformatics.* 2020;21(1):269.
382. Di Tommaso P, Chatzou M, Floden EW, Barja PP, Palumbo E, Notredame C. Nextflow enables reproducible computational workflows. *Nat Biotechnol.* 2017;35(4):316-9.
383. Thomas PD, Ebert D, Muruganujan A, Mushayahama T, Albu LP, Mi H. PANTHER: Making genome-scale phylogenetics accessible to all. *Protein Sci.* 2022;31(1):8-22.
384. Hayashi Y, Kuroda T, Kishimoto H, Wang C, Iwama A, Kimura K. Downregulation of rRNA transcription triggers cell differentiation. *PLoS One.* 2014;9(5):e98586.
385. Boulon S, Westman BJ, Hutten S, Boisvert FM, Lamond AI. The nucleolus under stress. *Mol Cell.* 2010;40(2):216-27.
386. Grummt I. The nucleolus—guardian of cellular homeostasis and genome integrity. *Chromosoma.* 2013;122(6):487-97.
387. Kuroda T, Murayama A, Katagiri N, Ohta YM, Fujita E, Masumoto H, et al. RNA content in the nucleolus alters p53 acetylation via MYBBP1A. *Embo j.* 2011;30(6):1054-66.
388. Kreiner G, Bierhoff H, Armentano M, Rodriguez-Parkitna J, Sowodniok K, Naranjo JR, et al. A neuroprotective phase precedes striatal degeneration upon nucleolar stress. *Cell Death Differ.* 2013;20(11):1455-64.
389. Subramanian A, Tamayo P, Mootha VK, Mukherjee S, Ebert BL, Gillette MA, et al. Gene set enrichment analysis: a knowledge-based approach for interpreting genome-wide expression profiles. *Proc Natl Acad Sci U S A.* 2005;102(43):15545-50.
390. Kim HJ, Lee HN, Jeong MS, Jang SB. Oncogenic KRAS: Signaling and Drug Resistance. *Cancers (Basel).* 2021;13(22).
391. Yu X, Zhang J, Sun S, Zhou X, Zeng T, Chen L. Individual-specific edge-network analysis for disease prediction. *Nucleic Acids Res.* 2017;45(20):e170.
392. An Y, Yao J, Niu X. The Signaling Pathway of PGE2 and Its Regulatory Role in T Cell Differentiation. *Mediators of Inflammation.* 2021;2021:1-7.
393. Wu J, Wang Y, Zhou Y, Wang Y, Sun X, Zhao Y, et al. PPAR γ as an E3 Ubiquitin-Ligase Impedes Phosphate-Stat6 Stability and Promotes Prostaglandins E(2)-Mediated Inhibition of IgE Production in Asthma. *Front Immunol.* 2020;11:1224.
394. De Paz Linares GA, Opperman RM, Majumder M, Lala PK. Prostaglandin E2 Receptor 4 (EP4) as a Therapeutic Target to Impede Breast Cancer-Associated Angiogenesis and Lymphangiogenesis. *Cancers (Basel).* 2021;13(5).
395. Lee J, Banu SK, Burghardt RC, Starzinski-Powitz A, Arosh JA. Selective inhibition of prostaglandin E2 receptors EP2 and EP4 inhibits adhesion of human endometriotic epithelial and stromal cells through suppression of integrin-mediated mechanisms. *Biol Reprod.* 2013;88(3):77.
396. Punyawatthanakool S, Matsuura R, Wongchang T, Katsurada N, Tsuruyama T, Tajima M, et al. Prostaglandin E(2)-EP2/EP4 signaling induces immunosuppression in human cancer by impairing bioenergetics and ribosome biogenesis in immune cells. *Nat Commun.* 2024;15(1):9464.
397. Doherty GA, Byrne SM, Molloy ES, Malhotra V, Austin SC, Kay EW, et al. Proneoplastic effects of PGE2 mediated by EP4 receptor in colorectal cancer. *BMC Cancer.* 2009;9:207.
398. Pastille E, Frede A, McSorley HJ, Gräb J, Adamczyk A, Kollenda S, et al. Intestinal helminth infection drives carcinogenesis in colitis-associated colon cancer. *PLoS Pathog.* 2017;13(9):e1006649.

399. Hang L, Blum AM, Setiawan T, Urban JP, Jr., Stoyanoff KM, Weinstock JV. Heligmosomoides polygyrus bakeri infection activates colonic Foxp3+ T cells enhancing their capacity to prevent colitis. *J Immunol.* 2013;191(4):1927-34.
400. Saito T, Nishikawa H, Wada H, Nagano Y, Sugiyama D, Atarashi K, et al. Two FOXP3(+)/CD4(+) T cell subpopulations distinctly control the prognosis of colorectal cancers. *Nat Med.* 2016;22(6):679-84.
401. Schreiber RD, Old LJ, Smyth MJ. Cancer immunoediting: integrating immunity's roles in cancer suppression and promotion. *Science.* 2011;331(6024):1565-70.
402. Karpiński P, Frydecka D, Szaśadek MM, Misiak B. Reduced number of peripheral natural killer cells in schizophrenia but not in bipolar disorder. *Brain Behav Immun.* 2016;54:194-200.
403. Weiss E, de la Grange P, Defaye M, Lozano JJ, Aguilar F, Hegde P, et al. Characterization of Blood Immune Cells in Patients With Decompensated Cirrhosis Including ACLF. *Front Immunol.* 2020;11:619039.
404. Weng M, Huntley D, Huang IF, Foye-Jackson O, Wang L, Sarkissian A, et al. Alternatively activated macrophages in intestinal helminth infection: effects on concurrent bacterial colitis. *J Immunol.* 2007;179(7):4721-31.
405. Oliphant CJ, Barlow JL, McKenzie AN. Insights into the initiation of type 2 immune responses. *Immunology.* 2011;134(4):378-85.
406. van der Flier LG, Haegbarth A, Stange DE, van de Wetering M, Clevers H. OLFM4 is a robust marker for stem cells in human intestine and marks a subset of colorectal cancer cells. *Gastroenterology.* 2009;137(1):15-7.
407. Ariyaratne A, Kim SY, Pollo SMJ, Perera S, Liu H, Nguyen WNT, et al. Trickle infection with Heligmosomoides polygyrus results in decreased worm burdens but increased intestinal inflammation and scarring. *Front Immunol.* 2022;13:1020056.
408. Herszényi L, Barabás L, Hritz I, István G, Tulassay Z. Impact of proteolytic enzymes in colorectal cancer development and progression. *World J Gastroenterol.* 2014;20(37):13246-57.
409. Roche J. The Epithelial-to-Mesenchymal Transition in Cancer. *Cancers (Basel).* 2018;10(2).
410. Jacobs BA, Prince S, Smith KA. Gastrointestinal Nematode-Derived Antigens Alter Colorectal Cancer Cell Proliferation and Migration through Regulation of Cell Cycle and Epithelial-Mesenchymal Transition Proteins. *Int J Mol Sci.* 2020;21(21).
411. Wang C, Lei H, Tian Y, Shang M, Wu Y, Li Y, et al. Clonorchis sinensis granulin: identification, immunolocalization, and function in promoting the metastasis of cholangiocarcinoma and hepatocellular carcinoma. *Parasit Vectors.* 2017;10(1):262.
412. Jacobs BA, Chetty A, Horsnell WGC, Schäfer G, Prince S, Smith KA. Hookworm exposure decreases human papillomavirus uptake and cervical cancer cell migration through systemic regulation of epithelial-mesenchymal transition marker expression. *Sci Rep.* 2018;8(1):11547.
413. Yang Y, Zhang H, Huang S, Chu Q. KRAS Mutations in Solid Tumors: Characteristics, Current Therapeutic Strategy, and Potential Treatment Exploration. *J Clin Med.* 2023;12(2).
414. Bieging KT, Mello SS, Attardi LD. Unravelling mechanisms of p53-mediated tumour suppression. *Nat Rev Cancer.* 2014;14(5):359-70.
415. Fernando M, Duijf PHG, Proctor M, Stevenson AJ, Ehmann A, Vora S, et al. Dysregulated G2 phase checkpoint recovery pathway reduces DNA repair efficiency and increases chromosomal instability in a wide range of tumours. *Oncogenesis.* 2021;10(5):41.
416. Cook ME, Jarjour NN, Lin CC, Edelson BT. Transcription Factor Bhlhe40 in Immunity and Autoimmunity. *Trends Immunol.* 2020;41(11):1023-36.
417. Shao C, Lu W, Du Y, Yan W, Bao Q, Tian Y, et al. Cytosolic ME1 integrated with mitochondrial IDH2 supports tumor growth and metastasis. *Redox Biol.* 2020;36:101685.
418. Hassn Mesrati M, Syafruddin SE, Mohtar MA, Syahir A. CD44: A Multifunctional Mediator of Cancer Progression. *Biomolecules.* 2021;11(12).

419. Sui Y, Jiang H, Kellogg CM, Oh S, Janknecht R. Promotion of colorectal cancer by transcription factor BHLHE40 involves upregulation of ADAM19 and KLF7. *Front Oncol.* 2023;13:1122238.
420. Fernandes LM, Al-Dwairi A, Simmen RCM, Marji M, Brown DM, Jewell SW, et al. Malic Enzyme 1 (ME1) is pro-oncogenic in *Apc(Min/+)* mice. *Sci Rep.* 2018;8(1):14268.
421. Ziranu P, Pretta A, Aimola V, Cau F, Mariani S, D'Agata AP, et al. CD44: A New Prognostic Marker in Colorectal Cancer? *Cancers (Basel).* 2024;16(8).
422. Maric J, Ravindran A, Mazzurana L, Björklund Å K, Van Acker A, Rao A, et al. Prostaglandin E(2) suppresses human group 2 innate lymphoid cell function. *J Allergy Clin Immunol.* 2018;141(5):1761-73.e6.
423. Luschnig-Schratl P, Sturm EM, Konya V, Philipose S, Marsche G, Fröhlich E, et al. EP4 receptor stimulation down-regulates human eosinophil function. *Cell Mol Life Sci.* 2011;68(21):3573-87.
424. Sturm EM, Schratl P, Schuligoi R, Konya V, Sturm GJ, Lippe IT, et al. Prostaglandin E2 inhibits eosinophil trafficking through E-prostanoid 2 receptors. *J Immunol.* 2008;181(10):7273-83.
425. Torres-Atencio I, Ainsua-Enrich E, de Mora F, Picado C, Martín M. Prostaglandin E2 prevents hyperosmolar-induced human mast cell activation through prostanoid receptors EP2 and EP4. *PLoS One.* 2014;9(10):e110870.
426. Kay LJ, Yeo WW, Peachell PT. Prostaglandin E2 activates EP2 receptors to inhibit human lung mast cell degranulation. *Br J Pharmacol.* 2006;147(7):707-13.
427. Rigoni A, Colombo MP, Pucillo C. Mast cells, basophils and eosinophils: From allergy to cancer. *Semin Immunol.* 2018;35:29-34.
428. Knight PA, Wright SH, Lawrence CE, Paterson YY, Miller HR. Delayed expulsion of the nematode *Trichinella spiralis* in mice lacking the mucosal mast cell-specific granule chymase, mouse mast cell protease-1. *J Exp Med.* 2000;192(12):1849-56.
429. Röszer T. Understanding the Mysterious M2 Macrophage through Activation Markers and Effector Mechanisms. *Mediators Inflamm.* 2015;2015:816460.
430. Chen S, Saeed A, Liu Q, Jiang Q, Xu H, Xiao GG, et al. Macrophages in immunoregulation and therapeutics. *Signal Transduct Target Ther.* 2023;8(1):207.
431. Casanova-Acebes M, Dalla E, Leader AM, LeBerichel J, Nikolic J, Morales BM, et al. Tissue-resident macrophages provide a pro-tumorigenic niche to early NSCLC cells. *Nature.* 2021;595(7868):578-84.
432. Zhou X, Khan S, Huang D, Li L. V-Set and immunoglobulin domain containing (VSIG) proteins as emerging immune checkpoint targets for cancer immunotherapy. *Front Immunol.* 2022;13:938470.
433. Inoue Y, Matsuura S, Yoshimura K, Iwashita Y, Kahyo T, Kawase A, et al. Characterization of V-set and immunoglobulin domain containing 1 exerting a tumor suppressor function in gastric, lung, and esophageal cancer cells. *Cancer Sci.* 2017;108(8):1701-14.
434. Hodzic Z, Schill EM, Bolock AM, Good M. IL-33 and the intestine: The good, the bad, and the inflammatory. *Cytokine.* 2017;100:1-10.
435. von Moltke J, Ji M, Liang HE, Locksley RM. Tuft-cell-derived IL-25 regulates an intestinal ILC2-epithelial response circuit. *Nature.* 2016;529(7585):221-5.
436. Arthur JC, Perez-Chanona E, Mühlbauer M, Tomkovich S, Uronis JM, Fan TJ, et al. Intestinal inflammation targets cancer-inducing activity of the microbiota. *Science.* 2012;338(6103):120-3.
437. Ben-Neriah Y, Karin M. Inflammation meets cancer, with NF- κ B as the matchmaker. *Nat Immunol.* 2011;12(8):715-23.
438. Colotta F, Allavena P, Sica A, Garlanda C, Mantovani A. Cancer-related inflammation, the seventh hallmark of cancer: links to genetic instability. *Carcinogenesis.* 2009;30(7):1073-81.

439. Elinav E, Nowarski R, Thaiss CA, Hu B, Jin C, Flavell RA. Inflammation-induced cancer: crosstalk between tumours, immune cells and microorganisms. *Nat Rev Cancer*. 2013;13(11):759-71.
440. Terzić J, Grivennikov S, Karin E, Karin M. Inflammation and colon cancer. *Gastroenterology*. 2010;138(6):2101-14.e5.
441. Pedraza-Fariña LG. Mechanisms of oncogenic cooperation in cancer initiation and metastasis. *Yale J Biol Med*. 2006;79(3-4):95-103.
442. Molinari M. Cell cycle checkpoints and their inactivation in human cancer. *Cell Prolif*. 2000;33(5):261-74.
443. Sims D, Sudbery I, Illott NE, Heger A, Ponting CP. Sequencing depth and coverage: key considerations in genomic analyses. *Nat Rev Genet*. 2014;15(2):121-32.
444. Liu Y, Ferguson JF, Xue C, Silverman IM, Gregory B, Reilly MP, et al. Evaluating the impact of sequencing depth on transcriptome profiling in human adipose. *PLoS One*. 2013;8(6):e66883.
445. Babarinde IA, Hutchins AP. The effects of sequencing depth on the assembly of coding and noncoding transcripts in the human genome. *BMC Genomics*. 2022;23(1):487.
446. Li D, Gong B, Xu J, Ning B, Tong W. Impact of Sequencing Depth and Library Preparation on Toxicological Interpretation of RNA-Seq Data in a "Three-Sample" Scenario. *Chem Res Toxicol*. 2021;34(2):529-40.
447. Schurch NJ, Schofield P, Gierliński M, Cole C, Sherstnev A, Singh V, et al. How many biological replicates are needed in an RNA-seq experiment and which differential expression tool should you use? *Rna*. 2016;22(6):839-51.
448. Tamayo P, Steinhardt G, Liberzon A, Mesirov JP. The limitations of simple gene set enrichment analysis assuming gene independence. *Stat Methods Med Res*. 2016;25(1):472-87.
449. Muto S, Ozaki Y, Yamaguchi H, Mine H, Takagi H, Watanabe M, et al. Tumor β -catenin expression is associated with immune evasion in non-small cell lung cancer with high tumor mutation burden. *Oncol Lett*. 2021;21(3):203.
450. Khademian N, Mirzaei A, Hosseini A, Zare L, Nazem S, Babaheidarian P, et al. Expression pattern and clinical significance of β -catenin gene and protein in patients with primary malignant and benign bone tumors. *Sci Rep*. 2022;12(1):9488.
451. Elzagheid A, Buhmeida A, Korkeila E, Collan Y, Syrjanen K, Pyrhonen S. Nuclear beta-catenin expression as a prognostic factor in advanced colorectal carcinoma. *World J Gastroenterol*. 2008;14(24):3866-71.
452. Pozzi A, Yan X, Macias-Perez I, Wei S, Hata AN, Breyer RM, et al. Colon carcinoma cell growth is associated with prostaglandin E2/EP4 receptor-evoked ERK activation. *J Biol Chem*. 2004;279(28):29797-804.
453. Dunham AS, Beltrao P. Exploring amino acid functions in a deep mutational landscape. *Mol Syst Biol*. 2021;17(7):e10305.
454. Grabowski P, Kustatscher G, Rappsilber J. Epigenetic Variability Confounds Transcriptome but Not Proteome Profiling for Coexpression-based Gene Function Prediction. *Mol Cell Proteomics*. 2018;17(11):2082-90.
455. Chen H, Ye F, Guo G. Revolutionizing immunology with single-cell RNA sequencing. *Cell Mol Immunol*. 2019;16(3):242-9.
456. Yu YR, O'Koren EG, Hotten DF, Kan MJ, Kopin D, Nelson ER, et al. A Protocol for the Comprehensive Flow Cytometric Analysis of Immune Cells in Normal and Inflamed Murine Non-Lymphoid Tissues. *PLoS One*. 2016;11(3):e0150606.

Appendix

Appendix table 1. Top 100 proteins identified in HES 10,000 – 50,000 molecular weight fraction by LC/MS.

Rank	Description	Accession	Score Sequest HT
1	Venom allergen/ancylostoma secreted protein-like 1 isoform 2	G4XWW4	1702.62
2	Venom allergen/ancylostoma secreted protein-like 3 isoform 1	G4XWX0	1288.05
3	Venom allergen/ancylostoma secreted protein-like 1 isoform 1	G4XWW3	1282.26
4	Lysozyme-1	G3C8W1	970.89
5	Venom allergen/ancylostoma secreted protein-like 2 isoform 3	G4XWW9	942.18
6	Carboxylic ester hydrolase	F6LW93	885.5
7	Apyrase-2	G4WZX8	873.21
8	Venom allergen/ancylostoma secreted protein-like 2 isoform 2	G4XWW8	815.07
9	Transthyretin-related-1	G3C8V9	810.37
10	GLOBIN domain-containing protein	A0A183FNA3	744.69
11	GLOBIN domain-containing protein	A0A183FNA1	722.09
12	SCP domain-containing protein	A0A3P8APZ8	721.46
13	Vitellogenin domain-containing protein	A0A183G4X9	678.18
14	Lysozyme	A0A3P8DRS4	673.03

15	GLOBIN domain-containing protein	A0A183FC19	649.52
16	GLOBIN domain-containing protein 1	A0A183GV03	636.13
17	Venom allergen/ancylostoma secreted protein-like 9	G4XWX8	607.89
18	VWFD domain-containing protein	A0A3P7ZT66	586.45
19	SCP domain-containing protein	A0A183FE39	493.04
20	SCP domain-containing protein	A0A183GC37	467.62
21	Zinc metalloproteinase	A0A183GKC3	462.99
22	Venom allergen/ancylostoma secreted protein-like 7 isoform 2	G4XWX5	459.15
23	Venom allergen/ancylostoma secreted protein-like 7 isoform 3	G4XWX6	412.19
24	SCP domain-containing protein	A0A183GC36	410.06
25	Venom allergen/ancylostoma secreted protein-like 7 isoform 1	G4XWX4	389.42
26	Polyprotein allergen nematode domain-containing protein	A0A3P7ZEG5	385.06
27	SCP domain-containing protein	A0A3P8AQ08	380.89
28	Uncharacterized protein	A0A183FR70	366.99
29	Zinc metalloproteinase	A0A183GCF4	362.23
30	Zinc metalloproteinase	A0A183GCF3	361.68
31	GLOBIN domain-containing protein	A0A183G1J6	359.14
32	Apyrase	A0A3P8D4Q0	355.89

33	GLOBIN domain-containing protein	A0A183GH14	352.44
34	Major sperm protein	A0A183F4S0	337.4
35	Venom allergen/ancylostoma secreted protein-like 1 isoform 4	G4XWW6	336.72
36	Zinc metalloproteinase	A0A183GE59	335.89
37	Apyrase	A0A183G2S1	332.16
38	Apyrase	A0A183GJY2	324.57
39	SCP domain-containing protein	A0A183F9U8	322.45
40	Venom allergen/ancylostoma secreted protein-like 1 isoform 3	G4XWW5	321.29
41	Apyrase-1 isoform 4	G4WZX7	311.31
42	SCP domain-containing protein	A0A3P8C155	308.37
43	Carboxylic ester hydrolase	F6LW95	300.29
44	Acetylcholinesterase-2	F6LW94	292.1
45	GLOBIN domain-containing protein	A0A183FL83	288.46
46	SCP domain-containing protein	A0A183GL21	280.51
47	SCP domain-containing protein	A0A3P7XU79	279.32
48	Apyrase-1 isoform 1	G4WZX4	278.35
49	Venom allergen/ancylostoma secreted protein-like 14	G4XWY2	267.88
50	GLOBIN domain-containing protein	A0A183G0G6	266.76

51	Venom allergen/ancylostoma secreted protein-like 12	G4XWY0	257.26
52	Uncharacterized protein	A0A183F2W9	249.23
53	Legumain prodomain domain-containing protein	A0A8L8JU57	246.17
54	Venom allergen/ancylostoma secreted protein-like 5	G4XWX2	245.17
55	Enolase	A0A183GB30	244.44
56	SCP domain-containing protein	A0A3P8C0T7	239.18
57	Apyrase	A0A3P7YPR1	232.12
58	Metalloendopeptidase	A0A183G4Z8	220.24
59	Zinc metalloproteinase	A0A183FJU9	212.99
60	Transthyretin-like family protein	A0A183GUL4	200.16
61	Venom allergen/ancylostoma secreted protein-like 8 isoform 1	G4XWX7	195.23
62	Venom allergen/ancylostoma secreted protein-like 6	G4XWX3	194.17
63	Chitin-binding type-2 domain-containing protein	A0A3P7XC10	182.41
64	SCP domain-containing protein	A0A183GMB4	180.3
65	Novel secreted protein 16	G3C8V7	171.79
66	Metalloendopeptidase	A0A3P8AZS9	166.88
67	SCP domain-containing protein	A0A183FQW2	162.05
68	Metalloendopeptidase	A0A183GJB1	160.57

69	Fructose-bisphosphate aldolase	A0A3P8F538	159.44
70	PHA domain	G3C8V5	154.82
71	SCP domain-containing protein	A0A3P7Z2D6	153.73
72	Uncharacterized protein	A0A183F469	153.49
73	Peptidase family M13	A0A3P7WLY7	153.38
74	SCP domain-containing protein	A0A183FQW0	152.07
75	C-type lectin domain-containing protein	A0A3P7Z055	149.55
76	Cysteine protease inhibitor	LOHAX6	148.84
77	Heat shock protein 60	A0A183FJW2	148.72
78	Galectin	A0A3P7ZLW5	147.67
79	Novel secreted protein 4	G3C8V6	142.65
80	Metalloendopeptidase	A0A183GL74	142.02
81	Glutathione S-transferase 2 (Fragment)	Q9NJK6	141.65
82	Endoribonuclease	A0A183GBC6	140.02
83	phosphoglycerate mutase (2,3-diphosphoglycerate-independent)	A0A183G4B0	137.97
84	SnoaL-like domain-containing protein	A0A183F2I9	137.34
85	Metalloendopeptidase	A0A183GBM9	137.12
86	HTH_48 domain-containing protein	A0A3P8F4J5	135.41

87	Venom allergen/ancylostoma secreted protein-like 10	G4XWX9	134.68
88	glutathione transferase	A0A183FXU3	132.84
89	Thioredoxin domain-containing protein	A0A183FHF8	131.36
90	Calreticulin	Q0VJ74	130.29
91	arginine kinase	A0A3P8A4R0	129.89
92	Uncharacterized protein	A0A183GEN8	126.53
93	SERPIN domain-containing protein	A0A183G340	126.3
94	Lysozyme	A0A183GIP3	126.06
95	Glutathione transferase	A0A183FRS0	124.84
96	Peptidase_M13 domain-containing protein	A0A3P8C7K1	124.33
97	C-type lectin domain-containing protein	A0A3P8EMW2	124.04
98	Sushi domain-containing protein	A0A183FDQ8	121.25
99	Metalloendopeptidase	A0A183FXF0	119.27
100	Peptidase_M13_N domain-containing protein	A0A3P7XJ53	118.39

Appendix table 2. Alphabetical list of all proteins identified in 10,000 – 50,000 molecular weight HES fraction

Description	Accession	Score
10-formyltetrahydrofolate dehydrogenase	AOA3P7YDJ0	5.49
14_3_3 domain-containing protein	AOA183FYM3	94.61
26S proteasome non-ATPase regulatory subunit 13	AOA183FDE6	18.9
3'-5' exonuclease domain-containing protein	AOA3P8C5E3	3
3-hydroxyacyl-CoA dehydrogenase NAD binding domain-containing protein	AOA3P8BZG2	4.52
3-hydroxyacyl-CoA dehydrogenase type-2	AOA183FVT7	14.97
40S ribosomal protein S12	AOA183FWC6	5.42
4-hydroxyphenylpyruvate dioxygenase	AOA183FN18	33.84
6-pyruvoyl tetrahydrobiopterin synthase	AOA183F299	2.27
7-dehydrocholesterol reductase	AOA183G7Y5	0
A2M domain-containing protein	AOA183G3U2	41.25
A2M_N_2 domain-containing protein	AOA3P7YK03	81.04
A4_EXTRA domain-containing protein	AOA3P8ELF3	5.17
AA_permease_C domain-containing protein	AOA183F3T8	8.43
Aa_trans domain-containing protein	AOA183G0J8	4.74
Aa_trans domain-containing protein	AOA183F651	4.4
Aa_trans domain-containing protein	AOA183FF40	8.85
ABC transmembrane type-1 domain-containing protein	AOA3P8CHW6	2.4
ABC transporter domain-containing protein	AOA3P7ZW14	3.71
ABC transporter domain-containing protein	AOA3P7WH28	5.62
ABC transporter domain-containing protein	AOA183G9F9	2.5
Acetylcholine regulator unc-18	AOA183FDJ8	6.53
Acetylcholinesterase-2	F6LW94	292.1
Acetyl-CoA hydrolase	AOA183G409	7.18
Acetyltransferase component of pyruvate dehydrogenase complex	AOA3P7XU24	8.26

Acid phosphatase	A0A183GI99	12
Actin	A0A183GCV5	65.26
Actin	A0A183FFE7	73.28
Actin-binding cytoskeleton protein filamin (Fragment)	A0A3P8CU02	3.28
Activin_recp domain-containing protein	A0A3P7X186	17.12
ADAMTS/ADAMTS-like Spacer 1 domain-containing protein	A0A3P7U1D7	13.81
adenosine deaminase	A0A183F9L2	21.81
Adenylate cyclase-stimulating G alpha protein	A0A183FJC9	2.05
Adenylosuccinate synthetase	A0A3P8B7T8	15.9
Adenylyl cyclase-associated protein	A0A183FHN2	20.31
ADF-H domain-containing protein	A0A3P8A8R3	12.02
ADP-ribosylation factor 1	A0A183FZY2	14.17
ADP-ribosylation factor 1	A0A183GGY6	2.28
Aha1_N domain-containing protein	A0A183GGI3	10.87
AIRS domain-containing protein	A0A183F7N0	45.26
Alanine--glyoxylate aminotransferase 2, mitochondrial	A0A3P8DHM6	8
Alarmin release inhibitor	A0A3P7XL18	96.97
Aldedh domain-containing protein	A0A3P7Z9J4	2.3
Aldo_ket_red domain-containing protein	A0A183FTW3	15.65
Aldo_ket_red domain-containing protein	A0A3P7ZXY1	3.67
Aldo_ket_red domain-containing protein	A0A183FX21	14.74
Aldo_ket_red domain-containing protein	A0A3P8AFN7	2.76
Aldo_ket_red domain-containing protein	A0A3P8EHA3	49.45
Aldo_ket_red domain-containing protein	A0A183G6P1	15
Aldo_ket_red domain-containing protein	A0A183G6P2	17.88
Aldo_ket_red domain-containing protein	A0A183FDQ1	2.55
Aldo_ket_red domain-containing protein	A0A183GAK0	15.84
Aldo_ket_red domain-containing protein	A0A183G493	2.29
Aldoketomutase	A0A183GMK1	9.31
Aldolase_II domain-containing protein	A0A183G863	2

alpha-1,2-Mannosidase	AOA3P8BI18	17.11
Alpha-1,4 glucan phosphorylase	AOA3P8EHV5	23.66
Alpha-amylase	AOA183GEX6	111.23
Alpha-D-phosphohexomutase alpha/beta/alpha domain-containing protein	AOA183F5T6	58.24
Alpha-D-phosphohexomutase alpha/beta/alpha domain-containing protein	AOA183FM79	34.23
Alpha-galactosidase	AOA183F7W8	3.36
alpha-L-fucosidase	AOA183G1C6	59.08
Alpha-mann_mid domain-containing protein	AOA3P8B1I1	91.5
Alpha-mann_mid domain-containing protein	AOA183FL60	10.4
Amidohydro-rel domain-containing protein	AOA183FHE8	5.37
Amiloride-sensitive sodium channel	AOA183FZY1	4.13
Amino acid transporter transmembrane domain-containing protein	AOA3P8CZI2	2.02
Aminotran_5 domain-containing protein	AOA183GPW6	13.6
AMP_N domain-containing protein	AOA183GUA3	27.74
Annexin	AOA3P8E4E5	18.18
Annexin	AOA183GSW2	1.86
Annexin	AOA183GU85	3.05
Annexin	AOA183GUX9	92.22
Annexin	AOA183F9D9	87.99
Anti_proliftrn domain-containing protein	AOA183GKL5	26.93
Apple domain-containing protein	AOA183FIB6	25.17
Apple domain-containing protein	AOA3P7XYB2	2.53
Apyrase	AOA3P7YPR1	232.12
Apyrase	AOA183G2S1	332.16
Apyrase	AOA3P8D4Q0	355.89
Apyrase	AOA183GJY2	324.57
Apyrase	AOA183G8J6	54.48
Apyrase-1 isoform 1	G4WZX4	278.35
Apyrase-1 isoform 4	G4WZX7	311.31
Apyrase-2	G4WZX8	873.21

Aquaporin	AOA3P7ZUZ1	3.96
arginine kinase	AOA3P8A4R0	129.89
arginine kinase	AOA183GCV2	58.35
Aspartate aminotransferase	AOA3P8BWG8	9.72
Aspartate aminotransferase	AOA183FI07	86.13
Aspartate aminotransferase, mitochondrial	AOA183GUX6	12.81
Aspartate--tRNA ligase, cytoplasmic	AOA183GXJ9	0
Aspartyl aminopeptidase (Fragment)	AOA3P8D9G3	29.39
Aspartyl aminopeptidase	AOA3P7YPM0	12.05
aspartyl aminopeptidase	AOA183GRD6	12
Astacin domain-containing protein	AOA183GRK2	14.84
Astacin domain-containing protein	AOA183FXW7	3.82
ATP-citrate synthase	AOA183G8F3	3.24
ATP-dependent (S)-NAD(P)H-hydrate dehydratase	AOA183FD39	30.47
Battenin	AOA3P8B4Y3	6.98
Beta-galactosidase	AOA183FJL0	15.4
Beta-lactamase domain-containing protein	AOA183GG60	9.31
Beta-mannosidase	AOA183FYI7	5.81
beta-mannosidase	AOA3P8DLK3	2.21
beta-N-acetylhexosaminidase	AOA3P7Z4B1	15.74
beta-N-acetylhexosaminidase	AOA3P8ADB1	4.15
beta-N-acetylhexosaminidase	AOA3P8FYF4	3.91
Bis(5'-nucleosyl)-tetrphosphatase [asymmetrical]	AOA183FQ35	13.99
BMERB domain-containing protein	AOA3P8AFF3	2.17
BPTI/Kunitz inhibitor domain-containing protein (Fragment)	AOA3P8C4N6	21.72
BPTI/Kunitz inhibitor domain-containing protein	AOA183FRB2	49.07
BPTI/Kunitz inhibitor domain-containing protein	AOA183FRG6	5.33
BPTI/Kunitz inhibitor domain-containing protein	AOA3P7YCN1	60.04
BPTI/Kunitz inhibitor domain-containing protein	AOA183FXX1	16.01
BPTI/Kunitz inhibitor domain-containing protein	AOA183G181	9.52

BPTI/Kunitz inhibitor domain-containing protein	A0A183G978	13.46
BPTI/Kunitz inhibitor domain-containing protein	A0A3P8CDK5	4.33
BPTI/Kunitz inhibitor domain-containing protein	A0A3P8DGB2	8.64
BPTI/Kunitz inhibitor domain-containing protein	A0A183FHZ0	6.95
BPTI/Kunitz inhibitor domain-containing protein	A0A183FLA8	2.36
BPTI/Kunitz inhibitor domain-containing protein	A0A183FNM1	10.33
BPTI/Kunitz inhibitor domain-containing protein	A0A183GJ10	7.97
Branched-chain-amino-acid aminotransferase	A0A183G406	21.05
BRO1 domain-containing protein	A0A3P8EE78	8.41
BTB domain-containing protein	A0A183FA16	3.91
BTB domain-containing protein	A0A183GRK7	2.77
C2 domain-containing protein	A0A183FY51	8.87
C6 domain-containing protein	A0A3P8BIE7	2.31
C6 domain-containing protein	A0A183F2U6	75.74
Cadherin domain-containing protein	A0A3P7XEW6	2.56
Calnexin	A0A183GGH9	2.34
Calpain catalytic domain-containing protein	A0A3P7YRS2	3.6
Calponin-homology (CH) domain-containing protein	A0A3P7YPV2	27.04
Calponin-homology (CH) domain-containing protein	A0A183FW58	3.7
Calponin-homology (CH) domain-containing protein	A0A183G6K9	3.06
Calponin-homology (CH) domain-containing protein	A0A3P8B709	16.1
Calreticulin	Q0VJ74	130.29
Carbonic anhydrase	A0A3P8DER1	9.8
Carbonic anhydrase	A0A183FFC5	7.39
Carboxylic ester hydrolase	F6LW93	885.5
Carboxylic ester hydrolase	F6LW95	300.29
Carboxypeptidase	A0A3P8BSJ0	7.3
Carboxypeptidase	A0A3P7X3M2	63.03
Carboxypeptidase	A0A183FJF1	21.25
Carboxypeptidase Q	A0A183GQF6	16.08

CARMIL pleckstrin homology domain-containing protein	AOA3P8CHZ1	5.04
Catalase (Fragment)	AOA3P8CQM1	97.54
Cathepsin propeptide inhibitor domain-containing protein	AOA183FIT4	11.38
Cathepsin propeptide inhibitor domain-containing protein	AOA183F3W3	15.85
cathepsin X	AOA183FHF3	47.31
CCHC-type domain-containing protein	AOA183GVQ5	0
CD36 family protein	AOA183GI62	11.92
Chitin-binding type-2 domain-containing protein	AOA183G5A1	86.97
Chitin-binding type-2 domain-containing protein	AOA183GPG4	8.03
Chitin-binding type-2 domain-containing protein	AOA183GVF0	13.8
Chitin-binding type-2 domain-containing protein	AOA3P7XC10	182.41
Chitin-binding type-2 domain-containing protein	AOA183FA92	2.78
Chloride intracellular channel exc-4	AOA183FQR7	33.69
Chondroitin proteoglyca	AOA183FVC8	5.27
Chondroitin proteoglycan 3	AOA183FVC9	26.29
Chondroitin proteoglycan 3	AOA183G1J5	16.63
Chondroitin proteoglycan 4 domain-containing protein	AOA3P7X3Z3	18.11
Chondroitin proteoglycan 4 domain-containing protein	AOA183G4M8	4.64
Citrate synthase	AOA183F511	23.44
CN hydrolase domain-containing protein	AOA3P7ZEL6	2.7
CN hydrolase domain-containing protein	AOA183FTP3	55.1
CN hydrolase domain-containing protein	AOA3P8EN65	15.33
CN hydrolase domain-containing protein	AOA183GQW1	3.59
Col_cuticle_N domain-containing protein	AOA183GAU8	15.53
Col_cuticle_N domain-containing protein	AOA183FF94	3.98
Copper transporter	AOA3P7Z3E7	32.53
Core-2/I-Branching enzyme	AOA3P7YD99	2.36
CPG4 domain-containing protein	AOA183GQS0	25.14
CPG4 domain-containing protein	AOA183GQS1	10.45
CPG4 domain-containing protein	AOA183F602	6.94

CS domain-containing protein	A0A183G1Y3	9.13
CS domain-containing protein	A0A3P8CI41	2.52
C-type lectin domain-containing protein	A0A183FQV6	17.76
C-type lectin domain-containing protein	A0A3P7YZB6	3.17
C-type lectin domain-containing protein	A0A3P8BDR5	12.2
C-type lectin domain-containing protein	A0A183G695	6.61
C-type lectin domain-containing protein	A0A3P8EMW2	122.29
C-type lectin domain-containing protein	A0A183F725	12.17
C-type lectin domain-containing protein	A0A3P8CHW1	6.55
C-type lectin domain-containing protein	A0A183GHB3	6.69
C-type lectin domain-containing protein	A0A183GP42	15.44
C-type lectin domain-containing protein	A0A3P8AF78	3.57
C-type lectin domain-containing protein	A0A183FFZ6	3.31
C-type lectin domain-containing protein	A0A3P7Z055	149.55
C-type lectin domain-containing protein	A0A183FJI1	56.57
C-type lectin domain-containing protein	A0A183FMN1	96.13
C-type lectin domain-containing protein	A0A183FPC1	3.66
C-type lectin domain-containing protein	A0A3P8C7C9	1.68
C-type lectin domain-containing protein	A0A183F8S8	2.86
C-type lectin-1	D2D3S1	31.69
CUB domain-containing protein	A0A3P7ZFV0	8.73
CUB domain-containing protein	A0A183G717	3.28
CUB domain-containing protein	A0A183GVI9	59.48
CUB domain-containing protein	A0A183FUM1	18.42
Cyclin N-terminal domain-containing protein	A0A183GTM1	2.9
cystathionine gamma-lyase	A0A183F407	14.02
Cystatin domain-containing protein	A0A183G0P7	17.23
Cystatin domain-containing protein	A0A183G7K2	1.97
Cystatin domain-containing protein	A0A183GDW0	22.88
Cysteine protease inhibitor	L0HAX6	148.84

Cytochrome c domain-containing protein	A0A183GUB8	30.07
Cytochrome P450	A0A3P7T9L9	4.56
CYTOSOL_AP domain-containing protein	A0A183FV74	32.51
CYTOSOL_AP domain-containing protein	A0A183G0L3	28.5
DAO domain-containing protein	A0A3P8CDP5	2.36
Deoxyribonuclease II	A0A183FJ39	34.56
deoxyribose-phosphate aldolase	A0A3P7ZN57	13.53
Deoxyuridine 5'-triphosphate nucleotidohydrolase	A0A183G2G1	6.09
Dihydrolipoyl dehydrogenase	A0A3P8F2V0	62.62
Dihydropteridine reductase	A0A3P8C8G3	10.16
Dipeptidyl peptidase 3	A0A183G994	3.01
DJ-1_Pfpl domain-containing protein	A0A183FID5	44.68
DOMON domain-containing protein	A0A183FZU8	53.98
DOMON domain-containing protein	A0A3P8BLU1	9.45
DOMON domain-containing protein	A0A183F7Q0	1.62
DOMON domain-containing protein	A0A183GIV5	36.1
DOMON domain-containing protein	A0A183FJE7	2.44
DUF148 domain-containing protein	A0A183FWJ6	18.42
DUF148 domain-containing protein	A0A183FXJ2	8.76
DUF148 domain-containing protein	A0A183F5D5	2.29
DUF148 domain-containing protein	A0A183GC29	6.25
DUF148 domain-containing protein	A0A183GI10	8.26
DUF148 domain-containing protein	A0A183GNC2	3.8
DUF148 domain-containing protein	A0A183GXB0	24.67
DUF148 domain-containing protein	A0A183FBN5	20.25
DUF148 domain-containing protein	A0A183FGL7	10.56
DUF148 domain-containing protein	A0A183F3E8	12.28
DUF148 domain-containing protein	A0A183FJT0	3.71
DUF148 domain-containing protein	A0A183FN70	6.54
DUF148 domain-containing protein	A0A183F1W0	37.22

DUF1794 domain-containing protein	A0A183GCJ0	2.73
DUF19 domain-containing protein	A0A3P7YL75	15.86
DUF19 domain-containing protein	A0A3P7ZP34	77.61
DUF19 domain-containing protein	A0A183G709	9.99
DUF19 domain-containing protein	A0A3P8B8Y8	30.2
DUF19 domain-containing protein	A0A183GF06	14.54
DUF3105 domain-containing protein	A0A183G069	20.68
DUF3677 domain-containing protein	A0A3P7TBH4	2.85
DUF4139 domain-containing protein	A0A183GX17	2.72
DUF4440 domain-containing protein	A0A183FR50	11.39
DUF4440 domain-containing protein	A0A183G1U8	4.69
DUF4440 domain-containing protein	A0A183FHZ5	5.58
DUF775 domain-containing protein	A0A183G7R2	2.54
Dynamin-type G domain-containing protein	A0A3P8CZD7	46.99
Dynein light chain (Fragment)	A0A3P8DA75	5.29
E2 ubiquitin-conjugating enzyme	A0A183FNG4	4.31
EB domain-containing protein	A0A183FVC7	11.35
EB domain-containing protein	A0A183FZB0	4.83
EB domain-containing protein	A0A183G718	26.18
EB domain-containing protein	A0A183G7Y1	5.77
EB domain-containing protein	A0A183GHG2	3.17
EB domain-containing protein	A0A183F4S3	6.68
EB1 C-terminal domain-containing protein	A0A3P8AVT6	2.46
EF1_GNE domain-containing protein	A0A183FWW6	9.32
EF-hand domain-containing protein	A0A183FSK9	2.13
EF-hand domain-containing protein	A0A183G1K0	11.09
EF-hand domain-containing protein	A0A3P8DWZ1	9.61
EF-hand domain-containing protein	A0A183G9L2	6.16
EF-hand domain-containing protein	A0A183GES0	5.71
EF-hand domain-containing protein	A0A183FJM4	37.35

EF-hand domain-containing protein	AOA183F3L3	26.75
EF-hand domain-containing protein	AOA183FPD1	23.92
EF-hand domain-containing protein	AOA183GRV0	5.91
EF-hand domain-containing protein	AOA183G580	2.3
EF-hand_10 domain-containing protein	AOA3P7YAZ9	9.3
EGF-like domain-containing protein (Fragment)	AOA3P7ZG08	2
EGF-like domain-containing protein	AOA183FRA7	3.51
EGF-like domain-containing protein	AOA3P7ZH87	47.6
EGF-like domain-containing protein	AOA183FUV5	32.75
EGF-like domain-containing protein	AOA3P8A187	7.79
EGF-like domain-containing protein	AOA183G9C4	3.22
EGF-like domain-containing protein	AOA3P8FLF9	3.29
ELFV_dehydrog_N domain-containing protein	AOA183FP10	18
Elongation factor 1-alpha	AOA183GHW9	30.11
Elongation factor 1-alpha	AOA183GKS9	33.15
Elongation factor 1-gamma	AOA183GLK4	17.64
Endonuclease/exonuclease/phosphatase domain-containing protein	AOA183GTV6	2.04
Endonuclease/exonuclease/phosphatase domain-containing protein	AOA3P7YFD8	3.16
Endoplasmic reticulum oxidoreductin-1	AOA3P8DKB0	2.58
Endoribonuclease	AOA183FVF8	28.4
Endoribonuclease	AOA183GBC6	144.21
Endoribonuclease	AOA3P8BNI7	36.85
Endoribonuclease	AOA183GE42	37.1
Endoribonuclease	AOA183FKR9	12.12
Enolase	AOA183GB30	246.61
Ephrin RBD domain-containing protein	AOA183G4G1	6.77
ERAP1_C domain-containing protein	AOA183G4Z1	8.21
ERAP1_C domain-containing protein	AOA183GNG0	3.02
ERAP1_C domain-containing protein	AOA183F9M3	4.7
Eukaryotic translation initiation factor 2A	AOA183F7F4	2.22

Eukaryotic translation initiation factor 5A	AOA183FUA7	6.15
FABP domain-containing protein	AOA183G7I2	95.46
FABP domain-containing protein	AOA183GBA0	84.64
FABP domain-containing protein	AOA3P8BXV7	14.45
FABP domain-containing protein	AOA183FKC6	28.05
Fatty-acid and retinol-binding protein 1	AOA3P8D9C1	49.48
Fatty-acid and retinol-binding protein 1	AOA183GLK6	98.28
Fatty-acid and retinol-binding protein 1	Q962H2	42.33
F-box domain-containing protein	AOA3P8B5E6	3.06
Ferritin	AOA183FLG6	60.33
FG-GAP repeat protein	AOA183F281	3.85
Fibrinogen C-terminal domain-containing protein	AOA183F5Y8	14.44
Fibronectin type III domain protein	AOA183GRF5	1.75
Fibronectin type-III domain-containing protein	AOA183GKI6	23.09
Fibronectin type-III domain-containing protein	AOA183FLC4	2.36
Follistatin-like domain-containing protein	AOA183FYL2	10.95
Follistatin-like domain-containing protein	AOA3P8AG68	7.43
Follistatin-like domain-containing protein	AOA3P8BLC5	5.31
fructose-bisphosphatase	AOA3P8BJH0	11.81
fructose-bisphosphatase	AOA183F3S6	3.4
Fructose-bisphosphate aldolase	AOA3P7Z267	55.77
Fructose-bisphosphate aldolase	AOA3P8AR25	38.44
Fructose-bisphosphate aldolase	AOA3P8F538	159.44
Fucosyltransferase	AOA183FY04	8.41
Fucosyltransferase	AOA183GW99	2.18
fumarate hydratase	AOA183F3M4	46.93
Fumarylacetoacetase	AOA3P8DN73	5.35
G_PROTEIN_RECEP_F1_2 domain-containing protein	AOA3P8C1H0	2.05
Galectin	AOA3P7ZLW5	147.67
Galectin	AOA183FUQ2	18.82

Galectin	AOA3P8DGW1	24.4
Galectin	AOA3P8BJI0	77.62
Galectin	AOA183GQ70	22.53
Galectin	AOA183GSH1	9.52
Galectin	AOA3P7XMX7	21.25
Galectin	AOA183FBB3	39.36
Galectin	AOA183FUQ3	5.47
Gamma-amino-N-butyrate transaminase	AOA183GHJ2	2.96
Gamma-glutamyltranspeptidase	AOA3P8BLR6	12.9
GATA-type domain-containing protein	AOA3P7TFL5	1.93
GH18 domain-containing protein	AOA183GR89	5.54
GIY-YIG domain-containing protein	AOA183GHQ0	13.45
GLOBIN domain-containing protein	AOA183G0G6	266.76
GLOBIN domain-containing protein	AOA183G1J6	359.14
GLOBIN domain-containing protein	AOA183F277	102.75
GLOBIN domain-containing protein	AOA183GH14	352.44
GLOBIN domain-containing protein	AOA183GHQ5	20.67
GLOBIN domain-containing protein	AOA183GHQ6	21.89
GLOBIN domain-containing protein	AOA183GM67	39.39
GLOBIN domain-containing protein	AOA183GM68	19.02
GLOBIN domain-containing protein	AOA183GV03	636.13
GLOBIN domain-containing protein	AOA183FC19	649.52
GLOBIN domain-containing protein	AOA183FL83	288.46
GLOBIN domain-containing protein	AOA183FNA1	722.09
GLOBIN domain-containing protein	AOA183FNA3	744.69
Globin family profile domain-containing protein	AOA183G022	26.06
Glucosamine 6-phosphate N-acetyltransferase	AOA183FKK1	4.81
Glucose-6-phosphate isomerase	AOA3P8AVX7	96.56
glutamate dehydrogenase [NAD(P)(+)]	AOA3P8AZN8	29.15
Glutamate dehydrogenase	AOA183FP08	105.99

glutaminyl-peptide cyclotransferase	AOA3P7XAZ5	37.96
Glutaredoxin domain-containing protein	AOA3P8AFI1	7.02
Glutathione peroxidase	AOA183FZL9	2.57
Glutathione peroxidase	AOA183G5K9	0
Glutathione S-transferase 2 (Fragment)	Q9NJQ6	141.65
Glutathione transferase	AOA183FRS0	124.84
Glutathione transferase	AOA183FRS1	60.84
glutathione transferase	AOA183FXU2	15.96
glutathione transferase	AOA183FXU3	132.84
Glutathione transferase	AOA183G3W8	0
Glutathione transferase	AOA3P7WLV8	24.35
Glyceraldehyde-3-phosphate dehydrogenase]	AOA3P7XJP6	27.07
glycerol kinase	AOA3P7ZWX6	17.85
Glyco_18 domain-containing protein	AOA183GQY9	2.04
Glyco_hydro_19_cat domain-containing protein	AOA183FRG5	112.73
Glyco_hydro_38C domain-containing protein	AOA3P8BQG6	13.25
Glyco_trans_2-like domain-containing protein	AOA183FRP6	2.84
Glyco_transf_20 domain-containing protein	AOA3P8EQX9	0
Glycoside hydrolase family 31 TIM barrel domain-containing protein	AOA183F6E2	28.46
Glycosyltransferase family 92 protein	AOA183FVI6	2.47
Golgi apparatus protein 1	AOA3P8CU50	42.61
G-protein alpha subunit	AOA3P8A765	4.38
GPS domain-containing protein	AOA183FVC3	2.26
GRAM domain-containing protein	AOA183G8C4	6.12
Ground-like domain-containing protein	AOA3P8CQW0	1.81
Group XV phospholipase A2	AOA3P7XPT5	17.09
GST N-terminal domain-containing protein	AOA183GCB3	72.05
GST N-terminal domain-containing protein	AOA183GPP6	42.18
GST N-terminal domain-containing protein	AOA3P7YKT9	4.33
Guanine nucleotide-binding protein alpha-12 subunit	AOA183F4L7	3.31

Guanine nucleotide-binding protein G(O) subunit alpha	AOA3P7Y0V2	3.49
Guanine nucleotide-binding protein G(Q) subunit alpha	AOA183G4U3	29.09
Guanine nucleotide-binding protein subunit gamma	AOA183GQM3	6.48
H(+)-transporting two-sector ATPase OS=Heligmosomoides polygyrus OX=6339 GN=HPBE_LOCUS13670 PE=3 SV=1	AOA3P8AYE2	27.78
HATPase_c domain-containing protein	AOA183FL08	24.03
HATPase_c domain-containing protein	AOA183GNL5	51.34
Heat shock protein 60	AOA183FJW2	148.72
Heat shock protein 70	AOA183FPM9	75.6
Helicase ATP-binding domain-containing protein	AOA183GP46	0
Helicase C-terminal domain-containing protein	AOA183F4Y2	9.16
Histidine acid phosphatase	AOA183GJN3	1.68
Histidine acid phosphatase	AOA183FNB4	5.41
Histone H2A	AOA183GKE2	9.13
Histone H4	AOA183GKE3	24.2
HIT domain-containing protein	AOA183GJ95	5.05
Homogentisate 1,2-dioxygenase	AOA183FMZ2	2.77
HTH_48 domain-containing protein (Fragment)	AOA3P8DMU9	2.6
HTH_48 domain-containing protein	AOA183G2M0	2.4
HTH_48 domain-containing protein	AOA3P8F4J5	135.41
HTH_48 domain-containing protein	AOA183GN43	3.2
Hyaluronidase	AOA3P8AQV6	55.16
Hydrolase, TatD family	AOA183FGB3	5.05
hydroxyacylglutathione hydrolase	AOA183FLK6	27.65
Ig_mannosidase domain-containing protein	AOA183FYI6	5.87
Ig-like domain-containing protein	AOA183G385	2.81
Ig-like domain-containing protein	AOA3P8AV95	5.09
inorganic diphosphatase	AOA183FPE2	38.56
Inositol-polyphosphate 5-phosphatase	AOA183FQ25	2.64
Insulin-degrading enzyme	AOA3P7Z4W9	5.53

Integrase_H2C2 domain-containing protein	AOA183FSS1	9.83
Isochorismatase domain-containing protein 1	AOA183FDZ3	14.5
Isochorismatase domain-containing protein 2	AOA183GQJ2	5.52
IU_nuc_hydro domain-containing protein	AOA183FP67	14.14
KASH domain-containing protein	AOA3P8AH06	7.74
Kynureninase	AOA3P8B8I3	17.1
kynurenine--oxoglutarate transaminase	AOA183FSP5	10.09
Lactate/malate dehydrogenase C-terminal domain-containing protein	AOA183FXA7	48.49
Laminin EGF-like domain-containing protein	AOA3P8ALL3	8.27
Laminin IV type A domain-containing protein	AOA3P7YZD1	12.12
Large ribosomal subunit protein uL10	AOA183F257	62.22
Ldh_1_C domain-containing protein	AOA183G8Q9	7.15
L-dopachrome isomerase	AOA183GT37	33.12
Legumain prodomain domain-containing protein	AOA183FHI5	43.12
Legumain prodomain domain-containing protein	AOA8L8JU57	246.17
Leucine Rich Repeat family protein	AOA183FIA5	2.64
Lipase	AOA183GH76	52.88
Lipase_3 domain-containing protein	AOA183FQY5	28.73
Lipase_3 domain-containing protein	AOA183FNC2	16.95
Lipase_GDSL domain-containing protein	AOA183GDT7	1.99
L-lactate dehydrogenase	AOA183FXA4	16.94
Long-chain-fatty-acid--CoA ligase	AOA183FRY3	2.16
LRRNT domain-containing protein	AOA3P8DDF6	2.48
LRRNT domain-containing protein	AOA183G5T5	2.99
LTD domain-containing protein	AOA183F2R8	5.77
LTD domain-containing protein	AOA183FE98	3.63
L-type lectin-like domain-containing protein	AOA3P8CW80	3.38
L-type lectin-like domain-containing protein	AOA183FFR8	2.4
Lysozyme	AOA3P8CJH8	23.15
Lysozyme	AOA183GIP3	126.06

Lysozyme	AOA3P8DRS4	673.03
lysozyme	AOA183GR22	41.35
Lysozyme-1	G3C8W1	973.87
Lysozyme-3	G3C8W3	51.23
M20_dimer domain-containing protein	AOA183FRN9	9.52
M20_dimer domain-containing protein	AOA183FV65	26.69
Mago nashi protein	AOA3P8DGM9	5.29
Major facilitator superfamily (MFS) profile domain-containing protein	AOA183FVM4	4.91
Major sperm protein	AOA183F4S0	337.4
Major sperm protein	AOA183FMF6	6.89
Malate dehydrogenase	AOA3P8B629	59.78
Malate dehydrogenase	AOA183F9A6	16.41
Malectin domain-containing protein	AOA183FLU4	1.97
Malic enzyme	AOA3P8G4E9	1.86
Malic enzyme	AOA183FD03	4.33
Malic enzyme	AOA3P8AHZ5	5.85
mannose-6-phosphate isomerase	AOA183GSX7	2.82
MARVEL domain-containing protein	AOA183GHC2	5.37
MD-2-related lipid-recognition domain-containing protein	AOA183GWE4	16.38
Melibiase_C domain-containing protein	AOA183G0Z2	4.81
Mesencephalic astrocyte-derived neurotrophic factor homolog	AOA183FNV3	4.35
Metalloendopeptidase	AOA183FS83	79.47
Metalloendopeptidase	AOA183FUM2	8.88
Metalloendopeptidase	AOA183FXF0	119.27
Metalloendopeptidase	AOA183G107	4.83
Metalloendopeptidase	AOA183G1C7	5.76
Metalloendopeptidase	AOA3P8AZS9	166.88
Metalloendopeptidase	AOA183G4Z8	220.24
Metalloendopeptidase	AOA183GBM9	137.12
Metalloendopeptidase	AOA183GJB1	160.57

Metalloendopeptidase	A0A183GKG5	24.8
Metalloendopeptidase	A0A183GL74	142.02
Metalloendopeptidase	A0A183GV64	116.08
Metalloendopeptidase	A0A183F959	75.85
Metalloendopeptidase	A0A183FGE7	80.63
Metalloendopeptidase	A0A183FP76	5.75
Metalloendopeptidase	A0A183FQE3	24.31
Metalloendopeptidase	A0A183G8U6	31.13
Metallophos domain-containing protein	A0A183F6K3	5.77
Metallophos domain-containing protein	A0A183G8E0	18.2
Metallophos domain-containing protein	A0A183F8I5	5.72
Methyltransfer_dom domain-containing protein	A0A183GGG1	2.38
Methyltransf_11 domain-containing protein	A0A3P7ZE54	2.43
Methyltransf_21 domain-containing protein	A0A183G725	1.83
Methyltransf_21 domain-containing protein	A0A183G896	31.56
MFS domain-containing protein	A0A3P7UDH2	2.69
MFS domain-containing protein	A0A3P7WFX3	2.48
MIF domain-containing protein	A0A183FYG9	44.48
MIR domain-containing protein	A0A183GS42	2.99
Mitochondrial fission 1 protein	A0A183FKK2	2.97
ML domain-containing protein	A0A183GB67	30.76
ML domain-containing protein	A0A183FK87	2.22
Mo25-like protein	A0A183FUU5	9.19
Moesin/ezrin/radixin homolog 1	A0A3P7YWN7	85.07
MSP domain-containing protein	A0A183FX2	25.15
MSP domain-containing protein	A0A183G134	20.04
MSP domain-containing protein	A0A183G8J1	31.82
MSP domain-containing protein	A0A183GD01	6.86
MSP domain-containing protein	A0A183GK57	20.8
MSP domain-containing protein	A0A183GWN9	2.54

MSP domain-containing protein	A0A183FBX1	11.37
MSP domain-containing protein	A0A3P7WIX3	11.89
MSP domain-containing protein	A0A183FET4	9.14
MSP domain-containing protein	A0A183FMF5	14.61
MSP domain-containing protein	A0A183FQ54	3.23
MSP domain-containing protein	A0A183F6T7	4.85
Mss4-like protein	A0A183GX04	7.76
Myosin motor domain-containing protein	A0A183G9Z8	3.51
Myosin motor domain-containing protein	A0A183GT80	5.41
Myosin motor domain-containing protein	A0A183FJV6	9.62
Myosin tail domain-containing protein	A0A3P7YXR1	2
Myosin_tail_1 domain-containing protein	A0A183GJ55	5.65
N(4)-(Beta-N-acetylglucosaminy)-L-asparaginase	A0A3P7XJG3	10.7
Na_H_Exchanger domain-containing protein	A0A183G162	1.69
N-acetyl-D-glucosamine kinase	A0A183F4H7	0
N-acetylglucosamine-6-phosphate deacetylase	A0A183FHE7	3.63
NAD(P)H oxidase (H2O2-forming)	A0A3P8DDR0	8.93
NAD(P)H-hydrate epimerase	A0A183FEC8	17.89
non-specific serine/threonine protein kinase	A0A183FVK9	9.06
non-specific serine/threonine protein kinase	A0A183GMU9	2.83
Novel secreted protein 16	G3C8V7	171.79
Novel secreted protein 4	G3C8V6	142.65
Nuclear migration protein nudC	A0A183GA25	9.22
Nucleoside diphosphate kinase	A0A183FHH5	80.25
Nucleosome assembly protein	A0A183FIH4	27.61
Nudix hydrolase domain-containing protein	A0A3P8A7I5	6.29
Obg-like ATPase 1	A0A3P7YNY5	3.79
Oxidoreductase, short chain dehydrogenase/reductase family protein	A0A183GWK6	3.13
Palmitoyl-protein thioesterase 1	A0A183G937	9.47
PALP domain-containing protein (Fragment)	A0A3P8AQB9	5.72

PAN domain protein	A0A183GCJ4	8.02
Paramyosin	A0A183FMY6	10.05
PDZ domain-containing protein	A0A183FT59	1.79
PDZ domain-containing protein	A0A183GFG9	15.12
PDZ domain-containing protein	A0A183FKB0	11.68
Pepsin inhibitor-3-like repeated domain-containing protein	A0A183FL91	82.67
Pept_C1 domain-containing protein	A0A183FV18	43.1
Pept_C1 domain-containing protein	A0A183GN22	16.44
Peptidase A1 domain-containing protein (Fragment)	A0A3P7WU33	11.81
Peptidase A1 domain-containing protein	A0A3P8DWX8	3.58
Peptidase A1 domain-containing protein	A0A183G8F2	84.38
Peptidase A1 domain-containing protein	A0A183G8H7	27.53
Peptidase A1 domain-containing protein	A0A183GGQ1	2.14
Peptidase A1 domain-containing protein	A0A183GUB0	23.91
Peptidase A1 domain-containing protein	A0A3P8AWB4	91.63
Peptidase A1 domain-containing protein	A0A183FFX8	78.01
Peptidase A1 domain-containing protein	A0A183FQC1	2.37
Peptidase C1A papain C-terminal domain-containing protein	A0A3P8B8X5	1.99
Peptidase C1A papain C-terminal domain-containing protein	A0A3P8AKK5	40.44
Peptidase family M13	A0A3P7WLY7	153.38
Peptidase M1 membrane alanine aminopeptidase domain-containing protein	A0A183GG91	21.72
Peptidase S1 domain-containing protein	A0A183FW10	3.84
Peptidase S1 domain-containing protein	A0A3P7ZHP8	18.04
Peptidase S1 domain-containing protein	A0A183G2Z8	3.56
Peptidase S1 domain-containing protein	A0A183GAF9	2.5
Peptidase S1 domain-containing protein	A0A183FMW5	13.09
Peptidase S1 domain-containing protein	A0A183FQB4	37.86
Peptidase S1 domain-containing protein	A0A183FTK9	12.41
Peptidase S9 prolyl oligopeptidase catalytic domain-containing protein (Fragment)	A0A3P8AH42	44.57
Peptidase S9 prolyl oligopeptidase catalytic domain-containing protein	A0A3P7Y5X7	55.85

Peptidase_M1 domain-containing protein	AOA3P7Z8T6	50.94
Peptidase_M1 domain-containing protein	AOA183F3W7	6.33
Peptidase_M1 domain-containing protein	AOA183GDG0	19.49
Peptidase_M13 domain-containing protein	AOA183FV57	45.79
Peptidase_M13 domain-containing protein	AOA183F5I5	35.05
Peptidase_M13 domain-containing protein	AOA3P8B1C5	15.31
Peptidase_M13 domain-containing protein	AOA183G4V6	29.21
Peptidase_M13 domain-containing protein	AOA3P8C7K1	124.33
Peptidase_M13 domain-containing protein	AOA183GBX0	35.51
Peptidase_M13_N domain-containing protein	AOA183GFK3	45.84
Peptidase_M13_N domain-containing protein	AOA3P7XJ53	118.39
Peptidase_M23 domain-containing protein	AOA3P7YAD8	6.63
Peptidase_M24 domain-containing protein	AOA183F7B6	3.47
Peptidase_M24 domain-containing protein	AOA183GSE1	4.24
Peptidase_S28 domain-containing protein	AOA183FHI3	10.71
Peptidase_S9_N domain-containing protein	AOA183FZ31	2.28
Peptidylglycine monooxygenase (Fragment)	AOA3P7YI24	93.28
Peptidyl-prolyl cis-trans isomerase	AOA183G9Q2	65.95
Peptidyl-prolyl cis-trans isomerase	AOA183F9U3	58.12
Peptidyl-prolyl cis-trans isomerase	AOA183FEH2	57.24
Peptidyl-prolyl cis-trans isomerase	AOA183FEJ2	67.95
peptidylprolyl isomerase	AOA3P8FXN5	21.69
peptidylprolyl isomerase	AOA183F8D9	11.45
PGM_PMM_I domain-containing protein	AOA183FA08	2.97
PGM_PMM_IV domain-containing protein	AOA183FU52	15.19
PH domain-containing protein (Fragment)	AOA3P8AJC6	2.47
PHA domain	G3C8V5	154.82
Phosphatidylethanolamine-binding protein	AOA183F4J6	48.94
Phosphatidylethanolamine-binding protein	AOA183F387	79
Phosphatidylethanolamine-binding protein	AOA183FR13	42.2

phosphoacetylglucosamine mutase	AOA3P8BFC7	2.66
phosphoenolpyruvate carboxykinase (GTP)	AOA183FUW9	11.94
Phosphoglycerate kinase	AOA183GDT5	59.02
phosphoglycerate mutase (2,3-diphosphoglycerate-independent)	AOA183G4A8	49.11
phosphoglycerate mutase (2,3-diphosphoglycerate-independent)	AOA183G4B0	137.97
Phospholipase A2 domain-containing protein	AOA183G694	69.91
Phospholipase A-2-activating protein	AOA3P8ASS9	2.6
Phospholipase B-like	AOA183F5P3	1.76
Phospholipase B-like	AOA3P8EH69	9.62
Phospholipase B-like	AOA183GJJ1	6.01
Phospholipase B-like	AOA183FP37	4
Phosphotransferase	AOA3P8EKM8	21.75
Phosphotransferase	AOA183FEZ9	75.74
Phosphotransferase	AOA183GKY8	7.07
Phosphotransferase	AOA183FFA2	2
PID domain-containing protein	AOA183F2Z3	22.58
PITH domain-containing protein	AOA183FFV2	6.12
Piwi domain-containing protein	AOA183G0Y0	114.18
PKS_ER domain-containing protein	AOA183FJY9	8.99
PLD phosphodiesterase domain-containing protein	AOA183GPL5	64.75
PLD phosphodiesterase domain-containing protein	AOA183GWA6	33.79
PNP_UDP_1 domain-containing protein	AOA183GWD9	37.29
Polyprotein allergen nematode domain-containing protein	AOA3P7ZEG5	383.22
PRELI/MSF1 domain-containing protein	AOA183GA36	11.77
Pribosyltran domain-containing protein	AOA183FGV2	3
Pribosyltran domain-containing protein	AOA183FZ74	3.47
PRKCSH_1 domain-containing protein	AOA183F8L5	2.34
Profilin	AOA183FG55	63.06
proline--tRNA ligase	AOA3P7XHK6	2.24
Propep_M14 domain-containing protein	AOA3P7ZUD8	2.47

Proteasome endopeptidase complex	A0A183G0D5	5.59
Proteasome endopeptidase complex	A0A183FG57	11.48
proteasome endopeptidase complex	A0A3P8AQ73	2.62
proteasome endopeptidase complex	A0A183FPX3	14.78
Proteasome subunit alpha type	A0A183FS25	8.44
Proteasome subunit alpha type	A0A3P8AIM0	6.71
Proteasome subunit alpha type	A0A183GNP5	25.99
Proteasome subunit alpha type-1	A0A3P7Y128	18.36
Protein amnionless	A0A3P8A4X3	20.17
Protein disulfide-isomerase	A0A183FHB8	38.89
Protein kinase domain-containing protein	A0A3P8BFH8	10.35
Protein kinase domain-containing protein	A0A183GU45	2.08
Protein kinase domain-containing protein	A0A183G4K6	5.09
Protein quiver	A0A183G8H3	12.77
protein-disulfide reductase	A0A183G9Q9	19.7
protein-disulfide reductase	A0A183FIX2	8.81
protein-disulfide reductase	A0A183G1H2	2.47
protein-L-isoaspartate(D-aspartate) O-methyltransferase	A0A3P7ZFG4	37.62
P-type domain-containing protein	A0A3P8DUU4	35.2
PurA ssDNA and RNA-binding protein	A0A183FM88	5.72
purine-nucleoside phosphorylase	A0A183GKM8	21.2
Purple acid phosphatase	A0A3P8ESA0	10.74
Purple acid phosphatase	A0A183F3S8	17.36
Putative hydroxypyruvate isomerase	A0A3P7WH29	10.18
Pyr_redox_2 domain-containing protein	A0A183GM42	16.5
Pyr_redox_dim domain-containing protein	A0A183GCC4	5.01
pyridoxal 5'-phosphate synthase	A0A183G4B1	2.39
Pyridoxal kinase	A0A3P8CE29	3.4
Pyruvate kinase	A0A3P8ATJ4	72.64
pyruvate kinase	A0A3P7XQW6	4.97

Rab GDP dissociation inhibitor	AOA183FNT2	54.82
Rab proteins geranylgeranyltransferase component A	AOA3P7XTD1	27.04
Ras-like GTP-binding protein Rho1	AOA183GG80	29.49
Ras-like protein 3	AOA183FDS0	7.91
Ras-like protein	AOA183FJ25	10.27
Ras-related protein Rab-11A	AOA183G948	7.05
Ras-related protein Rab-11A	AOA3P7Z5S4	15.3
Ras-related protein Rab-1A	AOA3P8CAG5	10.16
Ras-related protein Rab-2	AOA183G049	3.77
Ras-related protein Rab-5C	AOA3P8B7P0	4.89
Ras-related protein Rab-7a	AOA183GTC8	2.13
Ras-related protein Ral-a	AOA183GTJ4	2.72
Recep_L_domain domain-containing protein	AOA183FDJ9	2.09
Receptor expression-enhancing protein	AOA183GGH7	3.84
Receptor expression-enhancing protein	AOA183F947	10.25
Receptor expression-enhancing protein	AOA183F2D6	1.85
Receptor L-domain domain-containing protein	AOA3P8BIN7	5.02
Regulator of chromosome condensation	AOA3P8C3Q1	9.18
Renin receptor	AOA3P7Z6C4	16.86
Replication factor A protein 2	AOA183GF26	7.16
Reverse transcriptase domain-containing protein	AOA183FWV3	3.74
Reverse transcriptase domain-containing protein	AOA183G4U2	0
Reverse transcriptase domain-containing protein	AOA183G7F1	2.19
Reverse transcriptase domain-containing protein	AOA183G8F9	6.16
Reverse transcriptase domain-containing protein	AOA3P8AUD9	2.36
Reverse transcriptase domain-containing protein	AOA183GJN1	5.67
Reverse transcriptase domain-containing protein	AOA3P8BF86	21.21
Reverse transcriptase domain-containing protein	AOA183F1Y0	2.4
Rho GDP-dissociation inhibitor	AOA183FHG2	14.92
Ribonucleoside-diphosphate reductase small chain	AOA183GBN3	33.09

ribose-5-phosphate isomerase	A0A183GP05	9.17
Ribosome receptor lysine/proline rich domain-containing protein	A0A3P8AII7	2.34
RNA-binding protein 8A	A0A183FLW8	2.24
RRM domain-containing protein	A0A3P7YPE4	2.04
RRM domain-containing protein	A0A183GE35	0
RRM domain-containing protein	A0A3P7YNB5	9.45
S-(hydroxymethyl)glutathione dehydrogenase	A0A183G1X3	6.77
SAM domain-containing protein	A0A183GQK8	7.98
SAM_3 domain-containing protein	A0A183GE73	3.79
Saposin B-type domain-containing protein	A0A183G4H0	0
Saposin B-type domain-containing protein	A0A183F700	5.62
Saposin B-type domain-containing protein	A0A183F780	14.66
Saposin B-type domain-containing protein	A0A183GNG6	106.41
Saposin B-type domain-containing protein	A0A183GWL0	8.21
Saposin B-type domain-containing protein	A0A183FC23	7.62
Saposin B-type domain-containing protein	A0A183FKM2	6.33
Saposin B-type domain-containing protein	A0A183FM83	2.49
Saposin B-type domain-containing protein	A0A3P7XSC4	2.63
Saposin B-type domain-containing protein	A0A183FNA4	17.14
SCD domain-containing protein	A0A3P8EYX1	14.83
SCP domain-containing protein	A0A183FQV4	46.86
SCP domain-containing protein	A0A183FQW0	152.07
SCP domain-containing protein	A0A183FQW2	162.05
SCP domain-containing protein	A0A183FQW3	95.28
SCP domain-containing protein	A0A3P7Z2D6	153.73
SCP domain-containing protein	A0A183FUB7	27.5
SCP domain-containing protein	A0A183FUZ3	21.88
SCP domain-containing protein	A0A183FVD8	2.41
SCP domain-containing protein	A0A183FWD7	1.81
SCP domain-containing protein	A0A183FXF9	2.31

SCP domain-containing protein	AOA183G0M8	3.51
SCP domain-containing protein	AOA3P7T9T9	42.99
SCP domain-containing protein	AOA183G5V7	2.65
SCP domain-containing protein	AOA3P8C0T7	239.18
SCP domain-containing protein	AOA183GB18	57.45
SCP domain-containing protein	AOA3P8C833	7.39
SCP domain-containing protein	AOA3P7U7W5	38.05
SCP domain-containing protein	AOA183GC36	410.06
SCP domain-containing protein	AOA183GC37	469.85
SCP domain-containing protein	AOA183F790	47.51
SCP domain-containing protein	AOA183GL21	280.51
SCP domain-containing protein	AOA183F9U8	322.45
SCP domain-containing protein	AOA183FDN8	12.35
SCP domain-containing protein	AOA3P7WKN8	19.43
SCP domain-containing protein	AOA3P8APZ8	721.46
SCP domain-containing protein	AOA3P7XU79	279.32
SCP domain-containing protein	AOA183FE39	493.04
SCP domain-containing protein	AOA3P8AQ08	380.89
SCP domain-containing protein	AOA183FI95	8.78
SCP domain-containing protein	AOA3P7XCT8	47.45
SCP domain-containing protein	AOA3P7XQN6	44
SCP domain-containing protein	AOA3P8C155	308.37
SCP domain-containing protein	AOA183FQ65	61.4
SCP domain-containing protein	AOA183GMB4	180.3
SCP domain-containing protein	AOA183F334	44.84
SCP domain-containing protein	AOA183FQ66	19.15
SCP domain-containing protein	AOA183GVK9	2.66
SCP domain-containing protein	AOA183FDN9	2.21
SCP domain-containing protein	AOA183F348	1.9
Secreted protein	AOA183FTH2	4.17

Secreted protein	A0A183G531	1.75
Selenide, water dikinase	A0A3P8DVV3	60.33
SER_THR_PHOSPHATASE domain-containing protein	A0A183G5H5	7.99
SER_THR_PHOSPHATASE domain-containing protein	A0A183GSX4	3.61
Serine protease K12H4.7	A0A3P8CTT8	64.8
Serine/threonine-protein phosphatase	A0A183FBJ7	12.67
Serine/threonine-protein phosphatase	A0A183FLR9	5.66
Serine/threonine-protein phosphatase	A0A183FPN5	8.99
Serine/threonine-protein phosphatase	A0A183G537	4.81
serine--tRNA ligase	A0A183G1D6	1.9
SERPIN domain-containing protein	A0A183G340	126.3
SERPIN domain-containing protein	A0A183G711	26.02
SERPIN domain-containing protein	A0A183FBA8	60.41
SERPIN domain-containing protein	A0A183FH93	72.72
SGNH domain-containing protein	A0A3P8B808	16.68
SH3 domain-containing protein	A0A183FRS8	9.07
SH3 domain-containing protein	A0A183FIV8	10.65
ShKT domain-containing protein	A0A3P8DFF3	5.18
ShKT domain-containing protein	A0A183G4E7	2.56
ShKT domain-containing protein	A0A183G6L3	7.95
ShKT domain-containing protein	A0A3P8E8G5	3.47
ShKT domain-containing protein	A0A183G6T0	5.31
ShKT domain-containing protein	A0A183GCF5	2.7
ShKT domain-containing protein	A0A183F7G9	12.86
ShKT domain-containing protein	A0A3P8D883	10.73
ShKT domain-containing protein	A0A183GJB8	9.57
ShKT domain-containing protein	A0A183GSK1	88.71
ShKT domain-containing protein	A0A183FC18	39.45
ShKT domain-containing protein	A0A183FL78	8.26
SHSP domain-containing protein	A0A183FFA5	2.58

Sm domain-containing protein	AOA183FU27	1.89
Small nuclear ribonucleoprotein E	AOA183FYC3	2.18
Small nuclear ribonucleoprotein Sm D1	AOA3P7Y9V3	4.98
Small nuclear ribonucleoprotein Sm D2	AOA183FYH0	6.42
SMP-LTD domain-containing protein	AOA183GDD2	8.77
SnoL-like domain-containing protein	AOA183F2I9	137.34
Sorbitol dehydrogenase	AOA183GP48	8.2
Sphingomyelin phosphodiesterase C-terminal domain-containing protein	AOA183GQZ8	21.65
Splicing factor 3A subunit 1	AOA183FWX5	2.16
START domain-containing protein	AOA183FS05	0
SUI1 domain-containing protein	AOA183F423	2.78
Sulfhydryl oxidase	AOA183G339	53.19
Superoxide dismutase [Cu-Zn]	AOA183GDQ7	49.86
Superoxide dismutase [Cu-Zn]	AOA183F2J9	53.65
Superoxide dismutase	AOA183FRG8	43.04
Sushi domain-containing protein	AOA183F4D2	5.46
Sushi domain-containing protein	AOA183FTC0	45.27
Sushi domain-containing protein	AOA3P8AAL7	20.17
Sushi domain-containing protein	AOA183FY74	9.22
Sushi domain-containing protein	AOA183FZB9	79.22
Sushi domain-containing protein	AOA183G0Y8	3.87
Sushi domain-containing protein	AOA3P8E851	38.92
Sushi domain-containing protein	AOA183G5Z5	41.37
Sushi domain-containing protein	AOA183G6J9	6.8
Sushi domain-containing protein	AOA3P8EAW3	11.6
Sushi domain-containing protein	AOA183F730	43.43
Sushi domain-containing protein	AOA3P8FZW2	36.26
Sushi domain-containing protein	AOA183GNC9	4.37
Sushi domain-containing protein	AOA183GRJ4	45.65
Sushi domain-containing protein	AOA183F8Q1	2.11

Sushi domain-containing protein	A0A183GV89	31.08
Sushi domain-containing protein	A0A183FDI6	33.68
Sushi domain-containing protein	A0A183FDQ8	121.25
Sushi domain-containing protein	A0A183FDQ9	16.38
Sushi domain-containing protein	A0A183FDR1	32.24
Sushi domain-containing protein	A0A183F2Y8	21
Sushi domain-containing protein	A0A183F3L4	25.25
Sushi domain-containing protein	A0A183GVF6	47.53
Tetraspanin	A0A183GC41	16.96
Tetraspanin	A0A183GLS2	9.47
Tetraspanin	A0A183GWB6	2.3
Thioredoxin domain-containing protein	A0A183G8Y5	112.9
Thioredoxin domain-containing protein	A0A3P8ER50	5.49
Thioredoxin domain-containing protein	A0A183GE00	24.56
Thioredoxin domain-containing protein	A0A183GGR8	2.06
Thioredoxin domain-containing protein	A0A183GIN8	4.35
Thioredoxin domain-containing protein	A0A183GM32	7.72
Thioredoxin domain-containing protein	A0A183FHF8	131.36
thioredoxin-dependent peroxiredoxin	A0A183GP77	62.68
thioredoxin-dependent peroxiredoxin	A0A183FLW9	9.64
Thioredoxin-like_fold domain-containing protein	A0A183GCL8	7.38
Thioredoxin-like_fold domain-containing protein	A0A183G8J2	7.78
Thymidylate synthase	A0A183GFG5	12.77
Thyroglobulin type-1 domain-containing protein	A0A3P7ZBR9	6.41
TIL domain-containing protein	A0A183FF46	13.13
TIL domain-containing protein	A0A183FI10	3.5
TIL domain-containing protein	A0A183GJK1	4.88
TPM domain-containing protein	A0A183GFA6	5.91
TPR_REGION domain-containing protein	A0A183FEC1	2.89
TPT domain-containing protein	A0A183FKL6	6.43

Transaldolase	A0A183FQ32	45.23
Transforming growth factor beta mimic 2	A0A2P1IQ76	16.96
Transforming growth factor beta mimic 3	A0A2P1IQ78	34.59
Transforming growth factor beta mimic 4	A0A2P1IQ81	32.37
Transforming growth factor beta mimic 5	A0A2P1IQ79	36.05
Transforming growth factor beta mimic 6	A0A2P1IQ80	67.7
Transforming growth factor beta mimic 7	A0A2P1IQ85	37.52
Transforming growth factor beta mimic 8	A0A2P1IQ89	18.73
Transforming growth factor beta mimic 9	A0A2P1IQ82	12.03
Transforming growth factor mimic	A0A2D1LW19	34.18
transketolase	A0A183GND1	50.38
Transmembrane protein 144	A0A3P8BYC3	7.43
Tranthyretin-like family protein	A0A183FRA1	86.31
Tranthyretin-like family protein	A0A183FSN3	45.95
Tranthyretin-like family protein	A0A183FU24	11.4
Tranthyretin-like family protein	A0A183FUI7	4.93
Tranthyretin-like family protein	A0A183FUQ6	11.08
Tranthyretin-like family protein	A0A183FWM6	6.97
Tranthyretin-like family protein	A0A183FZ27	22.42
Tranthyretin-like family protein	A0A3P8DR89	14.93
Tranthyretin-like family protein	A0A183FZH2	15.76
Tranthyretin-like family protein	A0A183G464	5.94
Tranthyretin-like family protein	A0A183G4U9	42.44
Tranthyretin-like family protein	A0A183G854	8.05
Tranthyretin-like family protein	A0A183G8M0	13.95
Tranthyretin-like family protein	A0A183GAT9	9.21
Tranthyretin-like family protein	A0A183GBK8	21.1
Tranthyretin-like family protein	A0A183GUL4	200.16
Tranthyretin-like family protein	A0A183FDH4	19.97
Tranthyretin-like family protein	A0A183FDM9	7.8

Transthyretin-like family protein	AOA183FDZ7	10.11
Transthyretin-like family protein	AOA183FJF0	16.78
Transthyretin-like family protein	AOA183FP04	85.89
Transthyretin-like family protein	AOA183FP05	52.84
Transthyretin-like family protein	AOA183GCM3	3.35
Transthyretin-like protein 46	AOA183F7L7	6.02
Transthyretin-related-1	G3C8V9	810.37
Trehalase	AOA3P7XS77	41.14
Triokinase/FMN cyclase	AOA3P8AVD4	2.8
Tropomyosin	AOA3P8AUN4	6.18
Tropomyosin	A8D2L1	4.58
TROVE domain-containing protein	AOA3P8B1H4	46.53
Tr-type G domain-containing protein	AOA183FR02	56.1
Tryptophan synthase beta chain-like PALP domain-containing protein	AOA3P7ZV58	3.15
t-SNARE coiled-coil homology domain-containing protein	AOA183G9G9	1.73
t-SNARE coiled-coil homology domain-containing protein	AOA3P7ZLE6	3.57
t-SNARE coiled-coil homology domain-containing protein	AOA183F2P3	24.63
Tubulin alpha chain	AOA183GTY4	14.64
Tubulin beta chain	AOA183FGY7	4.1
Tyrosinase_Cu-bd domain-containing protein	AOA183GMM4	12.84
Tyrosine-protein kinase	AOA3P7YV65	3.83
Tyrosine-protein kinase	AOA183FWL9	15.76
Tyrosine-protein kinase	AOA3P8C9Y4	0
Ubiquitin-like domain-containing protein	AOA183FLX5	7.34
Ubiquitin-ribosomal protein eL40 fusion protein	AOA3P8GUK7	30.95
UBX domain-containing protein	AOA3P7XH21	3.51
UCR_hinge domain-containing protein	AOA183G774	72.35
UDP-glucose:glycoprotein glucosyltransferase	AOA3P7YNE8	4.97
UEV domain-containing protein	AOA3P8BPS9	5.4
Uncharacterized protein (Fragment)	AOA3P8AH85	23.43

Uncharacterized protein (Fragment)	AOA3P8BAZ4	27.26
Uncharacterized protein	AOA183FQV5	38
Uncharacterized protein	AOA183FR70	366.99
Uncharacterized protein	AOA183FRE4	49.83
Uncharacterized protein	AOA183FRF5	9.05
Uncharacterized protein	AOA183FRK2	21.54
Uncharacterized protein	AOA183FRQ0	0
Uncharacterized protein	AOA183FRT4	14.06
Uncharacterized protein	AOA183FRV3	13.38
Uncharacterized protein	AOA183FS78	3.69
Uncharacterized protein	AOA3P8CPY2	10.07
Uncharacterized protein	AOA183FSI3	5.65
Uncharacterized protein	AOA3P8A955	0
Uncharacterized protein	AOA3P7YJ00	18.04
Uncharacterized protein	AOA3P7ZTI4	5.75
Uncharacterized protein	AOA3P8CL22	4.11
Uncharacterized protein	AOA3P7ZGP0	2.92
Uncharacterized protein	AOA3P7ZIN0	2.12
Uncharacterized protein	AOA183FUK7	1.61
Uncharacterized protein	AOA3P8A394	8.63
Uncharacterized protein	AOA183F4X0	5.25
Uncharacterized protein	AOA183FVV0	28.43
Uncharacterized protein	AOA183FWG4	0
Uncharacterized protein	AOA183FWM7	8.44
Uncharacterized protein	AOA183FWN1	76.95
Uncharacterized protein	AOA183FWN8	31.08
Uncharacterized protein	AOA3P7Z231	8.8
Uncharacterized protein	AOA183FWU8	5.91
Uncharacterized protein	AOA183FX54	6.57
Uncharacterized protein	AOA3P7ZWW5	11.07

Uncharacterized protein	AOA183FXA8	6.49
Uncharacterized protein	AOA183FXB4	9.21
Uncharacterized protein	AOA183FY25	53.05
Uncharacterized protein	AOA183FY92	10.6
Uncharacterized protein	AOA183FYB2	2.24
Uncharacterized protein	AOA3P8D902	6.92
Uncharacterized protein	AOA183FZ32	4.63
Uncharacterized protein	AOA3P8B1B9	7.76
Uncharacterized protein	AOA183FZN5	2.51
Uncharacterized protein	AOA183FZQ5	46.4
Uncharacterized protein	AOA3P8E311	13
Uncharacterized protein	AOA3P8BDV2	2.67
Uncharacterized protein	AOA183G2N6	20.16
Uncharacterized protein	AOA183G347	5.53
Uncharacterized protein	AOA183G3G3	3.01
Uncharacterized protein	AOA183G3L0	2.5
Uncharacterized protein	AOA3P8DX86	13.28
Uncharacterized protein	AOA183F610	37.61
Uncharacterized protein	AOA183G499	13.12
Uncharacterized protein	AOA183G4D2	2.56
Uncharacterized protein	AOA3P8B8H7	2.48
Uncharacterized protein	AOA183G4V8	4.64
Uncharacterized protein	AOA183G4W1	2.37
Uncharacterized protein	AOA3P8E2I6	0
Uncharacterized protein	AOA3P8A2H4	27.22
Uncharacterized protein	AOA183F6A6	1.69
Uncharacterized protein	AOA183G5X3	1.99
Uncharacterized protein	AOA183G676	2.95
Uncharacterized protein	AOA3P8AV66	33.54
Uncharacterized protein	AOA183G6B0	4.06

Uncharacterized protein	AOA183F6D9	2.89
Uncharacterized protein	AOA183G7K1	4.03
Uncharacterized protein	AOA183G7Q5	17.77
Uncharacterized protein	AOA3P8BL27	7.09
Uncharacterized protein	AOA3P8A9V8	6.83
Uncharacterized protein	AOA183G951	2.65
Uncharacterized protein	AOA183G954	14.27
Uncharacterized protein	AOA183G9I0	41.91
Uncharacterized protein	AOA183G9M5	28.69
Uncharacterized protein	AOA183G9Q1	66.43
Uncharacterized protein	AOA183GAH0	65.67
Uncharacterized protein	AOA183F6Y0	6.18
Uncharacterized protein	AOA183GB45	11.84
Uncharacterized protein	AOA183F706	21.12
Uncharacterized protein	AOA183F711	10.88
Uncharacterized protein	AOA183GC10	4.59
Uncharacterized protein	AOA3P8BFB4	20.25
Uncharacterized protein	AOA183GC38	19.45
Uncharacterized protein	AOA183GCM2	7.44
Uncharacterized protein	AOA183GCY7	11.24
Uncharacterized protein	AOA183GDK5	2.38
Uncharacterized protein	AOA183GE62	28.21
Uncharacterized protein	AOA183GEN8	126.53
Uncharacterized protein	AOA183F7E1	7.98
Uncharacterized protein	AOA183GEV3	2.02
Uncharacterized protein	AOA183GFN7	2.74
Uncharacterized protein	AOA183GFS9	2.13
Uncharacterized protein	AOA183GGP9	111.56
Uncharacterized protein	AOA183GH04	6.49
Uncharacterized protein	AOA183GHF4	2.01

Uncharacterized protein	AOA183GHI1	13.02
Uncharacterized protein	AOA3P8BSN1	2.73
Uncharacterized protein	AOA183GHX2	7.53
Uncharacterized protein	AOA183GI15	26.94
Uncharacterized protein	AOA183F801	21.72
Uncharacterized protein	AOA183GK06	6.68
Uncharacterized protein	AOA183GKG0	3.42
Uncharacterized protein	AOA183GKY9	16.82
Uncharacterized protein	AOA183F298	3.17
Uncharacterized protein	AOA183GLD3	7.99
Uncharacterized protein	AOA183GM13	16.02
Uncharacterized protein	AOA183F8C8	8.43
Uncharacterized protein	AOA183GPP8	4.22
Uncharacterized protein	AOA183GPU3	22.2
Uncharacterized protein	AOA183GPU5	14.65
Uncharacterized protein	AOA183GQ78	8.98
Uncharacterized protein	AOA183GRD7	8.91
Uncharacterized protein	AOA183GRS4	0
Uncharacterized protein	AOA183GSH0	75.05
Uncharacterized protein	AOA183GSM6	1.91
Uncharacterized protein	AOA183GSM9	24.02
Uncharacterized protein	AOA183GTW0	8.44
Uncharacterized protein	AOA183GU98	1.74
Uncharacterized protein	AOA183GUH8	7.18
Uncharacterized protein	AOA183GUM5	48.22
Uncharacterized protein	AOA183GV24	24.65
Uncharacterized protein	AOA183GWI6	41.81
Uncharacterized protein	AOA183GWR3	27.84
Uncharacterized protein	AOA183GWU3	3.47
Uncharacterized protein	AOA183GWW1	2.6

Uncharacterized protein	AOA183GX80	8.64
Uncharacterized protein	AOA183GXX1	12.97
Uncharacterized protein	AOA183GXN7	9.44
Uncharacterized protein	AOA183F2E3	17.34
Uncharacterized protein	AOA183FAA5	30.92
Uncharacterized protein	AOA183F1T9	8.52
Uncharacterized protein	AOA183F2G7	7.29
Uncharacterized protein	AOA3P7U868	51.27
Uncharacterized protein	AOA183F2I4	3.95
Uncharacterized protein	AOA183FBH8	7.19
Uncharacterized protein	AOA3P7TFL0	15.45
Uncharacterized protein	AOA183FD26	24.4
Uncharacterized protein	AOA183FD27	76.4
Uncharacterized protein	AOA3P7X1Z1	8.17
Uncharacterized protein	AOA183F2P1	12.45
Uncharacterized protein	AOA183FD81	3.15
Uncharacterized protein	AOA183FD85	25.22
Uncharacterized protein	AOA183FDD1	1.75
Uncharacterized protein	AOA183FDQ7	2.51
Uncharacterized protein	AOA3P7WN17	74.19
Uncharacterized protein	AOA183FED7	19.98
Uncharacterized protein	AOA3P7X8L3	3.11
Uncharacterized protein	AOA3P7XSS6	2.59
Uncharacterized protein	AOA3P7Y146	2.43
Uncharacterized protein	AOA183FFP9	100.97
Uncharacterized protein	AOA183F317	71.46
Uncharacterized protein	AOA3P7WVN2	8.68
Uncharacterized protein	AOA3P7Y5C6	3.54
Uncharacterized protein	AOA3P7XSN6	17.34
Uncharacterized protein	AOA183F3B2	18.22

Uncharacterized protein	AOA183F3B3	11.67
Uncharacterized protein	AOA183FIE2	2.98
Uncharacterized protein	AOA3P7YDW4	1.89
Uncharacterized protein	AOA3P7X844	7.26
Uncharacterized protein	AOA183F3E1	71.22
Uncharacterized protein	AOA183FIT3	55.12
Uncharacterized protein	AOA3P7X8M9	21.72
Uncharacterized protein	AOA183FJ92	5.83
Uncharacterized protein	AOA183FJC2	2.99
Uncharacterized protein	AOA183FJF4	20.74
Uncharacterized protein	AOA183FJM9	69.08
Uncharacterized protein	AOA3P8BHQ9	2.68
Uncharacterized protein	AOA183FK39	37.06
Uncharacterized protein	AOA183FK40	17.45
Uncharacterized protein	AOA3P8BN52	23.65
Uncharacterized protein	AOA3P7XHP2	29.02
Uncharacterized protein	AOA183F3N9	2.87
Uncharacterized protein	AOA183FLM6	17.4
Uncharacterized protein	AOA183FLQ7	2.06
Uncharacterized protein	AOA183FMA1	3.31
Uncharacterized protein	AOA183FMP4	15.74
Uncharacterized protein	AOA3P7Z2T5	4.54
Uncharacterized protein	AOA183FN63	20.26
Uncharacterized protein	AOA183FPM5	9.32
Uncharacterized protein	AOA183F469	153.49
Uncharacterized protein	AOA183FKY2	88.4
Uncharacterized protein	AOA183FWJ0	35.91
Uncharacterized protein	AOA183GDY2	2.4
Uncharacterized protein	AOA183GIE9	1.72
Uncharacterized protein	AOA183F2W9	249.23

Uncharacterized protein	AOA183F9T5	77
Uncharacterized protein	AOA183FA35	76.75
Uncharacterized protein	AOA183GC15	60.17
Uncharacterized protein	AOA183FKA6	27.91
Uncharacterized protein	AOA183FRI5	15.53
Uncharacterized protein	AOA183GV56	11.39
Uncharacterized protein	AOA183FH84	11.34
Uncharacterized protein	AOA183GSD8	10.88
Uncharacterized protein	AOA183G4X1	9.53
Uncharacterized protein	AOA183GRI9	5.57
Uncharacterized protein	AOA183GWX0	5.47
Uncharacterized protein	AOA183GUP1	2.84
Uncharacterized protein	AOA183G394	2.63
Uncharacterized protein	AOA183GN85	2.56
Uncharacterized protein	AOA183GTT8	2.31
Uncharacterized protein	AOA183GER9	2.27
Uncharacterized protein	AOA183GG82	2.16
Uncharacterized protein	AOA183F6X7	1.9
Uncharacterized protein	AOA183F6W4	0
Uridine 5'-monophosphate synthase	AOA3P7ZXZ0	11.41
urocanate hydratase	AOA183FNT5	1.93
UTP--glucose-1-phosphate uridylyltransferase	AOA183F899	8.73
Vacuolar protein sorting-associated protein 13 VPS13 adaptor binding domain-containing protein	AOA3P8FM74	2.17
V-ATPase proteolipid subunit C-like domain-containing protein	AOA183GI85	4.34
Venom allergen/ancylostoma secreted protein-like 1 isoform 1	G4XWW3	1282.26
Venom allergen/ancylostoma secreted protein-like 1 isoform 2	G4XWW4	1702.62
Venom allergen/ancylostoma secreted protein-like 1 isoform 3	G4XWW5	321.29
Venom allergen/ancylostoma secreted protein-like 1 isoform 4	G4XWW6	336.72
Venom allergen/ancylostoma secreted protein-like 10	G4XWX9	134.68

Venom allergen/ancylostoma secreted protein-like 12	G4XWY0	257.26
Venom allergen/ancylostoma secreted protein-like 13	G4XWY1	16.32
Venom allergen/ancylostoma secreted protein-like 14	G4XWY2	267.88
Venom allergen/ancylostoma secreted protein-like 15	G4XWY3	93.27
Venom allergen/ancylostoma secreted protein-like 16	G4XWY4	61.12
Venom allergen/ancylostoma secreted protein-like 17	G4XWY5	42.79
Venom allergen/ancylostoma secreted protein-like 18	G4XWY6	37.24
Venom allergen/ancylostoma secreted protein-like 19 isoform 1	G4XWY7	37.64
Venom allergen/ancylostoma secreted protein-like 2 isoform 2	G4XWW8	815.07
Venom allergen/ancylostoma secreted protein-like 2 isoform 3	G4XWW9	942.18
Venom allergen/ancylostoma secreted protein-like 20	G4XWY8	37.4
Venom allergen/ancylostoma secreted protein-like 3 isoform 1	G4XWX0	1288.05
Venom allergen/ancylostoma secreted protein-like 5	G4XWX2	245.17
Venom allergen/ancylostoma secreted protein-like 6	G4XWX3	194.17
Venom allergen/ancylostoma secreted protein-like 7 isoform 1	G4XWX4	389.42
Venom allergen/ancylostoma secreted protein-like 7 isoform 2	G4XWX5	459.15
Venom allergen/ancylostoma secreted protein-like 7 isoform 3	G4XWX6	412.19
Venom allergen/ancylostoma secreted protein-like 8 isoform 1	G4XWX7	195.23
Venom allergen/ancylostoma secreted protein-like 9	G4XWX8	607.89
vesicle-fusing ATPase	A0A3P7Z3S7	8.2
Vitellogenin domain-containing protein	A0A183G4X9	678.18
VOC domain-containing protein	A0A183F608	21.4
VOC domain-containing protein	A0A183GCT5	17.69
Voltage-dependent anion-selective channel protein 3	A0A183F2W4	5.63
V-SNARE coiled-coil homology domain-containing protein	A0A183FZN3	2.7
V-SNARE coiled-coil homology domain-containing protein	A0A183GDP4	3.19
V-type proton ATPase proteolipid subunit	A0A183GFH4	13.79
V-type proton ATPase subunit a	A0A8L8KU62	8.49
V-type proton ATPase subunit C	A0A183G630	6.39
V-type proton ATPase subunit E	A0A183FQ34	10.13

V-type proton ATPase subunit G	A0A183FFJ0	7.98
V-type proton ATPase subunit H	A0A183G261	2.77
V-type proton ATPase subunit	A0A3P8F307	14.5
VWFA domain-containing protein	A0A183FW85	33.61
VWFA domain-containing protein	A0A3P8A5I9	17.61
VWFA domain-containing protein	A0A183FH91	1.89
VWFA domain-containing protein	A0A3P8B7Q7	11.36
VWFA domain-containing protein	A0A183FHR8	2.65
VWFD domain-containing protein	A0A3P7ZT66	584.16
WAP domain-containing protein	A0A183FSY0	17.84
WAP domain-containing protein	A0A183G3S6	2.85
WD_REPEATS_REGION domain-containing protein	A0A183GC65	15.31
WD_REPEATS_REGION domain-containing protein	A0A183GL35	9.02
WD_REPEATS_REGION domain-containing protein	A0A183GT30	8.44
WD_REPEATS_REGION domain-containing protein	A0A183FXD5	9.63
Zinc metalloproteinase	A0A183FRX3	7.52
Zinc metalloproteinase	A0A183G144	26.97
Zinc metalloproteinase	A0A183G6D0	32.17
Zinc metalloproteinase	A0A183GCF3	361.68
Zinc metalloproteinase	A0A183GCF4	362.23
Zinc metalloproteinase	A0A183GE59	335.89
Zinc metalloproteinase	A0A183GKC3	462.99
Zinc metalloproteinase	A0A183GL53	4.09
Zinc metalloproteinase	A0A183GP65	29.9
Zinc metalloproteinase	A0A183GS00	38.8
Zinc metalloproteinase	A0A183GVJ2	76.42
Zinc metalloproteinase	A0A183FJU9	212.99
Zinc metalloproteinase	A0A183GGW2	117.2
Zinc metalloproteinase	A0A8L8KA65	24.63
ZnMc domain-containing protein	A0A183GBA5	66.47

ZnMc domain-containing protein	AOA183GVJ6	31.4
ZP domain-containing protein	AOA183FZ10	12.4
ZP domain-containing protein	AOA183GH33	2.77
ZP domain-containing protein	AOA3P7Y3L6	10.56

Appendix table 3. GO terms of proteins identified in 10,000 – 50,000 molecular weight HES fraction

HES cellular compartment summary	Count	% total
None detected	419	57.95
Extracellular	91	12.59
Cytoplasm	69	9.54
Cell surface	28	3.87
Plasma membrane	24	3.32
Mitochondrion	16	2.21
Endoplasmic reticulum	13	1.80
Nucleus	12	1.66
Lysosome	11	1.52
Golgi apparatus	10	1.38
Cytoskeleton	7	0.84
Endosome	6	0.72
G-protein complex	4	0.48
Myosin filament	3	0.36
Spliceosome	3	0.36
Vacuole	2	0.24
Phosphopyruvate hydratase complex	1	0.12
Cell cortex	1	0.12
Peroxisome	1	0.12
Proton-transporting two-sector ATPase complex	1	0.12
NELF complex	1	0.12
HES biological process summary	Count	% total
None detected	476	57.42
Proteolysis	50	6.03
Carbohydrate metabolic process	15	1.81
Molting cycle	14	1.69
Protein folding	13	1.57

Glutathione metabolic process	10	1.21
Glucose metabolic process	8	0.97
Protein processing	8	0.97
Peptide catabolic process	7	0.84
Proteoglycan biosynthetic process	7	0.84
Actin cytoskeleton organisation	6	0.72
Cell redox homeostasis	6	0.72
Lipid metabolic process	6	0.72
Proteasomal protein catabolic process	6	0.72
Cell wall macromolecule catabolic process	4	0.48
Cysteine biosynthetic process	4	0.48
Fructose 1,6-bisphosphate metabolic process	4	0.48
Intracellular protein transport	4	0.48
Small molecule metabolic process	4	0.48
Acetylcholine catabolic process	3	0.36
Dephosphorylation	3	0.36
Glutamate catabolic process	3	0.36
Malate metabolic process	3	0.36
Mannose metabolic process	3	0.36
Phospholipid metabolic process	3	0.36
Adenylate cyclase-modulating GPCR signalling pathway	2	0.24
AMP biosynthetic process	2	0.24
Animal organ morphogenesis	2	0.24
Arachidonic acid secretion	2	0.24
Cellular response to insulin	2	0.24
Chaperone-mediated protein folding	2	0.24
Cytoplasmic microtubule organisation	2	0.24
Defense response to gram-positive bacterium	2	0.24
Endocytosis	2	0.24

Endoplasmic reticulum response	2	0.24
Exocytosis	2	0.24
Fatty acid transport	2	0.24
Fucosylation	2	0.24
GPCR signalling pathway	2	0.24
Glycogen metabolic process	2	0.24
Innate immune response	2	0.24
Lactate metabolic process	2	0.24
L-phenylalanine catabolic process	2	0.24
Microtubule cytoskeleton organisation	2	0.24
Mitochondrial electron transport	2	0.24
Mitotic cytokinesis	2	0.24
Negative regulation of MAPK	2	0.24
Nucleoside metabolic process	2	0.24
Phosphorylation	2	0.24
Photoreceptor cell maintenance	2	0.24
Purine ribonucleotide catabolic process	2	0.24
Response to oxidative stress	2	0.24
Response to stress	2	0.24
Signal transduction	2	0.24
Spliceosomal snRNP assembly	2	0.24
Sulfur compound metabolic process	2	0.24
Vacuolar acidification	2	0.24
10-formyltetrahydrofolate catabolic process	1	0.12
Acetate metabolic process	1	0.12
Acetyl-CoA biosynthesis from pyruvate	1	0.12
Action potential	1	0.12
Adenosine catabolic process	1	0.12
Amino acid biosynthetic process	1	0.12
Amyloid-beta metabolic process	1	0.12
Androgen metabolic process	1	0.12
Angiogenesis in wound healing	1	0.12

Apoptotic DNA fragmentation	1	0.12
Apoptotic mitochondrial changes	1	0.12
Aspartate biosynthesis	1	0.12
Aspartate catabolism	1	0.12
Autophagosome maturation	1	0.12
Axogenesis	1	0.12
Beta-alanine biosynthetic process	1	0.12
Biosynthetic process	1	0.12
Calcineurin-mediated signalling	1	0.12
Cell adhesion	1	0.12
Cell cycle	1	0.12
Cell development	1	0.12
Cellular response to cAMP	1	0.12
Cellular response to dexamethasone	1	0.12
Cellular response to oestrogen	1	0.12
Cellular response to heat	1	0.12
Cortical cytoskeleton organisation	1	0.12
Cytoskeleton organisation	1	0.12
Cytosolic ribosome assembly	1	0.12
NAD synthesis from tryptophan	1	0.12
Pyrimidine nucleobase biosynthetic process	1	0.12
Deoxyribonucleotide biosynthetic process	1	0.12
Detoxification of nitrogen compound	1	0.12
DNA damage response	1	0.12
Chromatin assembly	1	0.12
Dopaminergic neuron differentiation	1	0.12
D-ribose metabolic process	1	0.12
dTMP biosynthetic process	1	0.12
dUMP biosynthetic process	1	0.12
EGFR signalling	1	0.12
Establishment of protein localisation to extracellular region	1	0.12

Ethanol oxidation	1	0.12
ECM organisation	1	0.12
Fatty acid oxidation	1	0.12
Fumarate metabolic process	1	0.12
Glycerol catabolic process	1	0.12
Glycine biosynthesis	1	0.12
Glycolate biosynthesis	1	0.12
Glycolytic process	1	0.12
Glycoprotein catabolic process	1	0.12
Glycoside catabolic process	1	0.12
Glyoxylate catabolic process	1	0.12
Heterochromatin formation	1	0.12
Homogentisate formation	1	0.12
Hydrogen peroxide catabolic process	1	0.12
Intracellular sequestering of iron	1	0.12
Intracellular signal transduction	1	0.12
L-methionine salvage from methylthioadenosine	1	0.12
L-methylmalonyl-CoA metabolic process	1	0.12
Lysosome organisation	1	0.12
Metabolite repair	1	0.12
Methylglyoxal catabolic process	1	0.12
Muscle contraction	1	0.12
N-acetylglucosamine catabolic process	1	0.12
Negative regulation of protein ubiquitination	1	0.12
Negative regulation of transcription	1	0.12
Nervous system development	1	0.12
Nucleosome assembly	1	0.12
Nucleotide excision repair	1	0.12
One-carbon metabolic process	1	0.12
Organelle organisation	1	0.12

Organonitrogen compound catabolic process	1	0.12
Phosphatidylinositol-mediated signalling	1	0.12
Phosphocreatine biosynthetic process	1	0.12
Polyphosphate catabolic process	1	0.12
Positive regulation of early endosome to late endosome transport	1	0.12
Positive regulation of ruffle assembly	1	0.12
Positive regulation of translation	1	0.12
Positive regulation of Wnt signalling	1	0.12
Post-golgi mediated transport	1	0.12
Protein localisation to plasma membrane	1	0.12
Protein modification process	1	0.12
Protein polyubiquitination	1	0.12
Protein transport	1	0.12
Regulation of cytokine activity	1	0.12
Response to ER stress	1	0.12
Response to metal iron	1	0.12
Rho protein signal transduction	1	0.12
RNA splicing	1	0.12
Small GTP-ase mediated signal transduction	1	0.12
Sorbitol catabolic process	1	0.12
Translation	1	0.12
Trehalose catabolic process	1	0.12
tRNA processing	1	0.12
Ubiquitin-dependent protein catabolic process	1	0.12
Vesicle mediated transport	1	0.12
HES molecular function summary	Count	% total
None found	353	42.48
Metalloendopeptidase activity	45	5.42
ATP binding	23	2.77

Serine-type endopeptidase inhibitor activity	18	2.17
Calcium ion binding	17	2.05
Haem binding	17	2.05
Metal ion binding	17	2.05
GTP binding	13	1.56
Actin filament binding	12	1.44
Carbohydrate binding	10	1.38
Glutathione transferase activity	8	0.97
Oxidoreductase activity	8	0.97
Cysteine-type endopeptidase activity	7	0.84
Aspartic-type endopeptidase activity	6	0.72
Dipeptidyl-peptidase activity	6	0.72
Lipid binding	6	0.72
Peptidyl-prolyl cis-trans isomerase activity	6	0.72
Serine-type endopeptidase activity	6	0.72
Chitin binding	5	0.6
Copper ion binding	5	0.6
Hydrolase activity	5	0.6
Protein disulfide isomerase activity	5	0.6
DNA binding	4	0.48
Lysozyme binding	4	0.48
Manganese ion binding	4	0.48
Proton-transporting ATPase activity	4	0.48
Scavenger receptor activity	4	0.48
1-phosphatidylinositol binding	3	0.36
Acetylcholinesterase activity	3	0.36
Alpha-mannosidase activity	3	0.36
Flavin adenine dinucleotide binding	3	0.36
Fructose-bisphosphate aldolase activity	3	0.36
Glutamate dehydrogenase (NAD⁺) activity	3	0.36
Guanyl-nucleotide exchange factor activity	3	0.36
Magnesium ion binding	3	0.36

mRNA binding	3	0.36
Myosin phosphatase activity	3	0.36
Phosphatase activity	3	0.36
Phospholipase activity	3	0.36
RNA binding	3	0.36
Serine-type carboxypeptidase activity	3	0.36
Signalling receptor activity	3	0.36
2,3-bisphosphoglycerate-independent phosphoglycerate mutase activity	2	0.24
Acid phosphatase activity	2	0.24
Alanine-glyoxylate transaminase activity	2	0.24
Alditol NADP+ 1-oxidoreductase activity	2	0.24
Alpha,-1,4-glucosidase activity	2	0.24
Amino acid transmembrane transporter activity	2	0.24
Arginine kinase activity	2	0.24
ATPase binding	2	0.24
Beta-mannosidase activity	2	0.24
Beta-N-acetylglucosaminidase activity	2	0.24
Carbonate dehydratase activity	2	0.24
Catalytic activity	2	0.24
Chromatin binding	2	0.24
Cystathionine gamma-lyase activity	2	0.24
Cytokine activity	2	0.24
Electron transfer activity	2	0.24
Fatty acid binding	2	0.24
Flavin-dependent sulfhydryl oxidase activity	2	0.24
GDP binding	2	0.24
GDP-dissociation inhibitor activity	2	0.24
Glutathione hydrolase activity	2	0.24
Lipid transporter activity	2	0.24
L-lactate dehydrogenase activity	2	0.24

L-malate dehydrogenase activity	2	0.24
Phosphatidylinositol phospholipase C activity	2	0.24
Phospholipase A2 activity	2	0.24
Phosphopentomutase activity	2	0.24
Protein kinase activity	2	0.24
Structural molecule activity	2	0.24
Thioredoxin peroxidase activity	2	0.24
4-hydroxyphenylpyruvate dioxygenase activity	1	0.12
5'-nucleotidase activity	1	0.12
6,7-dihydropteridine reductase activity	1	0.12
ABC-type transporter activity	1	0.12
Acetate CoA-transferase activity	1	0.12
Adenosine deaminase activity	1	0.12
Adenylosuccinate synthase activity	1	0.12
Adenylylsulfatase activity	1	0.12
ADP binding	1	0.12
ADP-dependent NAD(P)H-hydrate dehydratase activity	1	0.12
ADP-ribose diphosphatase activity	1	0.12
Alcohol dehydrogenase activity	1	0.12
Aldehyde dehydrogenase activity	1	0.12
Alpha, alpha-trihalase activity	1	0.12
Alpha-amylase activity	1	0.12
Alpha-galactosidase activity	1	0.12
Alpha-L-fucosidase activity	1	0.12
Aminoacylase activity	1	0.12
Asparaginase activity	1	0.12
Beta-galactosiase activity	1	0.12
Beta-N-acetylhexosaminidase activity	1	0.12
Bis(5'-nucleosyl)-tetrphosphatase activity	1	0.12
bis(5'-adenosyl)-triphosphatase activity	1	0.12

Calmodulin binding	1	0.12
Carbohydrate transmembrane transporter activity	1	0.12
Carboxypeptidase activity	1	0.12
Chloride channel activity	1	0.12
Citrate (Si)-synthase activity	1	0.12
Complement component C1q complex binding	1	0.12
Corticotropin-releasing hormone receptor 1 binding	1	0.12
D5 dopamine receptor binding	1	0.12
Damaged DNA binding	1	0.12
Deaminase activity	1	0.12
Deoxyribonuclease II activity	1	0.12
Deoxyribose-phosphate aldolase activity	1	0.12
Dihydrofolate reductase activity	1	0.12
Dihydrolipoyl dehydrogenase activity	1	0.12
Dihydrolipoyllysine-residue acetyltransferase activity	1	0.12
dUTP diphosphatase activity	1	0.12
Dynein intermediate chain binding	1	0.12
Endopeptidase inhibitor activity	1	0.12
Endopolyphosphatase activity	1	0.12
Estradiol 17-beta-dehydrogenase	1	0.12
Ferric iron binding	1	0.12
Fibroblast growth factor binding	1	0.12
Fructose 1,6-bisphosphate 1-phosphatase activity	1	0.12
Fucosyltransferase activity	1	0.12
Fumarate hydratase activity	1	0.12
Fumarylacetoacetase activity	1	0.12
GPCR binding	1	0.12
Glutaminy-peptide cyclotransferase activity	1	0.12

GAPDH activity	1	0.12
Glycerol-3-phosphatase	1	0.12
Glycogen phosphorylase activity	1	0.12
Glycosyltransferase activity	1	0.12
G protein beta-subunit binding	1	0.12
GTPase activator activity	1	0.12
Heparin binding	1	0.12
Histone binding	1	0.12
Hsp90 protein binding	1	0.12
Hyaluronoglucosaminidase activity	1	0.12
Hydroxyacylglutathione hydrolase activity	1	0.12
Hydroxypyruvate isomerase activity	1	0.12
Inorganic diphosphate phosphatase activity	1	0.12
Kinase binding	1	0.12
Kynureninase activity	1	0.12
Kynurenine-oxoglutarate transaminase activity	1	0.12
Lactoylglutathione lyase activity	1	0.12
L-amino acid transmembrane transporter activity	1	0.12
Large ribosomal subunit rRNA binding	1	0.12
L-aspartate:2-oxoglutarate aminotransferase activity	1	0.12
L-iditol 2-dehydrogenase activity	1	0.12
Ligand-gated sodium channel activity	1	0.12
L-isoleucine transaminase activity	1	0.12
Malate dehydrogenase activity	1	0.12
Mannose binding	1	0.12
miRNA binding	1	0.12
N-acetylglucosamine-6-phosphate deacetylase activity	1	0.12
Nitrilase activity	1	0.12
O-acyltransferase activity	1	0.12

Oligosaccharide binding	1	0.12
Orotate phosphoribosyltransferase activity	1	0.12
Palmitoyl hydrolase activity	1	0.12
Peroxidase activity	1	0.12
Porin activity	1	0.12
Protein tag activity	1	0.12
Protein L-isoaspartate	1	0.12
Protein-membrane adaptor activity	1	0.12
Purine-nucleoside phosphorylase activity	1	0.12
Rho GDP-dissociation inhibitor activity	1	0.12
Ribonucleoside-diphosphate reductase activity	1	0.12
Ribose-5-phosphate isomerase activity	1	0.12
Ribosome binding	1	0.12
Signalling receptor complex adaptor activity	1	0.12
S-methyl-5-thioadenosine phosphorylase activity	1	0.12
SNAP receptor activity	1	0.12
Structural constituent of cytoskeleton	1	0.12
Structural constituent of ribosome	1	0.12
Syntaxin-1 binding	1	0.12
Thiamine pyrophosphate binding	1	0.12
Thioredoxin-disulfide reductase activity	1	0.12
Threonine-type endopeptidase activity	1	0.12
Transaldolase activity	1	0.12
Translation elongation factor activity	1	0.12
Transmembrane transporter activity	1	0.12
Unfolded protein binding	1	0.12
UTP:glucose-1-phosphate uridylyltransferase activity	1	0.12

Appendix table 4. Table listing all significantly differentially expressed genes in the colon of *H. polygyrus* infected mice vs naïve

Gene name	Log₂ Fold Change	P-adjusted value
Clec10a	1.81	0.004804
Kcnn3	1.87	1.52E-05
Cpa3	7.25	2.01E-13
Angptl4	4.46	1.20E-06
Lipe	1.56	0.013167
Hlf	1.99	0.000398
Adgre1	1.86	0.00231
Ccl24	3.32	0.001266
Prg4	7.83	1.06E-05
Cd163	2.71	1.09E-05
Ccl8	2.83	0.000131
Retn	2.54	0.004274
Pcolce2	2.41	8.12E-08
Hsd11b1	1.57	0.003005
Alox15	5.21	3.51E-14
Arg1	13.49	3.47E-11
Slc36a2	2.06	0.005317
Gfpt2	2.3	6.42E-12
Ltc4s	1.63	0.007184
Ccl11	1.9	0.000193
Per1	1.63	0.000487
Tshr	2.79	0.001766
Pygl	2.71	2.87E-06
Serpina3n	1.8	0.001053
Sfrp4	3.11	1.18E-09
Nr1d2	1.52	3.98E-05
Gdf10	2.2	1.23E-07
Scara5	1.89	1.88E-06
Dab2	1.63	0.00056
Slc7a8	1.6	1.72E-05
Mcpt2	6.79	1.06E-14
Mcpt1	5.48	1.06E-14
Col14a1	1.74	5.07E-05
Tef	1.57	0.00231
Apod	2.16	0.000109
Retnlb	6.67	0.00017
Ccdc80	1.64	0.000174
Pi16	2.4	1.44E-07
Emilin2	2.13	3.99E-06
C3	2.87	1.10E-05
Tpsab1	11.9	6.80E-06
Ms4a4c	-1.58	0.015463
Alas2	3.76	9.57E-06
Adhfe1	1.66	0.006165
Cfh	2.09	5.13E-07
Mptx1	5.93	9.00E-05
lfi202b	1.62	0.005703

F5	3.83	3.99E-06
Prrx1	3.13	0.000504
Mtarc1	6.1	0.000399
Fcgr2b	1.53	0.00055
Mrc1	1.86	0.000327
Plxdc2	1.69	0.001223
Fcna	3.19	9.89E-11
Fbn1	1.77	1.98E-08
Ccn5	2.38	0.006659
Slc6a17	1.53	0.002707
Enpep	2.04	0.000164
Clca1	2.07	1.28E-11
Bnc2	1.96	0.002186
Per3	1.85	9.67E-05
Nsg1	1.53	0.000195
Slc34a2	-2.35	0.002951
Gm20605	-1.54	0.000257
Mfap5	1.85	0.000324
Emp1	1.76	8.45E-06
Itgam	2.27	2.56E-07
Adgrg2	2.65	0.000131
Car5b	3.07	6.54E-05
Cd209d	1.82	0.013256
Dusp4	1.66	0.005632
Slc7a2	4.19	3.76E-05
Lctl	1.64	0.020838
Me1	4.87	0.000408
Folr2	2.57	1.01E-05
Troap	-1.72	0.000615
Tpsb2	10.71	2.16E-10
B3galt2	2.3	0.0005
Ankmy1	-1.74	0.013066
Scn7a	1.54	0.00319
Ints6	-1.71	0.000204
Thrsp	1.74	0.01526
Acss3	2.92	0.002033
Myrf	2.8	0.00028
Colec12	1.57	1.77E-05
Glb1l2	1.52	0.01723
Lum	1.6	2.08E-05
Apln	2.32	0.001515
Scd1	2.16	0.00945
Itln1	4.98	5.70E-06
Pkhd1l1	2.8	1.40E-05
Irs2	2.37	4.47E-07
F13a1	3.15	1.43E-07
Orm1	2.24	0.004856
Dse	1.56	0.004047
Mrap	3.12	0.001503
Saa3	18.91	8.91E-37

Usp45	1.55	0.000145
Ildr2	2.1	1.06E-05
Chil3	4375.16	1.37E-17
Atp1a3	2.82	5.70E-06
Abca9	1.51	0.01066
Cmklr1	1.8	0.000101
A530016L24Rik	6.37	0.00045
Col6a6	7.03	1.13E-07
Adgrd1	2.05	5.05E-09
Vsig4	12.42	0.000193
Irs3	1.85	0.006361
Rnase2a	28.22	2.97E-09
BC049715	-1.77	0.001225
Nat8l	2.03	0.008507
Clec4a1	1.9	0.003823
Ccr2	1.64	0.002431
Mrgprg	81.48	5.68E-08
Cd209f	1.82	0.0118
Hbb-bs	2.77	0.000112
Mogat2	1.66	0.019883
H1f3	2.19	0.002695
Creb5	1.67	0.000367
Arntl	-1.54	0.003244
Timd4	3.18	0.00028
Slit3	1.63	0.000552
Cd248	1.64	0.000316
Rps18-ps3	1.82	0.004781
Mcpt4	7.8	2.16E-10
Retnla	9.65	6.40E-13
Serpib2	10.6	9.79E-05
Paqr9	4.05	0.0019
Cd209b	7.56	2.62E-07
Cma2	17.09	5.77E-06
Col28a1	1.87	9.67E-05
H2bc24	1.73	0.000218
Cd300ld3	1.84	0.004036
Hba-a2	2.75	8.56E-05
Hba-a1	3.19	7.74E-10
Lrrn4cl	1.73	0.000267
C4b	1.68	0.000542
Cdkn2b	-1.85	4.76E-12
Hbb-bt	1.81	0.01059
Amy1	2.33	0.002425
Ankef1	3.17	0.003823
Arrdc3	1.79	5.47E-11
Igkv1-88	2.42	0.008749
Igkv12-46	3.6	0.00388
Igkv8-27	3.23	0.001953
Igkv3-10	7.5	8.98E-06
Ighg1	8.9	1.01E-05

Cd209g	1.77	0.009573
Mptx2	4.94	0.000114
Gm11830	1.63	0.008749
Gm15693	1.87	0.004784
Ighe	4.06	0.00354
Cyp2d10	-1.65	3.64E-05
Ighv2-9-1	2.36	0.008414
Ighv2-2	1.55	0.024132
Igkv3-4	5.16	1.73E-05
5730419F03Rik	1.56	0.015287
Exosc6	-3.01	2.91E-23
Btbd8	1.62	5.16E-05
Gm7049	6.84	0.000594
Gm36161	2.2	0.004189
Gm50388	-2.95	0.00028
Serpina3h	1.63	0.002178
Clec10a	1.81	0.004804
Kcnn3	1.87	1.52E-05
Cpa3	7.25	2.01E-13
Angptl4	4.46	1.20E-06
Lipe	1.56	0.013167
Hlf	1.99	0.000398
Adgre1	1.86	0.00231
Ccl24	3.32	0.001266
Prg4	7.83	1.06E-05
Cd163	2.71	1.09E-05
Ccl8	2.83	0.000131
Retn	2.54	0.004274
Pcolce2	2.41	8.12E-08
Hsd11b1	1.57	0.003005
Alox15	5.21	3.51E-14
Arg1	13.49	3.47E-11
Slc36a2	2.06	0.005317
Gfpt2	2.3	6.42E-12
Ltc4s	1.63	0.007184
Ccl11	1.9	0.000193
Per1	1.63	0.000487
Tshr	2.79	0.001766
Pygl	2.71	2.87E-06
Serpina3n	1.8	0.001053
Sfrp4	3.11	1.18E-09
Nr1d2	1.52	3.98E-05
Gdf10	2.2	1.23E-07
Scara5	1.89	1.88E-06
Dab2	1.63	0.00056
Slc7a8	1.6	1.72E-05
Mcpt2	6.79	1.06E-14
Mcpt1	5.48	1.06E-14
Col14a1	1.74	5.07E-05
Tef	1.57	0.00231

Apod	2.16	0.000109
Retnlb	6.67	0.00017
Ccdc80	1.64	0.000174
Pi16	2.4	1.44E-07
Emilin2	2.13	3.99E-06
C3	2.87	1.10E-05
Tpsab1	11.9	6.80E-06
Ms4a4c	-1.58	0.015463
Alas2	3.76	9.57E-06
Adhfe1	1.66	0.006165
Cfh	2.09	5.13E-07
Mptx1	5.93	9.00E-05
Ifi202b	1.62	0.005703
F5	3.83	3.99E-06
Prrx1	3.13	0.000504
Mtarc1	6.1	0.000399
Fcgr2b	1.53	0.00055
Mrc1	1.86	0.000327
Plxdc2	1.69	0.001223
Fcna	3.19	9.89E-11
Fbn1	1.77	1.98E-08
Ccn5	2.38	0.006659
Slc6a17	1.53	0.002707
Enpep	2.04	0.000164
Clca1	2.07	1.28E-11
Bnc2	1.96	0.002186
Per3	1.85	9.67E-05
Nsg1	1.53	0.000195
Slc34a2	-2.35	0.002951
Gm20605	-1.54	0.000257
Mfap5	1.85	0.000324
Emp1	1.76	8.45E-06
Itgam	2.27	2.56E-07
Adgrg2	2.65	0.000131
Car5b	3.07	6.54E-05
Cd209d	1.82	0.013256
Dusp4	1.66	0.005632
Slc7a2	4.19	3.76E-05
Lctl	1.64	0.020838
Me1	4.87	0.000408
Folr2	2.57	1.01E-05
Troap	-1.72	0.000615
Tpsb2	10.71	2.16E-10
B3galt2	2.3	0.0005
Ankmy1	-1.74	0.013066
Scn7a	1.54	0.00319
Ints6	-1.71	0.000204
Thrsp	1.74	0.01526
Acss3	2.92	0.002033
Myrf	2.8	0.00028

Colec12	1.57	1.77E-05
Glb1l2	1.52	0.01723
Lum	1.6	2.08E-05
Apln	2.32	0.001515
Scd1	2.16	0.00945
Itln1	4.98	5.70E-06
Pkhd1l1	2.8	1.40E-05
Irs2	2.37	4.47E-07
F13a1	3.15	1.43E-07
Orm1	2.24	0.004856
Dse	1.56	0.004047
Mrap	3.12	0.001503
Saa3	18.91	8.91E-37
Usp45	1.55	0.000145
Ildr2	2.1	1.06E-05
Chil3	4375.16	1.37E-17
Atp1a3	2.82	5.70E-06
Abca9	1.51	0.01066
Cmklr1	1.8	0.000101
A530016L24Rik	6.37	0.00045
Col6a6	7.03	1.13E-07
Adgrd1	2.05	5.05E-09
Vsig4	12.42	0.000193
Irs3	1.85	0.006361
Rnase2a	28.22	2.97E-09
BC049715	-1.77	0.001225
Nat8l	2.03	0.008507
Clec4a1	1.9	0.003823
Ccr2	1.64	0.002431
Mrgprg	81.48	5.68E-08
Cd209f	1.82	0.0118
Hbb-bs	2.77	0.000112
Mogat2	1.66	0.019883
H1f3	2.19	0.002695
Creb5	1.67	0.000367
Arntl	-1.54	0.003244
Timd4	3.18	0.00028
Slit3	1.63	0.000552
Cd248	1.64	0.000316
Rps18-ps3	1.82	0.004781
Mcpt4	7.8	2.16E-10
Retnla	9.65	6.40E-13
Serpinb2	10.6	9.79E-05
Paqr9	4.05	0.0019
Cd209b	7.56	2.62E-07
Cma2	17.09	5.77E-06
Col28a1	1.87	9.67E-05
H2bc24	1.73	0.000218
Cd300ld3	1.84	0.004036
Hba-a2	2.75	8.56E-05

Hba-a1	3.19	7.74E-10
Lrrn4cl	1.73	0.000267